

Dipl. Ing. Johannes Kofler Bsc.

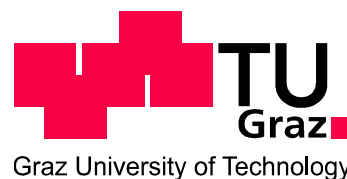
**Organic pulstrodes and
potentiometric ion sensors:
Reference-electrode-free ion
sensing**

DOCTORAL THESIS

For obtaining the academic degree of

Doktor der technischen Wissenschaften

Doctoral Programme of Technical Sciences
Technical Physics



Graz University of Technology

Supervisor:

Ao. Univ.-Prof. Dipl.-Ing. Dr.techn. Emil J.W. List-Kratochvil
Institute of Solid State Physics

In cooperation with
NanoTecCenter Weiz Forschungsgesellschaft mbH

Graz, April 2015

EIDESSTÄTLICHE ERKLÄRUNG

AFFIDAVIT

Ich erkläre an Eides statt, dass ich die vorliegende Arbeit selbstständig verfasst, andere als die angegebenen Quellen/Hilfsmittel nicht benutzt, und die den benutzten Quellen wörtlich und inhaltlich entnommenen Stellen als solche kenntlich gemacht habe. Das in TUGRAZonline hochgeladene Textdokument ist mit der vorliegenden Masterarbeit/Diplomarbeit/Dissertation identisch.

I declare that I have authored this thesis independently, that I have not used other than the declared sources/resources, and that I have explicitly indicated all material which has been quoted either literally or by content from the sources used. The text document uploaded to TUGRAZonline is identical to the present master's thesis/diploma thesis/doctoral dissertation.

Datum / Date

Unterschrift / Signature

To Martina

ACKNOWLEDGEMENT

I would like to especially thank Professor Emil J. W. Kratochvil-List for his guidance and for inspiring me with his deep love for science. I would also like to thank him for his forbearance and understanding during some of the more difficult periods of my tenure in his lab.

Special thanks goes to the well-organized, motivating, terrific, supercalifragilisticexpialidocious¹ Kerstin Schmoltner. A great part of this work was carried out in collaboration with her and I really enjoyed our vivid discussions, our teamwork and her honesty and reliability. I would also like to thank Sebastian Nau, Florian Kolb and Manuel Auer for support, good laughs, a joyful atmosphere and valuable discussions.

I also want to express my sincere gratitude to Josef Harrer who helped me with technical problems and who was always there to help me fix the e-line. He also gave me the opportunity to see things from the birds' eye view. I would also like to thank Angelika Nigg and Cornelia Ranz who created a joyful atmosphere in the lab. I also thank all the other members of the lab, both past and present, for their collegiality and friendship. Especially, Markus Postl and Stefan Sax for the 3D printed measurement setup, their support and their technical counsel.

Moreover I would like to thank Andreas Klug and Stefan Sax who allocated the funding for the MIEC-Devs and BioOFET2 project.

For funding I want to acknowledge the research project BioOFET2 and MIEC-DEVs and the Styrian government.

I would like to thank my parents for me being here and their unconditional support throughout the years. Last but most important I would like to thank Martina for her patience, understanding and her love.

ABSTRACT

Based on recent advances within the fields of organic electronics and polymeric ion selective membranes (ISMs), two novel low-cost and organic ion sensing concepts are presented within this work.

The first concept is based on an integrated electrolyte gated organic field-effect transistor (EGOFET) in combination with a polymeric ion-selective membrane. The membrane potential, which depends on the ion activity within the sample, modulates the effective gate potential and therefore drives the EGOFET. The advantage of this concept is that the potentiometric high impedance input signal of the membrane is transformed into an amplified low impedance amperometric output signal. Moreover, in contrast to the conventional OFET architecture, the semiconductor is in direct contact with the electrolyte. Consequently, there is no need for an expensive encapsulation or an elaborate deposition of a dielectric. In contrast, an electric double layer of high capacitance is formed, due to the direct contact between the electrolyte and the organic semiconductor. This extremely high capacitance induces a high charge carrier density in the semiconductor. For that reason, stable and low voltage operation (< 600 mV) becomes feasible. The architecture of this sensing platform was chosen to be modular and sensitivities towards other ions can be achieved, simply by exchanging the ion selective membrane. To prove the versatility of this concept, an H⁺ ion-selective and Na⁺ ion selective EGOFET is presented.

The second concept is a reference-electrode free, all organic K⁺ sensitive ion sensing platform fabricated on a plain sheet of paper by simplest means. This unique sensing platform consists of two identical ion selective electrodes (ISEs) which are assembled by bonding a polymeric ion selective membrane (ISM) directly onto a drop-casted PEDOT:PSS electrode on paper. Taking full advantage of the so called pulsetrode/flash-chronopotentiometry concept, a current pulse is used to measure the concentration of the targeted ion. This current forces an

ion flux out of the first ISE, through the sample and into the second ISE. This flux leads to a well-defined potential jump at the second ISE, as soon as the target ion locally depletes within the analyte, whereas the current induced potential change at the first ISE does not depend noticeably on the sample composition. Hence, the potential difference between the ISEs is directly related to the ion concentration within the sample. This concept allows for a 20-fold sensitivity enhancement compared to classical potentiometric measurements in physiological backgrounds. As mutual potential drifts of the ISEs cancel out, the sensor response showed excellent stability and did not change for over three months. Additionally, the response of the sensor could be modelled numerically, identifying the mechanisms and limitations of this promising sensor platform.

KURZFASSUNG

In dieser Arbeit werden zwei neuartige Ionenkonzepte vorgestellt. Diese basieren auf den jüngsten Erkenntnissen in den beiden Forschungsgebieten der organischen Elektronik und Polymer basierender Ionen-selektiver Membranen (ISM).

Das erste Konzept beruht auf einer Ionen-selektiven Membran in Kombination mit einem integrierten elektrolyt-gegateten organischen Feldeffekttransistor (EGOFET). Dabei fungiert der Transistor als Signalwandler und die Ionen-selektive Membran als sensitive Einheit. Das effektive Gate-Potential, das den Transistor ansteuert, wird vom Ionenkonzentrations-abhängigen Membranpotential moduliert. Der Vorteil dieses Messkonzeptes ist, dass ein potentiometrisches Eingangssignal mit hoher Impedanz in ein verstärktes Strom-Ausgangssignal übertragen wird. Im Vergleich zu herkömmlichen Transistoren benötigen EGOFETs keine kostenintensive Einkapselung oder eine aufwendige Aufbringung von Dielektrika. Ganz im Gegenteil, der direkte Kontakt zwischen dem Elektrolyten und dem organischen Halbleiter führt zur Ausbildung einer elektrischen Doppelschicht mit einer sehr hohen Kapazität. Diese außerordentlich hohe Kapazität erzeugt eine sehr hohe Ladungsträgerdichte im Halbleiter. Dadurch wird es möglich den Transistor, bei sehr niedrigen Spannungen ($< 1\text{ V}$) und gleichzeitig hohen Strömen ($> 1\ \mu\text{A}$) stabil zu betreiben. Die Architektur dieser Sensorplattform ist modular und die Sensitivität gegenüber eines spezifischen Ions kann durch die entsprechende Auswahl eines Ionophores erzielt werden. Die Vielseitigkeit dieses Konzeptes wird anhand einer Na^+ und H^+ sensitiven EGOFETs demonstriert.

Das zweite Konzept ist ein referenzelektrodenfreier, komplett organischer K^+ sensitiver Ionensensor. Um größtmögliche Kosteneffizienz zu gewährleisten, wurde dieser Sensor auf einem herkömmlichen Papierblatt mit einfachsten Fabrikationstechniken gefertigt. Dieses Messprinzip basiert auf zwei identischen Ionen-selektiven Elektroden, bestehend aus einer

ISM und einer auf das Papier auf getropften PEDOT:PSS Elektrode. Die Ionenkonzentration wird gemessen, indem ein konstanter Ionenstrom durch die erste ISE in den Analyten und von dort in die zweite ISE gepumpt wird. Zu einem bestimmten konzentrationsabhängigen Zeitpunkt, verarmt das Analyt-Ion in unmittelbarer Umgebung der zweiten ISE. Um den Ionenstrom aufrecht zu erhalten müssen daher andersartige Ionen in die zweite ISE extrahiert werden. Da diese Extraktion aber ein höheres Potential erfordert, führt die Verarmung zu einem definierten Potentialsprung. Der strominduzierte Potentialabfall über die erste ISE wird hingegen im Wesentlichen nicht von der Analyt-Zusammensetzung beeinflusst. Das Potential zwischen den ISEs, das benötigt wird den Ionenstrom aufrecht zu erhalten, ist daher direkt von der Konzentration des gewünschten Ions im Analyten abhängig. Im direkten Vergleich zu klassisch potentiometrischen Messungen ermöglicht dieses Konzept eine 20-fach höhere Sensitivität. Da sich gemeinsame, umgebungsbedingte Potentialveränderungen der ISEs gegenseitig aufheben, ist die Reproduzierbarkeit und Stabilität des Messsignals exzellent und blieb für mehr als drei Monate unverändert. Zusätzlich war es auch möglich das Verhalten der ISEs während dem Betrieb numerisch zu Modellieren und dadurch parasitäre Mechanismen zu identifizieren und die Grenzen des Messprinzips zu bestimmen.

List of included publications

This doctoral thesis is based on the articles published within the journals mentioned below. The author of this thesis is the first author of the listed publications and wrote the manuscripts, unless otherwise noted. The permission to reproduce the content was obtained from each journal and indicated within the corresponding chapters. Parts of the reproduced content have been modified and the original work can be found in the appendix.

A paper based, all organic, reference electrode free ion sensing platform

J. Kofler, S. Nau, Emil J.W. List-Kratochvil

Accepted by Journal of Chemical Materials B

Contribution: The author carried out all experimental work and wrote the manuscript. The manuscript was finalized with the co-authors.

Hydrogen ion-selective electrolyte-gated field-effect transistor for pH-sensing

J. Kofler*, K. Schmoltner*, A. Klug, E. J. W. List-Kratochvil

Applied Physics Letter 104, 193305 (2014)

*both authors contributed equally.

Contribution: The author contributed equally with K. Schmoltner to experiments related to the ion-selective EGOFETs and sensor characterization. The author wrote the manuscript, finalized the manuscript together with the K. Schmoltner.

Electrolyte-gated field-effect transistor for selective and reversible ion detection

K. Schmoltner*, J. Kofler*, A. Klug and E. J. W. List-Kratochvil,

Advanced Materials 25 (47), 6895–6899 (2013)

©WILEY-VCH Verlag GmbH & Co.

*both authors contributed equally.

Contribution: The author contributed equally with K. Schmoltner to experiments related to the ion-selective EGOFETs and sensor characterization. K. Schmoltner wrote the manuscript, finalized the manuscript together with the author.

Ion-selective electrolyte-gated field-effect transistors: Prerequisites for proper functioning

J. Kofler, K. Schmoltner and E.J.W. List-Kratochvil,

Proceedings of SPIE 9185, Organic Semiconductors in Sensors and Bioelectronics VII, 91851U-1 (2014)

©Society of Photo Optical Instrumentation Engineers

Contribution: All experimental work. The author wrote the manuscript. The manuscript was finalized with K. Schmoltner.

Highly robust electron beam lithography lift-off process using chemically amplified positive tone resist and PEDOT:PSS as a protective coating

J. Kofler, K. Schmoltner, A. Klug, E. J. W. List-Kratochvil

Contribution: All experimental work. The author wrote the manuscript. The manuscript was finalized with K. Schmoltner.

List of not included publications

Photolithographic processing and its influence on the performance of organic field-effect transistors

K. Schmoltner, A. Klug, J. Kofler and E. J.W. List

Proceedings of SPIE 8479, Organic Semiconductors in Sensors & Bioelectronics V, 84790J, (2012)

©Society of Photo Optical Instrumentation Engineers

Contribution: Carried out the SEM images were recorded and final editing with the co-authors.

Electrolyte-gated field-effect transistors for sensing applications in aqueous media

K. Schmoltner, J. Kofler, A. Klug and E. J. W. List-Kratochvil

Proceedings of SPIE 8831, Organic Field-Effect Transistors XII; Organic Semiconductors in Sensors & Bioelectronics VI, 88311N (2013)

©Society of Photo Optical Instrumentation Engineers

Contribution: Final editing with the co-authors.

CONTENT

1. Introduction and scope of the thesis	14
1.1 <i>Structure of this work</i>	17
2. Theory	19
2.1 <i>Organic electronics</i>	19
2.1.1 Organic semiconducting materials	20
2.1.1.1 Organic semiconducting material properties.....	21
2.1.1.2 Charge carriers	21
2.1.1.3 Conducting polymers - doping	22
2.1.2 Organic field-effect transistors	23
2.1.2.1 Operation principles.....	24
2.1.2.2 Organic field-effect transistors for sensing applications.....	26
2.2 <i>Electrolyte gated organic field-effect transistors</i>	28
2.3 <i>Electrochemistry at conducting/semiconducting electrodes</i>	31
2.3.1 Charge transfer at conducting- and semiconducting-electrolyte interfaces	31
2.3.2 Electric double layer	34
2.3.3 Polarizable vs. non-polarizable interfaces	35
2.3.4 Potentiometric measurements.....	36
2.4 <i>Ion selective electrodes</i>	38
2.4.1 Simple and facilitated ion transfer between immiscible electrolytes	38
2.4.2 Numerical modeling of ion selective membranes	41
2.4.2.1 Parameters used for the numerical calculations.....	44
2.4.3 Working principle of ion selective electrodes.....	46
2.4.3.1 Lower detection limit	50
2.4.3.2 Upper detection limit	52
2.4.4 Solid contact	52
2.4.5 Dynamically electrochemistry with ISEs	55
3. Ion selective electrolyte gated field-effect transistors	57

3.1	<i>Introduction</i>	58
3.2	<i>Experimental</i>	59
3.2.1	Fabrication procedures.....	59
3.2.2	Characterization methods	61
3.3	<i>Towards an ion selective EGOFET</i>	61
3.3.1	EGOFETs used as electric transducers	62
3.3.2	EGOFETs used for ion sensing applications	67
3.3.2.1	Ion sensitivity of EGOFETs	67
3.3.2.2	Gate electrode.....	68
3.3.2.3	Ion selective membrane.....	69
3.4	<i>The sensing concept</i>	70
3.5	<i>Ion selective sensing platform based on EGOFETs</i>	72
3.5.1	Na ⁺ sensitive EGOFET	72
3.5.2	H ⁺ selective EGOFET.....	75
3.5.2.1	Inner filling solution	75
3.5.2.2	Stability investigation.....	78
3.5.2.3	Constant current operation mode	80
3.5.2.4	Sensitivity and calibration	80
3.6	<i>Summary & conclusion</i>	82
4.	All organic paper based ion sensing platform	84
4.1	<i>Introduction into the sensing concept</i>	86
4.2	<i>Experimental</i>	88
4.2.1	Chemicals and Materials.....	88
4.2.2	Sensor fabrication.....	88
4.2.3	Measurement setups/procedures	89
4.3	<i>Results and discussion</i>	90
4.3.1	Conventional setup.....	90
4.3.1.1	Dynamic response at small pulse times	96
4.3.2	Ion selective electrodes on paper.....	98
4.4	<i>Conclusion & Outlook</i>	103

5. Summary & Conclusion	104
6. REFERENCES	107
7. Appendix	116
7.1 <i>A paper based, all organic, reference electrode free ion sensing platform</i>	116
7.2 <i>Hydrogen ion-selective electrolyte-gated field-effect transistor for pH-sensing</i>	127
7.3 <i>Electrolyte-gated field-effect transistor for selective and reversible ion detection</i>	133
7.4 <i>Ion-selective electrolyte-gated field-effect transistors: Prerequisites for proper functioning</i>	139
7.5 <i>Highly robust electron beam lithography lift-off process using chemically amplified positive tone resist and PEDOT:PSS as a protective coating</i>	153

1. INTRODUCTION AND SCOPE OF THE THESIS^a

The scope of this thesis is the investigation of two novel, organic and low-cost ion sensing platforms based on recent advances within the fields of organic electronics and polymeric ion selective membranes. Ion sensors are required in many fields ranging from food safety control², water quality monitoring³⁻⁵ to various applications in pharmaceutical and cosmetics industry.⁶ Especially, within the emerging fields of clinic analysis low-cost sensor platforms for in-situ sensing of ions and biological substances in appropriate aqueous media and physiological backgrounds are required.⁷ Within this field, potentiometric ion-selective electrodes (ISEs) are established tools as a routine methodology in clinical diagnostics for the determination of small hydrophilic target ions.⁸ In particular, ISEs based on polymeric ion selective membranes (ISMs) containing neutral or charged carriers (ionophores) have been improved to such an extent that it has resulted in a “new wave of ion-selective electrodes”.^{8,9} This was achieved by considerable improvements of the lower detection limit, new membrane materials, and a deeper theoretical understanding of the potentiometric response of ISMs. The discovery of transmembrane fluxes and the fact that leaking of target ions into the sample reduces the lower detection limit, revolutionized the field.¹⁰⁻¹⁴ Today, ISEs with extremely high selectivity⁸ and detection limits down to low nano-molar levels are available.¹⁵⁻²² If such powerful ion sensing elements are combined with suitable solid-state transducers, mass-producible, miniaturized ion-sensor systems with unforeseen analytical capabilities are within reach.^{8,23,24} Especially organic conductors are currently emerging as transducers for low cost organic potentiometric sensors.²⁵⁻²⁹

^a The content of the introduction is based on the work that has been published and submitted: J. Kofler, K. Schmoltner, A. Klug, and E.J.W. List-Kratochvil, *Appl. Phys. Lett.* 193305 (2014) and J. Kofler, S. Nau, and E.J.W. List-Kratochvil accepted by *J. Mater. Chem. B* (2015).

The sensitivity of all of these electrodes is typically given through the Nernst equation limiting it to ~ 59 mV for a 10-fold sample activity change in case of a monovalent ion. A second important limitation of ISEs is that in order to reliably measure the electromotive force (EMF) and to obtain a stable sensing signal, at least one reference electrode is required. However, the bridge electrolyte and the liquid junction of classical reference electrodes require regular maintenance, a vertical working position and it may also contaminate the sample. Although promising liquid junction-free all solid state reference electrode concepts were demonstrated^{28,30-35}, the potential stability upon varying the ionic strength²⁹ and response time of these novel solid-state reference electrodes still bear challenges.

The first presented ion sensing concept, combines these powerful ISMs with a highly promising transducer, namely, an electrolyte gated organic field-effect transistor (EGOFET). EGOFETs are characterized by their small size, portability, low-energy consumption and low cost³⁶⁻³⁸ and they have already proved to be ideal transducers for the detection of biomolecules such as DNA, dopamine, enzymes and proteins in an electrolytic background with a constant ionic strength.³⁹⁻⁴² An additional benefit of EGOFETs is that in contrast to the conventional ion-selective field-effect transistor (ISFET) architecture, the semiconductor is in direct contact with the electrolyte. Consequently, there is no need for elaborate and expensive encapsulation of the semiconductor. On the contrary, due to the direct contact between the electrolyte and the organic semiconductor, an electric double layer (EDL) at the semiconductor/electrolyte interface is formed. The EDL has an extremely high capacitance (1-10 $\mu\text{F}/\text{cm}^2$) inducing a high charge carrier density in the semiconductor.⁴³⁻⁴⁵ For that reason, stable and low voltage operation (< 600 mV) at currents which are sufficiently large for further signal processing (> 1 μA), becomes feasible. The major advantage of EGOFETs is that the potentiometric high impedance input signal of the membrane is transformed into an amplified low impedance, amperometric output signal. Therefore, they are ideal candidates, not only as transducers, but also as intrinsic signal amplifiers.⁴⁶ Consequently, the Nernstian sensitivity of the (ISM)s is intrinsically increased, easing data analysis. Using this concept a Na^+ ²⁵ and H^+ ^{26,47} sensitive ion sensing platform is demonstrated. Though this sensing concept is

very promising for low cost applications, one reference electrode is still required. In a second step an advanced electrodynamic concept, which does not require a reference electrode was pursued.

Typically ISEs are operated potentiometrically in chemical equilibrium. However, recently various attractive non-equilibrium, electrodynamic current and potential techniques have emerged.^{6,48-56} These techniques can overcome the limits of conventional ISEs. In particular flash chronopotentiometry (pulsetrodes), which allows for 10 to 20-fold sensitivity enhancement compared to classical potentiometry, seems to be especially suited for ion sensing in physiological backgrounds.⁵⁷⁻⁵⁹ The pulsetrode principle is based on a constant current pulse which forces an ion flux into the ISM. At a certain transition time, the target ion locally depletes within the analyte, leading to a drastic potential change (potential jump). The transition time and therefore also the potential recorded at a fixed time, are a function of the labile ion concentration within the analyte.^{6,58} Consequently, the potential can be used as a measurement signal, which exhibits a very high sensitivity within a narrow concentration range.⁵⁸ After each measurement the ISM has to be regenerated by applying the initial equilibrium potential measured before the current pulse is applied.⁵⁷ For that reason, conventional pulsetrodes still require reference electrodes.

The second investigated ion sensing concept is a flash-chronopotentiometric, all organic and reference electrode free K⁺ sensing platform on paper. This unique platform is based on two identical PEDOT:PSS-based solid contact ISEs (SC-ISEs) fabricated on a paper sheet by simplest means. The novelty of the proposed measurement method is that the commonly used reference electrode is replaced by a second, identical ISE. To measure the concentration of the target ion a current pulse is forced through the ISEs while the potential difference between the ISEs is measured at a fixed measurement time. The current forces an ion flux through the sample and through both ISEs. The ISE operated in forward direction, extracting target ions into the membrane from the sample side, will exhibit the typical potential jump upon target ion depletion. The ISE operated in backward direction just shifts the potential difference between the ISEs by a constant value and thus does not disturb the measurement

signal. Since both ISEs are identical, the equilibrium potentials of both ISEs are equal with respect to the analyte and the ISEs can be regenerated simply by shortening them after each measurement. Consequently, the second ISE serves two purposes. Firstly, it provides a reference potential during the measurement pulse and secondly it allows to regenerate the ISEs without using a reference electrode. Additionally, mutual potential drifts of the ISEs cancel out, leading to a very stable and reproducible response.

The results of both approaches are very promising and constitute an important step towards a low-cost disposable sensor array for multiple ion detection. This array is of high relevance for biomedical diagnostics, food-monitoring, industrial process- and water-control.

1.1 Structure of this work

The scope of this thesis is to investigate two novel ion sensing concepts based on recent advances within the fields of organic electronics and polymeric ion selective membranes. Accordingly, the work is divided into one common theory chapter and two separate chapters discussing the ion sensing concepts individually.

2nd chapter - theory: This chapter introduces basic theoretical concepts and operating principles which are later on used throughout the work. First the basics of organic electronics are introduced. Hereby, organic field effect transistors (OFETs) and electrolyte gated organic field effect transistors (EGOFETs) are discussed in detail. Subsequently, the relevant electrochemical mechanisms are discussed. A separate section is dedicated to the working principle of ion selective electrodes which is explained on the basis of numerical calculations. The numerical calculations carried out within this work are able to model static as well as the dynamic behavior of ISEs. Consequently, they are a very interesting tool to investigate the influence of the membrane or analyte composition in detail. The numerical methods used, are also presented.

3rd chapter - EGOFETs: In the 3rd chapter a novel sensing concept, based on a combination of ion selective membranes and EGOFETs is presented. First, the concept is critically examined and the prerequisites imposed on EGOFETs, used as transducers, are discussed. Subsequently, a Na⁺ and H⁺ sensitive EGOFETs are demonstrated. The sensing concept was developed/investigated and published in close collaboration with Dr. techn. Kerstin Schmoltner, who presented the Na⁺ sensitive EGOFET in detail in her PhD thesis.⁶⁰ For that reason, this work focuses on the H⁺ sensitive EGOFET.

4rd chapter – paper based flash-chronopotentiometric organic ion sensors: In the 3rd chapter a novel reference electrode free all organic ion sensing platform based on paper is presented. This sensing platform takes full advantage of flash-chronopotentiometry or the so called pulsetrode concept, which is introduced first. Subsequently, the proposed sensing concept is investigated on the basis of two conventional ISEs containing an aqueous inner filling solution. The response curves of these ISEs are modelled numerically, identifying the mechanisms and limits of this sensing platform. Finally, a sensing platform fabricated on a plain paper sheet is demonstrated using the same concept.

5th chapter – conclusion

6th chapter – references

7th chapter – appendix: The original texts of the works published in the course of this thesis.

2. THEORY

The ion sensing platforms developed within this thesis combine three broad fields of research. Namely, electrochemistry at conducting and semiconducting electrodes, polymeric ion selective electrodes and organic electronics. Due to the interdisciplinary, the basic concepts of these fields are introduced first. The first chapter introduces the principles of organic electronics with an emphasis on electrolyte gated organic field-effect transistors (EGOFETs). The second chapter deals with electrochemical mechanisms occurring at conducting and semiconducting electrodes. The third chapter discusses the principle working mechanisms of polymeric ion selective membranes (ISMs) operated in a potentiometric and dynamic mode.

2.1 Organic electronics

Unlike conventional inorganic electronics, organic electronics are constructed from carbon based compounds. Using modern organic synthesis, the properties and structure of these compounds can be specifically tailored to meet certain requirements. Another benefit of organic electronics is that they are low cost and solution processable. Thus, elaborate ion implantation or expensive vapor deposition processes, as in case of inorganic semiconductors, are not required. Furthermore, these materials can be designed to be biodegradable.⁴⁶ Considering recent advances within this field, the term green electronics can be envisioned.

First, the underlying physics of organic semiconducting materials such as their charge carriers and charge transfer processes are introduced. Subsequently, the working principles of organic field-effect transistors are presented. At the end of the section, the advantages of organic field-effect transistors and their device architectures for sensing applications are discussed.

2.1.1 Organic semiconducting materials

Organic semiconductors are based on conjugated carbon compounds. Their electronic properties arise from their special bonding configuration. Conjugated carbon compounds have a sp^2p_z hybridization. This means that each carbon atom has three sp^2 orbitals and one unpaired p_z orbital. The sp^2 orbitals form covalent σ -bonds with the neighboring atoms (see Figure 14 (a)). Whereas the perpendicular oriented p_z orbital, overlaps with the neighboring p_z orbitals forming π -bonds. The electrons within the p_z orbitals are not associated with a certain atom and are delocalized over the whole chain, forming a conduction band. Consequently, one would expect polyacetylene (see Figure 14 (b)) to behave like a 1D metal. In reality, this structure is energetically unfavorable and the single and double bonds are alternated leading to the so called conjugation. According to the Peierls theorem, the band splits into a bonding π and anti-bonding π^* band leading to the formation of a bandgap.^{135,136} The π band is fully occupied while the π^* band is empty. In terminology of molecular orbitals the π band corresponds to the HOMO (highest occupied molecular orbital) and the π^* band to the LUMO (lowest unoccupied molecular orbital).¹³⁷ In context of inorganic semiconductors, the HOMO is similar to the conduction band whereas the LUMO to the valence band. Theoretically, as the conjugation length and thus the number of carbon atoms, is increased, the energy gap gets smaller resulting in a continuous energy band. Practically, due to defects, twists and kinks, the π -conjugation is limited to a few repeating units.¹³⁵ Other than the conjugation length, the bandgap greatly depends on the molecular structure of the repeat units. Therefore, through intelligent design at a molecular level the properties of the organic semiconductors can be tuned.¹³⁵

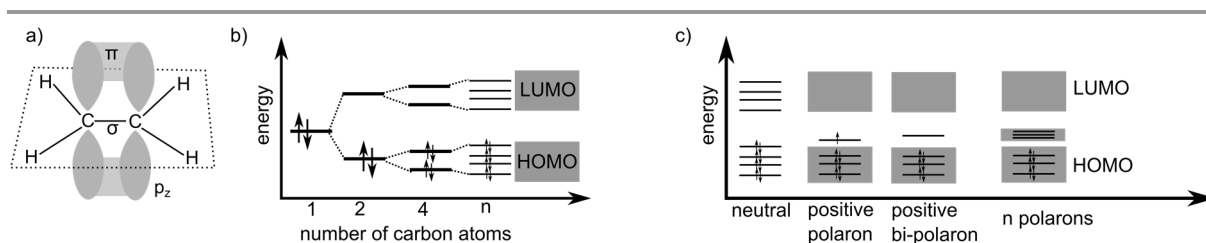


Figure 1: a) Illustration of the σ and π bonding of ethylene; b) illustration the occupation of the bonding π orbitals (HOMO) and anti-bonding π^* orbitals (LUMO) of polyacetylene; c) energy levels

2.1.1.1 Organic semiconducting material properties

Organic semiconductors can be classified into conjugated small molecules and conjugated polymers. Typically, small organic molecules are deposited via physical vapor deposition, whereas conjugated polymers are solution processable and can be deposited via spin coating, inkjet printing and roll to roll techniques.

The performance of organic semiconducting materials is generally characterized through their charge carrier mobility (μ) and their stability in ambient conditions. Typically, small molecules which form well-organized polycrystalline/crystalline films where the π orbitals of adjacent molecules overlap, generally outperform conjugated polymers. Mobilities μ as high as 15-40 $\text{cm}^2 \text{V}^{-1} \text{s}^{-1}$ ^{138,139} were measured in single crystalline films while conjugated polymers such as the commonly used regioregular poly(3-hexylthiophene-2,5-diyl) (P3HT, structure see Figure 2 (a)) exhibits mobilities in the range of $10^{-1} \text{cm}^2 \text{V}^{-1} \text{s}^{-1}$.¹⁴⁰ Though the charge carrier mobilities of conjugated polymers is magnitudes lower, the simple processability is a very persuasive argument for many sensing applications. Within this context, P3HT was used in this work. P3HT is one of the most studied organic polymers, commercially available, relatively cheap and it is easy to process.¹⁴¹⁻¹⁴³¹⁴⁴ Additionally, P3HT forms stable homogenous films on glass and PET substrates which do not delaminate in water. For that reason, P3HT is an ideal candidate as a model to investigate novel sensing methods ion aqueous environments. The implementation of other polymers with a higher environmental stability can then be carried out in a subsequent step.

2.1.1.2 Charge carriers

Doping or electrochemical gradients within the polymer create charge carriers. The charge carriers are not free electrons or holes but quasi particles corresponding to coupled charge-lattice entities. The presence of electronic charge leads to local changes in the atomic geometry which in turn leads to a self-localization of the electronic structure. All of the conducting polymers within this work have a non-degenerate ground state; i.e. they have a single geometric structure (the aromatic structure) and one ground energy. If an electron is removed, the structure changes from aromatic to quinoid, leading to a so called polaron. The

polaron is a quasi-particle coupling the conformational change of the polymer with the charge.^{135,137} If two electrons are removed then a bipolaron instead of two independent polarons is formed. The polarons/bipolarons create intermediate states within the band gap. In highly doped conducting polymers, the polaron states broaden until they eventually merge the HOMO and LUMO, closing the bandgap and leading to a metallic behavior.¹³⁵⁻¹³⁷

The charge transport of these charge carriers occurs via hopping in a distribution of localized states. In contrast to the band transport in inorganic single crystal semiconductors, where the charge transport is limited by phonon scattering, the transport in organic polymers is phonon assisted.¹³⁵⁻¹³⁷ For that reason, the charge carrier mobilities of organic semiconductors usually increase with temperature. There are many theoretical models describing the charge transport. However, these would by far exceed the scope of this work.

2.1.1.3 Conducting polymers - doping

Similar to inorganic semiconductors, organic semiconductors have to be doped to obtain high conductivities and metallic like properties. Doping in inorganic semiconductors is achieved by implanting impurity atoms into the semiconducting lattice. The dopant can be either a donor (n-type) or an acceptor (p-type) of an electron. Small impurity concentrations of a few ppm are sufficient to increase the conductivity. In contrast, organic semiconductors are doped by adding a high concentration of separate units which exchange an electron and form an ionic complex with the organic semiconductor.¹³⁶ Typical dopants are ions, charged molecules or polyelectrolytes. These are introduced during the synthesis, electrochemically or by diffusion.

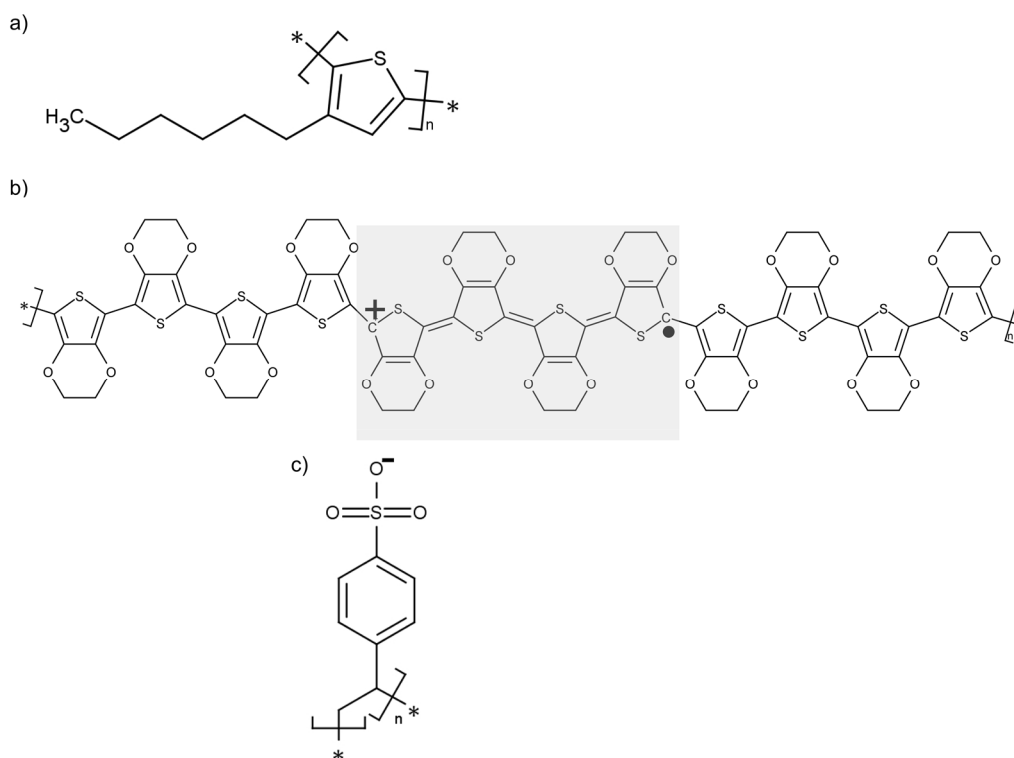


Figure 2: a) Structure of P3HT; b) shows the formation of a polaron (grey box) on a PEDOT backbone (thus PEDOT⁺);¹³⁵ c) shows the structure of the counterbalancing PSS⁻

One of the most popular conducting polymers is poly(3,4-ethylenedioxythiophene) polystyrene sulfonate (PEDOT:PSS). It is known to have a high conductivity, to be environmentally stable, commercially available, low cost and easy to process.^{145–148} For that reason, it was used within this work as a polymer to investigate new sensing methods. The structure of the PEDOT:PSS is shown Figure 2 b and c. The sulfonate group on the PSS chain takes on electron from the PEDOT backbone creating a positive charge. The charge is not localized in one monomer but is delocalized creating a polaron and therefore a positively charged charge carrier.¹³⁵

2.1.2 Organic field-effect transistors

FETs (field-effect transistors) are the backbone of modern microelectronics and the basis of the digital revolution of the 80s. Nowadays, the application field of organic field-effect transistors (OFETs) is not believed to be in the area of high performing integrated circuits where they cannot compete against state of the art silicon based FETs. Their application area

is in the field of low-cost, green and large area electronics where they compete against amorphous hydrogenated silicon thin film transistors (TFTs).¹⁴⁹ TFTs differ from FETs in that the conducting channel is formed by accumulation rather than by an inversion layer. Successful realizations include for example flexible displays and radio frequency identification tags.^{150–152} However, aside of these already highly industrialized consumer-electronics, OFETs are very promising candidates for various sensing applications. Especially electrolyte gated organic field effect transistors (EGOFETs) which are used to electronically detect DNA, enzyme and proteins are currently without alternative.¹⁵³

First the general operation principles of OFETs are introduced. Subsequently recent OFET based sensing devices are presented. A separate chapter is dedicated to a special kind of OFET, namely the EGOFETs.

2.1.2.1 Operation principles

The OFET is a three terminal device consisting of a source, a drain and a gate electrode. The source and drain electrodes are in direct contact with the OSC and the gate electrode is separated from the OSC by a dielectric (see Figure 3 (a)). The gate voltage (V_{GS}) induces charge carriers in the channel between the source and drain electrodes. If a source drain voltage (V_{DS}) is applied a current starts to flow. The magnitude of this current depends on the induced charge carrier density and thus gate voltage. The gate electrode-OSC stack can be considered as a capacity (if $V_{DS} = 0$). Accordingly, the induced charge carrier density is given by¹³⁵:

$$Q = C (V_{GS} - V_{th}) = \frac{\epsilon}{A d} (V_{GS} - V_{th}) \quad 2.1.1$$

Where Q is the charge, C is the capacity, ϵ is the dielectric constant of the dielectric, d the thickness of the dielectric, A the area of the channel (W x L) and V_{th} is called the threshold voltages which is a constant related to the work function difference of the gate dielectric and the OSC or to residual charges at the OSC-dielectric interface.

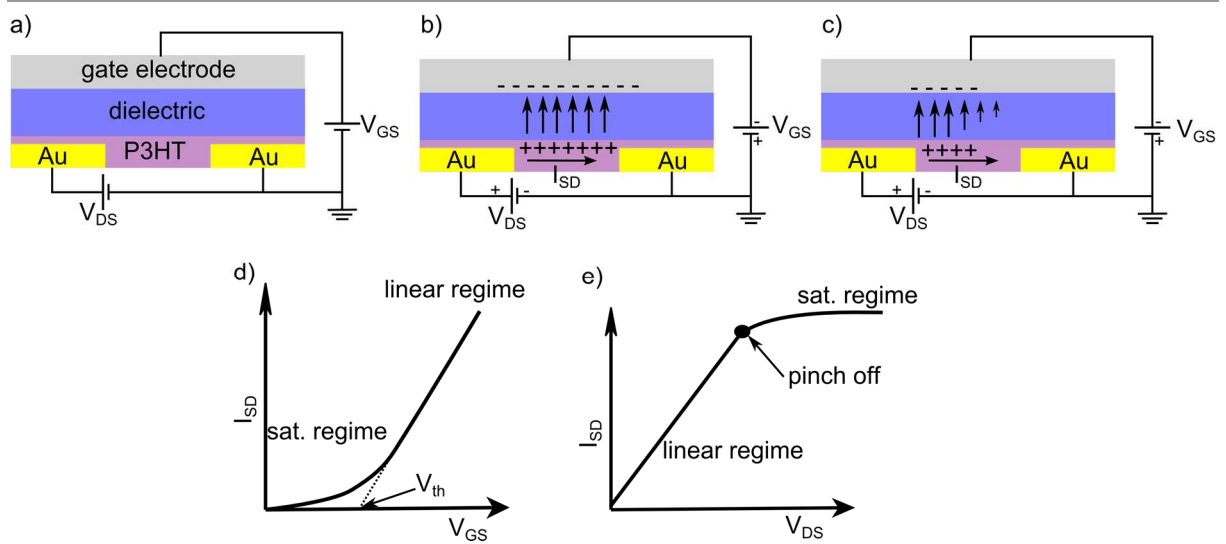


Figure 3: a) Illustration of the operation principle of an OFET. The distance between the source and drain is called the channel length (L) and the perpendicular dimension is called the width (W). The potential difference between the gate and the source electrode contact is called the gate voltage (V_{GS}) and the potential difference between the source and the drain contact is called the source voltage (V_{SD}). The charge carriers during an operation within the linear regime are shown in b) and in the saturation regime in c). The source drain current (I_{SD}) as a function of the gate voltage (transfer characteristic) is shown in d) and as a function of the source drain voltage is shown in e).

In case of a p-type semiconductor, such as P3HT, a negative gate bias has to be applied ($V_{GS} - V_{th} < 0$) to accumulate positive and mobile charge carriers at the OSC-dielectric interface. These accumulated charge carriers form a conductive channel (Figure 3 (b)). At V_{DS} potentials, which are small compared to the gate voltage ($V_{gate,eff} < V_{DS}$), the potential drop over the OSC can be neglected and the current flowing between the source and drain contact (I_{SD}) is given by¹³⁵:

$$I_{SD} = \frac{W}{L} \mu Q V_{DS} = \frac{W}{L} \mu C (V_{GS} - V_{th}) V_{DS} = \frac{W}{L} \mu C V_{gate,eff} \cdot V_{DS} \quad 2.1.2$$

Where I_{SD} is the source drain current and μ the mobility of the OSC and $V_{gate,eff}$ is the effective gate potential.

Consequently, at small V_{DS} , I_{SD} depends linearly on the applied gate voltage. Accordingly, this regime is called the linear regime.

At higher V_{GS} potentials, the conducting channel is pinched off as soon as $V_{DS} \sim V_{gate,eff}$ and a charge carrier depletion region is formed at the source contact. Within this depletion layer,

the effective gate potential cannot induce positive and mobile charge carriers. Hence, a further increase of V_{DS} does not lead to an increasing I_{SD} but to a wider depletion layer. Consequently, the current I_{SD} saturates. Accordingly, this regime is called the saturation regime. The I_{SD} current can then be described by¹³⁵:

$$I_{DS} = \frac{W}{2L} \mu C (V_{gate,eff})^2 \quad 2.1.3$$

For sensing applications two parameters are of especial importance. First the transconductance g_m which describes the drain current change per gate voltage change at a constant drain voltage and second the leakage current between the gate electrode and the OSC. The transconductance determines the amplification and should be as high as possible. The second parameter, the leakage current, determines the input impedance of the gate voltage and should be as low as possible.

The transconductance in the linear regime and in the saturation regime is given by:

$$g_{m,lin} = \frac{W\mu}{L} C V_{DS}; \quad g_{m,sat} = \frac{W\mu}{L} C V_{gate,eff} \quad 2.1.4$$

Practically, the OFETs are operated in the linear regime, V_{SD} is kept constant and I_{SD} is measured. Thus, there is a linear dependence between the output signal and the input signal, which eases data analysis.

One can see from eq. 2.1.4 and 2.1.3 that the higher the capacitance the more favorable the transconductance and the lower the required operation voltages V_{DS}/V_{GS} to obtain a certain I_{SD} . Due to the low charge carrier mobility of organic semiconductors, high V_{SD} voltages are required to obtain I_{SD} currents which are sufficiently large for further signal processing ($> 1 \mu A$). The charge carrier mobility is mainly a property of the semiconducting material. However, the capacitance is a property of the dielectric and device architecture.

2.1.2.2 Organic field-effect transistors for sensing applications

OFETs have proven to be ideal candidates as transducers for sensing applications.^{38,40,144,154–}

¹⁵⁶ Other than their low-cost and simple fabrication technique, their major advantage is that they transduce a high impedance input signal (the gate voltage) in an amplified low

impedance output signal (the source drain current). There are several approaches and different OFET architectures that have been published in literature.

In case of ion-sensitive OFETs, which are the organic counterparts of ISFETs/CHEMFETs (ion selective FETs, chemical FETs), the electric field/potential drop across the insulating gate dielectric is influenced by targeted ions at the electrolyte-dielectric interface. A successful realization of pH sensitive OFETs using silicon nitrite¹⁵⁷ and a Mylar™ foil¹⁵⁸ as a sensitive dielectric have been demonstrated. Furthermore, the sensing of biomolecules using tantalum oxide dielectric or K⁺ using a valinomycin modified dielectric, has been published.^{159,160} Though, these results seem to be very promising, due to the low charge carrier mobility of the organic semiconducting materials, these devices suffer from high operational voltages exceeding 10 V. Another approach was to use a classical OFET which is in direct contact with an electrolyte. The electrolyte was kept floating and the transistor was operated by an underlying gate. The sensing mechanism of these OFETs is not well understood as it relies on the semiconductors/dielectric inherent response to many chemical compounds.¹⁶¹ Nevertheless, sensitivities towards glucose, pH, cysteine, etc. were demonstrated.^{143,161}

However, electrolyte gated organic field-effect transistors, described in the following section seem to be the most promising candidates within this field.

2.2 Electrolyte gated organic field-effect transistors

Electrolyte gated organic field-effect transistors (EGOFETs) exhibit an exceptional performance at very low operational voltages (see Figure 4 (a)). This can be ascribed to the formation of an electric double layer with extremely high capacitances in the range of $10 \mu\text{F}/\text{cm}^2$ ^{43–45} at the semiconductor-electrolyte interface. This high capacitance induces a high charge carrier density and therefore source drain currents which are sufficiently high for further signal processing, at very low operational voltages (see equ. 2.1.1 and 2.1.2). Furthermore, an elaborate and expensive deposition of a gate dielectric can be omitted bringing low-cost, disposable sensor arrays within reach. Additionally, the semiconducting materials used, are also known for their good biocompatibility.^{36,157}

A large variety of different electrolytic systems, such as polyelectrolytes^{162,163}, polymer electrolytes^{164,165}, ionic liquids¹⁶⁶, ion gels¹⁶⁶ and electrolyte solutions^{43–45,167} have been examined. One of the most important milestones within this field was set by Kergoat et al. who reported on the stable operation of water-gated OFETs.⁴³ The thereafter following works such as the successful detection of biomolecules (DNA, dopamine, enzymes, proteins, ...) ^{39–42,168} gave rise to a whole new field of biological and ion sensors.

A very similar device is the so called electrochemical organic transistor (OECT). This device is based on doping/de-doping processes of the semiconductor (see Figure 4 (b)). Though EGOFETs and OECTs have the same architecture, they have different semiconducting materials. In contrast to EGOFETs, OECTs materials are typically hydrophilic polymers easing ion penetration in to the semiconductor and doping.^{45,169} Similar to EGOFETs, OECTs are also frequently used as transducers.^{37,170–172} However, their switching speed and their leakage currents are significantly larger than in case of EGOFETs.³⁷

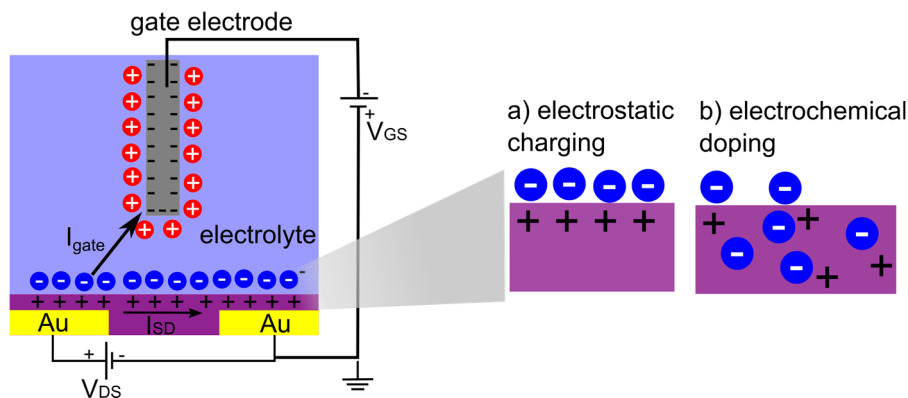


Figure 4: Illustration of the working principle of an EGOFET (a) and of an electrochemical transistor (OECT) (b).

There are different approaches to implement the EGOFET as a transducer in sensing applications (see Figure 5). The first and most simply approach is to modify a gold – gate electrode by a functional monolayer which captures biomolecules such as DNA or dopamine in a background electrolyte with constant ionic strength(Figure 5 (b)).^{173,174} Due to a modification of the gate-electrolyte interface (EDL changes), the potential drop over the gate-electrolyte interface is modified. Hence, the potential of the electrolyte (effective gate potential), which drives the EGOFET, depends on the biomolecules in the electrolyte. In another approach a DNA sensitive floating gate electrode was used (Figure 5 (c)).¹⁵³ This architecture has the advantage that it is possible to separate the EGOFETs from the sample solution. However, the most promising approach is to use modified semiconductors with functionalized monolayers (Figure 5 (a)).^{41,175} Their sensing signal arises due to a modification of the EDL at the semiconductor-electrolyte interface and a thereof varying charge carrier density within the semiconductor. Or in other words, these devices indirectly measure the differential capacity (potential dependent capacity) of the stern layer. Hence, this approach really takes full advantage of the EGOFET concept. The physics of these devices (interactions within the stern layer) is very rich and the possibilities of sensing applications are tremendous. Actually, EGOFETs are most likely the only devices which can measure adsorption processes at a polarizable interface within the stern layer in static and facil manner.

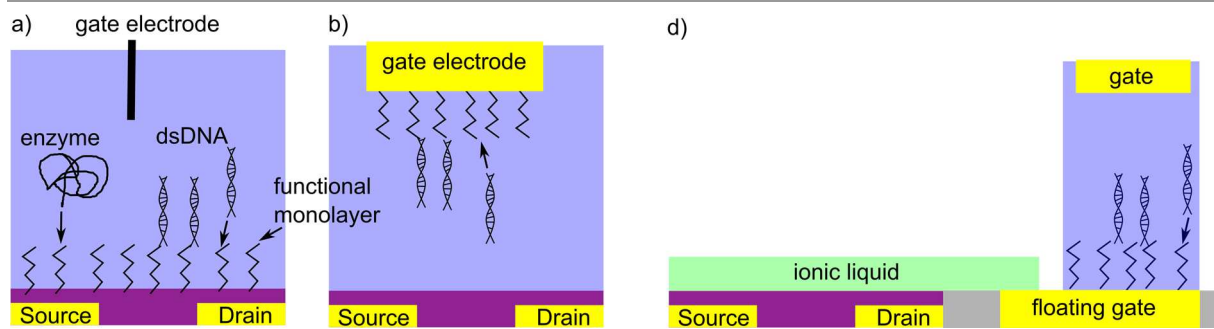


Figure 5: Illustration of the approaches to use EGOFETs as transducers in sensing applications: a) The semiconducting material is modified by a functional monolayer; b) the gate electrode is functionalized by a monolayer; c) the semiconductor solely used as a transducer and is driven by a floating gate. The floating gate is functionalized by a monolayer.

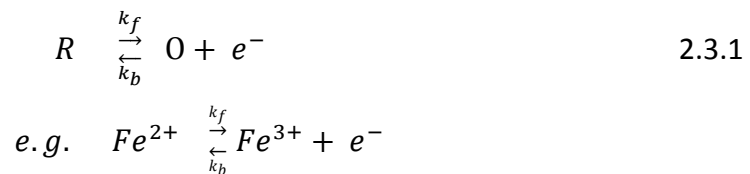
It is important to note that in order for the EGOFET to work, the semiconductor-electrolyte interface must be polarizable. If this is not the case, a large leakage current is flowing between the gate electrode and the source-drain contacts. Moreover, the capacity of the gate electrode must be significantly higher than the capacity of the semiconductor-electrolyte interface or must be non-polarizable. If one of these two conditions is not fulfilled, the effective gate potential within the analyte would not correspond to the potential applied to the gate electrode. Hence, the transistor characteristic would be degraded.

2.3 Electrochemistry at conducting/semiconducting electrodes

For a better understanding of the sensing concepts presented within this work, two omnipresent electrochemical phenomena, namely charge transfer at conducting-/semiconducting- electrolyte interfaces and the electric double layer, are discussed first. Subsequently, polarizable and non-polarizable interfaces and their implications for potentiometric measurements are presented.

2.3.1 Charge transfer at conducting- and semiconducting-electrolyte interfaces

Charge transfer processes occur as soon as a conducting- and semiconducting- electrode is immersed into an electrolyte. These processes are driven by electrochemical potential differences. For the sake of simplicity, let's consider a simple redox couple in contact with a metal electrode (see Figure 6 (a)):



Where k_f and k_b are the forward/backward rate constants and e^- is an electron.

The charge transfer is driven by the electrochemical potential difference of the electrons in the metal electrode and in the solution. The electrochemical potentials in the respective phase are given by:

$$\bar{\mu}_e^m = E_F + zF \varphi^M$$

$$\bar{\mu}_e^s = \bar{\mu}_R^s - \bar{\mu}_O^s = \bar{\mu}_R^{s,0} - \bar{\mu}_O^{s,0} + RT \ln(a_R^s/a_O^s) - zF \varphi^s$$

$$\bar{\mu}_{R/O}^s = \bar{\mu}_{R/O}^{s,0} + RT \ln(a_{R/O}^s) + zF \varphi^s$$

Where $\bar{\mu}_e^m$ is the electrochemical potential of the electron within the metal which equivalent to the familiar Fermi energy (at least for a Physicist); $\bar{\mu}_e^s$ can be seen as the Fermi energy of the electron in the solution; $\bar{\mu}_{R/O}^s$ is the electrochemical potential of the reduced/oxidized species; $\bar{\mu}_{R/O}^{s,0}$ is the standard chemical potential of the reduced/oxidized species and $a_{R/O}^s$ are the respective activity coefficients and φ^s is the potential in the solution.

As the electrons can be transferred from the metal electrode into the solution, their electrochemical potential must be equal in both phases, in equilibrium:

$$\bar{\mu}_e^m = \bar{\mu}_e^s$$

$$\varphi^M - \varphi^s = \frac{1}{F} (E_F - (\bar{\mu}_R^{s,0} - \bar{\mu}_O^{s,0})) + RT/F \ln\left(\frac{a_R}{a_O}\right)$$

$$E_{eq} = \varphi^M - \varphi^s = E_0 + RT/F \ln\left(\frac{a_R}{a_O}\right) \quad 2.3.2$$

Where E_0 is the standard redox potential which corresponds to $\frac{1}{F} (E_F - (\bar{\mu}_R^{s,0} - \bar{\mu}_O^{s,0}))$ and E_{eq} is the Nernstian equilibrium potential difference between the electrode and the electrolyte.

Consequently, the equilibrium potential depends on the relative activities of the reduced on oxidized species within the electrolyte. The other way around, if a potential is applied, the relative activities can be changed. In analogy to the bandstructures of semiconductors the direction of the current flowing upon applying a potential can be illustrated by band diagrams^b (see Figure 6 (a)). If a positive potential relative to the equilibrium potential is applied, the electrochemical potential is shifted and a positive current starts to flow and in case of a negative potential vice versa. The potential is typically expressed in terms of overpotential which is defined as the difference between the equilibrium potential and the actually applied potential.

^b Note that the magnitude of the current has to be described by a kinetic model similar to the one described in section 2.4.1. Furthermore note that the electrons within the solution are not "free" as proposed by the band-diagramm. The only charge carriers within the solution are the reduced and oxidized species. Thus, the band-diagramm should be considered as an abstract picture.

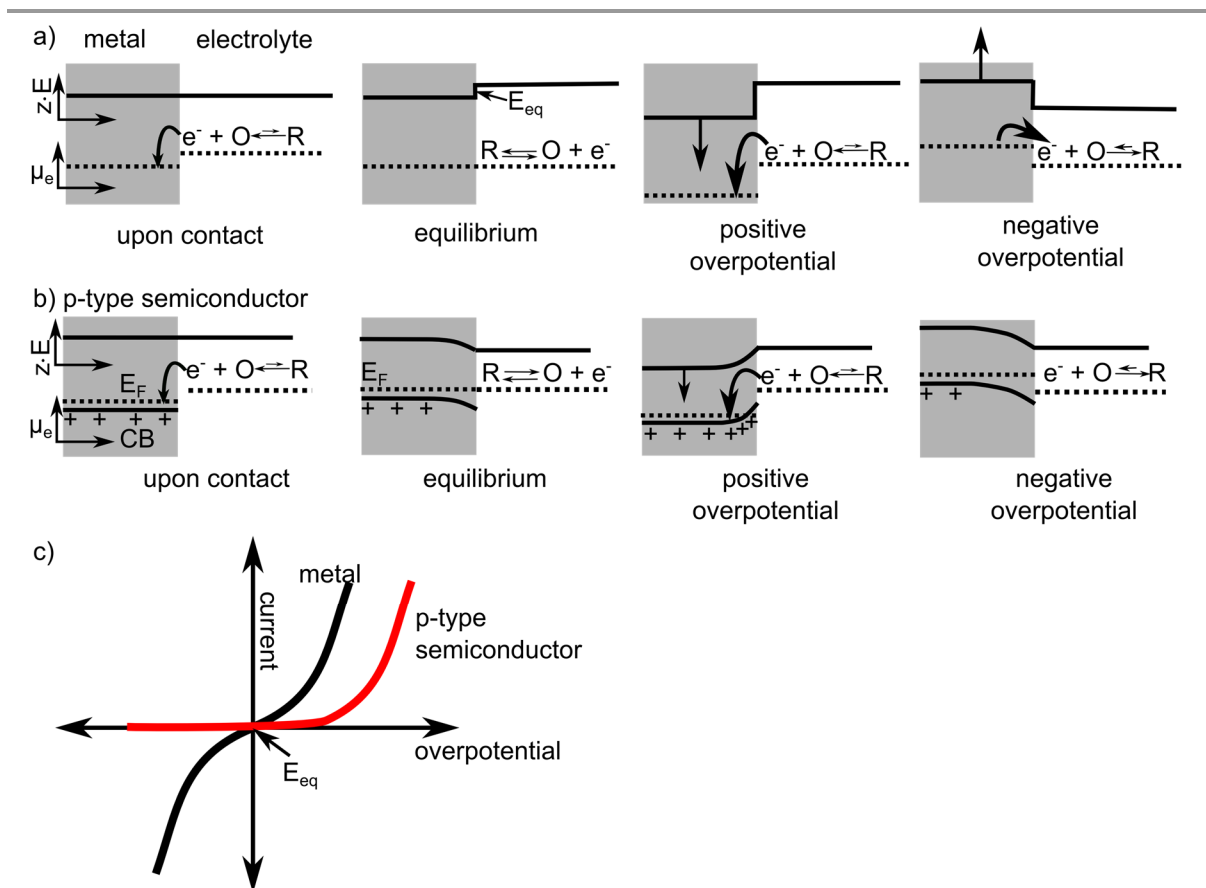


Figure 6: Illustration of the electrochemical potentials (μ_e) and the electric potentials (E) (before contact, in equilibrium, at a positive overpotential and a negative overpotential) of a redox couple in contact with a metal electrode (a) and a semiconductor (b). The currents flowing upon applying an overpotential are illustrated in c).

Lets' consider the same redox couple but a p-type semiconducting electrode. In this case, the majority charge carriers are positive holes. In the situation illustrated in Figure 6 (b)), where the E_F of the semiconductor lies above that in the solution, mobile positive charge carriers (hohles) are depleted at the interface leaving back negatively charged dopants. Consequently, a certain space charge region and a potential drop is formed, inducing a so called bend bending. If a negative overpotential is applied, the holes are further depleted within the semiconductor. Thus, the additionally applied potential drops within the semiconductor while the potential at the electrolyte interface remains unchanged. Hence, the current is not increased with increasing negative potential. Whereas if a sufficiently large positive overpotential is applied, holes are accumulated at the interface and the semiconductor

behaves metal like. Hence, a p-type semiconductor-electrolyte interface has a diode like overpotential-current characteristic (see Figure 6 (c)).

2.3.2 Electric double layer

The electric double layer (EDL) is formed as soon as a conducting electrode is immersed into an aqueous solution. Charge transfer processes into the electrolyte and ions which are adsorbed on the surface lead to surface charge at the electrode (see Figure 7). The plane through the center of the specifically adsorbed ions is called the inner Helmholtz (IHP) plane. The surface charge is shielded by solvated ions within the solution. Due to the solvation shell of these ion, they can only approach the electrode at a certain distance. The center of these nearest solvated ions is called the outer Helmholtz plane (OHP) or the Stern layer. The thickness of the Stern layer is in the range of 1-2 nm.⁶¹ Due to thermal agitations in the solution and concentration gradients the nonspecifically adsorbed ions are distributed in a three dimensional region called the diffuse layer Gouy-Chapman-Layer, which extends from the OHP into the bulk of the solution. The thickness of this diffusion layer depends on the ionic concentration in the solution and is on the order of 10 nm at electrolyte concentrations of 10 mM.⁶² The potential within this diffuse layer decreases exponentially according to the Poisson-Boltzmann assumption, while it decreases linearly within the Stern layer.⁶¹

The EDL formation has a very important implication: As soon as an electrode/semiconductor is immersed into an aqueous solution, ions get adsorbed. The adsorption and charge transfer process and therefore also the interfacial potential depends on the chemical properties of the involved ions and the electrode. Hence, neither the absolute potential of an electrolyte nor the potential drop at an electrode-electrolyte interface can be measured experimentally. However, it is possible to measure the relative potential (potential difference) between two electrodes.

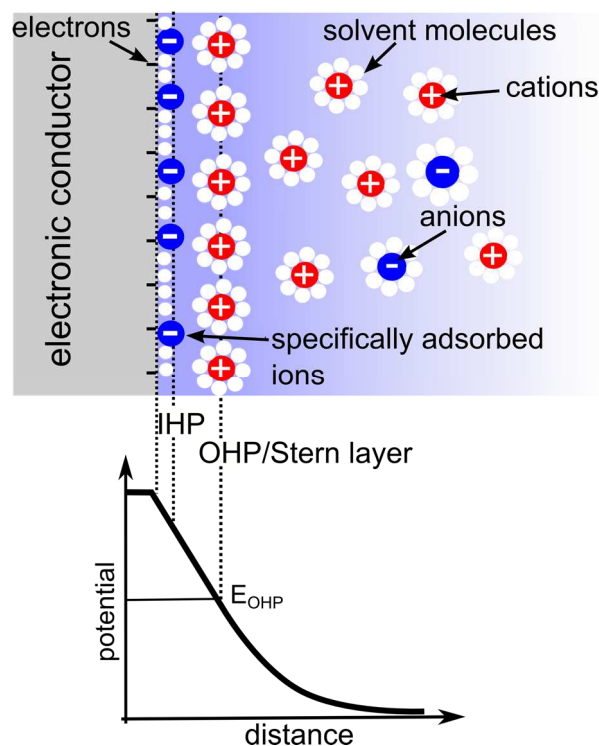


Figure 7: Illustration of an electric double layer at an electronic conductor-solution interface and corresponding the potential profile.

2.3.3 Polarizable vs. non-polarizable interfaces

There are two important ideal types of electrode-analyte interfaces. The first one, is the so called polarizable interface. In this case, zero net faradaic current should be flowing, regardless of the interface potential applied (see Figure 8). The prime example of a polarizable interface is a metal electrode which is covered by an insulating dielectric. However, within this work all electrodes are conductors or semiconductors, which are in direct contact with the electrolyte. Consequently, upon applying a potential deviating from the equilibrium potential, there is always a current flowing. The magnitude of this current depends on the composition of the electrolyte, the type of electrode and the exchange current density of the dominant redox active species. The potential difference between the equilibrium potential of the dominant redox couple and the applied potential at which experimentally significant currents are flowing is called the anodic/cathodic overpotential. Therefore, as long as the applied potential is smaller than the anodic/cathodic overpotential of the relevant redox

active species, the interface can be considered as polarizable and a negligible current is flowing.

In case of a non-polarizable interface the potential to force a current over the interface, should be as small as possible; i.e. the potential should not change significantly upon applying a current. A typical example of non-polarizable interfaces are reference electrodes. Reference electrodes must be non-polarizable in order to guarantee a stable potential even if small currents (e.g. leakage currents of a potentiometer) are flowing. Note that the polarizability of the interface is a property of the electrode and the composition of the electrolyte. For example, adding an electroactive species (ascorbic acid) which is easily reduced or oxidized can depolarize the initially polarizable interface.

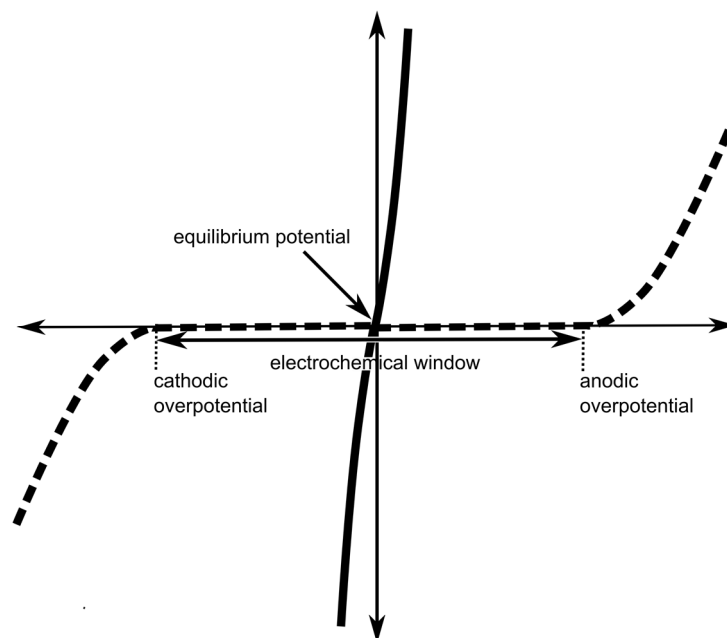


Figure 8: Illustration of a polarizable (dashed line) and a non-polarizable (solid line) interface electronic conductor – electrolyte interface.

2.3.4 Potentiometric measurements

Potentiometry passively measures the potential between two electrodes. Due to the formation of EDLs at conducting electrodes, potentiometric measurements are only able to measure the potential of an electrode with respect to the potential of another electrode.

Consequently, neither the absolute potential of an electrolyte nor the potential drop at an electrode-electrolyte interface can be measured. This is not a hindrance if all potentials are measured relative to a reference electrode which has a well-known and constant potential with respect to the analyte. Let's consider a typical Ag/AgCl reference electrode which is illustrated in Figure 9. This electrode is composed of a silver wire coated with AgCl immersed into a so called inner filling solution (IFS). The IFS has a known and constant composition (e.g. 3 M KCl) and contacts the analyte over a porous membrane. Though in chemical equilibrium the composition of the IFS approaches the composition of the analyte through diffusion, the timescale to reach this chemical equilibrium is magnitudes higher than the timescale to reach a uniform potential. Consequently, as long as the composition of the IFS is not changed, the potential drop over the Ag/AgCl-IFS interface remains constant and the potential within the IFS corresponds to the potential of the analyte (see Figure 9 on the left).

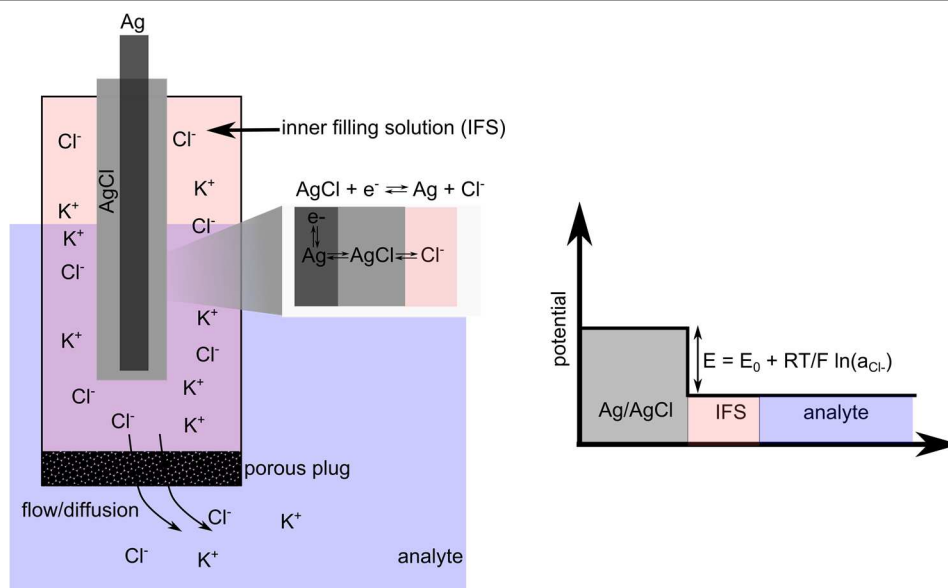


Figure 9: Illustration of the working principle of an Ag/AgCl reference electrode. The Ag wire is immersed into an inner filling solution (IFS) which has a constant Cl⁻ concentration. The inner filling solution contacts the analyte via a porous plug. The potential drop over the AgCl-IFS interface depends on the activity of the Cl⁻ within the IFS and remains constant as long as the Cl⁻ concentration is not changed. If the liquid junction potential (potential drop over the porous plug) is negligible, the potential of the IFS corresponds to the potential of the analyte.

Another important issue to consider is that two polarizable interfaces in series can be regarded as two capacities in series. The potential measured between these capacities is

given through noise or through charging of the capacities by parasitic currents. As the potentiometer itself can already be regarded as a polarizable interface, all other interfaces have to be non-polarizable. Consequently, every electrode must have at least one dominant redox couple which depolarizes the interface. Note that the transition between polarizable and non-polarizable is smooth and the measurements get increasingly challenging as the polarizability of the electrodes increases. Furthermore, also note that the lower the parasitic measurement current of the potentiometer gets, the less problematic the polarizability issue.

In order to reliably measure this potential two important rules have to be full-filled:

- In order to measure the potential of the analyte, reproducible and independently of the sample composition, reference electrodes are required.
- Never use two polarizing interfaces in series. As a potentiometer (used potentiometric measurements) already corresponds to a polarizable interface, all other interfaces contacting the analyte solution have to be non-polarizable.

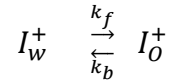
2.4 Ion selective electrodes

The sensing principle of ion selective electrodes (ISEs) is typically based on the potentiometric measurement of a concentration dependent phase boundary potential arising at an ion selective membrane-analyte interface. The underlying principle can be traced back to the ion transfer at immiscible electrolyte solutions (ITIES). For that reason, the fundamental relationships of ITIES are discussed first. Using these relationships, a numerical model is proposed in the thereafter following section. On the basis of this numerical model, the working principle, the limits and the optimization of ISEs are discussed in detail.

2.4.1 Simple and facilitated ion transfer between immiscible electrolytes

The underlying principle of highly ion selective plasticized PVC membranes is the ion transfer at immiscible solutions (ITIES) which can be described by the Butler-Volmer model, one of the most fundamental relationships in dynamic electrochemistry. The model describes the simple

heterogeneous mass transfer of charged ions between two immiscible phases; i.e. between an analyte and an ISM. In order to introduce this model and for the sake of simplicity, let's consider a heterogeneous, simple ion transfer of a monovalent ion between an aqueous and an organic phase (e.g. between an analyte and an ion selective membrane). Furthermore assume that the activity coefficients within the organic and aqueous phase are unity:



Where I_w^+ is an ion dissolved in the analyte; I_o^+ is an ion dissolved in the organic phase and k_f/k_b are the forward/backward rate constants

The transfer rate and the current densities are given by:

$$\begin{aligned} \frac{j_f}{F} &= v_f = k_f C_w \\ \frac{j_b}{F} &= v_b = k_b C_o \\ \frac{j_{net}}{F} &= v_{net} = k_f C_w - k_b C_o \end{aligned} \quad \text{Eq. 2.4.1}$$

Where j_f/j_b are the forward/backward current densities; v_b is the reaction rate; C_R/C_O are the concentrations of the reduced/oxidized species and i_{net}/v_{net} is the net reaction rate/current densities.

Within the Butler-Volmer model, the rate constants are assumed to have an Arrhenius form and can be described as:

$$k_f = k_0 \exp \left[-\frac{zF}{RT} \alpha (E - E^0) \right] \quad \text{Eq. 2.4.2}$$

$$k_b = k_0 \exp \left[\frac{zF}{RT} (1 - \alpha) (E - E^0) \right] \quad \text{Eq. 2.4.3}$$

Where E is the potential drop over the interface (transfer potential); E^0 is the standard transfer potential^c at $k_f = k_b$ ^d; α is the transfer coefficient which describes the symmetry of

^c Note that standard transfer potentials are used instead of formal transfer potentials. Consequently, it is assumed that the activity coefficients within the organic phase and the aqueous phase are unity.

^d In case of a symmetric reaction ($\alpha = 1/2$), the standard transfer potential E^0 is given by $E^0 = F\Delta_o^w G^0 / zF$ ($\Delta_o^w G^0$ is the free energy of transfer between the organic and aqueous phase). In literature this value is also called the standard energy of partition

the reaction; k_0 is the standard homogenous rate constant; k_f / k_b forward/backward homogenous rate constant; z is the charge of the transferring ion; F is the Farraday constant; R the gas constant and T the temperature.

In equilibrium, the net current is zero and an equilibrium potential is established. Accordingly, the equilibrium potential can be calculated by setting equation 2.4.1 to zero, leading to the classical Nernst equations^e:

$$E_{eq} = E^0 + \frac{RT}{zF} \ln \left(\frac{C_W}{C_O} \right) \quad \text{Eq.2.4.4}$$

Where E_{eq} is the equilibrium potential.

In equilibrium, the concentration of the organic and aqueous phase is given through:

$$\frac{k_f}{k_b} = K = \frac{C_W}{C_O} \quad \text{Eq. 2.4.5}$$

Where K is the partitioning coefficient.

Highly ion selective plasticized PVC membranes are chemically based on the recognition of an aqueous target ion by an ionophore, which thermodynamically facilitates selective ion transfer (IT) into the organic phase. In this case, the ion transfer be considered as a heterogeneous on step process⁶³:



Where L is the ionophore and n the complex stoichiometry.

The energy required to transfer the ion into the membrane is decreased by the complex formation constant (β) of the ionophore. According to the thermodynamic cycle approximation the formal potential E^0 can be described by⁶⁴:

$$E^0 = E_i^0 + \frac{RT}{zF} \ln \beta_n L^n$$

^e The Nernst equations are typically derived using thermodynamic assumptions. However, the Butler Volmer equations, which are based on the empirical assumption that the transfer rates have an Arrhenius form lead to the same conclusion. Such an agreement is required: In equilibrium a kinetic model must collapse to relations of the thermodynamic form.

Where β_n is the complex formation constant within the ISM and E_i^0 is the simple ion transfer potential and L^n is the concentration of the free ionophore within the membrane.

The Butler Volmer equations do not take into account an EDL at the interface. This effects were included by Frumkin who assumed that the closest approach of the reacting species to the electrode is the OHP. This assumption has the following implications: Due to the diffuse layer, the potential at the OHP is not equal to the potential in the solution. Furthermore, the concentration of the reacting species at the OHP is not equal to the bulk concentration; e.g. if an electrode has a negative charge the concentration of positively charged ions at the OHP will be higher than within the bulk electrolyte (see Figure 7). The Frumkin model extends the Butler-Volmer model by replacing the bulk concentration and the bulk potential with the concentrations and potentials at the OHP. Accordingly, the transfer rates and the equilibrium potential are described by:

$$k_f = k_0 \exp \left[-\frac{zF}{RT} \alpha (E_{OHP} - E^0) \right] \quad 2.4.6$$

$$k_b = k_0 \exp \left[\frac{zF}{RT} (1 - \alpha) (E_{OHP} - E^0) \right] \quad 2.4.7$$

$$\frac{j_f}{F} = v_f = k_f C_W^* \quad 2.4.8$$

$$\frac{i_b}{F} = v_b = k_b C_O^* \quad 2.4.9$$

$$E_{eq} = E^0 + \frac{RT}{zF} \ln \left(\frac{C_W^*}{C_O^*} \right) \quad 2.4.10$$

Where C_O^*/C_R^* are the concentrations of the reduced/oxidized species at the OHP; E_{OHP} is the potential difference between the electrode and the OHP(see Figure 6).^f

Though, the Frumkin model is analytically more challenging to solve, it actually accommodates numerical calculations (see section 2.4.2).

2.4.2 Numerical modeling of ion selective membranes^g

There are well established theoretical models which describe ITIES and assisted ITIES and consequently ion selective membranes (ISM) under equilibrium conditions.^{10,65–71}

^f In literature E_{OHP} is typically expressed by $E_{OHP} = E - \varphi_2$ where φ_2 is the potential drop over the diffuse layer.

^g The section is based on the work submitted to J. Kofler, S. Nau, and J.W.L.-K. Emil, J. Mater. Chem. B (2015).

Furthermore, there are also analytical as well as numerical models for non-equilibrium operation modes.^{66,72–76} Within these models, the potential at the interface is calculated by inserting the boundary concentrations of the relevant ions in the respective phase into the Nernst equations and the mass transport through the interfaces is described by constant heterogeneous rate constants. The ratio of the heterogeneous rate constants of a specific ion are assumed to be equal to the partitioning coefficient as described in equation 2.4.5. Hence, these models assume that the thermodynamically facilitated IT is fast and instantaneously, reaching local thermodynamic equilibrium across the interface even under dynamic mass transport conditions. Though, the equilibrium assumption is usually completely justified, the major drawback of these models is that they neglect the influence of the electric potential on the transfer rates.

For that reason, a new numerical method was developed. The presented method models the transfer rates in between the phases using Butler-Volmer-type relations and the bulk of the electrolytes is modelled using the well-established Nernst Planck and Poisson drift-diffusion equations (NPP). Hence, this model uses basic kinetic electrochemical principles which describe the response of ISEs under equilibrium as well as dynamic conditions.

Similar to the method described by J.J. Jasielc et al.⁷⁷ and Bartosz Gryszakowski et al.⁷³ the system was separated into three separate layers (analyte, ISM, inner filling solution) (see Figure 10). The bulk of these layers were calculated by solving the NPP equations in the following form^{73,77}:

$$\frac{\partial c_i(x,t)}{\partial t} = \frac{\partial J_i(x,t)}{\partial x} \quad 2.4.11$$

$$\frac{\partial E(x,t)}{\partial t} = \frac{1}{\varepsilon_{o/w}} I(t) - \frac{F}{\varepsilon_{o/w}} \sum_{i=1}^r c_i J_i(x,t) \quad 2.4.12$$

$$J_i(x,t) = -D_i^{o/w} \frac{\partial c_i(x,t)}{\partial x} + \frac{F}{RT} D_i^{o/w} z_i \cdot c_i(x,t) \cdot E_i(x,t) \quad 2.4.13$$

Where E is the electric field, $\varepsilon_{o/w}$ is the dielectric constant in the organic/water phase, c_i is the concentration of the i^{th} ion, J_i is the flux, z_i the charge, $D_i^{o/w}$ is the diffusion constant in the water and all other letters have their usual meaning.

The mass transport of a specific ion in between the layers and thus through interfaces was modelled using the Butler-Volmer-type relations as described in equations 2.4.9-2.4.12 . The NPP equations approximate the ions by point charges with an infinite small size not accounting for any concentration dependent activity changes or adsorption effects at the ISM-water interface. Thus the NPP equation models the diffuse Gouy-Chapman layer. However, the stern layer, which greatly depends on the size of the ions, on adsorption phenomena, interaction of present ions and other complex processes, cannot be modelled. For that reason, to calculate the potential drop over the interface (E_{OHP} in equation 2.4.9 and 2.4.10) the stern layer is approximated by a capacity; i.e. the potential is obtained by multiplying the electric field at the phase boundary by the distance in between the interfaces. The dielectric constant of the capacity was assumed to be the arithmetic average of the dielectric constant of the water and the organic phase.

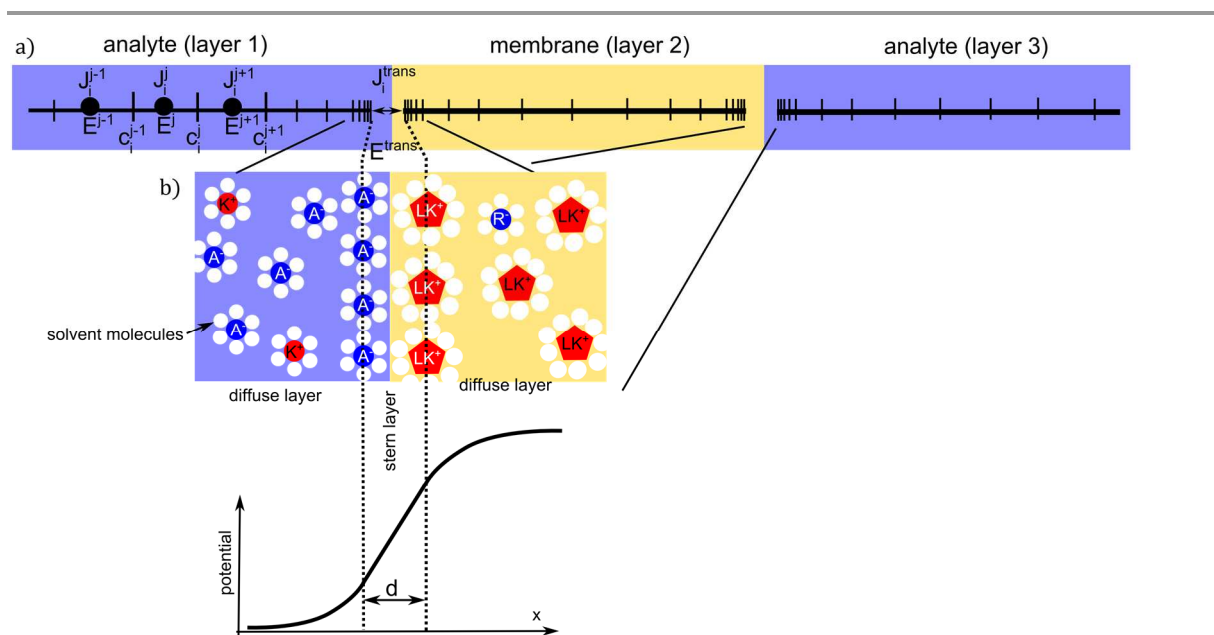


Figure 10: a) Illustration of the numerical calculations and the discretisation used. The spacing of the grid where the concentration was calculated was chosen to be smaller closer to the interfaces. The flux and the electric field are calculated at intermediate points lying half way between the concentration points. The transfer rates/transfer potentials were calculated by assuming a stern layer at the interface with a discrete distance d (b). The LK^+ complex is illustrated by a red pentagon; A^- corresponds to anions present in the analyte, R^- to background anions in the membrane and K^+ to potassium ions in the analyte.

Similar to the method proposed by J.J. Jasielec et al.⁷³ the method of lines was used to discretize the differential equations. This method is illustrated in Figure 10. The ionic flux and the electric field are calculated at intermediate grid points situated half way between the concentration grid points. The time derivative of the electric field (eq. 2.4.15) and the ionic flux (eq. 2.4.16) are obtained by calculating the central first order derivative of the concentration. The concentration is then obtained by calculating the central first order derivative of the flux (eq. 2.4.14). The program was written in Octave, which is an open source pendant of matlab. The equations were integrated using the Octave Isode solver. Alternatively, it is also possible to use the odesx solver of the odepkg (wrapper of the fortran seulex solver). The calculations were carried out on a 64 bit - windows 8 system taking full advantage of the new 64 bit Octave build.

2.4.2.1 Parameters used for the numerical calculations

Though, the components used in the membrane were not discussed yet, the parameters used for the numerical calculations are already introduced. Please refer to section 2.4.3 or the experimental section of chapter 3 and 4 for details). The parameters were taken from literature (see table 1 and table 2), if they were available. Due to very complex experimental setup and assumptions which have to be made (e.g. diffusion constants), there is a large discrepancy of the experimental values in literature. To qualitatively model the sensor response, this is obviously not a hindrance as the simulated response curves are in good agreement with the experimental results.

Most of the simple ion transfer potentials measured in literature are measured at a NPOE/W micro interface. As the PVC does not seem to influence the transfer potentials significantly (just ~20 mV)⁸⁷, the values obtained at NPOE/W interfaces seem to be justified. Another issue to consider is that the (TCIPB⁻) is known to temporarily complex alkali metal ions at the NPOE/W interface leading to a so called shuttling mechanism and thus to a reduced formal transfer potential⁸⁸. For that reason, only formal transfer potentials measured in a TCIPB⁻ background were considered within this work.

Table 1: Parameters used to numerical compute the NPP equations.

Ion	D_o [m ² /s]	D_w [m ² /s] ^f	φ_i^0 [mV]	Log β
K ⁺	1.3 10 ^{-11,a}	1.96 10⁻⁹	440^g	11.63^l
IL ⁺	3.01 10^{-12,b}	n.a.	n.a.	11.63^l
Cl ⁻	1.3 10 ^{-11,a}	2.03 10 ⁻⁹	-521^h	0
Na ⁺	8.8 10 ^{-12,a}	1.33 10 ⁻⁹	518^g	7.63 ^m
TCIPB ⁻	1.1 10 ^{-12,c}	1.66 10 ⁻¹⁰	-335ⁱ	0
Ca ²⁺	5 10 ^{-11,a}	7.54 10 ⁻¹⁰	550 ^j	0
TDA ⁺	0.6 10 ^{-12,d}	0.9 10 ⁻¹¹	-500 ^j	0
Ionophore I	1.9 10^{-12,b}	n.a.	n.a.	n.a.
SO ₄ ²⁻	7 10 ^{-11,a}	10.7 10 ⁻⁹	-600 ^k	0
TFPB ⁻	1.1 10 ^{-12,e} .	1.66 10 ⁻¹⁰	n.a.	0

a) the diffusion coefficients were calculated using the estimated ratio of $D_o/D_w = 6.6 \times 10^{-3}$ as proposed in ref. ⁷⁸; b) taken from ref ⁷⁹; c) assumed to be equal to the diffusion coefficient of TFPB⁻, which has a very similar size and structure; d) The diffusion coefficient of TDA was assumed to be twice as big as TFPB⁻ which is ~ 2 times smaller; e) taken from ref. ⁸⁰; f) taken from ref. ⁸¹ and ref. ⁸²; g) taken from ⁸³; h) taken from ⁸⁴; i) taken from ref. ⁸²; j) taken from ref. ⁸⁴. The value of TDA was estimated from the graphs available in ⁸⁴; k) The value was estimated from the data available in ref. ⁸⁵ in a nitrobenzene/water interface as proposed in ref. ⁸⁴ and ⁸²; l) taken from ⁸⁶; m) assumed.

In case of highly hydrophilic ions (Ca²⁺, SO₄²⁻) no experimentally obtained values of the formal transfer potential are available yet. Typically the ion transfer potentials are measured by CV measurements which require a background electrolyte in the organic phase. This background electrolyte within the membrane typically gets extracted before these lipophilic ions are extracted into the membrane. For that reason, the transfer potentials were assumed to be larger than the transfer potentials of the background electrolyte within the membrane used.

Table 2: Parameters used to numerical compute the NPP equations.

Parameter	Value
ϵ_{water}	80
$\epsilon_{\text{membrane}}$	40 ^a
membrane thickness	150 μm
water layer thickness	400 μm
interface distance (d)	2 nm ^d
k_0	9 10^{-3} cm/s ^c
α	0.48 ^c

a) taken from ⁷¹; c) the standard rate constants and the transfer coefficients were assumed to be equal for all transferring ions. The value was taken from ref. ⁶³; d) this parameter does not influence the final response curve noticeably but the initial potential distribution.

2.4.3 Working principle of ion selective electrodes

Polymer ion selective membranes are made out of a polymeric matrix which is soaked with a water immiscible solvent (plasticizer) and contains a highly selective ionophore and fixed ionic sites. The most popular polymeric ISMs are based on a polyvinylchloride (PVC) matrix and either nitrophenyl octyl ether (NPOE) or dioctyl sebacate (DOS) plasticizers.^{89–91} Note that the plasticizer content of the ISM is actually very high (66 wt%).^{92,93} and that these membranes are therefore also called solvent polymeric membranes. However, there is a broad variety of other matrixes and plasticizers available.^{94–96} Discussing these would exceed the scope of this work and the reader is referred to an excellent review on state of the art ISMs written by Bühlmann et al.⁸⁹ This work focuses on PVC-NPOE based membranes. As described in section 2.4.1, highly ion selective plasticized PVC membranes are chemically based on the recognition of an aqueous target ion by an ionophore, which thermodynamically facilitates selective ion transfer (IT) into the membrane. The strong ion - ionophore interaction overcomes the unfavorable free energy of transfer and hydrophilic ions are extracted into the hydrophobic membrane, developing a Nernstian phase boundary potential in equilibrium:⁸⁹

$$E_{eq,PB} = E_i^0 + \frac{RT}{z_i F} \ln \left(\frac{a_{i,water}}{a_{i,membrane}} \right) \quad \text{Eq. 2.4.14}$$

Where $E_{eq,PB}$ is the phase boundary potential and; E_i^0 is the standard transfer potential of the targeted ion and $a_{i,water}$ is the activity of the target ion within the water and $a_{i,membrane}$ is the activity of the target ion within the membrane.

To measure this phase boundary potential, the ISM is typically contacted by an inner filling solution (IFS) with a known target ion concentration as illustrated in Figure 11. Hence, there are two phase boundary potentials, one at the IFS side and one at the analyte side. The membrane potential $E_{membrane}$ is given by the sum of the individual phase boundary potentials:

$$E_{membrane} = \left[E_i^0 + \frac{RT}{z_i F} \ln \left(\frac{a_{i,water}}{a_{i,membrane}} \right) \right] + \left[-E_i^0 + \frac{RT}{z_i F} \ln \left(\frac{a_{i,membrane}}{a_{i,IFS}} \right) \right]$$

$$= \frac{RT}{z_i F} \ln \left(\frac{a_{i,analyte}}{a_{i,IFS}} \right) \quad \text{Eq. 2.4.15}$$

Hence, as long as the target ion activity within the IFS solution is kept constant, the membrane potential depends on the target ion activity within the sample in a Nernstian fashion (59.16 mV per tenfold activity change in case of a monovalent ion).

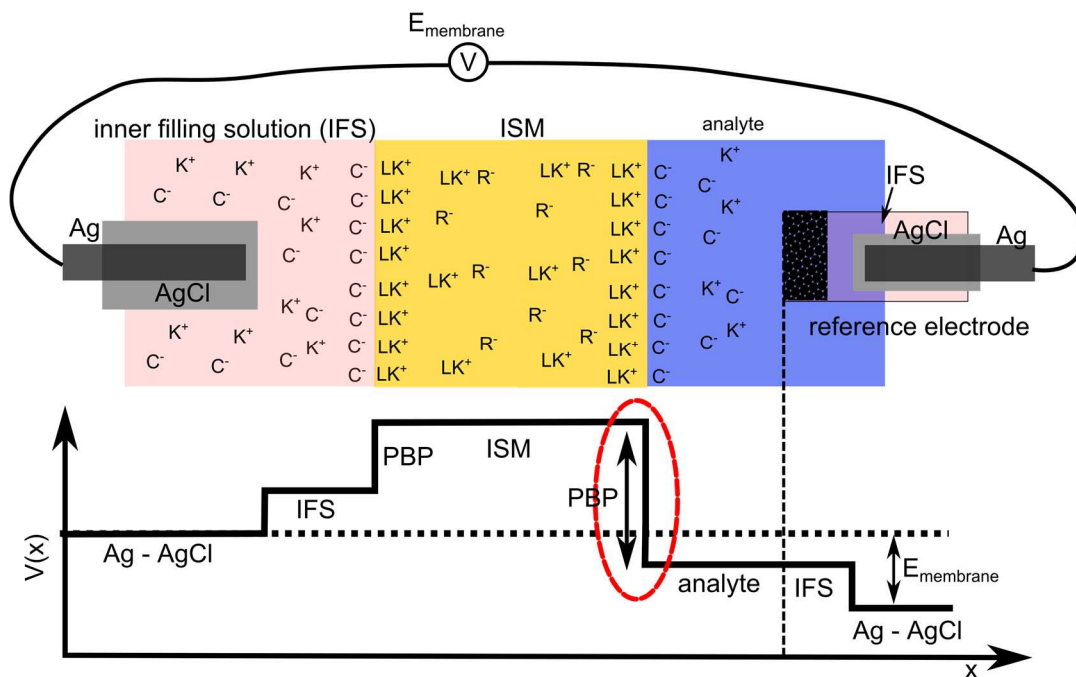


Figure 11: Illustration of a classical ion selective electrode and the potential profile along the measurement setup. The phase boundary potential (PBP) on the analyte side of the ISM depends on the target ion activity within the analyte (marked with a red circle)

Figure 12 shows numerically calculated response curves of a K^+ sensitive membrane in a background of constant ionic strength (10 mM NaCl) and an IFS containing (10 mM KCl), four different theoretical restrictions. The first configuration is that the ISM only contains a selective ionophore and that only target ions are allowed to be transferred into the ISM. In this case a Nernstian response with respect to the activity of the target ion within the analyte (black in Figure 12 (a)) is obtained. Furthermore, the concentration of complexed target ions (LK^+) within the ISM does not depend on the activity within the analyte and the curves at a concentration of 1 nM and 10 nM K^+ overlap (Figure 12 (b), black solid line). However, this picture is oversimplified: If the transfer of negatively charged ions (Cl^-) is allowed, the response curve towards a K^+ concentration changes is negligible (see Figure 12 (a)). Though, the Cl^- concentration within the IFS and the analyte are constant (constant ionic background), the Cl^- concentration at the analyte side is lower than at the IFS side (at a K^+ concentration of 1 nM, see Figure 12 (c) red).

Furthermore, the LK^+ concentration within the bulk membrane is magnitudes higher and equal to the Cl^- concentration (see Figure 12 (b) red). This can be ascribed to the so called co-extraction of Cl^- ions. In contrast to single K^+ ions which are confined to the ISM interfaces, K^+ and Cl^- pairs can penetrate the bulk-membrane changing the LK^+ bulk concentration because they fulfill the charge neutrality condition.^h Since, Cl^- ions are attracted by the positively charged LK^+ layer at the membrane side, the amount of co-extracted Cl^- ions depends on the K^+ concentration within the analyte (see Figure 12 (d), red box).ⁱ The Nernstian phase boundary potential is a function of the ratio of the respective LK^+ and K^+ activities at the phase boundary (also see section 2.4.5 and equation 2.4.14). As both concentrations are directly proportional to each other, the phase boundary potential at the analyte side does only negligibly depend on the K^+ concentration. Hence the total membrane response is almost zero. Practically, ISMs just containing ionophores exhibit long term potential drifts, memory

^h K^+ and Cl^- pairs are not actual atomic pairs and they are not actually “sticking” together. However, each charge unit Cl^- entering the bulk of the membrane, is accompanied by a charge unit of K^+ .

ⁱ The amount of co-extracted Cl^- ions depends on the K^+ concentration within the analyte and is therefore higher than predicted by the standard partitioning coefficient (see eq. 2.4.5).

effects and potential instabilities. Thus, the numerically calculated potential in Figure 12 (a) should be considered as an illustration.

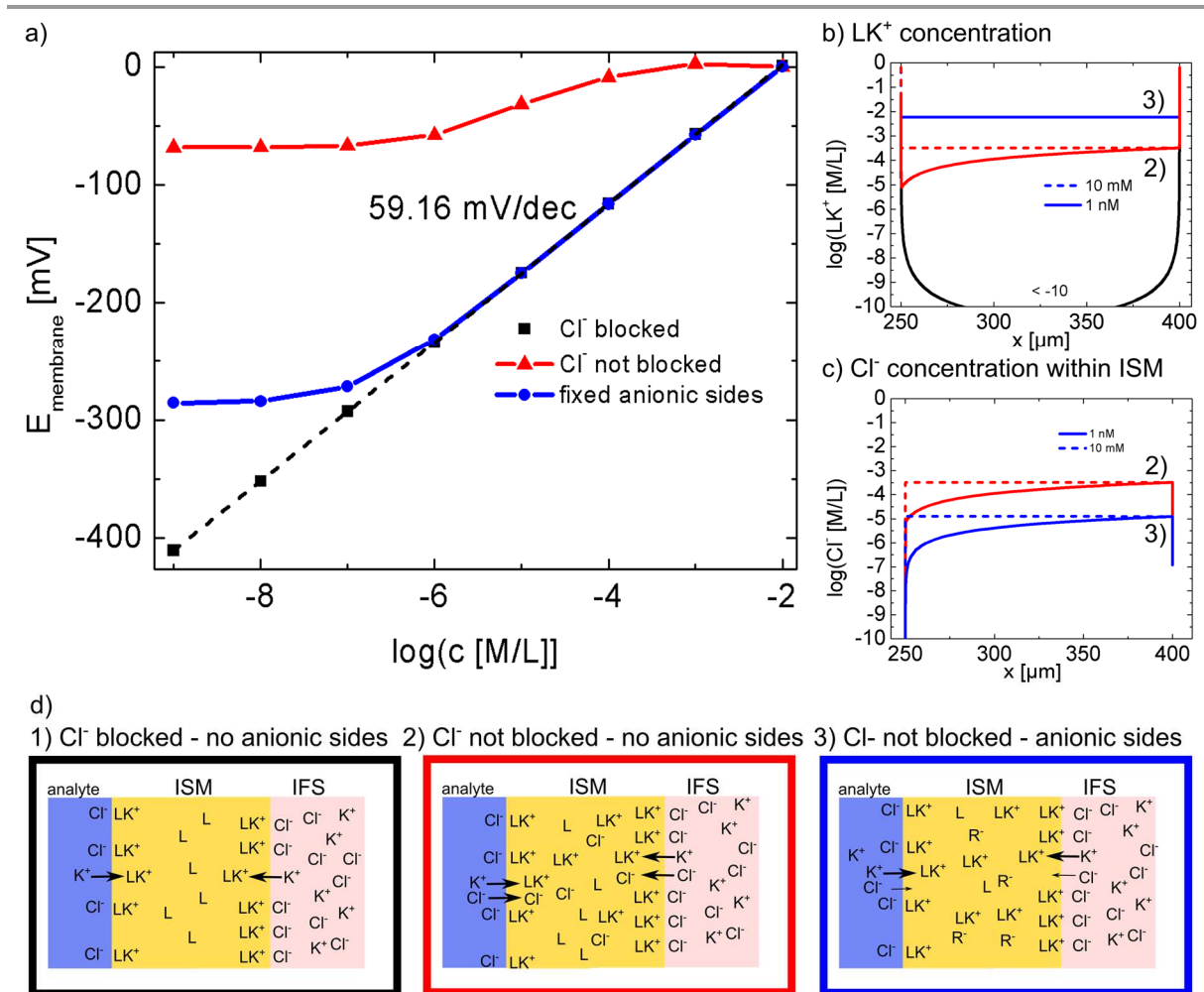


Figure 12: Illustration of the working principle of ion selective membranes within a background of constant ionic strength (10 mM NaCl) and an IFS containing 10 mM KCl. The membrane potential at different target ion concentrations for 3 configurations: 1) no anionic (Cl^-) transfer allowed and no anionic sides (black, the dashed line represents the thermodynamic limit (the Nernstian response)); 2) anionic transfer allowed and no anionic sides (red); 3) anionic transfer allowed and anionic sides (blue). The corresponding concentration profiles of the complexed K^+ ions (LK^+) and the Cl^- ions are shown in b) and c) at concentrations of 1 nM (solid lines) and 10 mM (dashed lines). The transfer processes are illustrated in d).

In order to keep the activity of the target ion within the membrane constant, fixed anionic sides (R⁻) have to be added to the membrane. Fixed anionic sides are lipophilic negatively

charged anions which are not dissolved in the water (e.g. tetrakis[3,5-bis(trifluoromethyl)phenyl]borate (TFPB⁻)). As ionophore-target ion complexes are already present within the membrane, the additional extraction of target ions with anions becomes chemically unfavorable (Figure 12 (b/c)). Consequently, the LK^+ activity within the membrane is independent of the K^+ activity within the analyte and the phase boundary potential of the ISM depends on the activity within the analyte in a Nernstian fashion (see Figure 12 (a)). The Nernstian behaviour is observed above the lowest detection limit (above 1 $\mu\text{M/L}$). The factors influencing/determining this lower detection limit are discussed in the following section.

2.4.3.1 Lower detection limit

The lower detection limit is given by diffusive fluxes through the membrane which locally increase the target ion concentration within the vicinity of the membrane (see Figure 13 (b)). The transmembrane fluxes are induced by concentration gradients of LK^+ within the bulk of the ISM. There are two mechanisms which induce these gradients: First, if no interfering ions are present, the relatively small amount of co-extracted Cl^- ions are sufficient to induce a concentration gradient. This concentration gradient leads to a diffusive flux of K^+ ions from the IFS into the analyte. The magnitude of this diffusive flux depends on the concentration difference between the target ion within the IFS and the analyte

At a concentration of 10 mM, the lower detection limit is 1 $\mu\text{M/L}$ (blue in Figure 13), whereas at a concentration of 0.1 μL the lower detection limit is as low as 1 nM (green in Figure 13). However, this is at the cost of a lower upper detection limit. Furthermore, such low concentrations within the IFS are very susceptible to contaminations. The second mechanism is caused by an ion exchange of interfering ions, such as Na^+ , with the targeted K^+ ions. The exchanged LNa^+ ions lower the concentration of LK^+ ions at the analyte side (see Figure 13 (b/c), red). As before, the LK^+ concentration gradient leads to a diffusive transmembrane flux which increases the target ion in the vicinity of the membrane. Hence, if interfering ions are present the lower detection limit is not given through the difference of the complex formation constant but through a transmembrane flux.

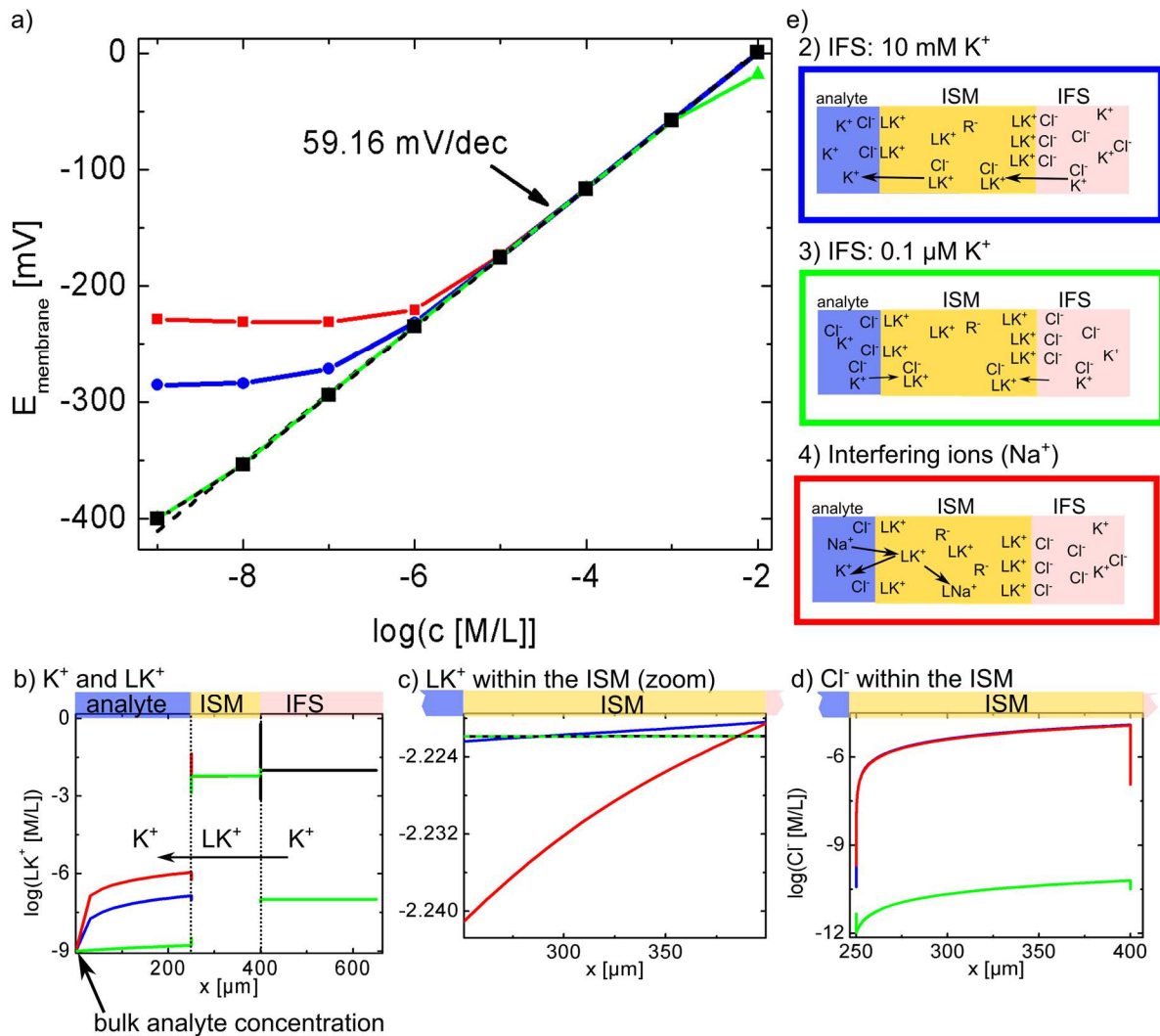


Figure 13: Illustration of the lower detection limit of ISMs within a background of constant ionic strength (10 mM NaCl) and an IFS containing 10 mM KCl. The membrane potential at different target ion concentrations for 4 different constellations: 1) no anionic transfer allowed (black); 2) anionic transfer allowed and 10 mM K^+ IFS (blue); 3) 0.1 μM K^+ IFS (green); 4) anionic transfer allowed and Na^+ transfer allowed and 10 mM IFS (red). The corresponding concentration of the complexed K^+/LK^+ ions and Cl^- ions are shown in a), b) and c) (at a target ion concentration of 1 nM). The relevant transfer processes are illustrated in e).

To summarize, the lower detection limit is given through transmembrane fluxes. One approach to reduce the transmembrane fluxes is to reduce the diffusion constant of the membrane components which comes at the cost of a higher membrane resistance and a more challenging measurement setup.^{12,97} Another approach to reduce the influence of these transmembrane fluxes is to use flow cells.⁹⁸ In flow cells, a high analyte flux reduces the

diffusion layer in the vicinity of the membrane. However, the most promising approach seems to be so called solid contact ISEs, discussed in section 2.4.4.⁹⁹

2.4.3.2 Upper detection limit

The upper detection limit of ISEs is given by significant extraction of anions (Cl^-) into the membrane. As soon as anions are extracted into the membrane, the concentration of LK^+ within the membrane changes and the concentration dependent signal is lost (see this section at the beginning and an ISM without anionic sides). The upper detection limit depends on the complexation constant of the ionophore and the concentration and type of counter anions: The stronger the ionophore binds the target ion, the likelier the extraction of counter anions. Consequently, in order to increase the upper detection limit a low complexation constant and a high energy of transfer of counter anions is required. This is in contrast to the lower detection limit, where a high complexation constant is advantageous.

2.4.4 Solid contact

Though liquid contacts are well defined and easy to setup in laboratories, they have a number of disadvantages such as evaporation of the inner filling solution, a challenging miniaturization and transmembrane diffusive fluxes.⁹⁹ Whereas, in case of solid contact ISEs (SC-ISEs) the ISM is sandwiched between the sample solution and a solid contact (SC) avoiding the above mentioned issues. However, providing a well-defined interface between an electron-conducting SC with an ion-conducting polymeric ion selective membrane is very challenging. One of the first solid contact ISEs were so called coated wire electrodes.¹⁰⁰ This electrodes consisted of an ISM which was directly bonded onto a metal wire. However, these electrodes suffer from poor reproducibility and potential drifts. This was ascribed to a poorly defined membrane-metal interface.^{99,101,102} First, due to condensation at the metal, a very thin water layer is formed at the metal electrode (see Figure 14 (c)). This water layer acts as an inner filling solution with a very small volume. Consequently, small transmembrane fluxes, diffusion of gas such as CO_2 can already induce significant composition changes and therefore potential drifts. ^{99,101,102} In the worst case, the ISM is delaminated which leads to a catastrophic failure. In addition to that, these electrodes violate a fundamental law of

electrochemistry: As no dominant redox couples are present, two polarizing interfaces are used in series. To circumvent this problem three major approaches were pursued in literature (see Figure 14): The first one is to use an ISM which is loaded with a redox couple as described in ref. ^{99,103–105} (see Figure 14 (a)). Though this approach seems to be very promising, it was not further pursued by other research groups. The reason might be ascribed to an interference of the redox couples with the targeted ion. The second one are the so called ion selective field-effect transistors (ISFETs), where the ISM is directly bonded onto the dielectric of a FET.^{106–110} The membrane potential of the ISM modulates the gate voltage which drives the transistor. In this case, the dielectric-ISM interface is the only polarizing interface and a redox couple can be omitted. ISFETs sensitive to K^+ , Na^+ and Ca^{2+} and heavy metals have been demonstrated using a variety of different architectures.^{94,110–112} Furthermore, integrated ISFET sensor arrays for pH¹¹³, enzymes¹⁰⁸ and DNA¹⁰⁶ detection have been published. However, other than the pH sensitive ISFETs, these devices were not brought to wide commercial applications so far.⁹⁹ This is most likely due to the expensive and elaborate fabrication of ISFETs. The third approach, are ion and electron conducting polymers. These polymers act as an electron to ion transducer depolarizing the ISM-conducting polymer (see Figure 14 (b)) interface. This interface is well defined and the suppression of transmembrane fluxes lead to SC-ISEs with very low detection limit in the nano-molar regime.^{114–118} The SC-ISEs based on conducting polymers did not solve all the problems. Many of the conducting polymers such as poly(3,4-ethylenedioxythiophene) polystyrene sulfonate (PEDOT:PSS) and 4-(1-Pyrrolidinyl)pyridin (PPy) are hygroscopic leading to an unintentionally formed water layer between the ISM and the SC (see Figure 14 (c)).^{99,119,120} Hence, their long term stability with respect to the standard transfer potential (E_0) at the SC-ISM interface, still bears challenges.¹⁰²

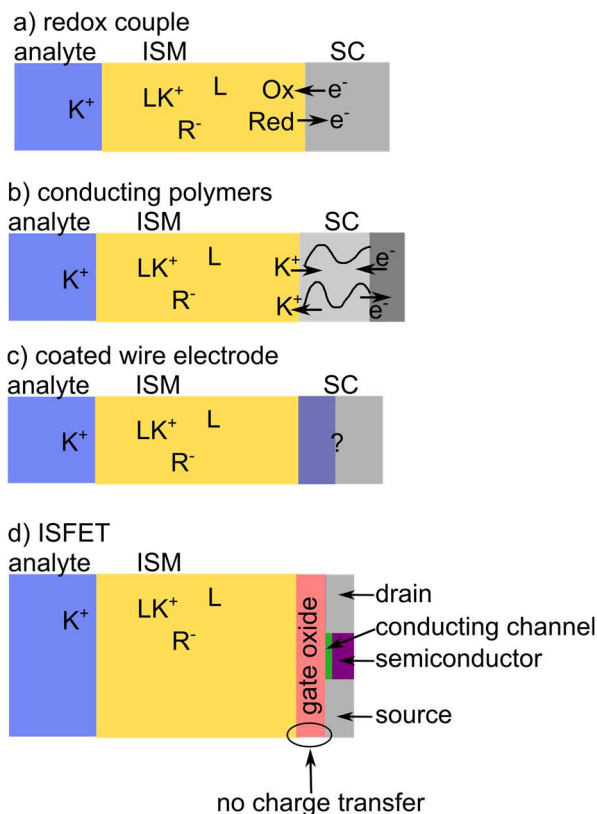


Figure 14: Illustration of a metal SC-ISE using an ISM loaded with a redox couple (a) and a conducting polymer SC-ISE (b). The conducting polymer (indicated with light grey) serves as an electron to ion transducer. The unintentional formed water layer at a solid contact is shown in c). This water contact leads to an undefined SC-ISM contact. d) illustration of an ISFET.

Within this work PEDOT:PSS was used as solid state transducer because its electrochemically stable and its known to perform well in combination with PVC-based ISMs.^{8,114,119,121} PEDOT is known to be stable in its oxidized form (PEDOT⁺) and the PSS⁻ anion acts as a polyanionic dopant neutralizing the positive charges of conducting PEDOT⁺ backbones. The conducting polymer turns electrically insulating if it is reduced to neutral PEDOT⁰. During reduction, the cationic charge carriers of the PEDOT⁺ are lost while foreign cations (K⁺) are influxed from the ISM into the film¹²²:



Where e⁻ are electrons, PSS⁻ is the polystyrene sulfonate and PEDOT^{0/+} the positively and neutral poly(3,4-ethylenedioxythiophene) backbone; $K_{membrane/Film}^+$ are cations within the film/membrane.

Consequently, the PEDOT:PSS turns insulating at the membrane side, if large inward currents are applied. This was reported to be a problem in case of stripping voltammetry or other related techniques where the PEDOT:PSS reduction gets the current limiting factor.¹²³ However, if a constant current pulse is applied as done in chapter 3, this is not a problem as the characteristic potential drop over the PEDOT:PSS ideally remains unchanged from measurement to measurement and just results in a time dependent offset.

2.4.5 Dynamically electrochemistry with ISEs

Most polymeric membranes are operated using potentiometry. However, recently various non-equilibrium techniques have emerged. ISMs operated with controlled current or potential techniques have a number of attractive analytical features. One example of such an emerging technique is stripping ion transfer voltammetry which allows for extremely low detection limits in the pico-molar regime.^{50,51,55,124–129} At higher concentrations, chronopotentiometric methods which exhibit a very high sensitivity and thus accuracy are of particular interest.^{52,57,58,130}

This work focused on the detection of alkali metals in physiological samples and therefore on chronopotentiometry. This method is based on a current pulse which is forced through the membrane while the potential is monitored. Though, a constant ion flux is forced through the ISM, the transfer at the interface is fast and instantaneous establishing a near-nernstian phase boundary potential, even under dynamic mass transport conditions.^{72,131} This near-nernstian phase boundary potential is not equal to the one measured under zero current conditions because the phase boundary activities/concentrations change:

$$E_{PB} \sim \ln \left(\frac{C_W^*(t)}{C_O^*(t)} \right)$$

Where C_W^* and C_O^* are the concentrations of the target ion at the phase boundary which are a function of the pulse time.

The current induced activity change greatly depends on the diffusion constant within the respective phase. Hence, as long as there are sufficient target ions or free ionophores

available, the phase boundary potential, remains Nernstian.^{53,132} If the concentration of the target ion is smaller than a critical concentration, the ion is depleted in the vicinity of the membrane at a certain transition time. This critical concentration is given by ¹³²:

$$\sqrt{t_{transition}} = \frac{-FA}{2I} \sqrt{D_{aq} c_{critical}}$$

Where D_{aq} is the diffusion coefficient in the aqueous solution, $c_{critical}$ is the critical concentration, I is the current, t is the duration of the current pulse, A is the membrane area and all other symbols have their usual meaning.

As soon as the target ion depletes other ions have to be extracted into the membrane or oppositely charged ions have to be extracted from the ISM into the analyte. As these transfers are energetically unfavourable, a higher potential has to be applied. Hence, a potential jump is observed at this depletion concentration/transition time.

Generally, in case of chronopotentiometry, the ISEs are operated using small current amplitudes where no depletion occurs^{133,134}, whereas in case of flash chronopotentiometry large current amplitudes which purposely deplete a specific ion, are used.⁵⁸ Flash chronopotentiometry relies on the measurement of the potential jump whose magnitude depends on the selectivity of the membrane. For that reason sensitivities which exceed the Nernstian limit by a factor 20, are possible. Within this work a new flash chronopotentiometry concept is introduced in chapter 3.

3. ION SELECTIVE ELECTROLYTE GATED FIELD-EFFECT TRANSISTORS

Within the following chapter a new sensing concept based on an integrated EGOFET used as a transducer in combination with an ionophore-doped polymeric ion-selective membrane serving as a sensing element, is presented. This new concept proved to be an important step towards a low-cost integrated ion sensor array for selective and multiple ion detection.

The content of this chapter is based on the work that has been published and was partly modified:

Hydrogen ion-selective electrolyte-gated field-effect transistor for pH-sensing

J. Kofler*, K. Schmoltner*, A. Klug, E. J. W. List-Kratochvil

Applied Physics Letter 104, 193305 (2014). Reproduced with permission from © AIP Publishing

*both authors contributed equally.

Contribution: The author contributed equally with K. Schmoltner to experiments related to the ion-selective EGOFETs and sensor characterization. The author wrote the manuscript, finalized the manuscript together with the K. Schmoltner.

Electrolyte-gated field-effect transistor for selective and reversible ion detection

K. Schmoltner*, J. Kofler*, A. Klug and E. J. W. List-Kratochvil,

Advanced Materials 25 (47), 6895–6899 (2013). Reproduced with permission from ©WILEY-VCH Verlag GmbH & Co.

*both authors contributed equally.

Contribution: The author contributed equally with K. Schmoltner to experiments related to the ion-selective EGOFETs and sensor characterization. K. Schmoltner wrote the manuscript, finalized the manuscript together with the author.

Ion-selective electrolyte-gated field-effect transistors: Prerequisites for proper functioning

J. Kofler, K. Schmoltner and E.J.W. List-Kratochvil,
Proceedings of SPIE 9185, Organic Semiconductors in Sensors and Bioelectronics VII,
91851U-1 (2014). Reproduced with permission from
©Society of Photo Optical Instrumentation Engineers
Contribution: All experimental work. The author wrote the manuscript. The
manuscript was finalized with K. Schmoltner.

3.1 Introduction^j

The presented sensing concept takes full advantage of recent advances within the research fields of ion selective membranes (ISMs) and organic field-effect transistors: Ion-selective membranes, containing neutral or charged ionophores, are available for the determination of a large number of organic and inorganic ions.¹³¹ During the past decade the chemical sensing abilities of ISMs have been significantly improved, resulting in a “new wave of ion-selective membranes”.⁸ If such powerful ion sensing elements are combined with suitable solid-state transducers, mass-producible, miniaturized ion-sensor systems with unforeseen analytical capabilities are within reach.⁸ Electrolyte-gated field-effect transistors (EGOFETs) already proved to be ideal candidates as transducers for the detection of biomolecules such as DNA, dopamine, enzymes and proteins in an electrolytic background with a constant ionic strength.^{39–42} Moreover, EGOFETs are characterized by their small size, portability, low-energy consumption and low cost.^{36–38} An additional benefit of EGOFETs is that in contrast to the conventional ion-selective field-effect transistor (ISFET) architecture, the semiconductor is in direct contact with the electrolyte. Consequently, there is no need for elaborate and expensive encapsulation of the semiconductor. On the contrary, due to the formation of an electric double layer (EDL) at the semiconductor/electrolyte interface and a resulting high capacity (1–10 $\mu\text{F}/\text{cm}^2$), a stable low-voltage operation ($< 1\text{ V}$) is possible.^{43–45} Therefore, they are ideal candidates, not only as transducers, but also as intrinsic signal amplifiers.⁴⁶

^j The section is based on the work that has been published. J. Kofler, K. Schmoltner, A. Klug, and E.J.W. List-Kratochvil, *Appl. Phys. Lett.* 193305 (2014).

Here, a novel, selective and reversible EGOFET based ion sensing platform for solutions with varying ionic strength, is demonstrated. The presented architecture is modular and the EGOFET serves exclusively as a transducer. For that reason, the detection of other ions can be realized “simply” by introducing appropriate ISMs. Furthermore, important sensor parameters such as lowest detection limit and selectivity can be tuned by modifying the membrane.

Firstly, the fabrication procedures and the characterization methods are presented. After that the building blocks of the EGOFET sensing platform namely the EGOFET, the ISM and the gate electrode are investigated separately, reasoning the chosen ion-sensor architecture. The results of these investigations are summarized in the section called “towards an ion selective EGOFET”. After that, the final concept of this novel sensing platform is presented. Subsequently, the versatility of the concept is demonstrated by means of an H⁺ selective and a Na⁺ selective EGOFET.

3.2 Experimental

Firstly, the fabrication and assembly procedures of the ion sensing platform are presented. The measurement methods used to characterize the sensor and electrodes are described subsequently.

3.2.1 Fabrication procedures

The EGOFETs and the electrodes for the normal pulse voltammetry measurements were fabricated on PET and glass substrates (Melinex, DuPont Teijin Films). The 50 nm gold source/drain (S/D) electrodes with 2 nm chromium adhesion layer were structured using conventional lift-off processing (channel length $\approx 7 \mu\text{m}$, channel width $\approx 3 \text{ mm}$). The electrodes used for the normal pulse voltammetry had an area of 28 mm^2 . Regioregular poly(3-hexylthiophene) (Plexcore OS purchased from Sigma-Aldrich) was deposited via spin-coating from a 4 g L^{-1} toluene solution and dried at $60 \text{ }^\circ\text{C}$ in Argon (Ar) for $\approx 10 \text{ min}$ and subsequently at $120 \text{ }^\circ\text{C}$ under high vacuum ($p \approx 4 \times 10^{-5} \text{ mbar}$) for 1 h. All devices were

assembled under inert atmosphere. The Na⁺ selective ISM membranes were prepared by drop-casting a high molecular weight polyvinyl chloride (31 wt%, Selectophore grade), 2-nitrophenyl octyl ether (2-NPOE) (68 wt%), potassium tetrakis- ((4-chlorophenyl)borate (KTPClPB) (0.7 wt%) and sodium ionophore X (0.2 wt%) in 5 mL tetrahydrofuran (THF) cocktail onto a glass slide. Whereas, the H⁺ selective ISM membranes were prepared by drop-casting a high molecular weight polyvinyl chloride (31 wt%, Selectophore grade), 2-nitrophenyl octyl ether (2-NPOE) (63 wt%), sodium tetrakis[3,5-bis(trifluoromethyl)phenyl]borate (NaTFPB) (2 wt%) and Hydrogen ionophore V (4 wt%) in 4 mL tetrahydrofuran (THF) cocktail onto a glass slide. The K⁺ selective ISM membranes were prepared by drop-casting a high molecular weight polyvinyl chloride (31 wt%, Selectophore grade), 2-nitrophenyl octyl ether (2-NPOE) (63 wt%), sodium tetrakis[3,5-bis(trifluoromethyl)phenyl]borate (NaTFPB) (0.5 wt%) and Potassium ionophore V (1 wt%) in 4 mL tetrahydrofuran (THF) cocktail onto a glass slide. The drop-cast membranes were allowed to dry overnight in a saturated THF environment conditions and were peeled off the glass slide for further implementation. All of the chemicals mentioned above were obtained from Fluka Sigma-Aldrich and were used as received.

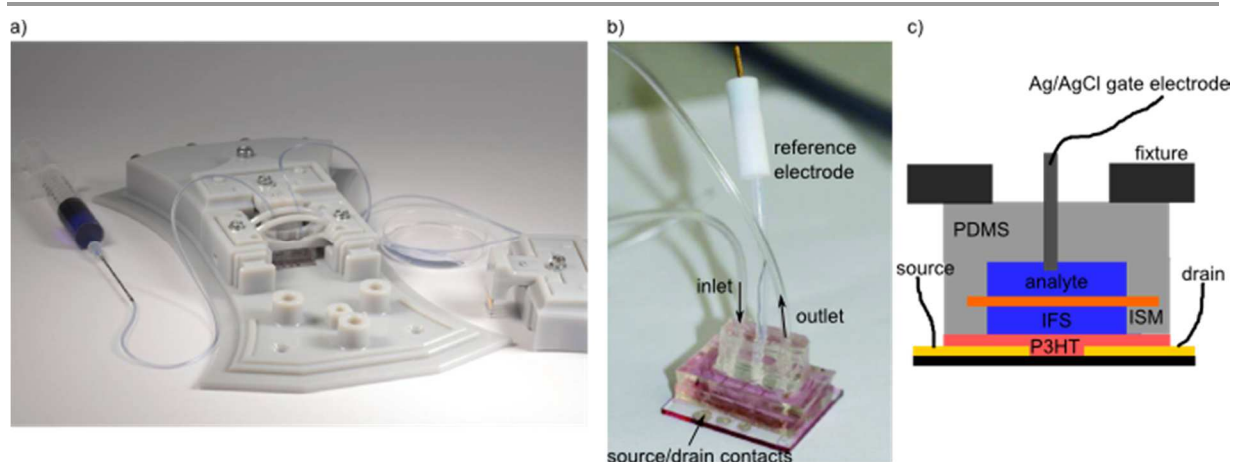


Figure 15: a) 3D printed fixture for the flow cell; b) assembled ion sensitive EGOFET; c) illustration of a side view of the assembled device.

The reservoir and the flow cell for the ion-sensitive EGOFETs were made of polydimethylsiloxane (PDMS, Sylgard 184) via a soft molding process, including a curing step

of ≈ 1 h at 100 °C. The already assembled flow cell is shown in Figure 15 (b) and (c). The flow cell was sealed by an appropriate fixture shown in Figure 15 (a).

3.2.2 Characterization methods

The saline solutions were prepared in concentrations varying from 10^{-4} M to 10^{-1} M NaCl (99.5%, p.a., ACS, ISO) and KCl (>99.0%) in deionized water, respectively. The 0.2 M potassium phosphate buffer solutions (PBS) were adjusted to pH 7. To continuously tune the pH value, the sample solution was buffered with 10 mM boric acid and 10 mM citric acid (unless noted otherwise) and drop-wise titrated with 0.5 M NaOH, while the pH was monitored with a calibrated glass electrode (Orion Thermo Sure Flow).

The electrical characterization of all devices was done in ambient air (at same light conditions) using an Agilent B1500 Parameter Analyzer. All potentials were applied with respect to an Ag/AgCl reference electrode containing a 3 M KCl inner filling solution. All normal pulse voltammetry measurements were carried out by a common three electrode setup: Pt counter electrode, Ag/AgCl reference electrode and a working electrode (electrode which is examined). The currents were measured after applying a potential pulse for 10 s on three different electrodes not revealing significant differences.

3.3 Towards an ion selective EGOFET^k

Within this section the building blocks of the EGOFET sensing platform namely the EGOFET, the ISM and the gate electrode are investigated separately, reasoning the architecture of the presented sensing platform. First, EGOFETs are discussed in general terms, not specifically considering sensing applications; i.e. the prerequisites to achieve a proper electrical signal transduction are discussed. After that, the peculiarity and conceptual issues of EGOFETs used in ion sensing applications are presented.

^k The section is based on the work that has been published: J. Kofler, K. Schmoltner, and E.J.W. List-Kratochvil, Proc. SPIE **9185**, 91851U (2014).

3.3.1 EGOFETs used as electric transducers

As EGOFET – transducers are of high interest to the scientific community, a separate chapter was dedicated to the general prerequisites which have to be fulfilled to achieve a proper potentiometric signal transduction and amplification. In order to do so, the semiconductor-(P3HT) and gate- electrolyte interfaces were examined separately. Au electrodes and Au electrodes coated with P3HT (Au|P3HT electrodes) were fabricated and examined by normal pulse voltammetry measurements. Hence, a potential was applied to the electrolyte relative to the respective electrode and the current was measured after a 10 s potential pulse. This current is highly relevant to EGOFET devices, since it is directly related to the leakage current and to the potential drops at the semiconductor-/gate- electrolyte interfaces.

Two representative interface types were examined, namely one polarizable (no faradaic current) and one non-polarizable interface (faradaic current passes) (see Figure 16 (b)). The measurement setup of the pulse voltammetry measurements is illustrated in Figure 16 (a)). The measured currents of Au/P3HT-PBS (phosphate buffer solution) and Au– PBS interfaces are shown in Figure 16 (c)). The Au-PBS and the P3HT-PBS interfaces are polarizable within an electrochemical window of -500 mV to + 500 mV vs. an Ag/AgCl reference electrode. Thus, within this potential window, only negligible leakage current between the gate and the EGOFET device (source-/drain- pads, channel) will be flowing. The currents flowing across Au|P3HT and Au electrodes in a PBS solution containing 0.01 M ascorbic acid are shown in Figure 16 (d)). The currents are magnitudes higher than their PBS counterparts. This can be ascribed to the ascorbic acid which easily oxidized or reduced and acts as a depolarizer. Consequently, these interfaces are not polarizable and small potentials below +/- 500 mV already lead to currents in the range of a few μA . In both cases (PBS and PBS containing ascorbic acid), the currents flowing across the Au|P3HT electrodes at positive biases is magnitudes lower compared to Au electrodes. Since these currents increase significantly with time at potentials more positive than 500 mV (see Figure 17 (a)), the measured current depends on the history of the device, as indicated by an arrow (see Figure 16 (c)).

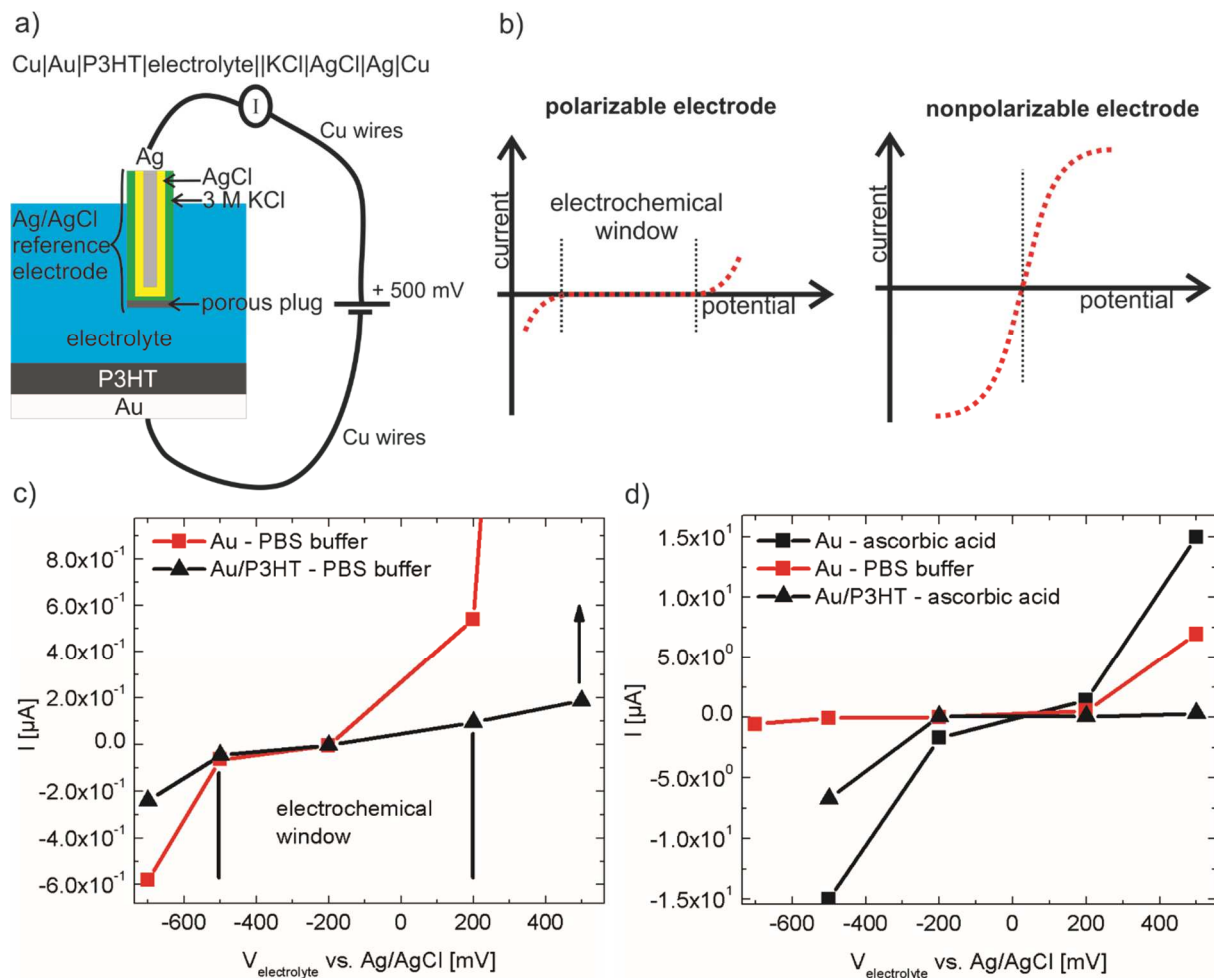


Figure 16: An illustration of the voltammetry measurement setup (a) and graphs of ideal polarizes and nonpolarized interfaces (b). The currents of the Au- and P3HT- PBS buffer and -ascorbic acid interfaces is shown in (c) and (d) respectively. The Au and P3HT- PBS buffer interface is polarizable within a -/+500 mV electrochemical window. Whereas the Au, P3HT-ascorbic acid solution interface is not polarizable and large currents > 1 mA are observed at voltages of -500 mV and +500 mV.

Figure 17 (a) shows the current as a function of time at -500 mV, -700 mV and +500 mV, +700 mV with respect to an AgCl reference electrode of an Au|P3HT electrodes. At a negatively biased gate electrolyte the current decreases with time, whereas at a positive bias the current increases. This could be ascribed to the p-type conduction of the P3HT. If the electrolyte is biased negatively, holes are injected from the underlying Au electrode to shield the external electric field induced by the potential difference between the gate and the gold electrode/P3HT (see theory section 2.3). Consequently, the potential should ideally drop over the P3HT-electrolyte interface (see Figure 17 (b)). Whereas, if the electrolyte is biased

positively the potential drops over the whole P3HT coating as a result of the p-type conduction. The potential drop at the P3HT-electrolyte interface which drives the electrochemical reaction and thus the faradaic current is therefore reduced. However, the electric field increases the migration of water/ions towards the gold pads. As the water/ion content is increased, the P3HT loses its blocking capabilities and the current starts to increase.

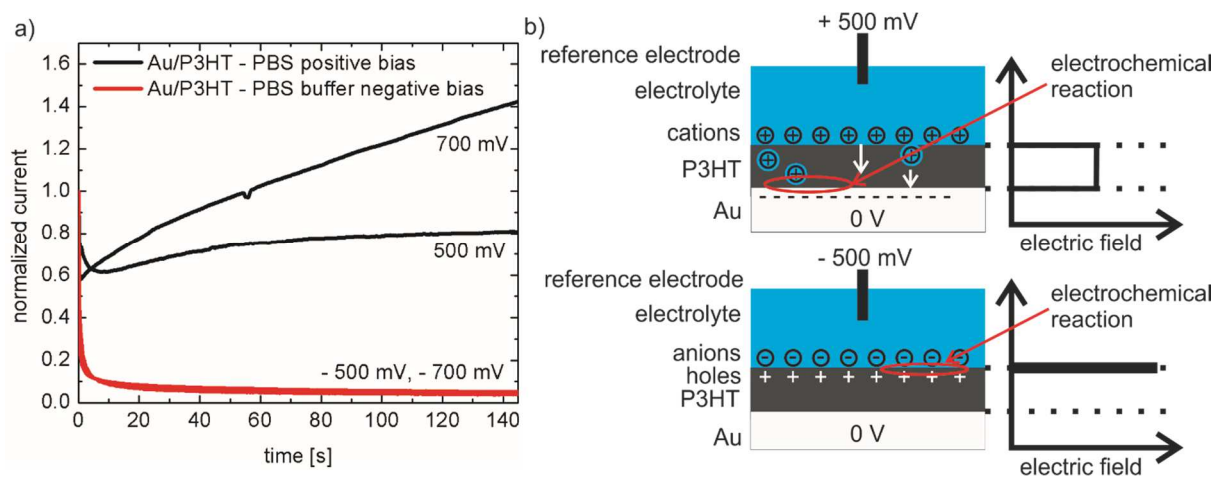


Figure 17: Normalized current as a function of time at positive and negative biased electrolyte solution (PBS) of an Au electrode coated with P3HT (a). The current was normalized by the initial current at time $t = 0$. At positive bias the current increases with time whereas at negative bias the current decreases. This could be attributed to an electric field which increases the ion/water migration towards the gold pad and as a result leads to decreasing blocking capabilities of the P3HT as illustrated in a simplified model (b).

In case of an EGOFET there are three interface combinations possible: 1) both interfaces polarizable; 2) semiconductor interface polarizable and gate electrode non-polarizable; 3) both interface non-polarizable. The distinct EGOFET characteristics corresponding to these interface combinations are shown in Figure 18 1) (b), 2) (c), 3) (d) respectively. Figure 18 (a) shows a simplified circuit diagram of an EGOFET which neglects potential differences between the source and drain pads and describes the interfaces by a capacitor in parallel to a resistor. The potential difference between the source/drain contacts and the gate electrolyte lead to an EDL formation with a high capacitance which controls the source-drain current. Ideally, the potential of the gate electrolyte should solely be given through the potential of the gate electrode; i.e. the effective gate potential should be independent of potential applied to the source/drain contacts. If this is not the case, the transistor does not show a proper transistor

characteristic/amplification. Thus, if the gate electrode-electrolyte interface and the P3HT-electrolyte interface is polarizable (R_{Gate} and R_{P3HT} large), the capacity of the gate electrode has to be significantly higher compared to the capacity of the source/drain contacts. That is why the EGOFET gated with a small area polarizable Au-gate electrode shows a poor performance compared to a porous large polarizable Pt-electrode (see Figure 18 (b)). These two cases mentioned above are certainly extreme cases. Practically, the transition between polarizing and non-polarizing interface is continuous and separating the capacitive contributions from the resistive contributions of the two interfaces is not possible. So far only polarizable gates-electrodes have been discussed. For that reason, the characteristics of a non-polarizable gate electrode (Ag/AgCl) using the same electrolyte (R_{Gate} small, R_{P3HT} large) are shown in Figure 18 (c). In this case, the capacity of the gate electrode does not matter and as the P3HT-electrolyte interface is polarizable, the characteristics are identical the ones obtained in Figure 18 (b). Figure 18 (d) shows the transfer characteristics in case of non-polarizable P3HT and gate-electrolyte interfaces (R_{Gate} and R_{P3HT} are small) in comparison to a polarizable interface. To do so, the EGOFET was gated with pure PBS, subsequently with a phosphate buffer containing ascorbic acid acting as a depolarizer and finally again with pure PBS. Due to the ascorbic acid the leakage current dominates the transistor characteristics. After replacing the ascorbic acid containing buffer with pure PBS again, the initial good transistor characteristics and low leakage currents are restored, not indicating any degradation of the P3HT.

To conclude, there are two conditions to achieve a proper EGOFET performance in terms of amplifications: First, the P3HT-electrolyte interface has to be polarizable and secondly, the gate electrode should either be non-polarizable or have a large capacity.

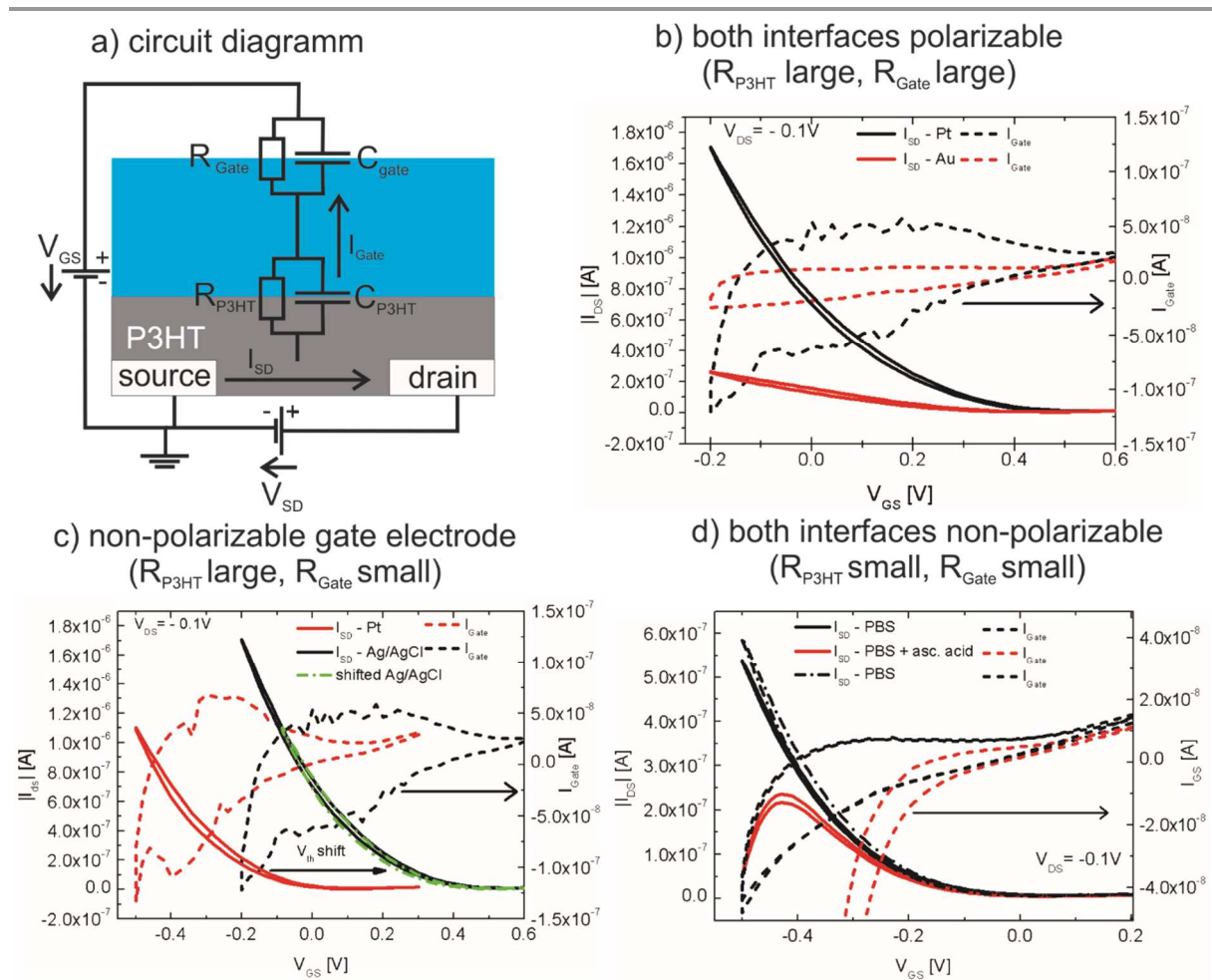


Figure 18: EGOFET operation modes: a) Simplified circuit diagram of the relevant interfaces of an EGOFET; b) transfer characteristics of an EGOFET gated with a small Au electrode (1 cm^2) (small C_{Gate}) is compared to an EGOFET gated with a porous Pt electrode (large C_{Gate}); c) transfer characteristics of an EGOFET gated with an Ag/AgCl electrode (non-polarizable) and a Pt electrode (polarizable). d) transfer-characteristics gated with an Ag/AgCl electrode and a PBS electrolyte containing ascorbic acid (non-polarizable) compared to a pure PBS electrolyte (polarizable).

3.3.2 EGOFETs used for ion sensing applications

Within this section the sensitivities of the major building blocks (EGOFET, gate electrode and ISM) towards various electrolytes and their implications for the sensing concept, are examined.

3.3.2.1 Ion sensitivity of EGOFETs

In order to investigate the prerequisites to obtain a good performance with respect to the targeted sensing applications, the influence of electrolytes with varying ionic strength was examined first. Figure 19 (a) shows the transfer characteristic of an EGOFET gated with a 10^{-2} M NaCl solution, subsequently with a 10^{-4} M NaCl solution and finally with a 10^{-4} M NaCl solution containing a 10^{-2} M CaCl_2 background. An Ag/AgCl reference electrode was used as a gate-electrode to ensure a constant gate potential which is independent of the electrolyte composition. The source drain currents are decreased with decreasing ionic strength. However, if the Cl^- concentration is kept constant using a CaCl_2 background, the transfer characteristics (including I_{Gate}) are almost unaltered. This can be attributed to a modification of the electrolyte/semiconductor interface depending on the concentration and type of the anion in the electrolyte.¹⁷⁶

Hence, EGOFET-characteristics non-selectively depend on the ionic strength/composition of the gating solution due to a modification of the electrolyte/semiconductor interface. For that reason, EGOFETs cannot be in direct contact with the sample solution as this would lead to a mixed signal between the selective signal of the ISM and the non-selective signal of the EGOFET.¹⁷⁶ Thus, a different approach has to be pursued: The EGOFET has to be in contact with an inner filling solution of constant composition which is separated from the analyte by an ion selective membrane. Note that for the same reason, modifying the gate electrode with an ISM as frequently done in literature¹⁷⁶, is not an option.

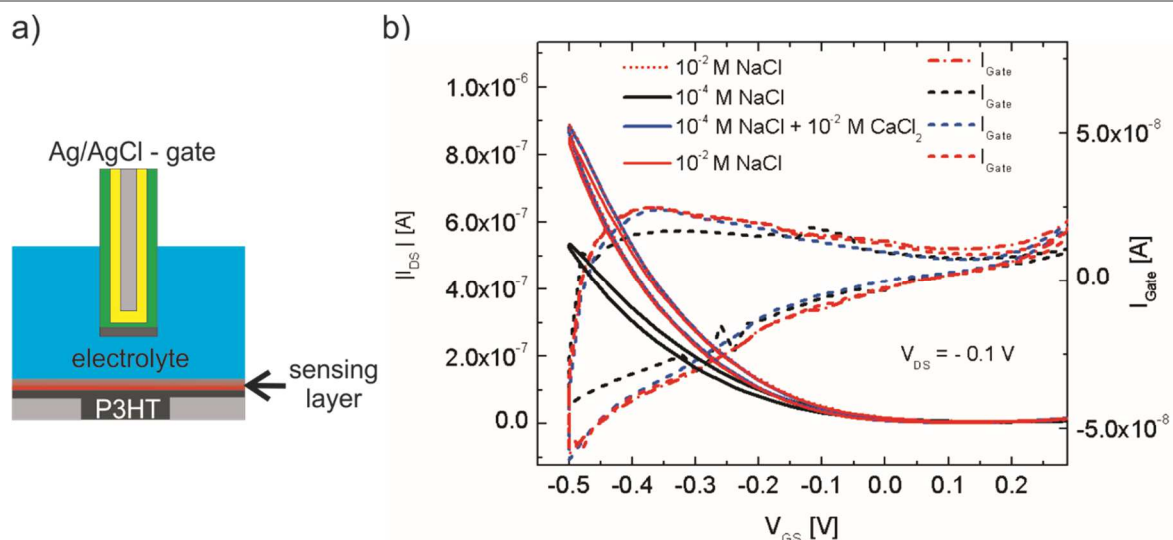


Figure 19: a) Illustration of an EGOFET using the semiconductor as a sensing layer; b) transfer characteristic of an EGOFET gated with a 10^{-2} M NaCl solution, with a 10^{-4} M NaCl solution and a 10^{-4} M NaCl solution containing a 10^{-2} M $CaCl_2$ background. An Ag/AgCl reference electrode was used as a gate-electrode to ensure a constant gating potential which is independent of the composition of the electrolyte.

3.3.2.2 Gate electrode

Though various electrodes such as Pt or PEDOT:PSS can be used as a gate without changing the electrical performance of the EGOFETs, the electrochemical cell potential (gate electrode|analyte) typically changes with the sample composition. Figure 20 (b) shows the electrode potential of a PEDOT:PSS electrode relative to a Ag/AgCl reference electrode. As the ionic strength is changed from 10^{-2} M KCl to 10^{-6} M KCl, the potential varies for ~ 80 mV. However, if the KCl concentration is decreased within a constant ionic NaCl background (10^{-2} M), keeping the ionic strength almost constant, the potential just varies for 20 mV. This potential drift would lead to a mixed signal between the sensing signal of the ISM and a non-selective signal from the gate electrode as shown in Figure 20 (b). Consequently, Ag/AgCl reference electrodes which guarantee a constant potential, independently from the sample composition have to be used, which is currently the major drawback of ion selective EGOFETs.

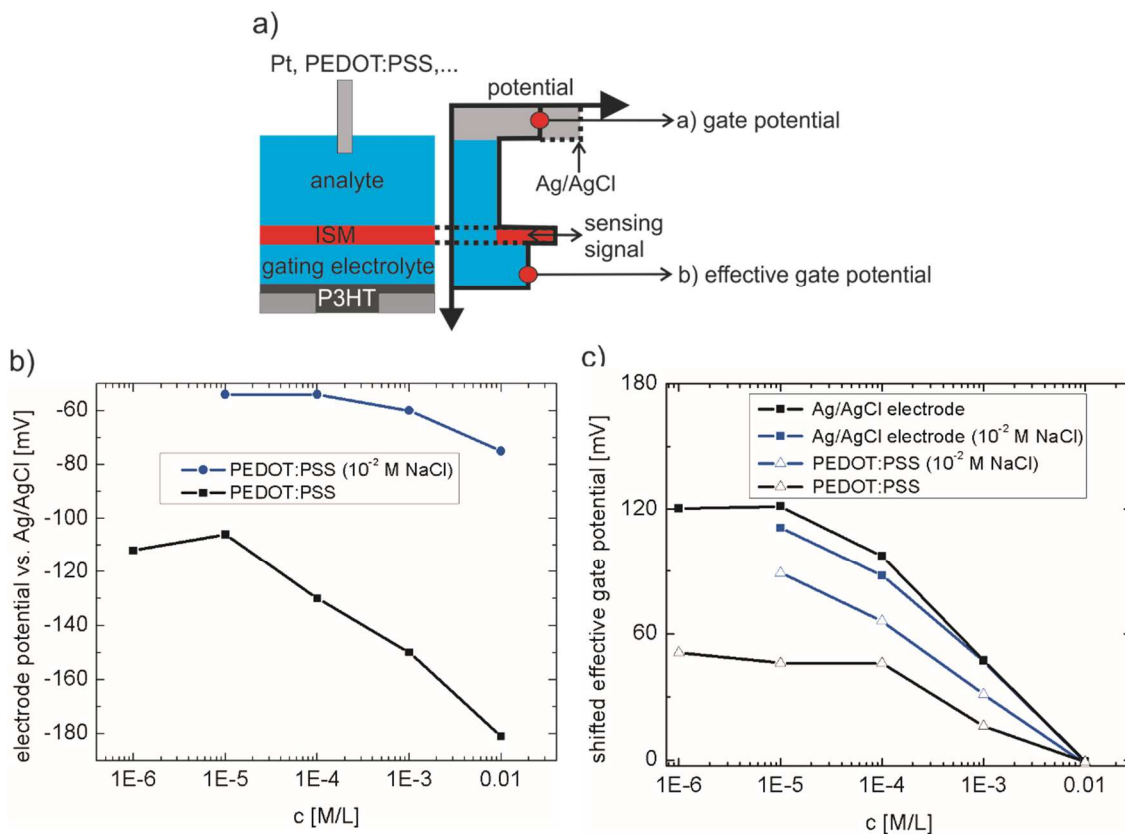


Figure 20: a) illustration of the functional principle of an ion selective EGFET b) The electrode potential of PEDOT:PSS electrodes vs. the constant potential of a Ag/AgCl reference electrode as a function of K^+ concentration. The potential was measured within a constant NaCl background (blue) and de-ionized water (black); c) Effective gate potentials of a K^+ selective membrane measured with an Ag/AgCl reference electrode (squares) and with a PEDOT:PSS electrode (triangles) shifted to 0 mV at a concentration of 10^{-2} M for better comparison. The potentials were measured with a constant NaCl background (blue) and de-ionized water (black).

3.3.2.3 Ion selective membrane

Due to the direct contact between the semiconductor and the electrolyte, a small leakage current is flowing between the gate and the EGFET. This leakage current is also flowing through the ISM. This might be a negative side effect (discussed in section 2.4.5). High leakage currents densities can lead to a polarization of the membrane. Figure 21 shows the response curve of a Na^+ selective ISM while applying a constant current. During EGFET operation and a leakage current density of -10 nA/mm^2 , cations are driven from the inner filling solution into the sample solution. Consequently, the Na^+ concentration is increased, right in the vicinity of the ISM which leads to a higher lowest-detection limit. This also indicates that the area of the membrane has to have a certain size compared to the size of the transistor. Thus, typical

leakage currents in the range of 1 nA require a minimum membrane size around 1 mm². The leakage current could also be used to pump ions from the sample into the inner filling solution (+10 nA/mm²), which could possibly lead to a lower detection limit. Unfortunately, as P3HT is a p-type conductor, this results in an EGOFET which is turned off.

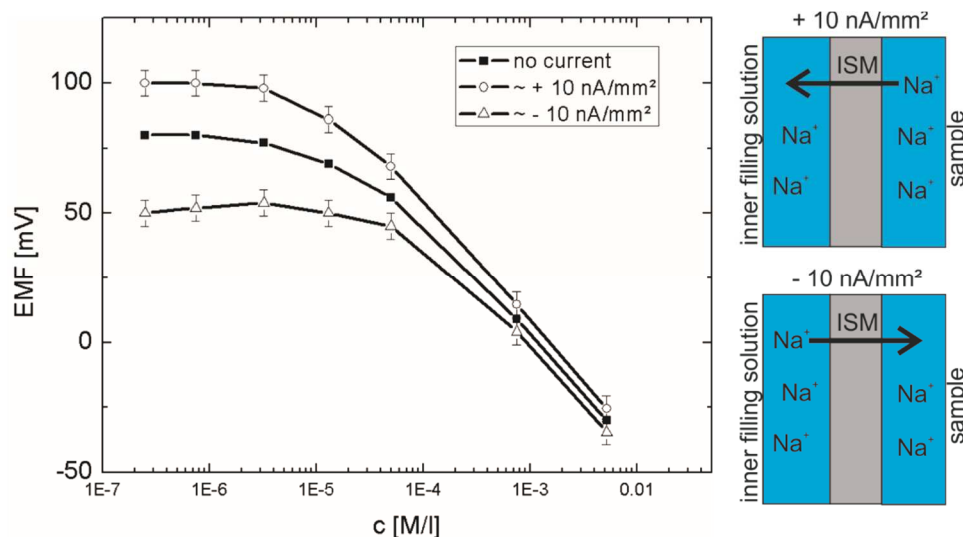


Figure 21: Membrane potential of a Na⁺ selective membrane as a function of Na⁺ concentration while applying a constant current (Na⁺ ions flow from sample to inner filling solution) and negative currents (Na⁺ ions flow from the inner filling solution to the sample). The potentials were not corrected for ohmic drops within the electrolyte. The error bars are due to noisy measurements. The current density (+/- 10 nA/mm²) is an estimation as the real surface area of the membrane which is slightly corrugated, is not exactly known.

3.4 The sensing concept

There are different approaches to implement the EGOFET as a transducer in sensing applications (see section 2.4). Though it was already demonstrated that EGOFETs based on specifically designed semiconductors can be directly used as sensing elements for biomolecules such as DNA, dopamine, enzymes and proteins³⁹⁻⁴² in a background of constant ionic strength, this approach does not seem to be suitable for the detection of metal ions such as Na⁺ or K⁺ in analytes with varying ionic strength. First, only analytes with a large electrochemical window can be measured. This is not a drawback for biological analytes which have a known composition. Secondly, the EGOFET-characteristics non-selectively depend on

the ionic strength/composition of the gating solution due to a modification of the electrolyte/semiconductor interface.

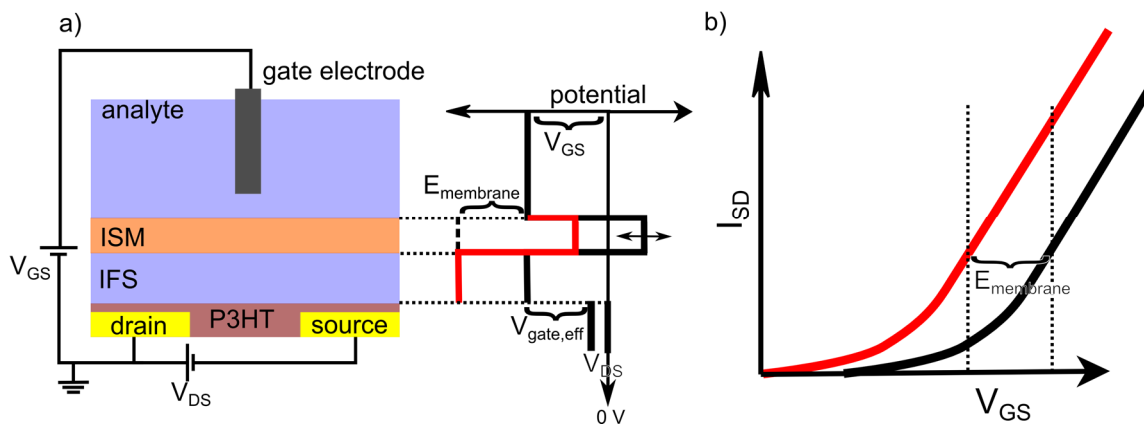


Figure 22: Illustration of the sensing mechanism: a gate potential is applied to the sample solution relative to the source contact. The effective gate potential ($V_{\text{gate,eff}}$) which drives the EGOFET is given through the sum of the gate (V_{GS}) and membrane potential (E_{membrane}). E_{membrane} stems from two Nernstian phase boundary potentials at the ISM/inner filling solution (IFS) and at the sample/ISM interface, each depending on the respective activity. If a transfer characteristic is recorded, the transfer curve would be shifted by the membrane potential as demonstrated in our recent publication²⁶ and as illustrated in b).

For that reason, a novel sensing concept is proposed. An illustration of this concept is shown in Figure 22 (a)). The EGOFET serves as a transducer and is in direct contact with an inner filling solution which is separated from the sample solution by the ISM. The sensing signal itself is given through the potential drop over the ISM, referred to as the membrane potential (E_{mem}). E_{mem} depends on the activity of target ion within the sample (a_{sample}) relative to the activity of target ion in the inner filling solution (a_{IFS}) in a Nernstian fashion: $E_{\text{mem}} = E_0 + \frac{RT}{zF} \ln\left(\frac{a_{\text{sample}}}{a_{\text{IFS}}}\right)$, E_0 is a constant, R the gas constant, z_i the valency of the analyte ion, F the Faraday's constant.⁸⁹ During operation, a gate potential is applied to the sample solution with respect to the source contact through an Ag/AgCl reference electrode. The potential of the inner filling solution, which actually drives the EGOFET, is given through the sum of the membrane potential and the gate potential, and is further on referred to as effective gate potential. As the ion concentration within the analyte is decreased, the membrane potential is increased leading to a higher effective gate potential and therefore also to a higher source drain current (Figure 22 (b)).

In contrast to other OFET sensor concepts such as organic electrochemical transistors, this approach is potentiometric and no direct modification of the organic semiconductor takes place, which leads to a higher overall device stability.²⁶

3.5 Ion selective sensing platform based on EGOFETs

To demonstrate the versatility of the concept, an H⁺ selective and a Na⁺ selective EGOFET are presented. The Na⁺ sensor was developed first and the results and implementation of the sensor is discussed in detail in the PhD thesis of Kerstin Schmoltner.⁶⁰ However, as this work formed the basis for the thereafter following publications, the most important results of this sensor are presented. The H⁺ sensitive sensor was a further development and is presented in detail within this work.

3.5.1 Na⁺ sensitive EGOFET[†]

The Na⁺ sensitive EGOFET was based on a state of the art ISM. Based on the discussion of section 3.4, an IFS with a high ionic strength was used (10⁻² M NaCl). The fabrication procedure is described in the experimental section 3.2. In a first approach, in order to demonstrate the sensitivity of the ion-selective EGOFET to Na⁺, the source-drain current was recorded at a constant gate and source-drain potential while the Na⁺ concentration in the water (analyte) was increased stepwise (see Figure 23 (a), V_{DS} = -0.1 V, V_{GS} = -0.2 V). As a sensitive response a source-drain current decrease of ~250-500 nA/dec (depending on the point of operation) was observed while varying the Na⁺ concentration between 10⁻⁶ M and 10⁻¹ M. The source-drain current decrease reflects the change in effective gate potential. The latter can be calculated by using the fitted transfer curve at V_{SD} = -0.1 V of the EGOFET, if the Na⁺ concentration in the inner filling solution and the analytes are equal. In this case E_{membrane} is zero and the transistor

[†] This work is discussed in detail in the PhD thesis of Kerstin Schmoltner⁶⁰ and is based on the work that has been published: K. Schmoltner, J. Kofler, A. Klug, and E.J.W. List-Kratochvil, *Adv. Mater.* **25**, 6895 (2013). The original text was written by K. Schmoltner in collaboration with the author.

characteristics are superimposable to a “simple” EGOFET without an ISM. Figure 23 (b) shows the calculated effective gate voltage versus the Na^+ concentration following a linear relation with a slope of 62 mV/dec which is in good agreement with the theoretically predicted value of 59.2 mV/dec, calculated from the Nernst equation at 25°C.

The flow cell was required to obtain a reversible sensor response and to lower the detection limit from 10^{-5} M Na^+ down to $\sim 10^{-6}$ M Na^+ .¹² This can be clearly seen by comparing the source-drain current before and after applying a flow of DI water through the cell (see Figure 23, first 300 s): If there is no flow, ions which diffuse out of the inner filling solution into the analyte lead to an artificially increased ion concentration in the vicinity of the ISM (also see section 2.4).⁹⁷ Hence, the effective gate potential and therefore also the source-drain current is decreased. Note that, these low Na^+ concentrations and the resulting high effective gate voltages (here < -400 mV) lead to significant drifts (decreasing channel currents, see Figure 23 (a), 200-400 s). This is in accordance with the results obtained in case of the H^+ sensor discussed in section 3.5.2. In section 3.5.2 detailed stability investigations were carried out. This drift can in principle be avoided by keeping the effective gate potential constant at a stable operating point, regardless of the ion concentration in the analyte. An appropriate read-out circuit was later on implemented in the H^+ sensitive EGOFET (see section 3.5.2). The reported lowest detection limit and response time of about ~ 30 s is not a property of the ion-sensitive EGOFET itself, but is rather determined by the flow cell used (high dead volume).

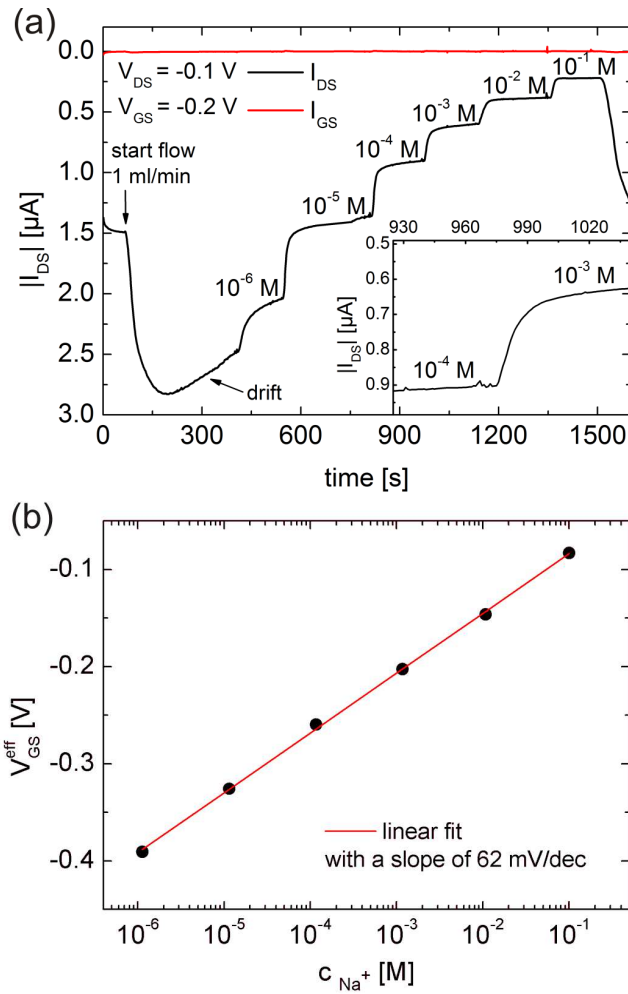


Figure 23: a) Source-drain current response to increasing Na⁺ concentration of a typical ion-sensitive EGOFET with a PVC ion-selective membrane, exhibiting a response time of ~30 s (see inset). b) Calculated effective gate potential versus Na⁺ concentration.

3.5.2 H⁺ selective EGOFET^m

As a further development and to prove the versatility of the concept a pH sensitive EGOFET was investigated. Glass electrodes, having a relatively high selectivity and a wide response range, are the most widely used devices for pH measurements in various samples. However, they also have a number of limitations, including high electrical resistance and brittleness. Particularly for applications in bioanalysis such as in-vivo blood pH measurements, electrodes based on ionophore-doped liquid polymeric membranes are often preferred over traditional glass electrodes.⁹¹ Here we demonstrate a novel, selective and reversible EGOFET based pH sensor for a broad detection range between pH 3 and pH 12. As described in section 3.4, first it is verified whether the IFS is appropriate with respect to sensing and electrical performance. Subsequent stability investigations show the importance of operating the EGOFET at a constant low-voltage working point. This was ensured by the implementation of a new dynamic measurement protocol which guarantees a constant effective gating potential independent of the sample composition.

3.5.2.1 Inner filling solution

As described in section 3.4, in order for this sensor concept to work, the inner filling solution of the sensor has to fulfill two conditions. First, the inner filling solution has to have a large electrochemical window which ensures a polarizable interface and thus a negligible leakage current (I_G) between the transistor and the gate. The second condition is related to the ISM: In order to guarantee a stable pH value and to avoid membrane potential drifts, pH buffers have to be used as an inner filling solution. Otherwise, processes such as co-extraction of counter-cations into the membrane and resulting diffusive transmembrane fluxes of H⁺ lead to undesired pH value change of the inner filling solution.^{12,65,67,68,70,178,179} Furthermore, solvent polymeric membranes are permeable to CO₂ and other small neutral molecules which can also influence the pH value of the inner filling solution.^{99,180,181}

^m The section is based on the work that has been published: J. Kofler, K. Schmoltner, A. Klug, and E.J.W. List-Kratochvil, Appl. Phys. Lett. 193305 (2014).

Here, a standard 0.2 M phosphate buffer solution (PBS, pH 7), as commonly used in conventional ISE-setups, was employed as an inner filling solution. To verify whether the first condition is fulfilled, the EGOFET performance was studied without an ISM, i.e. the Ag/AgCl reference electrode was in direct contact with the inner filling solution (see inset in Figure 24). Figure 24 depicts the corresponding transfer (a) and output (b) characteristics, showing a good overall performance (on-current $\sim 1.7 \mu\text{A}$ and on/off ratio $\sim 2 \times 10^2$). These results are comparable with other values found in literature^{26,43,182} and prove the suitability of this buffer as a gating electrolyte. To demonstrate the effect of an inner filling solution which does not fulfill the aforementioned conditions (i.e. small electrochemical window), ascorbic acid (10^{-2} M) was added to the PBS. Figure 24 (c) shows the source-drain current (left) and gate current/leakage current (right) of an EGOFET gated with pure PBS, subsequently with a phosphate buffer containing ascorbic acid and finally again with pure PBS. Similar measurements were performed at higher gate potentials exhibiting the same trend (see Figure 25). In case of ascorbic acid, the leakage current (open circles) increased by two orders of magnitude (from 10^{-10} to 10^{-8} A) and the channel current decreased accordingly. However, after replacing the ascorbic acid containing buffer with pure PBS again, the initial good transistor characteristics and low leakage currents were restored. Interestingly, the channel currents (at $V_{\text{DS}} = -100$ mV, $V_{\text{GS}} = -200$ mV) were slightly higher compared to the first measurement, indicating the absence of any degradation of the P3HT.

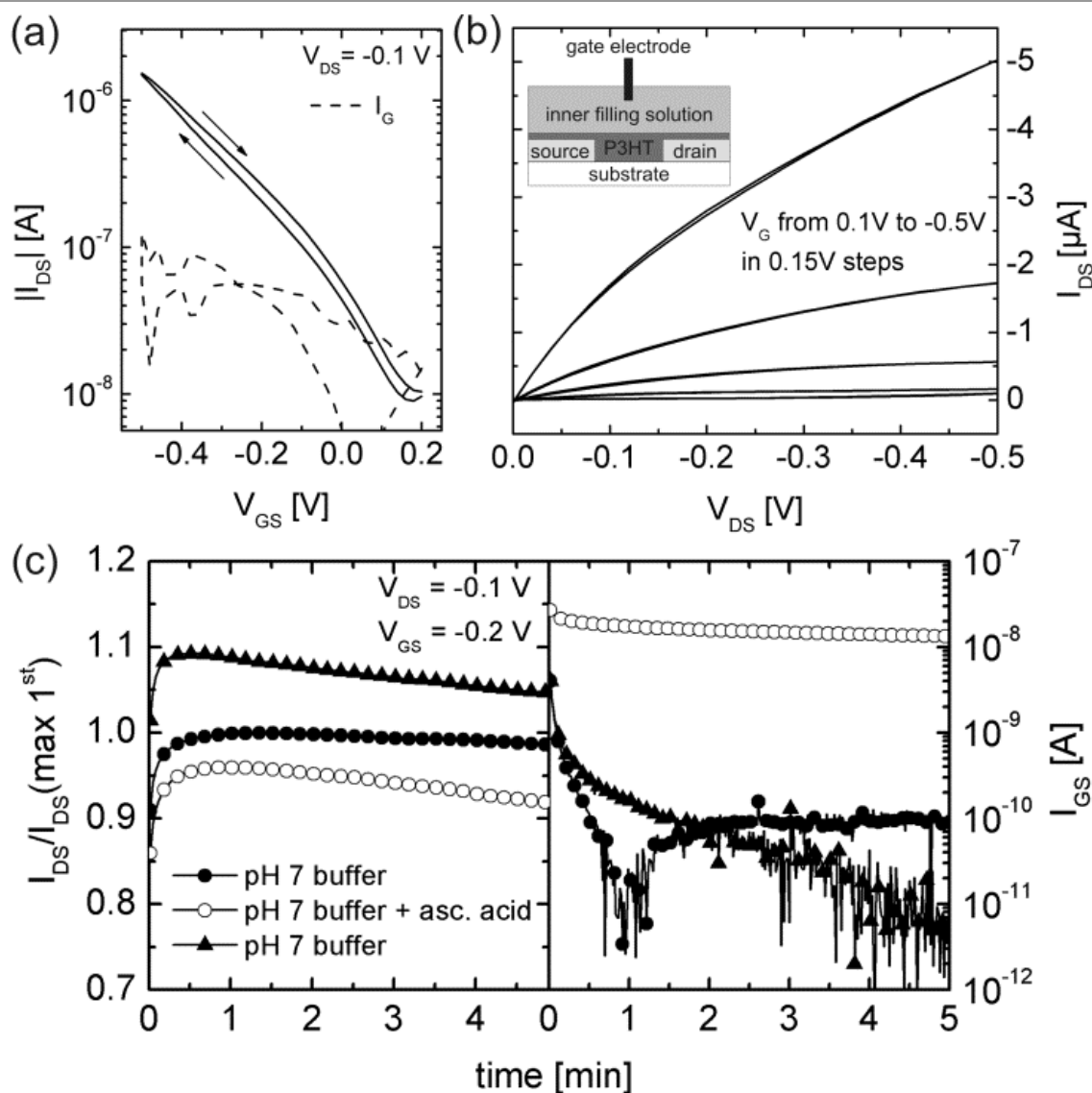


Figure 24 Transfer (a) and output (b) characteristics of EGOFETs gated with a 0.2 M phosphate buffer (PBS, pH 7); (c) source-drain current (left) and leakage current (right) as a function of time: first, the EGOFET was gated with PBS (filled circles), subsequently with PBS containing ascorbic acid (open circles) and finally again with PBS (filled triangles).

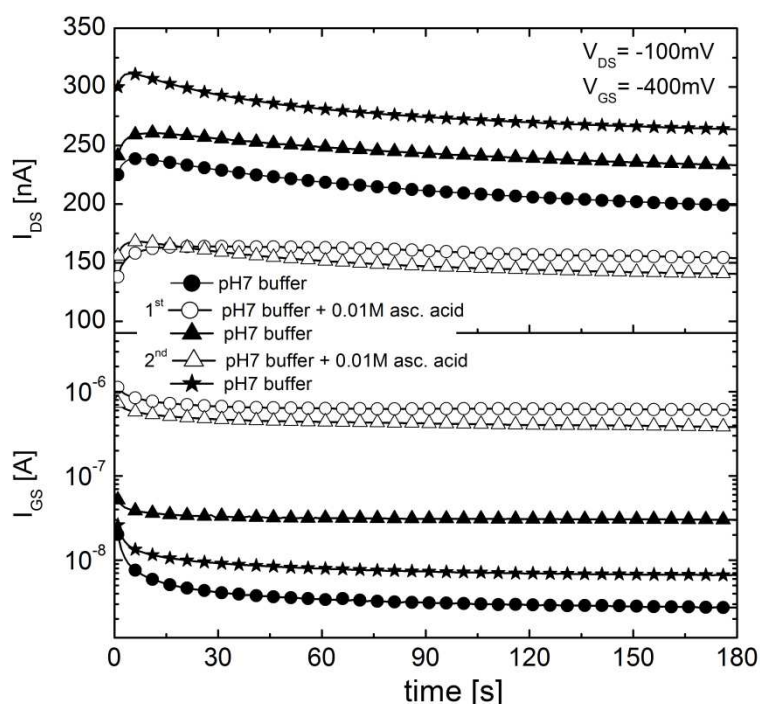


Figure 25: Source-drain current (top) and leakage current (bottom) as a function of time: first, the EGOFET was gated with pure PBS (filled symbols), subsequently with PBS containing ascorbic acid (open symbols) and finally again time with pure PBS (filled symbols)

The observed high steady-state gate currents can be ascribed to the ascorbic anion which is easily oxidized at the P3HT/electrolyte interface upon applying a negative potential to the gate electrode. Thus, the phosphate buffer containing ascorbic acid is a good example of a solution with a small electrochemical window. Another negative side effect at high gate currents can be a polarization of the membrane (also see section 3.3.2.3),^{57–59,183} which can lead to deviations from the linear Nernstian behavior and to a higher lowest-detection limit. These results highlight the importance of an appropriate inner filling solution and the separation of the EGOFET from the sample solution.

3.5.2.2 Stability investigation

EGOFETs typically exhibit drifts.²⁶ For that reason, stability investigations were carried out by measuring the drain and leakage currents at different gate voltages while keeping the source-drain potential constant. Figure 26 (a) shows the relative source-drain current changes for stepwise increased gate voltages. At gate voltages of -200 mV, -400 mV and -600 mV negligible source-drain current drifts are observed within the measurement period of 8 min.

High gate potentials of -800 mV lead to a significant channel current decrease of about 60% within 8 min indicating an irreversible degradation of the transistor. This is also confirmed by a significantly lower channel current of ~ 80 nA in comparison to the initial reference measurement at -200 mV (~ 450 nA). Moreover, the leakage current did not change, except during the first few seconds due to repolarization/charging and is typically ~ 1 nA (see Figure 26 (b)).

The reason behind the observed channel current degradation is believed to be attributed to electrolysis and subsequent degradation of P3HT through oxygen oxidation^{184,185} and decrease of the charge carrier mobility due to ions/water molecules which diffuses into the organic semiconductor (also see section 3.3.1).¹⁸⁶

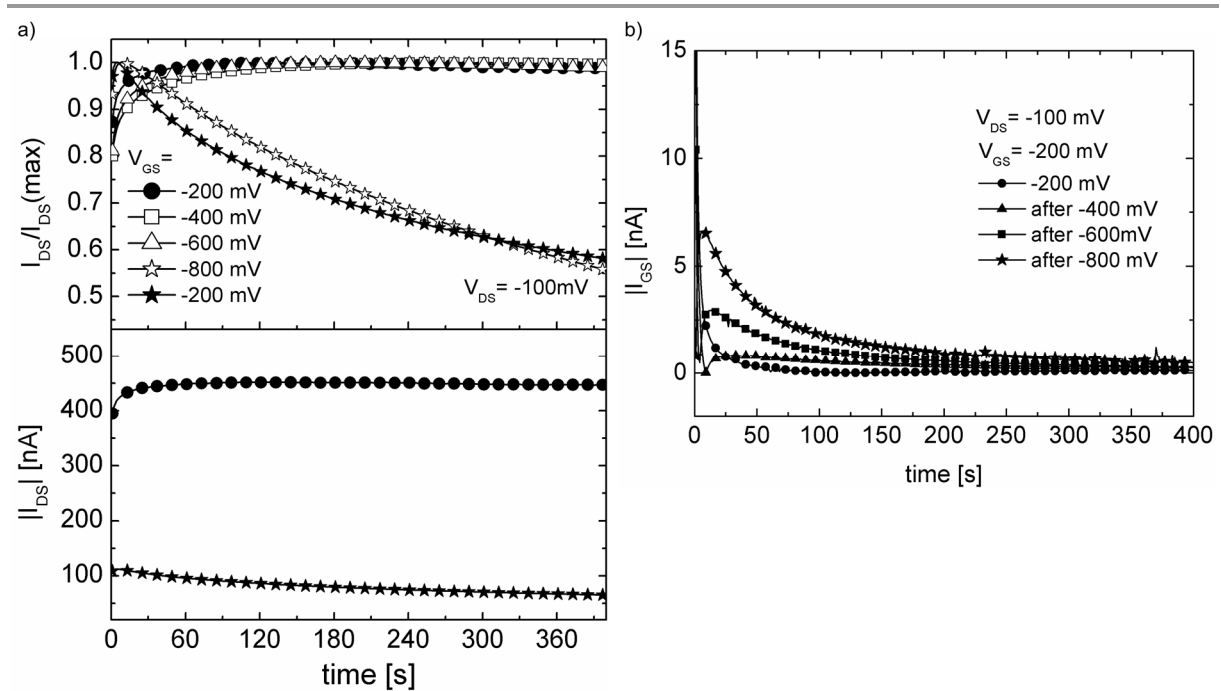


Figure 26: a) Relative change of the source-drain current of an EGOFET gated with PBS as a function of time for different applied gate voltages (top): Open symbols represent measurements with stepwise increased gate voltages (-400 mV, -600 mV, -800 mV), closed symbols represent the subsequent reference measurements at -200 mV. The curves were normalized with respect to their maximum current. (bottom) Absolute change of source-drain current at $V_{GS} = -200$ mV before and after applying elevated gate potentials for 8 min (> 600 mV). b) Source-gate current as a function of time of a typical EGOFET gated with a phosphate buffer (pH7) after applying increased gate potentials: the leakage current was recorded at constant potentials of: $V_{GS} = -200$ mV and $V_{DS} = -100$ mV.

3.5.2.3 Constant current operation mode

Regardless of the exact degradation mechanism, the results demonstrate that EGOFETs must be operated well below -600 mV in order to guarantee a stable operation. As the state of the art H⁺ selective ISM membrane used in this work exhibits a broad detection range between pH 3 and pH 12 with a near Nernstian response of 52 mV/pH and a high selectivity⁹¹, the membrane potential can vary for more than 400 mV. Consequently, in case of an IFS with a pH 7, the membrane potentials can vary for more than +/- 200 mV. If the EGOFET is operated at a gate potential of -400 mV, the membrane potential can either lead to irreversible degradation ($V_{\text{gate,eff}} = -600$ mV) at pH 12 or negligible source-drain currents ($V_{\text{gate,eff}} = -200$ mV) at pH 3. For that reason, ion selective EGOFETs have to be operated at a constant working point and consequently also at a constant source-drain current. This implies that the effective gate potential has to be independent of the membrane potential and thus also ion activity within the sample. This can be achieved by adjusting the gate voltage through a feed-back loop which keeps a constant source-drain current constant. The measurement signal is then given by the gate potential change required to keep the same source-drain current. Other than the operational stability, this operation mode has another benefit: The measured signal corresponds directly to the membrane potential change which eases data analysis. As a result, it is not necessary to record the whole transfer curve in order to correlate the source-drain current changes with membrane potential changes/concentration changes. As in case of conventional ISEs, two solutions with known pH values are sufficient to calibrate the sensor.

The feedback loop was implemented using two Keithley 2400 SMUs which were controlled in real time via VBA-Excel. One SMU (source-drain SMU) measured the current at a constant source-drain voltage. The second one was connected to the gate electrode (gate SMU). Both SMUs shared a common ground.

3.5.2.4 Sensitivity and calibration

The pH calibration curves of a boric/citric acid solution with a molarity of 10 mM each, are shown in Figure 27 (a). Additionally, a calibration of a 5 mM boric/citric acid solution with and without a 10 mM NaCl background was recorded. The pH value was adjusted by titrating with

a NaOH solution. As a result, the Na^+ concentration is increased at high pH values depending on the initial molarity of the citric and boric acid. Despite of a high concentration of the interfering alkali metal ion Na^+ , the response curve reveals a near Nernstian slope between pH values 6 and 12, with a slope of 52 mV/dec. There is only a limited influence of interfering Na^+ ions at high pH values where the slope is slightly decreased. This is due to the high selectivity of the membrane over alkali metal ions.⁹¹ At low pH values ($< \text{pH } 6$), anion interference leads to a deviation from the Nernstian slope ($\sim 25 \text{ mV/dec}$).⁹¹ The anionic interference is increased with increasing anionic strength, i.e. with increasing NaCl or citric acid concentration (see section 2.4.3/2.4.5). Figure 27 (b) shows the response curve of the sensor device exposed to a pH 12.2 buffer-solution and subsequently to a pH 2.7 buffer-solution. The response is reversible and even long continuous measurements of 30 min did not show any significant drifts. The response time of this device is limited by the time necessary to flush the flow cell with the buffer solution.

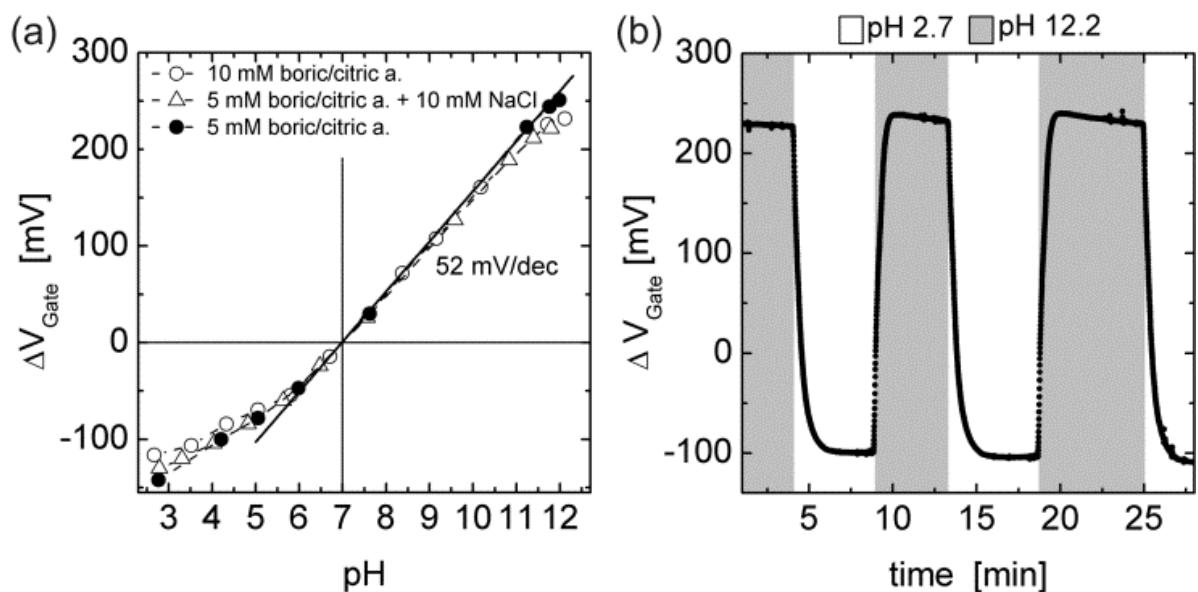


Figure 27: (a) pH value calibration curves: gate voltage change as a function of the pH value; (b) response curve upon a pH-value change from pH 2.7 to pH 12

3.6 Summary & conclusion

In conclusion, a novel sensor platform based on electrolyte-gated OFETs for selective and reversible ion detection was successfully demonstrated. The novelty of this design compared to conventional ISFETs is the direct contact between the electrolyte and the semiconductor without the use of a solid dielectric, making low-voltage operation in aqueous media feasible. Furthermore, this architecture benefits from a modular approach, allowing for the detection of various ions simply by choosing an appropriate ion-selective membrane. To demonstrate the versatility of this concept a pH and a Na⁺ sensitive sensor based on highly selective state of the art ISMs was successfully demonstrated.

In order to obtain a general picture of ion selective EGOFETs, the requirements imposed on the gating electrolyte, the gate electrode and the semiconductor-electrolyte interface were investigated first. It is crucial that the whole gate potential actually drops at the semiconductor-electrolyte interface and that the leakage current flowing between the gate and the semiconductor is as small as possible. Consequently, the semiconductor – electrolyte interface should be polarizable. The electrolyte – gate interface, on the other hand must not be polarizable, as long as its capacity is larger than that of the EGOFET including the source/drain contacts. However, if analytes with varying ionic strength are targeted, a non-polarizable Ag/AgCl reference electrode (or other equivalent reference electrodes) is required to apply a concentration independent gate-potential. Furthermore, as the characteristics of the EGOFETs change non-selectively with the ionic strength of the gate electrolyte, the EGOFET should be in contact with a constant, well defined inner filling solution which is separated from the sample by an ISM. Accordingly, the sensing signal which solely relies on the highly selective ISM, is amplified and transduced into a low impedance output signal by the EGOFET.

Even though all physical requirements are met, EGOFETs typically exhibit irreversible degradation, if the gate potential exceeds a certain level. Due to a dynamic measurement protocol which operates the EGOFET at a constant and stable low-voltage working point

independent of the sample composition, a broad detection range between pH 2.7 and pH 12 was possible. The response of the sensor was near Nernstian in the range between pH 6 and 12 and a sub-Nernstian response between pH 2.7 and 6. The presented potentiometric sensor based on a Na⁺ sensitive PVC membrane showed a Nernstian behavior for a broad detection range between 10⁻⁶ M and 10⁻¹ M Na⁺.

These results constitute an important step towards a low-cost integrated sensor array for multiple ion detection facilitated by a facile integration of different state-of-the-art ISMs, being of high relevance for biomedical diagnostics, food-monitoring, industrial process- and water-control.

4. ALL ORGANIC PAPER BASED ION SENSING PLATFORM

The content of this chapter is based on the work that has been published and was partly modified:

A paper based, all organic, reference electrode free ion sensing platform

J. Kofler, S. Nau, Emil J.W. List-Kratochvil

Accepted by Journal of Chemical Materials B

Reproduced with permission from © Royal society of chemistry

Contribution: The author carried out all experimental work and wrote the manuscript. The manuscript was finalized with the co-authors

The aim of this chapter is to present a flash-chronopotentiometric, all organic and reference electrode free K^+ sensing platform on paper. This unique platform is based on two identical PEDOT:PSS-based solid contact ISEs (SC-ISEs) fabricated on a paper sheet by simplest means (see Figure 28 a). The novelty of the proposed measurement method is that the commonly used reference electrode is replaced by a second, identical ISE. To measure the concentration of the target ion a current pulse is forced through the ISEs while the potential difference between the ISEs is measured at a fixed measurement time t_{meas} (see Figure 28 b, V_{SENS}). The current forces an ion flux through the sample and through both ISEs. The ISE operated in forward direction (ISE_{IN}), extracting target ions into the membrane from the sample side, will exhibit the typical potential jump upon target ion depletion (see Figure 28 b V_{IN} and Figure 28 c). The ISE operated in backward direction (ISE_{OUT}) just shifts the potential difference between the ISEs by a constant value, and thus does not disturb the measurement signal (see Figure 28 V_{OUT}). Since both ISEs are identical, the equilibrium potentials of both ISEs are equal with

respect to the analyte and the ISEs can be regenerated simply by shortening them after each measurement.

Consequently, the second ISE serves two purposes. Firstly, it provides a reference potential during the measurement pulse and secondly it allows to regenerate the ISEs without using a reference electrode. Additionally, mutual potential drifts of the ISEs cancel out, leading to a very stable and reproducible response.

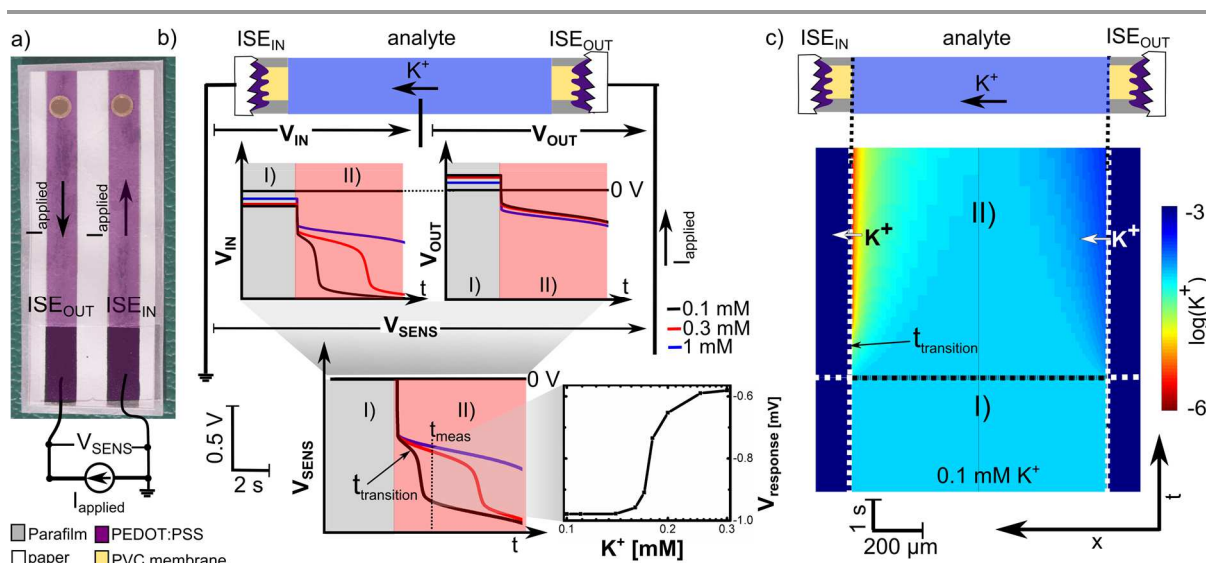


Figure 28 a) An image of a fabricated sensor and its circuit diagram (the materials are additionally dyed for a better understanding); b) Illustration of the sensing principle: A measurement cycle consists of a regeneration (I, both ISEs are shortened) a constant-current measurement pulse (II) and an inverse regeneration pulse (III, not shown). The membrane potentials of ISE_{IN} (V_{IN}), ISE_{OUT} (V_{OUT}) and the potential difference between the ISEs (V_{SENS}) during a measurement cycle at different K^+ concentrations (0.1 mM black, 0.3 mM red, 1 mM blue), is shown on the top left, top right and left bottom. To measure the concentration a constant-current pulse is applied ($I_{applied}$) while the potential V_{SENS} is recorded at a fixed time t_{meas} . The according response ($V_{response}$) is shown on the bottom right; c) the numerically calculated K^+ concentration during a measurement cycle (bulk analyte concentration 0.1 mM K^+).

To generalize the proposed sensing method and to demonstrate that the sensing signal solely arises at the ISM-sample interface, two conventional ISEs containing aqueous inner filling solutions were used in a first step. The results were modelled by numerical calculations, gaining insight into the response mechanisms and revealing the limits of the measurement-parameters, namely the maximum current density and pulse time. In a second step, the response of the all organic PEDOT:PSS-based SC-ISEs is investigated, exhibiting the same

characteristics as the conventional setup. In accordance with the results reported by S. Makarychev-Mikhailov et al.²⁷, a 20-fold sensitivity enhancement compared to classical potentiometric measurement was obtained. Furthermore, repeated measurements over a period of 3 months reveal that the response signal was stable for at least 3 months.

4.1 Introduction into the sensing concept

Generally, chronopotentiometric measurements are based on ion transfer at immiscible electrolyte solutions (ISM, aqueous analyte).⁵ For that reason, to describe the response of a chronopotentiometrically operated ISM, all transferring ions within the analyte and the ISM have to be considered. Highly ion selective plasticized PVC membranes contain an ionophore (L), anionic sites (R^-) and a background electrolyte (B^+/B^-) (see Figure 29 a). These anionic sites fix the concentration of ionophore-target ion concentration (LK^+) and the background electrolyte ensures a high conductivity of the membrane.⁵ However, the sensing mechanism is chemically based on the recognition of an aqueous target ion by an ionophore, which thermodynamically facilitates selective ion transfer (IT) into the membrane. The strong ion - ionophore interaction overcomes the unfavorable free energy of transfer and hydrophilic ions are extracted into the hydrophobic membrane developing a Nernstian phase boundary potential in equilibrium²⁸. The Nernstian phase boundary potential is used as a measurement signal for potentiometric measurements, limiting the response to a sensitivity of ~ 59 mV per 10 fold activity change in case of a monovalent ion. Upon applying a current pulse, ions are forced into the membrane on the front side of ISE_{IN} and out of the membrane on the back side of ISE_{OUT} . As the transfer of the target ion (K^+) into the membrane is facilitated by the ionophore, exclusively K^+ ions are extracted into ISE_{IN} . Likewise, K^+ ions are extracted into the analyte at ISE_{OUT} (mechanism 1' in Figure 29 b). At the beginning of the pulse, as long as the ion concentrations at the interface are proportional to the bulk ion concentrations, the response obeys a near-Nernstian slope towards the respective activity (see theory section 2.4.5).^{29,30} At larger pulse times, the target ion is depleted. The square root of the time when the target ion depletes (transition time) is linearly proportional to the concentration and

inversely proportional the current density. As soon as the target ion depletes within the sample, other positively charged ions have to be transferred into the membrane or negatively charged ions within the membrane have to be extracted into the analyte (see mechanism 2' in Figure 29). As the free energy of transfer of these ions is higher, a larger potential has to be applied to keep the ion flux through the ISM-analyte interface constant. The magnitude of this potential change (potential jump) is directly related to the selectivity of the membrane; i.e. to the difference of the free energy of transfer between the target ion and the alternatively included/extracted ion. However, similar depletion effects can also occur within the membrane. The freely available ionophores (L) at ISE_{IN} or the complexed target ions (LK⁺) at ISE_{OUT} can deplete earlier than the target ion. Likewise, alternative ions are extracted into the analyte or the membrane (see Figure 29 b, mechanisms 3' and 4').

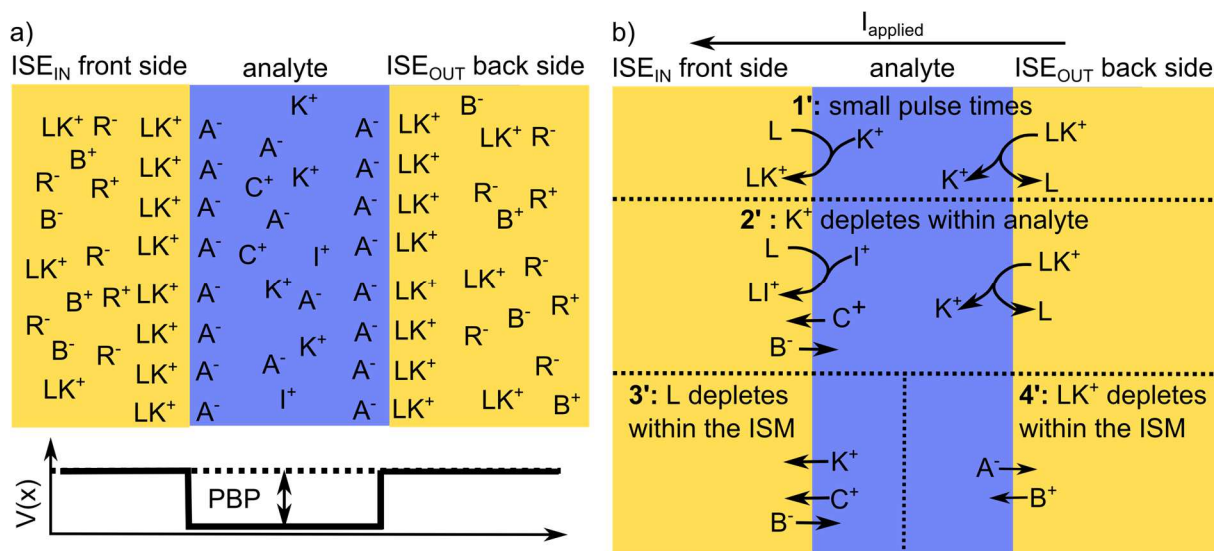


Figure 29: a) Illustration of the ions present within the membrane/analyte and the formation of the Nernstian phase boundary potential (PBP) in equilibrium. K⁺ corresponds to the target ions, I⁺ to the interfering ions, C⁺/A⁻ to background cations/anions in the analyte, R⁻ to anionic sides in the ISM and B⁺/ B⁻ to background cations/anions in the ISM, L is the freely available ionophore and LK⁺/LI⁺ is the ionophore-K⁺/L⁺ complex; b) illustrations of possible mechanisms occurring at the front side and backside of an ISM during a current pulse (for further details see text).

4.2 Experimental

4.2.1 Chemicals and Materials

The ISM contained the cation exchanger sodium tetrakis[3,5-bis(trifluoromethyl)phenyl]borate (NaTFPB) (15 mM/kg), the potassium ionophore I (valinomycin, 5 mM/kg) and the background electrolyte tetradodecylammonium (TDA) tetrakis(4-chlorophenyl)borate (TCIPB) (ETH 500, 20 mM/kg). The membrane matrix contained high molecular weight polyvinyl chloride (33 wt%, Selectophore grade) and the plastisizer 2-nitrophenyl octyl ether (2-NPOE) (67 wt%). The ISM cocktails were dissolved in tetrahydrofuran (THF) and drop casted onto a confined glass sheet. The drop-cast membrane was allowed to dry overnight at ambient conditions in a saturated THF environment and was peeled off for further implementation. The final thickness of the ISM was $\sim 150 \mu\text{m}$. All of the chemicals mentioned above were obtained from Fluka Sigma- Aldrich and were used as received. The saline solutions were prepared with KCl (>99.0%), CaCl_2 (>99.0%) Na_2SO_4 (>99.0%) and deionized water (grade).

4.2.2 Sensor fabrication

First, the design of the PEDOT:PSS electrodes was printed in black & white on a copy-paper (copy paper "Blustar" 80 g/m²). The PEDOT:PSS electrodes are simply structured by drop casting PEDOT:PSS (CleviosTM PH 1000) onto these printed electrodes. As the inkjet printing paper is initially hydrophobic and the water based ink hydrophilic, PEDOT:PSS is confined to the hydrophilic printed areas. After drop casting PEDOT:PSS, the paper is transferred into an oven and dried for 1 h at 150 °C. The resistance of the PEDOT:PSS electrodes (1 cm wide and 5 cm long) is in the range of 30 k Ω . Subsequently, the paper is made water impermeable by laminating a Parafilm M[®] at $\sim 100^\circ\text{C}$ onto the top and the bottom side of the paper. Prior to lamination two holes (2 mm and 3 mm diameter), which accommodate the ISMs, were punched into the Parafilm M[®] using a biopsy punch. The ISMs are cut out of a bigger ISM sheet using a biopsy punch with a diameter of 4 mm. The sensor is finalized by gluing these ISMs onto the PEDOT:PSS electrodes. This is done by drop-casting 5 μL THF onto the ISM and

immediately thereafter placing the ISM with the THF side first onto the PEDOT:PSS electrodes. THF partly dissolves the ISM leading to a conformal contact between the ISM and the PEDOT:PSS electrodes and to a tight sealing at the ISM edges. After gluing, the sensor is left to rest for ~ 12 h in order to let the residual THF evaporate. After fabrication, the sensors were conditioned for ~ 5 h in a 1 mM KCl solution to exchange the Na^+ ions of the NaTFPB within the membrane with targeted K^+ ions. After the conditioning the sensors were blow dried and subsequently stored in dark under ambient conditions until measurement. Note that the ISEs were spaced 5 mm apart in order to avoid cross talk.

4.2.3 Measurement setups/procedures

Current and potentials were measured using a B1500A Parameter analyzer. To carry out potential measurements, the source-measurement units were operated as 0 A constant current sources while measuring the potential. To apply a current pulse, the current was set to the corresponding value and the potential was measured. To carry out the reference measurements (conventional setup) two custom made ISEs were used. The inner filling solutions (IFS) (10 mM KCl in a 10 mM CaCl_2 background) of the ISEs were contacted with Ag/AgCl reference electrodes, whereas the PEDOT:PSS based solid state ISEs were contacted by two alligator clamps. In order to investigate the ISEs separately, an additional reference electrode contacting the analyte, was used. The reference electrode was placed half way between the ISEs. A measurement cycle was carried out as follows. First, a base line potential-pulse is applied (0 V to both ISE terminals) while the current flowing between the ISEs is monitored. This current should ideally be 0 A in equilibrium. This base line pulse was applied for 6 min in between the current pulses. Subsequently, a current pulse and a reverse regeneration pulse was applied and the potential was monitored at all three reference electrodes. No working electrodes were used and the currents applied during the measurement cycles were passing through the reference electrodes contacting the IFS. The recorded potentials are therefore biased by a current induced potential drop at the reference electrodes. However, these potentials drops are constant and therefore solely result in a constant offset which does not influence the measurement signal as such. Furthermore, note

that all measurements were carried out using excess background electrolytes to avoid migration effects within the analyte.

4.3 Results and discussion

First, to generalize the measurement method, two conventional ISEs containing an aqueous inner filling solutions (liquid contact), were used. Liquid contacts are well-defined system which can be described numerically. Hence, it is possible to identify the mechanisms and the operational limits of the sensor. Furthermore, it is verified that the sensing signal solely arises at the ISM-sample interface and is not at the PEDOT:PSS solid contact, implying the possibility to use this measurement method for various other ISEs. In the thereafter following step, the PEDOT:PSS-paper based SC-ISEs are characterized and the sensitivity and long term stability of the sensing platform is demonstrated.

4.3.1 Conventional setup

The response curves and the applied currents at concentrations of 0.01, 1, 10 mM KCl in a 10 mM CaCl₂ M background of a measurement setup using two conventional ISEs are shown in Figure 30. First, both ISEs are forced to 0 V which is equivalent to shortening both ISEs (see region I in Figure 30). As both ISEs are identical they ideally have the same equilibrium potentials with respect to the analyte. Consequently, only a negligible faradaic current is flowing in between the ISEs (see Figure 30 (b) region I). After an equilibration time of 5 minutes, a current is applied to the ISEs, forcing K⁺ ions from the analyte into the membrane on one side and vice versa on the other side (see region II in Figure 30). The potential difference in between the ISEs corresponds to the measurement response which strongly depends on the target ion concentration within the analyte. After this first current pulse a second inverse pulse, with identical but negative current is applied. This leads to a faster regeneration of the membrane²⁵ (region III). After the measurement, both ISEs are forced to 0 V to regenerate the ISEs. During the regeneration, the current flowing between the ISEs decreases until it eventually reaches a very small steady state current (~0.7 nA/mm²).

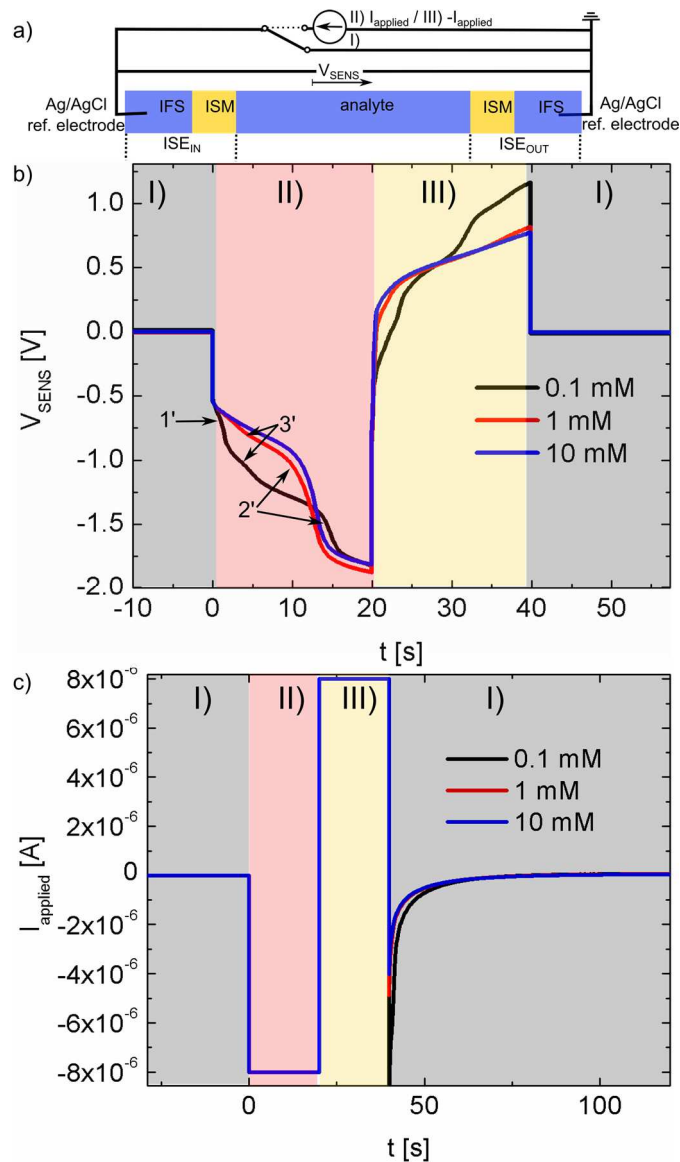


Figure 30: a) Simplified circuit diagram of the measurement setup showing two ISEs with identical inner filling solutions (IFS) which are operated in series. In between the measurements, the ISMs are regenerated by applying 0 V to both ISEs. This is equivalent to a shorting, which is illustrated by a switch in position I); during the measurement pulse and the reverse pulse the switch is in position II) or III) respectively; b) Sensing signal (V_{SENS}) measured in analytes at concentrations of 0.1 mM (black), 1 mM (red), 10 mM KCl (blue) and in an 10 mM CaCl_2 background during a full measurement cycle consisting of a regeneration (grey region I), a measurement pulse (red region II) and an inverse pulse (yellow region III). The observable transition times are marked with numbers 1'-3'. The applied current density was $0.4 \mu\text{A}/\text{cm}^2$. The corresponding currents are shown in c).

The remaining steady state current can be attributed to a small potential difference between the reference electrodes, non-idealities of the membranes or to the measurement setup itself (potential differences as small as of ~ 0.4 mV are sufficient to explain this current). However, currents of these small magnitudes are not sufficient to perturb the ISM and the thereafter following measurements at concentrations examined within this work.

There are three different potential jumps observable in Figure 30 b. In order to ensure that the sensing signal solely depends on the target ion concentration, it is crucial to identify the origins of the potential jumps. For that reason each ISE was investigated separately in various background electrolytes by monitoring the potential of the analyte with an Ag/AgCl reference electrode. The experimentally measured as well as numerically calculated response curves of ISE_{IN} at concentrations of 0.1, 1, 10 mM KCl in an 10 mM CaCl₂ and a highly interfering 10 mM NaCl background are shown in Figure 31. These two background cations represent two extremes; Ca²⁺ is very hydrophilic and non-interfering ion, whereas Na⁺ is one the major interfering ions (in case of the valinomycin ionophore). At the end of the regeneration the membrane potential depends on the concentration within the electrolyte in a near Nernstian fashion (56 mV per 10 fold activity change, see Figure 31, region I). This Nernstian offset at the beginning of the pulse results in a concentration dependent shift of the response curves of a single ISE, even before a potential jump has occurred. As two ISEs are operated in series, this potential shift cancels out in the final response curve (see Figure 28 (d) and Figure 30, region I). The inset of Figure 31 (a) shows the response curves which are corrected for the Nernstian equilibrium potential at the beginning. These corrected response curves are not noticeably concentration dependent as long as no characteristic potential jump is observed (refer to section 4.3.2 for details). The first potential jump is observed at a concentration of 0.1 mM K⁺ in a CaCl₂ electrolyte (point 1'). In case of the NaCl electrolyte the magnitude of this potential jump is not as pronounced and a second potential inflection is observed at larger pulse times (point 2*). At K⁺ concentrations of 1 mM and 10 mM one potential jump is observed in both background electrolytes (point 2').

Evidently, the numerical solutions of the NNP equations agree qualitatively with the response curves obtained. According to the numerical solutions of the NNP equations, the potential inflection in point 1' is due to the depletion of the target ion within the aqueous sample (see Figure 31 (c)). In case of the NaCl background, interfering Na⁺ ions can easily be extracted into the membrane as soon as the K⁺ ion depletes within the aqueous layer. Whereas in case of the CaCl₂ background, due to the high hydrophilicity of Ca²⁺, TCIPB⁻ ions (background electrolyte of the membrane) are forced from the membrane into the water. The extraction of TCIPB⁻ requires a higher potential than the assisted ion transfer of Na⁺. This is the reason why the magnitude of the potential jump is lower in case of the highly interfering NaCl background. The second inflection in point 2* can be ascribed to ionophore depletion within the membrane. As soon as the freely available ionophores deplete at the membrane surface, the assisted ion transfer gets halted. As Na⁺ is very hydrophilic, primarily TCIPB⁻ ions are extracted from the membrane into the water. The same mechanism is also responsible for the potential inflection at point 2'. At high K⁺ concentrations (1 mM and 10 mM) the ionophore depletes, leading to a potential inflection which is identical to the one observed at point 2*.

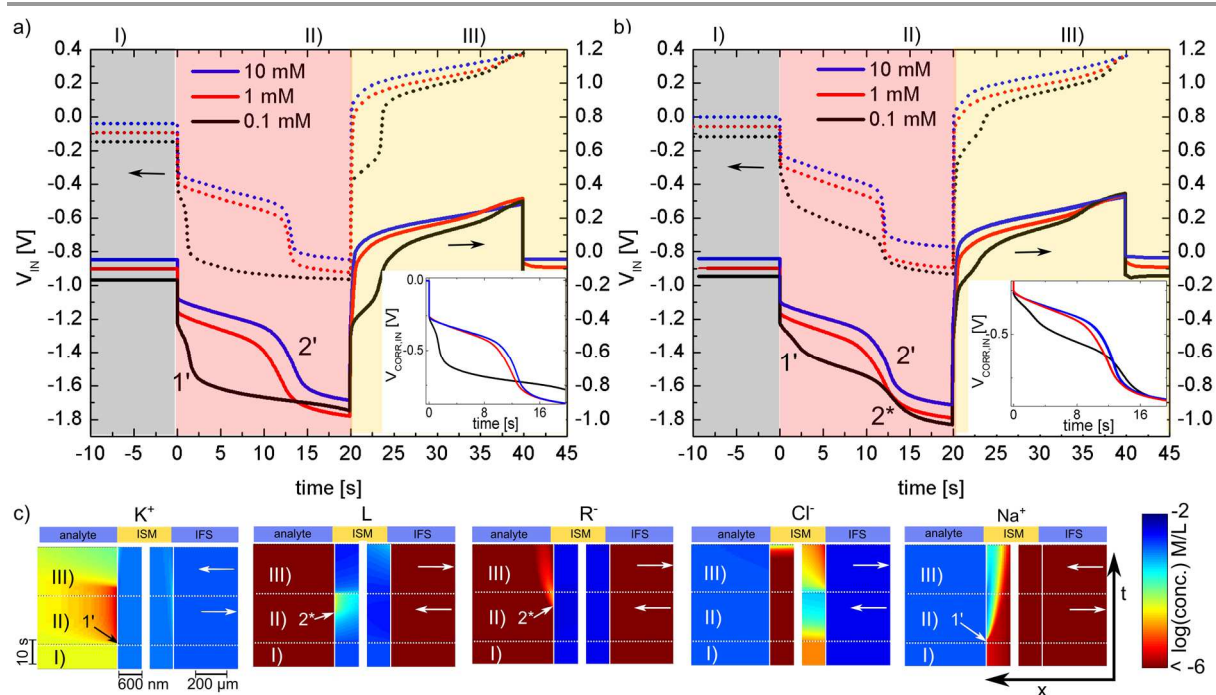


Figure 31: Measured (solid) and numerically calculated reponse (dotted) of ISE_{IN} during a measurement cycle at concentrations of 0.1 mM, 1 mM and 0.01 mM K^+ in a 10 mM $CaCl_2$ background (a) and a 10 mM NaCl background (b). The insets show the corrected potentials ($V_{IN}(t) - V_{IN}(t = -5\text{ s})$). The characteristic transition times are marked with numbers (for details see text). The applied current density was $0.4\ \mu\text{A}/\text{mm}^2$. c) Calculated concentration profiles at the interfaces of the relevant ions during a measurement cycle at a concentration of 0.1 mM K^+ in a NaCl background. The time and location where characteristic transitions occur are marked with numbers (for details see text). For better visibility, the x-axis are scaled differently for each ion in the membrane as well as in the aqueous solutions.

The experimental as well as the numerically calculated response curves of ISE_{OUT} in an analyte containing 0.1, 1, 10 mM KCl in an 10 mM NaCl and 10 mM Na_2SO_4 background are shown in Figure 32. This time the anion is drawn towards the membrane. This is why an alternative anion was studied. SO_4^{2-} is extremely hydrophilic (on the right in the Hoffmeister series) and will therefore require a significant higher potential to be extracted into the membrane than Cl^- . As in the case of ISE_{IN} , the corrected response curves do not depend noticeably on the target ion concentration or on the background electrolyte as long as no potential jump is observed (at current pulse times smaller than 2 s, for details refer to section 4.3.1.1). At higher pulse times and low K^+ concentrations of 0.1 mM, two inflection points are observable. According to the numerical solutions of the NPP equations, the second one (2') can again be ascribed to ionophore depletion and is identical to the one observed at 10 mM K^+ at ISE_{IN} .

Thus, the K^+ ions within the inner filling solution deplete the ionophore on the inner filling solution side. Though, the transition time of the first potential jump (1'), does not depend on the concentration or type of background analyte, the magnitude of the potential jump does. The magnitude decreases with increasing K^+ concentration until it completely disappears at 10 mM. According to the NPP equations this can be ascribed to a depletion of complexed LK^+ at the backside of the membrane and thus on the sample side. As soon as LK^+ depletes, anions from the sample are extracted into the membrane. As SO_4^{2-} (see Figure 32 (b)) has a higher free energy of transfer and is found to the right of Cl^- in the Hoffmeister series, a more prominent backside depletion is observable.

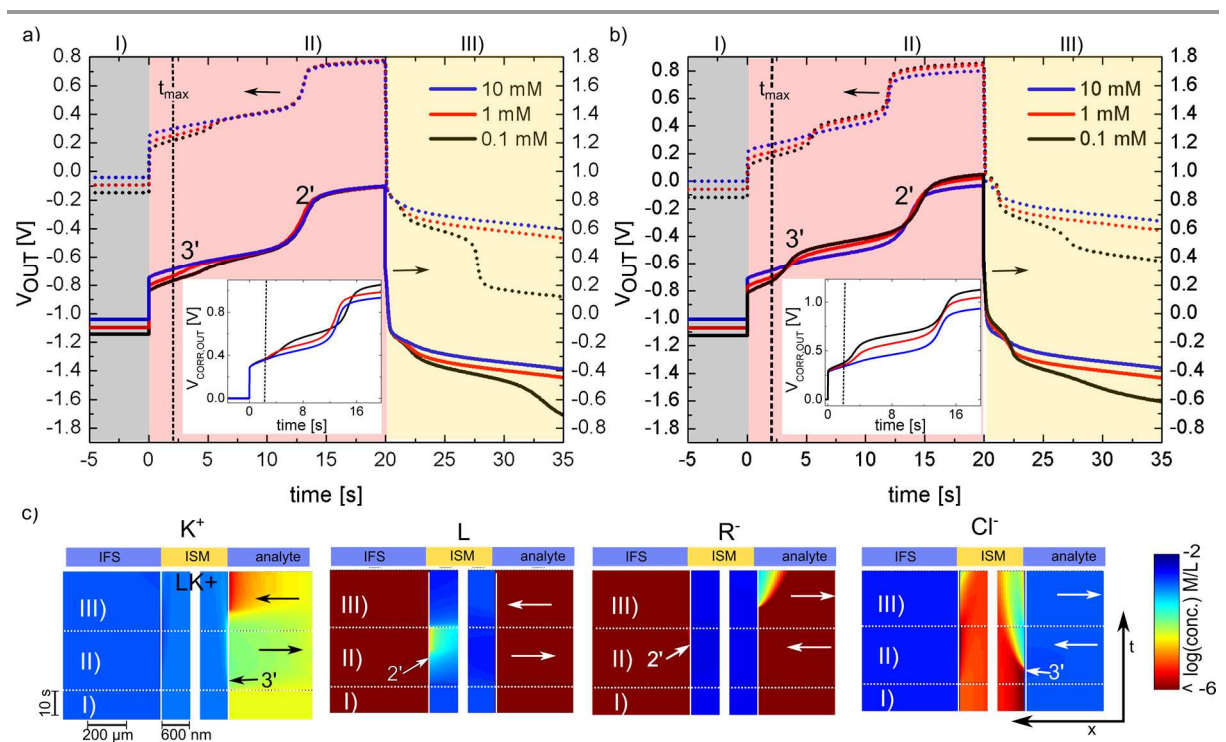


Figure 32: Measured (solid) and numerically calculated (dotted) response of ISE_{OUT} during a measurement cycle at concentrations of 0.1 mM, 1 mM and 10 mM K^+ in a 10 mM $CaCl_2$ background (a) and a 10 mM Na_2SO_4 background. The insets show the corrected potentials ($V_{CORR,OUT} = V_{OUT}(t) - V_{OUT}(t = -5 \text{ s})$). The characteristic transition times are marked with numbers (for details see text). The applied current density was $0.4 \mu A/mm^2$. The maximum applicable pulse time ($t_{max} \sim 2 \text{ s}$) is marked by a vertical line. c) Calculated concentration profiles at the interfaces of the relevant ions during a measurement cycle at a concentration of 0.1 mM in a $CaCl_2$ background. The times and locations where characteristic transition times occur are marked with numbers (for details see text). For better visibility, the x-axis are scaled differently for each ion in the membrane as well as in the aqueous solutions.

To summarize, the measurement response only depends explicitly on the K^+ concentration within the analyte as long as no backside depletion of ISE_{OUT} occurs. As soon as the ISE_{OUT} depletes on the backside, anions have to be extracted from the sample into the membrane leading to a potential jump. The magnitude of this potential jump and therefore also the sensor response depends on transferring anions present in the analyte. For that reason, the maximum applicable pulse time is limited to t_{max} (see vertical dotted line in Figure 32). Backside depletion can be avoided if the current density through ISE_{OUT} is smaller than through ISE_{IN} . Thus, the surface area of ISE_{OUT} has to be larger than of ISE_{IN} . However, ionophore depletion at the front side of ISE_{IN} leads to a selectivity breakdown giving rise to the upper detection limit. The response at concentrations exceeding this upper detection limit and concomitant higher current amplitudes, is rather determined by ionophore diffusion within the membrane than the concentration of target ions in aqueous phase.

4.3.1.1 Dynamic response at small pulse times

The actual response at small pulse time before depletion effects occur is not intuitive: The reactions at the interface are fast and instantaneous establishing a near Nernstian phase boundary potential, even under dynamic mass transport conditions (as long as no concentration polarization occurs)^{72,131}. This near-Nernstian phase boundary potential is not equal to the one measured under zero current conditions because the phase boundary activities change (see theory section 2.4.5). The current induced activity change greatly depends on the diffusion constant within the respective phase. Furthermore, the current induced change of the Nernstian phase boundary potential depends on the relative activity change and not on the absolute change.

Figure 33 (a) and (b) show the corrected experimental and numerically calculated response curves at small pulse times of ISE_{IN} and ISE_{OUT} respectively. The corrected potentials recorded at t_1 (1s) / t_2 (2s) are shown in c / d. Generally, the corrected potentials (absolute) measured at time t_1 are smaller than the ones measured at t_2 .

In case of ISE_{IN} and at large target ion concentrations (> 1 mM), the potential does not depend noticeably on the concentration of the target ions within the analyte. However, it increases

with time. This increase can be attributed to a magnitudes smaller ion diffusion-constant in the membrane than in the aqueous phase: The phase boundary concentrations within the membrane are gradually increased on the front and decreased on the backside. Whereas, the phase boundary concentration within the analyte remain almost unchanged. Consequently, the constant current induces a concentration independent response. At a concentration of 1 mM the target ion is depleted and the response depends on the ion concentration within the analyte.

Similar to ISE_{IN} , the response of ISE_{OUT} does not depend on the sample composition at high target ion concentrations (> 1 mM), as long as no backside depletion occurs. At a concentration of 0.1 mM the phase boundary concentration of the analyte is slightly changed giving rise to a response drift of ~ 20 mV which is a negligible contribution to the total sensor response. Note that this shift does not degrade the sensing signal as it depends selectively on the concentration of the target ion. However, if the signal would be measured at t_2 the response would strongly depend on the background anion present in the analyte (see Figure 33 (d)).

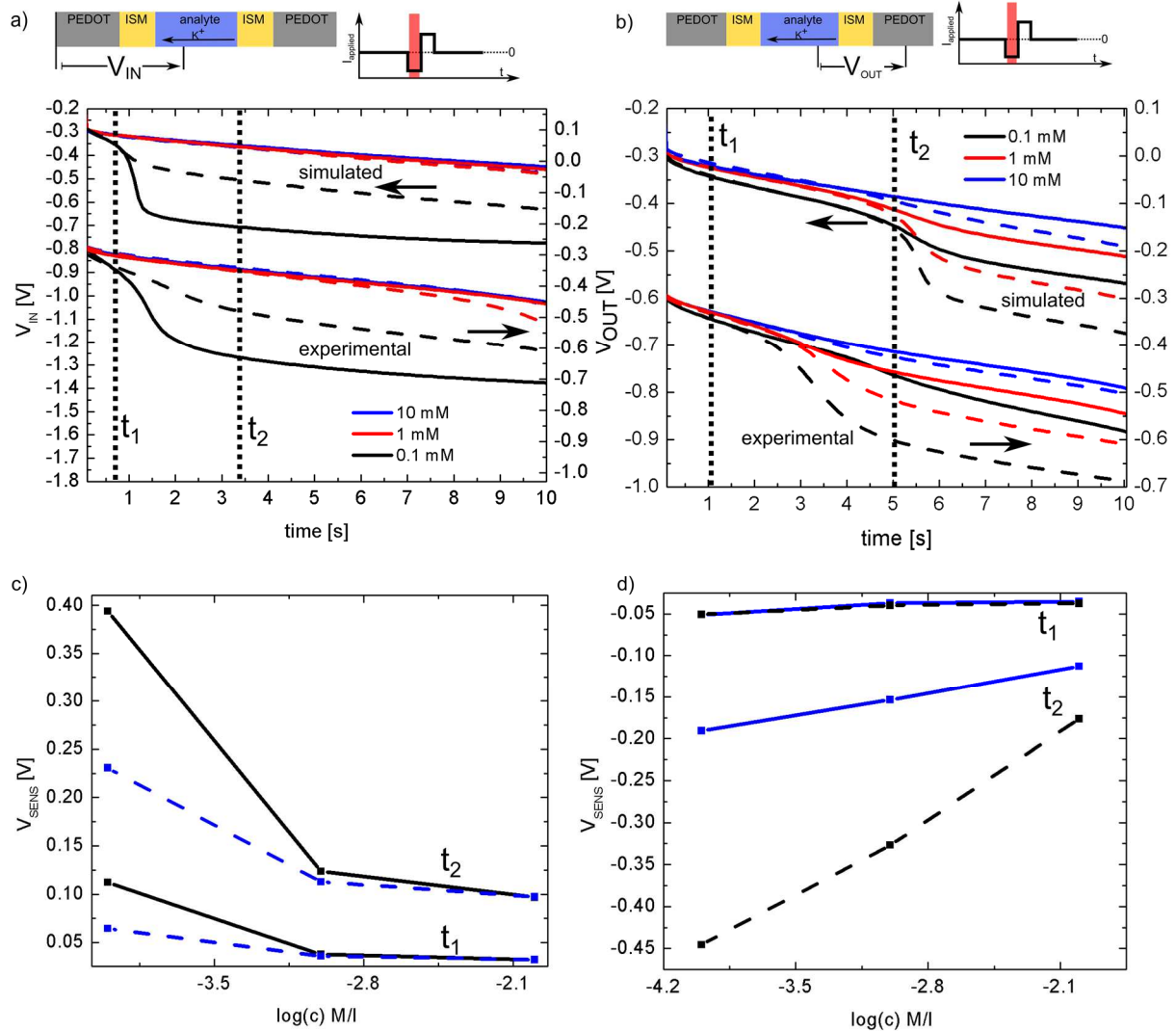


Figure 33: Experimentally and numerically calculated corrected response curves at small pulse times of ISE_{IN} (a) and ISE_{OUT} (b) recorded in a CaCl₂ (solid lines) and Na₂SO₄ (dashed lines) background at concentrations of 0.1 mM, 1 mM and 10 mM. The response curves were obtained by subtracting the equilibrium potential measured under zero current conditions at the end of the regeneration pulse. The response recorded at t_1 (1s) and t_2 (2s) are shown in c) (ISE_{IN}) and d) (ISE_{OUT}).

4.3.2 Ion selective electrodes on paper

Besides the presentation of the generalized concept, the aim of this work is also to present a fully functional low cost disposable sensor platform. For that reason, two SC-ISEs were fabricated on a paper sheet by simplest means. The SC-ISE consists of a ISM which is bonded onto a PEDOT:PSS layer which was drop casted on a paper sheet. The PEDOT:PSS layer serves

as an ion to electron transducer at the ISM interface and as an electrode at the same time. In order to avoid backside depletion, ISE_{OUT} was one and a half times larger than ISE_{IN} .

Figure 34 (a) shows the response curves of SC- ISE_{IN} and SC- ISE_{OUT} recorded in a 0.1 mM KCL solution. The first and second response curves exhibit significant drifts. After 15 measurement cycles the response curves reach a steady state and there are only small shifts in the thereafter following measurements. If the ISE is left idle for a day a significant change from measurement to measurement is observed in the beginning. Same as before, after 15 measurements the response curves reach a steady state and are almost identical to the ones measured on the first day. Consequently, 15 conditioning measurements have to be carried out prior to measurement. The response curves are generally more reproducible at the beginning of the pulse and even after three months and 120 measurements, the response curve remains almost unchanged. Figure 34 (a) also demonstrates the advantage of 2 ISEs operated in series. In equilibrium, before the measurement pulse is started, the potentials of the ISEs exhibited a drift of 130 mV after 3 months with respect to an Ag/AgCl reference electrode. If just one ISE would have been used this would have resulted in a potential shift of ~130 mV (see Figure 34 (b)). As both ISEs are identical they both exhibit approximately the same potential drift. For that reason, the net potential between the ISEs is not changed. Thus, the sensor response is not influenced by this drift.

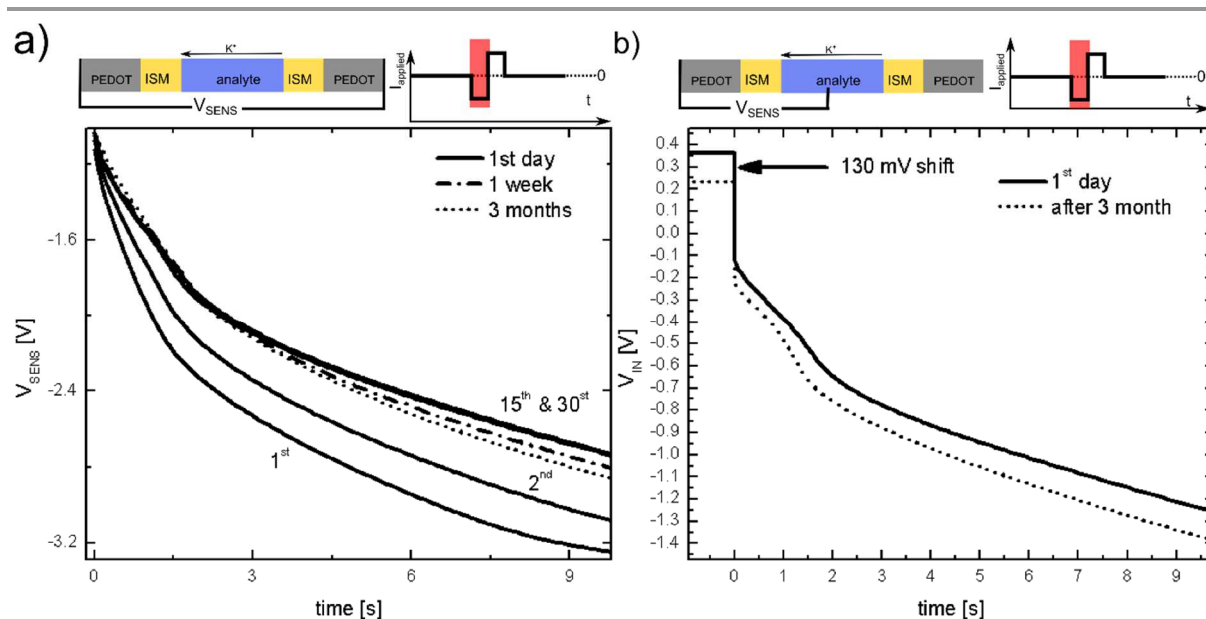


Figure 34: Sensor response (a) and response of ISE_{IN} only (b) during a current pulse (0.6 μA/mm²) in a 10⁻⁴ M K⁺ solution after 15 and 30 measurements on the first day (solid lines) and the thereafter following measurement at the second day (dash-dot lines) and after 3 months (dotted lines). The illustration on the top shows the measurement setup and the time span which is shown in the graph (red area)

Hence, the SC-ISE requires ca. 15 measurement cycles to obtain a steady state response curve. Similar to the previously presented Figure 30, Figure 35 (a) and (b) show the response curves of ISE_{IN} and ISE_{OUT} recorded at concentrations of 0.1 mM, 1 mM and 10 mM K⁺ in a CaCl₂ and Na₂SO₄ background after the conditioning protocol was carried out.

Compared to the curves obtained with the conventional setup, the potential of ISE_{IN} significantly increases with time. This can be ascribed to the reduction of the conducting PEDOT⁺ to isolating PEDOT⁰ at the backside of the ISM.^{34,35} The amount of PEDOT⁺, which gets reduced and consequently also the conductivity change, is defined through the current. As the current is kept constant, the dynamic potential change over PEDOT:PSS is not changed between measurements and just results in an offset. Disregarding this increasing potential, the curves are qualitatively similar to the ones obtained with the conventional setup. Accordingly, two potential jumps (1' and 2') are found. The characteristic potential peaks either correspond to the depletion of K⁺ within the sample (at point 1' in Figure 35) at a concentration of 0.1 mM K⁺ or the depletion of the ionophore at high K⁺ concentrations (at

point 2' in Figure 35). Note that due to the higher current density the transition times are shifted to smaller values compared to the conventional setup. In contrast the response curves of SC-ISE_{out} are different. The response curve of the SC-ISE_{out} is characteristic to a membrane which is immediately depleted on the backside and thus on the PEDOT:PSS side. The front-side depletion in the Na₂SO₄ background electrolyte is not as significant as observed with the conventional setup but still visible (marked with 3' in Figure 35). Interestingly no backside depletion at the PEDOT:PSS side is observed. This can be ascribed to the very rough interface ISM-PEDOT:PSS which leads to a lower current density through the interface.

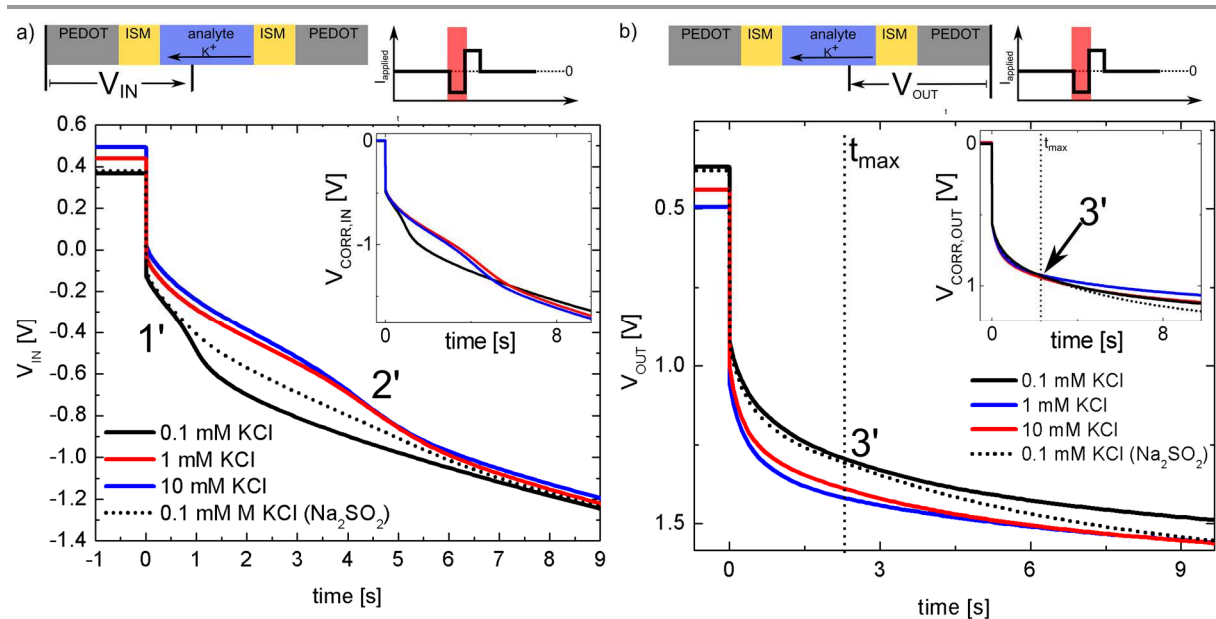


Figure 35: Response of the SC-ISE operated in forward direction (a) and the one operated in backward direction (b) at concentrations of 0.1 mM, 1 mM and 10 mM in a 10 mM CaCl₂ background (solid lines) and 10 mM CaCl₂ Na₂SO₂ background (dotted lines). The insets show the corrected potentials ($V_{CORR,IN/OUT}(t) = V_{IN/OUT}(t) - V_{IN/OUT}(t = -5 \text{ s})$). The sensor was driven at a current density of $\sim 0.6 \mu\text{A}/\text{mm}^2$ (ISE_{IN}) and $\sim 0.4 \mu\text{A}/\text{mm}^2$ (ISE_{OUT}). The maximum applicable pulse time ($t_{max} \sim 2 \text{ s}$) is marked by a vertical line. The illustration on the top shows the measurement setup and the time span which is shown in the graph (red area).

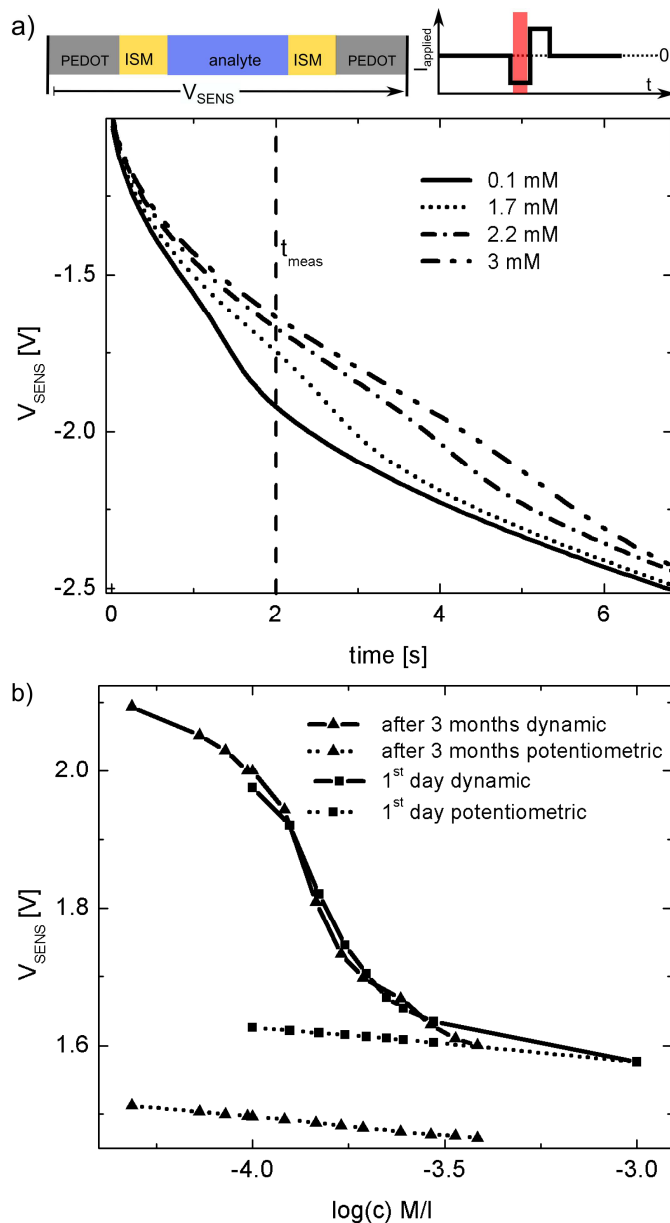


Figure 36: a) Response curve during a measurement pulse recorded in concentrations ranging from 0.1 mM to 10 M in a CaCl_2 background ($\sim 0.6 \mu\text{A}/\text{mm}^2$ (ISE_{IN}) and $\sim 0.4 \mu\text{A}/\text{mm}^2$ (ISE_{OUT})). The time t_{meas} at which the potential for various sample K^+ concentrations was recorded, is marked by a dotted line. b) The potential measured at t_{meas} for various K^+ concentrations in a CaCl_2 background (solid) compared to the ISM potential measured using a conventional potentiometric measurement (dotted) at the first day (squares) and after three months (triangles). All measurements were carried out on the same device. In order to compare the potentials of the potentiometric measurements to the dynamic measurements, they were both shifted by the same constant value.

Figure 36 shows the response curve of the sensor for K^+ concentrations ranging from 0.1 mM to 10 mM recorded in a CaCl_2 background. One can clearly see the shift of the transition time to

larger values upon increasing the K^+ concentration. To measure the concentration it is not necessary to record the whole response curve. Recording the potential at a certain time t_{meas} (see Figure 36 (a)) below t_{max} is sufficient. Figure 36 (b) shows the response recorded at a measurement time of 1.8 s compared to the potentiometric response which was measured before the dynamic measurements were carried out. The dynamic response shows a step drop at concentrations between $10^{-3.6}$ M and 10^{-4} M. Within this concentration range the sensitivity is increased by a factor ~ 20 compared to a potentiometric measurement (400 mV instead of 20 mV). The dynamic response remained stable, even after a period of 3 months and 120 measurements, whereas the potentiometric response exhibited a significant drift. This stability is caused by the two identical ISEs which exhibit the same potential drift. For that reason the net potential between the ISEs remains approximately zero. Consequently, the response is not influenced by mutual potential drifts of both ISMs as they cancel out.

4.4 Conclusion & Outlook

In conclusion we have presented a unique ion sensing platform based on two solid contact ISEs (SC-ISEs) which were fabricated on a paper sheet, by simplest means, using PEDOT:PSS and Parafilm M[®] for sealing. This concept proved to be very promising. Using this simple setup a 20 fold sensitivity enhancement compared to a potentiometric measurement was achieved without using a reference electrode. Due to the ISEs operated in series, potential drifts of the membranes cancel out and the response of this sensor turned out to be stable for at least 3 months and 120 measurements. The response is clearly well suited for cheap disposable threshold ion sensors under conditions with physiological backgrounds. The K^+ sensitive membrane served as a model and simply by exchanging the ionophore sensitivities toward other ions can be achieved. Thus, this concept can be extended to all sorts of analytical applications.

5. SUMMARY & CONCLUSION

The scope of this thesis is the investigation of two low-cost and organic ion sensing platforms based on recent advances within the fields of organic electronics and polymeric ion selective membranes.

First, a novel sensor platform based on an electrolyte-gated organic field effect transistor (EGOFET) for selective and reversible ion detection was successfully demonstrated. The major advantage of EGOFETs is that they can transduce a potentiometric input signal with high impedance into an amplified low impedance output signal. In other words, EGOFETs can replace potentiometers which would otherwise be required to measure the potentials of ion selective membranes (ISMs). Compared to conventional ion selective field effect transistors (ISFETs), the novelty of this design is the direct contact between the electrolyte and the semiconductor. Hence, there is no need for an expensive encapsulation or an elaborate deposition of a dielectric. On the contrary, due to the direct contact between the electrolyte and the organic semiconductor, an electric double layer (EDL) at the semiconductor-electrolyte interface is formed. The EDL has a high capacitance inducing a high charge carrier density in the semiconductor. For that reason, a stable and low voltage operation (< 600 mV) at currents which are large enough for further signal processing (> 1 μ A), is possible. However, investigations of the transfer-characteristics in various background electrolytes revealed that they non-selectively depend on the ionic strength of the gating solution. Furthermore, examinations of the semiconductor-electrolyte interface demonstrated that the semiconductor-electrolyte interface has to be polarizable. Accordingly, electrolytes containing electroactive substances such as ascorbic acid, degraded the transistor characteristics significantly. Either way, a direct contact of the EGOFET with the sample solution would lead to a mixed signal between the selective signal of the ISM and the non-selective signal of the EGOFET. This is why the sensing platform was

assembled by an EGOFET-inner filling solution-ISM-analyte stack. This architecture has the advantage that the EGOFET is in contact with an electrolyte of constant composition, being separated from the analyte by an ISM. To measure the ion activity, a gate potential is applied through an Ag/AgCl reference-electrode contacting the analyte. The effective gate potential of the inner filling solution, which actually drives the EGOFET, is given through the sum of the membrane potential and the gate potential. Hence, the EGOFET serves exclusively as a transducer while the highly selective ISM serves as a sensing element. Consequently, the presented architecture is modular and the detection of other ions can be realized “simply” by introducing appropriate ISMs. Furthermore, important sensor parameters such as the lowest detection limit and selectivity can be tuned by modifying the membrane. To demonstrate the versatility of this concept a pH and a Na⁺ sensitive sensor based on highly selective state of the art ISMs were presented. Due to a dynamic measurement protocol, which operates the EGOFET at a constant and stable low-voltage working point independently from the sample composition, a broad detection range between pH 2.7 and pH 12 was possible. Furthermore, the Na⁺ sensitive EGOFET showed a Nernstian response for a broad detection range between 10⁻⁶ M and 10⁻¹ M Na⁺.

The second investigated ion sensing concept is a flash-chronopotentiometric, reference-electrode free, all organic ion sensing platform fabricated on a paper sheet by simplest means. This sensing platform consists of two identical ion selective electrodes (ISEs) which are assembled by bonding a polymeric ion selective membrane (ISM) directly onto a drop-casted PEDOT:PSS electrode on paper. As the ISEs are identical, the equilibrium potential difference between the ISEs is zero, independently from the sample composition. It is therefore not possible to use conventional potentiometry to measure the ion concentration/activity. However, it is feasible using a non-equilibrium measurement method, namely flash-chronopotentiometry. To measure the concentration a constant ion flux is forced through the first ISE into the analyte and from the analyte into the second ISE. To keep the ion flux constant, other ions have to be extracted into the membrane, as soon as the target ion depletes at the second ISE. As the transfer of these ions requires a higher potential, a drastic potential jump is observed. Whereas, the current induced potential change at the first ISE does not noticeably depend on the composition of the analyte.

Consequently, the potential difference between the ISEs, required to apply the current is directly related to the ion concentration within the sample. After the current pulse, the ISEs have to be regenerated by applying the initial equilibrium potential. Thus, they can be regenerated simply by short-circuiting them. Hence, the second ISE serves two purposes. Firstly, it provides a reference potential during the measurement pulse and secondly it allows to regenerate the ISEs without using a reference electrode. To generalize the proposed sensing method and to demonstrate that the sensing signal solely arises at the ISM-sample interface, two conventional ISEs containing aqueous inner filling solutions were additionally investigated. The numerical model was able to describe the response curves of these ISE in equilibrium and under dynamic operation within different electrolytes. Consequently, it was possible to gain insights in the working principles of flash-chronopotentiometrically operated ISEs. Furthermore, the numerical model allowed to rationally choose the measurement parameters, such as current amplitude and pulse time, prior to experiment.

Using this simple setup and measurement method a 20 fold sensitivity enhancement compared to a potentiometric measurement was achieved, without using a reference electrode. Due to the ISEs operated in series, potential drifts of the membranes cancel out and the response of this sensor turned out to be stable for at least 3 months and 120 measurements. The response is obviously well suited for low-cost disposable threshold ion sensors under conditions with physiological backgrounds. The K^+ sensitive membrane served as a model. Simply by exchanging the ionophore sensitivities toward other ions can be achieved. Thus, this concept can be extended to all sorts of analytical applications.

To summarize, both concepts constitute an important step towards a low-cost integrated sensor array for multiple ion detection facilitated by a facile integration of different state-of-the-art ISMs, being of high relevance for biomedical diagnostics, food-monitoring, industrial process- and water-control.

6. REFERENCES

- ¹ R. Stevenson, *Marry Poppins* (USA, 1964).
- ² M. Tudorache and C. Bala, *Anal. Bioanal. Chem.* **388**, 565 (2007).
- ³ C. Jimenez-Jorquera, J. Orozco, and A. Baldi, *Sensors* **10**, 61 (2010).
- ⁴ G. Hanrahan, D.G. Patil, and J. Wang, *J. Environ. Monit.* **6**, 657 (2004).
- ⁵ R. De Marco, G. Clarke, and B. Pejcic, *Electroanalysis* **19**, 1987 (2007).
- ⁶ G. Crespo and E. Bakker, *RSC Adv.* **3**, 25461 (2013).
- ⁷ Y. Wang, H. Xu, J. Zhang, and G. Li, *Sensors* **8**, 2043 (2008).
- ⁸ J. Bobacka, A. Ivaska, and A. Lewenstam, *Chem. Rev.* **108**, 329 (2008).
- ⁹ E. Bakker, E. Pretsch, and P. Bühlmann, *Anal. Chem.* **72**, 1127 (2000).
- ¹⁰ A. Ceresa, A. Radu, S. Peper, E. Bakker, and E. Pretsch, *Anal. Chem.* **74**, 4027 (2002).
- ¹¹ T. Sokalski, A. Ceresa, T. Zwickl, and E. Pretsch, *J. Am. Chem. Soc.* **119**, 11347 (1997).
- ¹² A. Ceresa, T. Sokalski, and E. Pretsch, *J. Electroanal. Chem.* **501**, 70 (2001).
- ¹³ V.I. Slaveykova, K.J. Wilkinson, A. Ceresa, and E. Pretsch, *Environ. Sci. Technol.* **37**, 1114 (2003).
- ¹⁴ Z. Szigeti, T. Vigassy, E. Bakker, and E. Pretsch, *Electroanalysis* **18**, 1254 (2006).
- ¹⁵ A. Malon, T. Vigassy, E. Bakker, and E. Pretsch, *J. Am. Chem. Soc.* **128**, 8154 (2006).
- ¹⁶ G. Lisak, T. Sokalski, J. Bobacka, L. Harju, and A. Lewenstam, *Talanta* **83**, 436 (2010).
- ¹⁷ X.-G. Li, H. Feng, M.-R. Huang, G.-L. Gu, and M.G. Moloney, *Anal. Chem.* **84**, 134 (2012).
- ¹⁸ A. Radu, S. Peper, C. Gonczy, W. Runde, and D. Diamond, *Electroanalysis* **18**, 1379 (2006).
- ¹⁹ E. Bakker and E. Pretsch, *Trends Anal. Chem.* **20**, 11 (2001).
- ²⁰ Z. Szigeti, I. Bitter, K. Tóth, C. Latkoczy, D.J. Fliegel, D. Günther, and E. Pretsch, *Anal. Chim. Acta* **532**, 129 (2005).

- ²¹ M.A. Rahman, P. Kumar, D.-S. Park, and Y.-B. Shim, *Sensors* **8**, 118 (2008).
- ²² Z. Szigeti, A. Malon, T. Vigassy, V. Csokai, A. Grün, K. Wygladacz, N. Ye, C. Xu, V.J. Chebny, I. Bitter, R. Rathore, E. Bakker, and E. Pretsch, *Anal. Chim. Acta* **572**, 1 (2006).
- ²³ J. Bobacka, *Electroanalysis* **18**, 7 (2006).
- ²⁴ A. Michalska and K. Maksymiuk, *Anal. Chim. Acta* **523**, 97 (2004).
- ²⁵ J. Kofler, K. Schmoltner, A. Klug, and E.J.W. List-Kratochvil, *Appl. Phys. Lett.* 193305 (2014).
- ²⁶ K. Schmoltner, J. Kofler, A. Klug, and E.J.W. List-Kratochvil, *Adv. Mater.* **25**, 6895 (2013).
- ²⁷ J.E. Zachara, R. Toczyłowska, R. Pokrop, M. Zagórska, A. Dybko, and W. Wróblewski, *Sensors Actuators B Chem.* **101**, 207 (2004).
- ²⁸ S. Anastasova-Ivanova, U. Mattinen, A. Radu, J. Bobacka, A. Lewenstam, J. Migdalski, M. Danielewski, and D. Diamond, *Sensors Actuators B Chem.* **146**, 199 (2010).
- ²⁹ H. Xu, Y. Pan, Y. Wang, G. Li, Y. Chen, and Y. Ye, *Meas. Sci. Technol.* **23**, 125101 (2012).
- ³⁰ U. Mattinen, J. Bobacka, and A. Lewenstam, *Electroanalysis* **21**, 1955 (2009).
- ³¹ Y. Abbas, D. Balthazar de Graaf, W. Olthuis, and A. van den Berg, *Anal. Chim. Acta* **821**, 81 (2014).
- ³² W. Vonau, W. Oelßner, U. Guth, and J. Henze, *Sensors Actuators B Chem.* **144**, 368 (2010).
- ³³ T. Kakiuchi, T. Yoshimatsu, and N. Nishi, *Anal. Chem.* **79**, 7187 (2007).
- ³⁴ T. Blaz, J. Migdalski, and A. Lewenstam, *Analyst* **130**, 637 (2005).
- ³⁵ A. Kisiel, H. Marcisz, A. Michalska, and K. Maksymiuk, *Analyst* **130**, 1655 (2005).
- ³⁶ P. Lin and F. Yan, *Adv. Mater.* **24**, 34 (2012).
- ³⁷ L. Kergoat, B. Piro, M. Berggren, G. Horowitz, and M.-C. Pham, *Anal. Bioanal. Chem.* **402**, 1813 (2012).
- ³⁸ J.T. Mabeck and G.G. Malliaras, *Anal. Bioanal. Chem.* **384**, 343 (2006).
- ³⁹ L. Kergoat, B. Piro, M. Berggren, M.C. Pham, A. Yassar, and G. Horowitz, *Org. Electron.* **13**, 1 (2012).
- ⁴⁰ S. Casalini, F. Leonardi, T. Cramer, and F. Biscarini, *Org. Electron.* **14**, 156 (2013).
- ⁴¹ F. Buth, A. Donner, M. Sachsenhauser, M. Stutzmann, and J.A. Garrido, *Adv. Mater.* **24**, 4511 (2012).
- ⁴² M. Magliulo, A. Mallardi, M.Y. Mulla, S. Cotrone, B.R. Pistillo, P. Favia, I. Vikholm-Lundin, G. Palazzo, and L. Torsi, *Adv. Mater.* **25**, 2090 (2013).

- ⁴³ L. Kergoat, L. Herlogsson, D. Braga, B. Piro, M.-C. Pham, X. Crispin, M. Berggren, and G. Horowitz, *Adv. Mater.* **22**, 2565 (2010).
- ⁴⁴ F. Buth, D. Kumar, M. Stutzmann, and J. a. Garrido, *Appl. Phys. Lett.* **98**, 153302 (2011).
- ⁴⁵ A. Laiho, L. Herlogsson, R. Forchheimer, X. Crispin, and M. Berggren, *Proc. Natl. Acad. Sci. U. S. A.* **108**, 15069 (2011).
- ⁴⁶ T. Cramer, A. Campana, F. Leonardi, S. Casalini, A. Kyndiah, M. Murgia, and F. Biscarini, *J. Mater. Chem. B* **1**, 3728 (2013).
- ⁴⁷ J. Kofler, K. Schmoltner, and E.J.W. List-Kratochvil, *Proc. SPIE* **9185**, 91851U (2014).
- ⁴⁸ M.G. Afshar, X. Xie, and E. Bakker, *Anal. Chem.* (2014).
- ⁴⁹ C. Cheng, X. Tian, Y. Guo, Y. Li, H. Yuan, and D. Xiao, *Electrochim. Acta* **56**, 9883 (2011).
- ⁵⁰ Y. Kim and S. Amemiya, *Anal. Chem.* **80**, 6056 (2008).
- ⁵¹ B. Kabagambe, A. Izadyar, and S. Amemiya, *Anal. Chem.* **84**, 7979 (2012).
- ⁵² K.L. Gemene, A. Shvarev, and E. Bakker, *Anal. Chim. Acta* **583**, 190 (2007).
- ⁵³ A. Shvarev and E. Bakker, *Talanta* **63**, 195 (2004).
- ⁵⁴ E. Pergel, R.E. Gyurcsányi, K. Tóth, and E. Lindner, *Anal. Chem.* **73**, 4249 (2001).
- ⁵⁵ H. Katano and M. Senda, *Anal. Sci.* **14**, 63 (1998).
- ⁵⁶ J. Guo and S. Amemiya, *Anal. Chem.* **78**, 6893 (2006).
- ⁵⁷ S. Makarychev-Mikhailov, A. Shvarev, and E. Bakker, *J. Am. Chem. Soc.* **126**, 10548 (2004).
- ⁵⁸ M. Ghahraman Afshar, G.A. Crespo, and E. Bakker, *Anal. Chem.* **84**, 8813 (2012).
- ⁵⁹ S. Makarychev-Mikhailov, A. Shvarev, and E. Bakker, *Anal. Chem.* **78**, 2744 (2006).
- ⁶⁰ K. Schmoltner, *Environmentally Stable Organic Field-Effect Transistor Based Sensor Devices*, Technical University Graz (TUG), 2014.
- ⁶¹ H. Wang and L. Pilon, *J. Phys. Chem. C* **115**, 16711 (2011).
- ⁶² A.J. Bartt and L.R. Faulkner, in *John Wiley Sons*, edited by D. Harris and C. Robey, 2 nd (2001), pp. 12–15.
- ⁶³ R. Ishimatsu, A. Izadyar, B. Kabagambe, Y. Kim, J. Kim, and S. Amemiya, *J. Am. Chem. Soc.* **133**, 16300 (2011).

- ⁶⁴ R. Ishimatsu, A. Izadyar, B. Kabagambe, Y. Kim, J. Kim, and S. Amemiya, *J. Am. Chem. Soc.* **133**, 16300 (2011).
- ⁶⁵ W.E. Morf, E. Lindner, and W. Simon, *Anal. Chem.* **47**, 1596 (1975).
- ⁶⁶ T. Sokalski, P. Lingenfelter, and A. Lewenstam, *J. Phys. Chem. B* **107**, 2443 (2003).
- ⁶⁷ T. Zwickl and T. Sokalski, *Electroanalysis* **11**, 673 (1999).
- ⁶⁸ W.E. Morf, M. Badertscher, T. Zwickl, N.F. De Rooij, and P. Ernö, *J. Phys. Chem. B* **103**, 11346 (1999).
- ⁶⁹ E. Bakker, N. Mathias, and E. Pretsch, *Anal. Chem.* **71**, 1041 (1999).
- ⁷⁰ E. Bakker, R.K. Meruva, E. Pretsch, and M.E. Meyerhoff, *Anal. Chem.* **66**, 3021 (1994).
- ⁷¹ E. Lindner, E. Graf, Z. Niegreis, K. Toth, E. Pungor, and R.P. Buck, *Anal. Chem.* **60**, 295 (1988).
- ⁷² A. Shvarev and E. Bakker, *Anal. Chem.* **75**, 4541 (2003).
- ⁷³ B. Gryszakowski, A. Lewenstam, and M. Danielewski, *Diffus. Fundam.* **8**, 1 (2008).
- ⁷⁴ J.M. Zook, S. Bodor, R.E. Gyurcsányi, and E. Lindner, *J. Electroanal. Chem.* **638**, 254 (2010).
- ⁷⁵ J.M. Zook, R.P. Buck, R.E. Gyurcsányi, and E. Lindner, *Electroanalysis* **20**, 259 (2008).
- ⁷⁶ E. Bakker and a. J. Meir, *SIAM Rev.* **45**, 327 (2003).
- ⁷⁷ J.J. Jasielc, R. Filipek, K. Szyszkiewicz, J. Fausek, M. Danielewski, and a. Lewenstam, *Comput. Mater. Sci.* **63**, 75 (2012).
- ⁷⁸ T. Osakai, Y. Sato, M. Imoto, and T. Sakaki, *J. Electroanal. Chem.* **668**, 107 (2012).
- ⁷⁹ J.M. Zook, S. Bodor, E. Lindner, K. Tóth, and R.E. Gyurcsányi, *Electroanalysis* **21**, 1923 (2009).
- ⁸⁰ S. Bodor, J.M. Zook, E. Lindner, K. Tóth, and R.E. Gyurcsányi, *J. Solid State Electrochem.* **13**, 171 (2008).
- ⁸¹ Y.-H. Li and S. Gregory, *Geochim. Cosmochim. Acta* **38**, 703 (1974).
- ⁸² M. Imoto, T. Sakaki, and T. Osakai, *Anal. Chem.* **85**, 4753 (2013).
- ⁸³ H.J. Lee, C. Beriet, and H.H. Girault, *J. Electroanal. Chem.* **453**, 211 (1998).
- ⁸⁴ S. Wilke and T. Zerihun, *J. Electroanal. Chem.* **515**, 52 (2001).
- ⁸⁵ T. Osakai, T. Kakutani, Y. Nishiwaki, and M. Senda, *Anal. Sci.* **3**, 499 (1987).
- ⁸⁶ Y. Qin, Y. Mi, and E. Bakker, *Anal. Chim. Acta* **421**, 207 (2000).

- ⁸⁷ J. Langmaier, K. Stejskalová, and Z. Samec, *J. Electroanal. Chem.* **496**, 143 (2001).
- ⁸⁸ O.L. Francois, P. Sun, and M. V Mirkin, *J. Am. Chem. Soc.* **1128**, 15019 (2006).
- ⁸⁹ P. Buhlmann and L.D. Chen, in *Supramol. Chem. From Mol. to Nanomater.*, edited by Jonathan W. Steed and P.A. Gale, 1 st ed. (Wiley, 2012), pp. 2539–2577.
- ⁹⁰ M.M. Zareh, *Anal. Sci.* **25**, (2009).
- ⁹¹ X.-J. Liu, B. Peng, F. Liu, and Y. Qin, *Sensors Actuators B Chem.* **125**, 656 (2007).
- ⁹² E. Lindner, V. V Cosofret, S. Ufer, R.P. Buck, W.J. Kao, M.R. Neuman, and J.M. Anderson, *J. Biomed. Mater. Res.* **28**, 591 (1994).
- ⁹³ Y. Mi, C. Green, and E. Bakker, *Anal. Chem* **70**, 5252 (1998).
- ⁹⁴ S.-I. Wakida, M. Yamane, K. Higashi, K. Hihiro, and Y. Ujihira, *Sensors And Actuators* **B1**, 412 (1990).
- ⁹⁵ L.Y. Heng and E.A.H. Hall, *Anal. Chem* **72**, 581 (2000).
- ⁹⁶ N. Abramova and A. Bratov, *Sensors* **9**, 7097 (2009).
- ⁹⁷ S. Mathison and E. Bakker, *Anal. Chem.* **70**, 303 (1998).
- ⁹⁸ K. Toth, E. Lindner, and E. Pungor, *Anal. Chim. Acta* **234**, 57 (1990).
- ⁹⁹ E. Lindner and R.E. Gyurcsányi, *J. Solid State Electrochem.* **13**, 51 (2009).
- ¹⁰⁰ H. Tamura, K. Kimura, and T. Shono, *Anal. Chem* **1227**, 1224 (1982).
- ¹⁰¹ J. Bobacka, *Anal. Chem.* **71**, 4932 (1999).
- ¹⁰² U. Vanamo and J. Bobacka, *Electrochim. Acta* **122**, 316 (2014).
- ¹⁰³ T. Rosatzin, E. Bakker, K. Suzuki, and W. Simon, *Anal. Chim. Acta* **280**, 197 (1993).
- ¹⁰⁴ R.P. Buck and E. Lindner, *Acc. Chem. Res.* **31**, 257 (1998).
- ¹⁰⁵ R. Naegeli, J. Redepenning, and F.C. Anson, *J. Phys. Chem.* **90**, 6227 (1986).
- ¹⁰⁶ K. Nakazato, *Sensors* **9**, 8831 (2009).
- ¹⁰⁷ A. Van den Berg, A. Grisel, and G. Lyonnaise, *Sensors Actuators B* **4**, 235 (1991).
- ¹⁰⁸ S. V Dzyadevych, A.P. Soldatkin, A. V El'skaya, C. Martelet, and N. Jaffrezic-Renault, *Anal. Chim. Acta* **568**, 248 (2006).

- ¹⁰⁹ P. Bergveld, in *IEEE Sens. Conf. Toronto* (2003), pp. 1–26.
- ¹¹⁰ P.L.H.M. Cobben, R.J.M. Egberink, J. Bomerb, J.R. Haak, P. Bergveldb, and D.N. Reinhoudt, *Sensors Actuators B* **6**, 304 (1992).
- ¹¹¹ Z. Elbhiri, J.M. Chovelon, N. Jaffrezic-Renault, and Y. Chevalier, *Sensors Actuators B Chem.* **58**, 491 (1999).
- ¹¹² M. Chudy, W. Wroblewski, and Z. Brzozka, *Sensors Actuators B* **57**, 47 (1999).
- ¹¹³ S.-R. Chang and H. Chen, *Sensors* **9**, 8336 (2009).
- ¹¹⁴ J. Bobacka, A. Ivaska, and A. Lewenstam, *Electroanalysis* **15**, 366 (2003).
- ¹¹⁵ A. Michalska, M. Ocyga, and K. Maksymiuk, *Anal. Bioanal. Chem.* **385**, 203 (2006).
- ¹¹⁶ A. Michalska, *Anal. Bioanal. Chem.* **384**, 391 (2006).
- ¹¹⁷ A. Michalska, A. Konopka, and M. Maj-Zurawska, *Anal. Chem.* **75**, 141 (2003).
- ¹¹⁸ A. Michalska and K. Maksymiuk, *Talanta* **63**, 109 (2004).
- ¹¹⁹ J. Bobacka, *Anal. Chem.* **71**, 4932 (1999).
- ¹²⁰ M. Fibbioli, W.E. Morf, M. Badertscher, N.F. De Rooij, and È. Pretsch, *Electroanalysis* 1286 (2007).
- ¹²¹ J. Bobacka, A. Lewenstam, and A. Ivaska, *J. Electroanal. Chem.* **509**, 27 (2001).
- ¹²² H.-S. Park, S.-J. Ko, J.-S. Park, J.Y. Kim, and H.-K. Song, *Sci. Rep.* **3**, 2454 (2013).
- ¹²³ G. a. Crespo and E. Bakker, *RSC Adv.* **3**, 25461 (2013).
- ¹²⁴ Y. Kim, P.J. Rodgers, R. Ishimatsu, and S. Amemiya, *Anal. Chem.* **81**, 7262 (2009).
- ¹²⁵ S. Jadhav and E. Bakker, *Anal. Chem.* **71**, 3657 (1999).
- ¹²⁶ H.J. Lee, G. Lager, C.M. Pereira, A.F. Silva, and H.H. Girault, *Talanta* **78**, 66 (2009).
- ¹²⁷ A. Molina, C. Serna, J. a Ortuño, J. Gonzalez, E. Torralba, and a Gil, *Anal. Chem.* **81**, 4220 (2009).
- ¹²⁸ M.D. Scanlon, G. Herzog, and D.W.M. Arrigan, *Anal. Chem.* **80**, 5743 (2008).
- ¹²⁹ G. Herzog, V. Kam, A. Berduque, and D.W.M. Arrigan, *J. Agric. Food Chem.* **56**, 4304 (2008).
- ¹³⁰ S. Sawada, H. Torii, T. Osakai, and T. Kimoto, *Anal. Chem.* **70**, 4286 (1998).
- ¹³¹ E. Bakker, P. Bühlmann, and E. Pretsch, *Chem. Rev.* **97**, 3083 (1997).

- ¹³² J. Ding, X. Wang, and W. Qin, *ACS Appl. Mater. Interfaces* **5**, 9488 (2013).
- ¹³³ Y. Abbas, W. Olthuis, and A. van den Berg, *Sensors Actuators B Chem.* **188**, 433 (2013).
- ¹³⁴ J.M. Zook, J. Langmaier, and E. Lindner, *Sens. Actuators. B. Chem.* **136**, 410 (2009).
- ¹³⁵ Z. Bao and J. Locklin, *Organic Field-Effect Transistors*, 1st ed. (CRC Press, 2007).
- ¹³⁶ A.J. Heeger, *Rev. Mod. Phys.* **73**, 681 (2001).
- ¹³⁷ J. Bredas and G. Street, *Acc. Chem. Res.* **1305**, 309 (1985).
- ¹³⁸ O.D. Jurchescu, M. Popinciuc, B.J. Van Wees, and T.T.M. Palstra, *Adv. Mater.* **19**, 688 (2007).
- ¹³⁹ Y. Yuan, G. Giri, A.L. Ayzner, A.P. Zoombelt, S.C.B. Mannsfeld, J. Chen, D. Nordlund, M.F. Toney, J. Huang, and Z. Bao, *Nat. Commun.* **5**, 3005 (2014).
- ¹⁴⁰ H. Sirringhaus, N. Tessler, and R.H. Friend, *Science (80-.)*. **280**, 1741 (1998).
- ¹⁴¹ B.C.D. Dimitrakopoulos and P.R.L. Malenfant, *Adv. Mater.* **14**, 99 (2002).
- ¹⁴² S. Allard, M. Forster, B. Souharce, H. Thiem, and U. Scherf, *Angew. Chem. Int. Ed. Engl.* **47**, 4070 (2008).
- ¹⁴³ A.M. Münzer, K. Melzer, M. Heimgreiter, and G. Scarpa, *Biochim. Biophys. Acta* **1830**, 4353 (2013).
- ¹⁴⁴ G. Scarpa, A. Idzko, A. Yadav, and S. Thalhammer, *Sensors* **10**, 2262 (2010).
- ¹⁴⁵ P. Tehrani, a Kancierzewska, X. Crispin, N. Robinson, M. Fahlman, and M. Berggren, *Solid State Ionics* **177**, 3521 (2007).
- ¹⁴⁶ X. Crispin, F.L.E. Jakobsson, A. Crispin, P.C.M. Grim, P. Andersson, A. Volodin, C. Van Haesendonck, M. Van Der Auweraer, W.R. Salaneck, and M. Berggren, *Society* 4354 (2006).
- ¹⁴⁷ J. Ouyang, C.-W. Chu, F.-C. Chen, Q. Xu, and Y. Yang, *Adv. Funct. Mater.* **15**, 203 (2005).
- ¹⁴⁸ A.M. Nardes, *On the Conductivity of PEDOT:PSS Thin Films*, 2007.
- ¹⁴⁹ C. Wang, H. Dong, W. Hu, Y. Liu, and D. Zhu, *Chem. Rev.* **112**, 2208 (2012).
- ¹⁵⁰ T. Sekitani and T. Someya, *Mater. Today* **14**, 398 (2011).
- ¹⁵¹ G. Gelinck, P. Heremans, K. Nomoto, and T.D. Anthopoulos, *Adv. Mater.* **22**, 3778 (2010).
- ¹⁵² L. Zhou, A. Wanga, S.C. Wu, J. Sun, S. Park, and T.N. Jackson, *Appl. Phys. Lett.* **88**, 10 (2006).
- ¹⁵³ S.P. White, K.D. Dorfman, and C.D. Frisbie, *Anal. Chem.* **87**, 1861 (2015).

- ¹⁵⁴ Z. Zhu, J.T. Mabeck, C. Zhu, N.C. Cady, A. Batt, and G.G. Malliaras, *Mater. Sci.* **1556** (2004).
- ¹⁵⁵ Y. Guo, G. Yu, and Y. Liu, *Adv. Mater.* **22**, 4427 (2010).
- ¹⁵⁶ M. Berggren and a. Richter-Dahlfors, *Adv. Mater.* **19**, 3201 (2007).
- ¹⁵⁷ C. Bartic and G. Borghs, *Anal. Bioanal. Chem.* **384**, 354 (2005).
- ¹⁵⁸ A. Loi, I. Manunza, and A. Bonfiglio, *Appl. Phys. Lett.* **86**, 103512 (2005).
- ¹⁵⁹ C. Bartic¹, A. Campitelli, and S. Borghs, *Appl. Phys. Lett.* **82**, 475 (2003).
- ¹⁶⁰ T. Ji, P. Rai, S. Jung, and V.K. Varadan, *Appl. Phys. Lett.* **92**, 233304 (2008).
- ¹⁶¹ M.E. Roberts, S.C.B. Mannsfeld, N. Queraltó, C. Reese, J. Locklin, W. Knoll, and Z. Bao, *Proc. Natl. Acad. Sci. U. S. A.* **105**, 12134 (2008).
- ¹⁶² L. Herlogsson, X. Crispin, N.D. Robinson, M. Sandberg, O.-J. Hagel, G. Gustafsson, and M. Berggren, *Adv. Mater.* **19**, 97 (2007).
- ¹⁶³ O. Larsson, E. Said, M. Berggren, and X. Crispin, *Adv. Funct. Mater.* **19**, 3334 (2009).
- ¹⁶⁴ M.J. Panzer and C.D. Frisbie, *J. Am. Chem. Soc.* **129**, 6599 (2007).
- ¹⁶⁵ M.J. Panzer, C.R. Newman, and C.D. Frisbie, *Appl. Phys. Lett.* **86**, 103503 (2005).
- ¹⁶⁶ S.H. Kim, K. Hong, W. Xie, K.H. Lee, S. Zhang, T.P. Lodge, and C.D. Frisbie, *Adv. Mater.* (2012).
- ¹⁶⁷ M.J. Panzer and C.D. Frisbie, *Adv. Mater.* **20**, 3177 (2008).
- ¹⁶⁸ S. Cotrone, M. Ambrico, H. Toss, M.D. Angione, M. Magliulo, A. Mallardi, M. Berggren, G. Palazzo, G. Horowitz, T. Ligonzo, and L. Torsi, *Org. Electron.* **13**, 638 (2012).
- ¹⁶⁹ E. Said, O. Larsson, M. Berggren, and X. Crispin, *Adv. Funct. Mater.* **18**, 3529 (2008).
- ¹⁷⁰ M. Hamedi, L. Herlogsson, X. Crispin, R. Marcilla, M. Berggren, and O. Inganäs, *Adv. Mater.* **21**, 573 (2009).
- ¹⁷¹ C. Müller, M. Hamedi, R. Karlsson, R. Jansson, R. Marcilla, M. Hedhammar, and O. Inganäs, *Adv. Mater.* **23**, 898 (2011).
- ¹⁷² D. a. Bernardis, D.J. Macaya, M. Nikolou, J. a. DeFranco, S. Takamatsu, and G.G. Malliaras, *J. Mater. Chem.* **18**, 116 (2008).
- ¹⁷³ S. Casalini, A. Shehu, S. Destri, W. Porzio, M.C. Pasini, F. Vignali, F. Borgatti, C. Albonetti, F. Leonardi, and F. Biscarini, *Org. Electron.* (2012).

- ¹⁷⁴ L. a. Majewski, R. Schroeder, M. Grell, P. a. Glarvey, and M.L. Turner, *J. Appl. Phys.* **96**, 5781 (2004).
- ¹⁷⁵ K. Krishnamoorthy, R.S. Gokhale, A.Q. Contractor, A. Kumar, A. Asaf, and A. Marg, 820 (2004).
- ¹⁷⁶ K. Melzer, A.M.M. Münzer, E. Jaworska, K. Maksymiuk, A. Michalska, and G. Scarpa, *Org. Electron.* **15**, 595 (2014).
- ¹⁷⁷ P. Bergveld, *Sensors And Actuators* **88**, 1 (2003).
- ¹⁷⁸ T. Sokalski, A. Ceresa, M. Fibbioli, T. Zwickl, E. Bakker, and E. Pretsch, *Anal. Chem.* **71**, 1210 (1999).
- ¹⁷⁹ T. Sokalski, T. Zwickl, E. Bakker, and E. Pretsch, *Anal. Chem.* **71**, 1204 (1999).
- ¹⁸⁰ E. Lindner and R.P. Buck, *Fresenius. J. Anal. Chem.* **364**, 22 (1999).
- ¹⁸¹ S.Y. Hyoung, S.C. Geun, and M.E. Meyerhoff, *Anal. Chim. Acta* **237**, 115 (1990).
- ¹⁸² K. Schmoltner, J. Kofler, A. Klug, and E.J.W. List-Kratochvil, *Proc. SPIE* **8831**, 88311N (2013).
- ¹⁸³ J.M. Zook, R.P. Buck, J. Langmaier, and E. Lindner, *J. Phys. Chem. B* **112**, 2008 (2008).
- ¹⁸⁴ H.-H. Liao, C.-M. Yang, C.-C. Liu, S.-F. Horng, and H.-F. Meng, *J. Appl. Phys.* **103**, 104506 (2008).
- ¹⁸⁵ M.S.A. Abdou, F.P. Orfino, Y. Son, and S. Holdcroft, *J. Am. Chem. Soc.* **119**, 4518 (1997).
- ¹⁸⁶ T. Cramer, T. Steinbrecher, T. Koslowski, D. Case, F. Biscarini, and F. Zerbetto, *Phys. Rev. B* **79**, 155316 (2009).

7. APPENDIX

7.1 A paper based, all organic, reference electrode free ion sensing platform

J. Kofler, S. Nau, Emil J.W. List-Kratochvil

Accepted by Journal of Chemical Materials B

Contribution: The author carried out all experimental work and wrote the manuscript. The manuscript was finalized with the co-authors.

Note that the layout is not final and that the published publication will look differently.

ARTICLE

A paper based, all organic, reference electrode free ion sensing platform

Cite this: DOI: 10.1039/x0xx00000x

Johannes Kofler^a, Sebastian Nau^a and Emil J. W. List-Kratochvil^{a,b},Received 00th January 2012,
Accepted 00th January 2012

DOI: 10.1039/x0xx00000x

www.rsc.org/

We present a reference-electrode free, all organic K⁺ sensitive ion sensing platform fabricated on a plain sheet of paper by simplest means. This unique sensing platform consists of two identical ion selective electrodes (ISEs) which are assembled by bonding a polymeric ion selective membrane (ISM) directly onto a drop-casted PEDOT:PSS electrode on paper. Taking full advantage of the so called pulsetrode concept, a current pulse is used to measure the concentration of the targeted ion. This current forces an ion flux out of the first ISE, through the sample and into the second ISE. This flux leads to a well-defined potential jump at the second ISE, as soon as the target ion locally depletes within the analyte, whereas the current induced potential change at the first ISE does not depend noticeably on the sample composition. Hence, the potential difference between the ISEs is directly related to the ion concentration within the sample. This concept allows for a 20-fold sensitivity enhancement compared to classical potentiometric measurements in physiological backgrounds. As mutual potential drifts of the ISEs cancel out, the sensor response showed excellent stability and did not change for over three months. Additionally, the response of the sensor could be modelled numerically, identifying the mechanisms and limitations of this promising sensor platform.

Introduction

Ion sensors are required in many fields ranging from food safety control¹, water quality monitoring²⁻⁴ to various applications in pharmaceutical and cosmetics industry.⁵ Especially within the emerging fields of clinic analysis low-cost sensor platforms for in-situ sensing of ions and biological substances in appropriate aqueous media and physiological backgrounds are required.⁶ Potentiometric ion-selective electrodes (ISEs) are established tools as a routine methodology in clinical diagnostics for the determination of small hydrophilic target ions.⁷ In particular ISEs based on polymeric ion selective membranes (ISMs) containing neutral or charged carriers (ionophores) have been improved to such an extent that it has resulted in a "new wave of ion-selective electrodes".^{7,8} This was achieved by considerable improvements of the lower detection limit, new membrane materials, and a deeper theoretical understanding of the potentiometric response of ISMs. The discovery of transmembrane fluxes and the fact that leaking of target ions into the sample reduces the lower detection limit, revolutionized the field.^{9,10} Today, ISEs with extremely high selectivity⁸ and detection limits down to low nano-molar levels are available.¹¹⁻¹⁴ Recently, low cost organic potentiometric sensors have emerged.^{15,16} The sensitivity of all of these electrodes is typically given through the Nernst equation limiting it to ~59 mV for a 10 fold sample activity change in case of a monovalent ion. A second important limitation of ISEs is that in order to reliably

measure the electromotive force (EMF) and to obtain a stable sensing signal, at least one reference electrode is required. However, the bridge electrolyte and the liquid junction of classical reference electrodes require regular maintenance, a vertical working position, and it may also contaminate the sample. Although promising liquid junction-free all solid state reference electrode concepts were demonstrated¹⁷⁻²³, the potential stability upon varying the ionic strength²⁴ and response time of these novel solid-state reference electrodes still bear challenges.

Typically ISEs are operated potentiometrically in chemical equilibrium. However, recently various attractive non-equilibrium current and potential techniques have emerged.⁵ These techniques can overcome the limits of conventional ISEs. In particular flash chronopotentiometry (pulsetrodes), which allows for 10 to 20-fold sensitivity enhancement compared to classical potentiometry, seems to be especially suited for ion sensing in physiological backgrounds.²⁵⁻²⁷ The pulsetrode principle is based on a constant-current pulse which forces a ion flux into the ISM. This constant ion flux leads to a local depletion of the target ion in the analyte which is accompanied by a drastic potential change (potential jump) at a certain transition time. Hence, the potential recorded at a fixed pulse time is a function of the labile ion concentration within the analyte^{5,26} and exhibits a very high sensitivity within a narrow concentration range.²⁶ After each measurement the ISM has to be regenerated by applying the initial equilibrium potential measured before the

current pulse is applied.²⁵ For that reason, reference electrodes are still necessary.

The aim of this work is to present a flash-chronopotentiometric, all organic and reference electrode free K^+ sensing platform on paper. This unique platform is based on two identical PEDOT:PSS-based solid contact ISEs (SC-ISEs) fabricated on a paper sheet by simplest means (see figure 1a). The novelty of the proposed measurement method is that the commonly used reference electrode is replaced by a second, identical ISE. To measure the concentration of the target ion a current pulse is forced through the ISEs while the potential difference between the ISEs is measured at a fixed measurement time t_{meas} (see figure 1 b, V_{SENS}). The current forces an ion flux through the sample and through both ISEs. The ISE operated in forward direction (ISE_{IN}), extracting target ions into the membrane from the sample side, will exhibit the typical potential jump upon target ion depletion (see figure 1b V_{IN} and figure 1c). The ISE operated in backward direction (ISE_{OUT}) just shifts the potential difference between the ISEs by a constant value, and thus does not disturb the measurement signal (see figure 1 b V_{OUT}). Since both ISEs are identical, the equilibrium potentials of both ISEs are equal with respect to the analyte and the ISEs can be regenerated simply by shortening them after each measurement.

Consequently, the second ISE serves two purposes. Firstly, it provides a reference potential during the measurement pulse and secondly it allows to regenerate the ISEs without using a reference electrode. Additionally, mutual potential drifts of the ISEs cancel out, leading to a very stable and reproducible response.

To generalize the proposed sensing method and to demonstrate that the sensing signal solely arises at the ISM-sample interface, two conventional ISEs containing aqueous inner filling solutions were used in a first step. The results were modelled by numerical calculations, gaining insight into the response mechanisms and revealing the limits of the measurement-parameters, namely the maximum current density and pulse time. In a second step, the response of the all organic PEDOT:PSS-based SC-ISEs is investigated, exhibiting the same characteristics as the conventional setup. In accordance with the results reported by S. Makarychev-Mikhailov et al.²⁷, a 20-fold sensitivity enhancement compared to classical potentiometric measurement was obtained. Furthermore, repeated measurements over a period of 3 months reveal that the response signal was stable for at least 3 months.

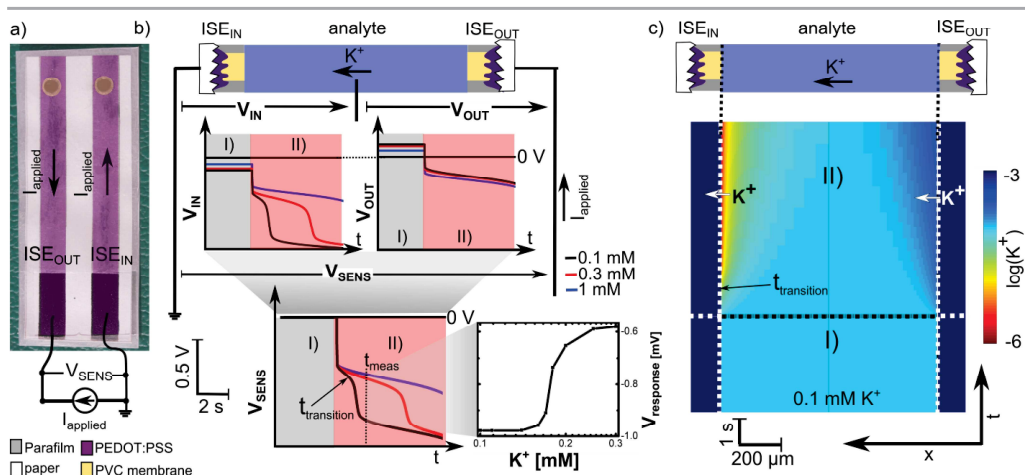


Figure 1: a) An image of a fabricated sensor and its circuit diagram (the materials are additionally dyed for a better understanding); b) Illustration of the sensing principle: A measurement cycle consists of a regeneration (I, both ISEs are shortened) a constant-current measurement pulse (II) and an inverse regeneration pulse (III, not shown). The membrane potentials of ISE_{IN} (V_{IN}), ISE_{OUT} (V_{OUT}) and the potential difference between the ISEs (V_{SENS}) during a measurement cycle at different K^+ concentrations (0.1 mM black, 0.3 mM red, 1 mM blue), is shown on the top left, top right and left bottom. To measure the concentration a constant-current pulse is applied (I_{applied}) while the potential V_{SENS} is recorded at a fixed time t_{meas} . The according response (V_{response}) is shown on the bottom right; c) the numerically calculated K^+ concentration during a measurement cycle (bulk analyte concentration 0.1 mM K^+).

Theory

Generally, chronopotentiometric measurements are based on ion transfer at immiscible electrolyte solutions (ISM, aqueous analyte).⁵ For that reason, to describe the response of a chronopotentiometrically operated ISM, all transferring ions within the analyte and the ISM have to be considered. Highly ion

selective plasticized PVC membranes contain an ionophore (L), anionic sides (R^-) and a background electrolyte (B^+/B^-) (see figure 2a). These anionic sides fix the concentration of ionophore-target ion concentration (LK^+) and the background electrolyte ensures a high conductivity of the membrane.⁵ However, the sensing mechanism is chemically based on the recognition of an aqueous target ion by an ionophore, which

thermodynamically facilitates selective ion transfer (IT) into the membrane. The strong ion-ionophore interaction overcomes the unfavorable free energy of transfer and hydrophilic ions are extracted into the hydrophobic membrane developing a Nernstian phase boundary potential in equilibrium²⁸. The Nernstian phase boundary potential is used as a measurement signal for potentiometric measurements, limiting the response to a sensitivity of ~ 59 mV per 10 fold activity change in case of a monovalent ion. Upon applying a current pulse, ions are forced into the membrane on the front side of ISE_{IN} and out of the membrane on the back side of ISE_{OUT}. As the transfer of the target ion (K^+) into the membrane is facilitated by the ionophore, exclusively K^+ ions are extracted into ISE_{IN}. Likewise, K^+ ions are extracted into the analyte at ISE_{OUT} (mechanism 1' in figure 2b). At the beginning of the pulse, as long as the ion concentrations at the interface are proportional to the bulk ion concentrations, the response obeys a near-Nernstian slope towards the respective activity (see also SUI S2).^{29,30} At larger pulse times, the target ion is depleted. The square root of the time when the target ion depletes (transition time) is linearly proportional to the concentration and inversely proportional the current density. As soon as the target ion depletes within the sample, other positively charged ions have to be transferred into the membrane or negatively charged ions within the membrane have to be extracted into the analyte (see mechanism 2' in figure 2). As the free energy of transfer of these ions is higher, a larger potential has to be applied to keep the ion flux through the ISM-analyte interface constant. The magnitude of this potential change (potential jump) is directly related to the selectivity of the membrane; i.e. to the difference of the free energy of transfer between the target ion and the alternatively included/extracted ion. However, similar depletion effects can also occur within the membrane. The freely available ionophores (L) at ISE_{IN} or the complexed target ions (LK⁺) at ISE_{OUT} can deplete earlier than the target ion. Likewise, alternative ions are extracted into the analyte or the membrane (see figure 2b, mechanisms 3' and 4'). There are analytical and numerical models which describe the chronopotentiometric operation of an ISM.^{29,31–35} These models only consider ion transfers of target and interfering ions and they neglect the influence of the electric potential. In contrast, the numerical calculations presented here, take all transferring ions as well as the electric potential, into account. A detailed description of the method can be found in the SUI (S1). Briefly, similar to the method described in ref. ³⁶ and ref. ³¹ the system was separated into three layers (analyte, ISM, inner filling solution). The bulk of these layers were calculated by solving the Nernst Planck and Poisson differential equations (NPP) as described in ref. ³¹. The mass transport of a specific ion in between the layers and thus through interfaces were modelled using the Butler-Volmer-type relations which describe the transfer rates as a function of the potential drop at the interface.²⁸

Experimental

Chemicals and Materials

The ISM contained the cation exchanger sodium tetrakis[3,5-bis(trifluoromethyl)phenyl]borate (NaTFPB) (15 mM/kg), the potassium ionophore I (valinomycin, 5 mM/kg) and the background electrolyte tetradodecylammonium (TDA) tetrakis(4-chlorophenyl)borate (TCIPB) (ETH 500, 20 mM/kg). The membrane matrix contained high molecular weight polyvinyl chloride (33 wt%, Selectophore grade) and the plasticizer 2-nitrophenyl octyl ether (2-NPOE) (67 wt%). The ISM cocktails were dissolved in tetrahydrofuran (THF) and drop casted onto a confined glass sheet. The drop-cast membrane was allowed to dry overnight at ambient conditions in a saturated THF environment and was peeled off for further implementation. The final thickness of the ISM was ~ 150 μ m. All of the chemicals mentioned above were obtained from Fluka Sigma-Aldrich and were used as received. The saline solutions were prepared with KCl (>99.0%), CaCl₂ (>99.0%) Na₂SO₄ (>99.0%) and deionized water (grade).

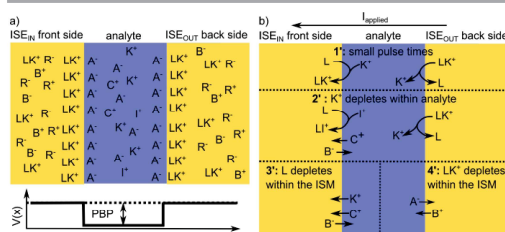


Figure 2: a) Illustration of the ions present within the membrane/analyte and the formation of the Nernstian phase boundary potential (PBP) in equilibrium. K⁺ corresponds to the target ions, L⁺ to interfering ions, C⁺/A⁻ to background cations/anions in the analyte, R⁻ to anionic sides in the ISM and B⁻/L⁺ to background cations/anions in the ISM, L is the freely available ionophore and LK⁺/L⁺ is the ionophore-K⁺/L⁺ complex; b) illustrations of possible mechanisms occurring at the front side and backside of an ISM during a current pulse (for further details see text).

Sensor fabrication

First, the design of the PEDOT:PSS electrodes was printed in black & white on a copy-paper (copy paper "Blustar" 80 g/m²). The PEDOT:PSS electrodes are simply structured by drop casting PEDOT:PSS (Clevios™ PH 1000) onto these printed electrodes. As the inkjet printing paper is initially hydrophobic and the water based ink hydrophilic, PEDOT:PSS is confined to the hydrophilic printed areas. After drop casting PEDOT:PSS, the paper is transferred into an oven and dried for 1 h at 150 °C. The resistance of the PEDOT:PSS electrodes (1 cm wide and 5 cm long) is in the range of 30 k Ω . Subsequently, the paper is made water impermeable by laminating a Parafilm M[®] at ~ 100 °C onto the top and the bottom side of the paper. Prior to lamination two holes (2 mm and 3 mm diameter), which accommodate the ISMs, were punched into the Parafilm M[®] using a biopsy punch. The ISMs are cut out of a bigger ISM sheet using a biopsy punch with a diameter of 4 mm. The sensor is finalized by gluing these ISMs onto the PEDOT:PSS electrodes. This is done by drop-casting 5 μ L THF onto the ISM and immediately thereafter placing the ISM with the THF side first

onto the PEDOT:PSS electrodes. THF partly dissolves the ISM leading to a conformal contact between the ISM and the PEDOT:PSS electrodes and to a tight sealing at the ISM edges. After gluing, the sensor is left to rest for ~ 12 h in order to let the residual THF evaporate. After fabrication, the sensors were conditioned for ~ 5 h in a 1 mM KCl solution to exchange the Na⁺ ions of the NaTFPB within the membrane with the targeted K⁺ ions. After the conditioning the sensors were blow dried and subsequently stored in dark under ambient conditions until measurement. Note that the ISEs were spaced 5 mm apart in order to avoid cross talk.

Measurement setups/procedures

Current and potentials were measured using a B1500A Parameter analyzer. To carry out potential measurements, the source-measurement units were operated as 0 A constant current sources while measuring the potential. To apply a current pulse, the current was set to the corresponding value and the potential was measured. To carry out the reference measurements (conventional setup) two custom made ISEs were used. The inner filling solutions (IFS) (10 mM KCl in a 10 mM CaCl₂ background) of the ISEs were contacted with Ag/AgCl reference electrodes whereas the PEDOT:PSS based solid state ISEs were contacted by two alligator clamps. In order to investigate the ISEs separately, an additional reference electrode contacting the analyte, was used. The reference electrode was placed half way between the ISEs. A measurement cycle was carried out as follows. First, a base line potential-pulse is applied (0 V to both ISE terminals) while the current flowing between the ISEs is monitored. This current should ideally be 0 A in equilibrium. This base line pulse was applied for 6 min in between the current pulses. Subsequently, a current pulse and a reverse regeneration pulse was applied and the potential was monitored at all three reference electrodes. No working electrodes were used and the currents applied during the measurement cycles were passing through the reference electrodes contacting the IFS. The recorded potentials are therefore biased by a current induced potential drop at the reference electrodes. However, these potentials drops are constant and therefore solely result in a constant offset which does not influence the measurement signal as such. Furthermore note that all measurements were carried out using excess background electrolytes to avoid migration effects within the analyte.

Results and discussion

First, to generalize the measurement method, two conventional ISEs containing an aqueous inner filling solutions (liquid contact), were used. Liquid contacts are well-defined system which can be described numerically. Hence, it is possible to identify the mechanisms and the operational limits of the sensor. Furthermore, it is verified that the sensing signal solely arises at the ISM-sample interface and is not at the PEDOT:PSS solid contact, implying the possibility to use this measurement method for various other ISEs. In the thereafter following step, the PEDOT:PSS-paper based SC-ISEs are characterized and the

sensitivity and long term stability of the sensing platform is demonstrated.

Conventional setup

The response curves and the applied currents at concentrations of 0.01, 1, 10 mM KCl in a 10 mM CaCl₂ M background of a measurement setup using two conventional ISEs are shown in figure 3. First, both ISEs are forced to 0 V which is equivalent to shortening both ISEs (see region I in figure 3). As both ISEs are identical they ideally have the same equilibrium potentials with respect to the analyte. Consequently, only a negligible faradaic current is flowing in between the ISEs (see figure 3b region I). After an equilibration time of 5 minutes, a current is applied to the ISEs, forcing K⁺ ions from the analyte into the membrane on one side and vice versa on the other side (see region II in figure 3). The potential difference in between the ISEs corresponds to the measurement response which strongly depends on the target ion concentration within the analyte. After this first current pulse a second inverse pulse, with identical but negative current, is applied. This leads to a faster regeneration of the membrane²⁵ (region III). After the measurement, both ISEs are forced to 0 V to regenerate the ISEs. During the regeneration, the current flowing between the ISEs decreases until it eventually reaches a very small steady state current (~0.7 nA/mm²). The remaining steady state current can be attributed to a small potential difference between the reference electrodes, non-idealities of the membranes or to the measurement setup itself (potential differences as small as of ~ 0.4 mV are sufficient to explain this current). However, currents of these small magnitudes are not sufficient to perturb the ISM and the thereafter following measurements at concentrations examined within this work.

There are three different potential jumps observable in figure 3b. In order to ensure that the sensing signal solely depends on the target ion concentration, it is crucial to identify the origins of the potential jumps. For that reason each ISE was investigated separately in various background electrolytes by monitoring the potential of the analyte with an Ag/AgCl reference electrode. The experimentally measured as well as numerically calculated response curves of ISE_{IN} at concentrations of 0.1, 1, 10 mM KCl in an 10 mM CaCl₂ and a highly interfering 10 mM NaCl background are shown in figure 4 a and b respectively. These two background cations represent two extremes; Ca²⁺ is very hydrophilic and non-interfering ion, whereas Na⁺ is one of the major interfering ions (in case of the valinomycin ionophore).

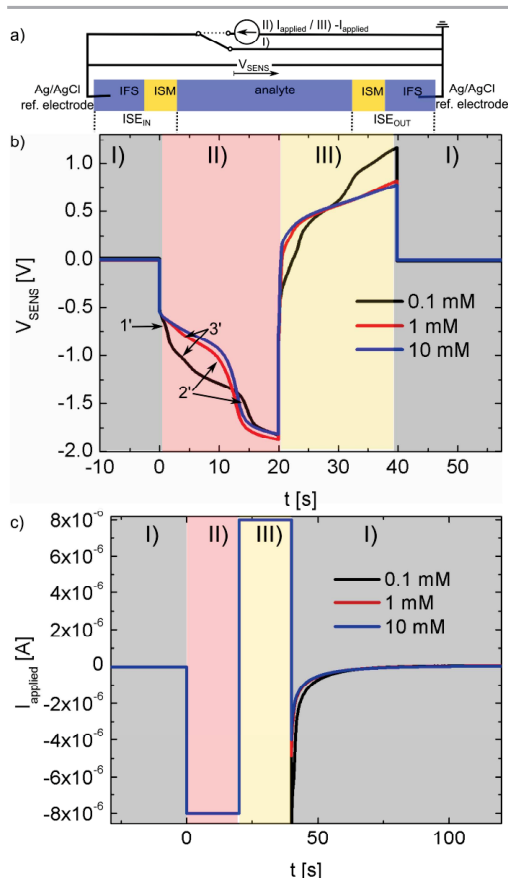


Figure 3: a) Simplified circuit diagram of the measurement setup showing two ISEs with identical inner filling solutions (IFS) which are operated in series. In between the measurements, the ISMs are regenerated by applying 0 V to both ISEs. This is equivalent to a shorting, which is illustrated by a switch in position I); during the measurement pulse and the reverse pulse the switch is in position II) or III) respectively; b) Sensing signal (V_{SENS}) measured in analytes at concentrations of 0.1 mM (black), 1 mM (red), 10 mM KCl (blue) and in an 10 mM CaCl_2 background during a full measurement cycle consisting of a regeneration (grey region I), a measurement pulse (red region II) and an inverse pulse (yellow region III). The observable transition times are marked with numbers 1'-3'. The applied current density was $0.4 \mu\text{A}/\text{cm}^2$. The corresponding currents are shown in c).

At the end of the regeneration, the membrane potential depends on the concentration within the electrolyte in a Nernstian fashion (56 mV per 10 fold activity change, see figure 4, region I). This Nernstian offset at the beginning of the pulse results in a concentration dependent shift of the response curves of a single ISE, even before a potential jump has occurred. As two ISEs are operated in series, this potential shift cancels out in the final response curve (see figure 1d and figure 3, region I). The inset of figure 4a shows the response curves which are corrected for the Nernstian equilibrium potential at the beginning. These corrected response curves are not noticeably concentration dependent as long as no characteristic potential jump is observed (refer to SUI S2 for details). The first potential jump is observed at a concentration of 0.1 mM K^+ in a CaCl_2 electrolyte (point 1'). In case of the NaCl electrolyte the magnitude of this potential jump is not as pronounced and a second potential inflection is observed at larger pulse times (point 2*). At K^+ concentrations of 1 mM and 10 mM one potential jump is observed in both background electrolytes (point 2').

Evidently, the numerical solutions of the NNP equations agree qualitatively with the response curves obtained. According to the numerical solutions of the NNP equations, the potential inflection in point 1' is due to the depletion of the target ion within the aqueous sample (see figure 4c). In case of the NaCl background, interfering Na^+ ions can easily be extracted into the membrane as soon as the K^+ ion depletes within the aqueous layer. Whereas in case of the CaCl_2 background, due to the high hydrophilicity of Ca^{2+} (high free energy of transfer from the aqueous analyte into the hydrophobic ISM), TCIPB^- ions (background electrolyte of the membrane) are forced from the membrane into the water. The extraction of TCIPB^- requires a higher potential than the assisted ion transfer of Na^+ . This is the reason why the magnitude of the potential jump is lower in case of the highly interfering NaCl background. The second inflection in point 2* can be ascribed to ionophore depletion within the membrane. As soon as the freely available ionophores deplete at the membrane surface, the assisted ion transfer gets halted. As Na^+ is very hydrophilic, primarily TCIPB^- ions are extracted from the membrane into the water. The same mechanism is also responsible for the potential inflection at point 2'. At high K^+ concentrations (1 mM and 10 mM) the ionophore depletes, leading to a potential inflection which is identical to the one observed at point 2*.

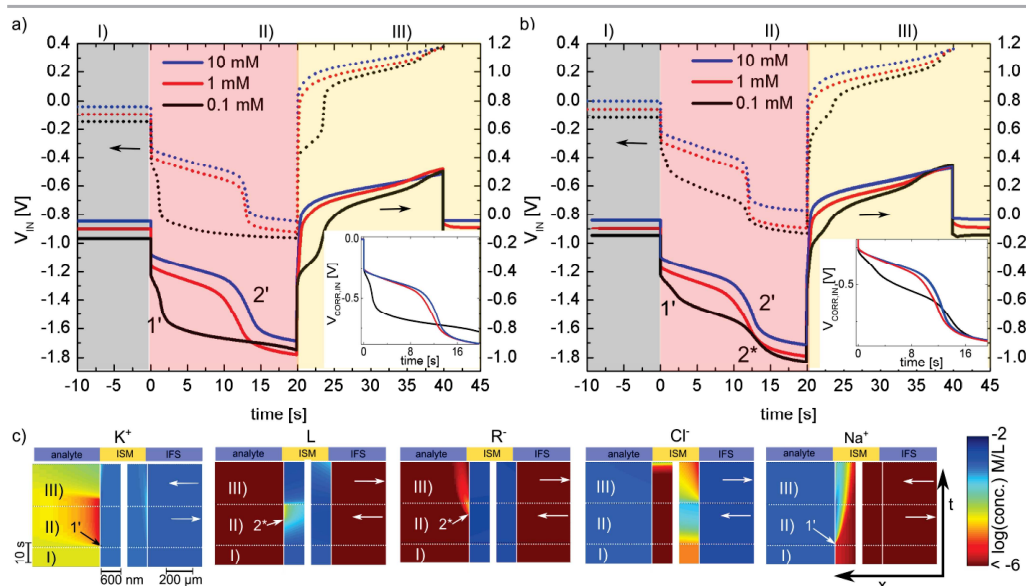


Figure 4: Measured (solid) and numerically calculated response (dotted) of ISE_{IN} during a measurement cycle at concentrations of 0.1 mM, 1 mM and 0.01 mM K^+ in a 10 mM CaCl_2 background (a) and a 10 mM NaCl background (b). The insets show the corrected potentials ($V_{IN}(t) - V_{IN}(t = -5 \text{ s})$). The characteristic transition times are marked with numbers (for details see text). The applied current density was $0.4 \mu\text{A}/\text{mm}^2$. c) Calculated concentration profiles at the interfaces of the relevant ions during a measurement cycle at a concentration of 0.1 mM K^+ in a NaCl background. The time and location where characteristic transitions occur are marked with numbers (for details see text). For better visibility, the x-axis is scaled differently for each ion in the membrane as well as in the aqueous solutions.

The experimental as well as the numerically calculated response curves of ISE_{OUT} in an analyte containing 0.1, 1, 10 mM KCl in an 10 mM NaCl and 10 mM Na_2SO_4 background are shown in figure 5 a and b respectively. This time the anion is drawn towards the membrane. This is why an alternative anion was studied. SO_4^{2-} is extremely hydrophilic (on the right in the Hoffmeister series) and will therefore require a significant higher potential to be extracted into the membrane than Cl^- . As in the case of ISE_{IN} , the corrected response curves do not depend noticeably on the target ion concentration or on the background electrolyte as long as no potential jump is observed (at current pulse times smaller than 2 s, for details refer to SUI S2). At higher pulse times and low K^+ concentrations of 0.1 mM, two inflection points are observable. According to the numerical solutions of the NPP equations, the potential jump 2' can again

be ascribed to ionophore depletion and is identical to the one observed at 10 mM K^+ at ISE_{IN} . Thus, the K^+ ions within the inner filling solution deplete the ionophore on the inner filling solution side. Though, the transition time of the potential jump 3', does not depend on the concentration or type of background analyte, the magnitude of the potential jump does. The magnitude decreases with increasing K^+ concentration until it completely disappears at 10 mM. According to the NPP equations this can be ascribed to a depletion of complexed LK^+ at the backside of the membrane and thus on the sample side. As soon as LK^+ depletes, anions from the sample are extracted into the membrane. As SO_4^{2-} (see figure 5b) has a higher free energy of transfer and is found to the right of Cl^- in the Hoffmeister series, a more prominent backside depletion is observable.

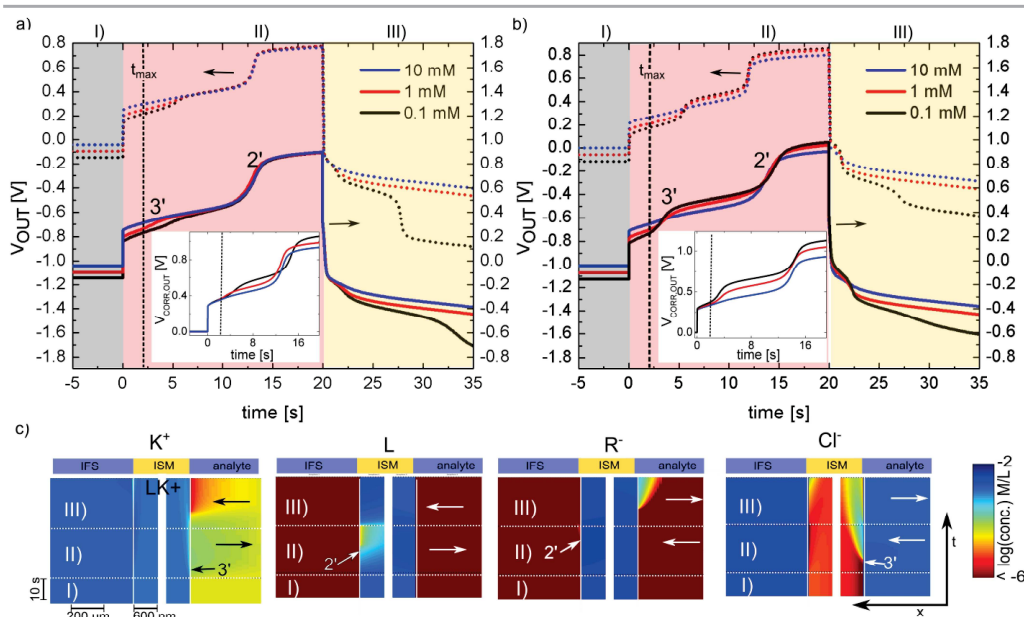


Figure 5: Measured (solid) and numerically calculated (dotted) response of ISE_{OUT} during a measurement cycle at concentrations of 0.1 mM, 1 mM and 10 mM K^+ in a 10 mM $CaCl_2$ background (a) and a 10 mM Na_2SO_4 background (b). The insets show the corrected potentials ($V_{CORR,OUT} = V_{OUT}(t) - V_{OUT}(t = -5 \text{ s})$). The characteristic transition times are marked with numbers (for details see text). The applied current density was $0.4 \mu\text{A}/\text{mm}^2$. The maximum applicable pulse time ($t_{max} \sim 2 \text{ s}$) is marked by a vertical line. c) Calculated concentration profiles at the interfaces of the relevant ions during a measurement cycle at a concentration of 0.1 mM in a $CaCl_2$ background. The times and locations where characteristic transition times occur are marked with numbers (for details see text). For better visibility, the x-axis are scaled differently for each ion in the membrane as well as in the aqueous solutions.

To summarize, the measurement response only depends explicitly on the K^+ concentration within the analyte as long as no backside depletion of ISE_{OUT} occurs. As soon as the ISE_{OUT} depletes on the backside, anions have to be extracted from the sample into the membrane leading to a potential jump. The magnitude of this potential jump and therefore also the sensor response depends on transferring anions present in the analyte. For that reason, the maximum applicable pulse time is limited to t_{max} (see vertical dotted line in figure 5). Backside depletion can be avoided if the current density through ISE_{OUT} is smaller than through ISE_{IN} . Thus, the surface area of ISE_{OUT} has to be larger than of ISE_{IN} . However, ionophore depletion at the front side of ISE_{IN} leads to a selectivity breakdown giving rise to the upper detection limit. The response at concentrations exceeding this upper detection limit and concomitant higher current amplitudes, is rather determined by ionophore diffusion within the membrane than the concentration of target ions in aqueous phase.

Ion selective electrodes on paper

Besides the presentation of the generalized concept, the aim of this work is also to present a fully functional low cost disposable sensor platform. For that reason two SC-ISEs were fabricated on a paper sheet by simplest means. The SC-ISE consists of an ISM which is bonded onto a PEDOT:PSS layer which was drop casted on a paper sheet. The PEDOT:PSS layer serves as an ion to electron transducer at the ISM interface and as an electrode at the same time. In order to avoid backside depletion, ISE_{OUT} was one and a half times larger than ISE_{IN} .

The SC-ISE requires ca. 15 measurement cycles to obtain a steady state response curve. Detailed stability and conditioning investigations can be found in the SUI (S3). Similar to the previously presented figure 4, figure 6a and b show the response curves of ISE_{IN} and ISE_{OUT} recorded at concentrations of 0.1

mM, 1 mM and 10 mM K^+ in a $CaCl_2$ and Na_2SO_4 background after the conditioning protocol was carried out.

Compared to the curves obtained with the conventional setup, the potential of ISE_{IN} significantly increases with time. This can be ascribed to the reduction of the conducting $PEDOT^+$ to isolating $PEDOT^0$ at the backside of the ISM. ^{37,38} The amount of $PEDOT^+$, which gets reduced and consequently also the conductivity change, is defined through the current. As the current is kept constant, the dynamic potential change over $PEDOT:PSS$ is not changed between measurements and just results in an offset. Disregarding this increasing potential, the curves are qualitatively similar to the ones obtained with the conventional setup. Accordingly, two potential jumps ($1'$ and $2'$) are found. The characteristic potential peaks either correspond to the depletion of K^+ within the sample (at point $1'$ in figure 6) at

a concentration of 0.1 mM K^+ or the depletion of the ionophore at high K^+ concentrations (at point $2'$ in figure 6). Note that due to the higher current density the transition times are shifted to smaller values compared to the conventional setup. In contrast the response curves of $SC-ISE_{OUT}$ are different. The response curve of the $SC-ISE_{OUT}$ is characteristic to a membrane which is immediately depleted on the backside and thus on the $PEDOT:PSS$ side. The front-side depletion in the Na_2SO_4 background electrolyte is not as significant as observed with the conventional setup but still visible (marked with $3'$ in Figure). Interestingly no backside depletion at the $PEDOT:PSS$ side is observed. This can be ascribed to the very rough interface $ISM-PEDOT:PSS$ which leads to a lower current density through the interface.

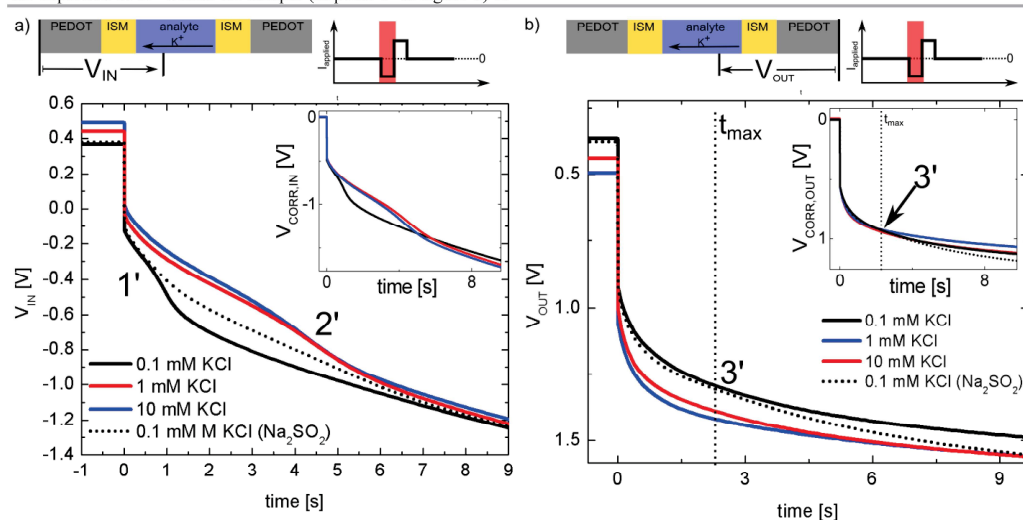


Figure 6: Response of the SC-ISE operated in forward direction (a) and the one operated in backward direction (b) at concentrations of 0.1 mM, 1 mM and 10 mM in a 10 mM $CaCl_2$ background (solid lines) and 10 mM $CaCl_2$, Na_2SO_4 background (dotted lines). The insets show the corrected potentials ($V_{CORR,IN/OUT}(t) = V_{IN/OUT}(t) - V_{IN/OUT}(t - 5\text{ s})$). The sensor was driven at a current density of $\sim 0.6 \mu A/mm^2$ (ISE_{IN}) and $\sim 0.4 \mu A/mm^2$ (ISE_{OUT}). The maximum applicable pulse time ($t_{max} \sim 2\text{ s}$) is marked by a vertical line. The illustration on the top shows the measurement setup and the time span which is shown in the graph (red area).

Figure 7 shows the response curve of the sensor for K^+ concentrations ranging from 0.1 mM to 10 mM recorded in a $CaCl_2$ background. One can clearly see the shift of the transition time to larger values upon increasing the K^+ concentration. To measure the concentration it is not necessary to record the whole response curve. Recording the potential at a certain time t_{meas} (see figure 7a) below t_{max} is sufficient. Figure 7b) shows the response recorded at a measurement time of 1.8 s compared to the potentiometric response which was measured before the dynamic measurements were carried out. The dynamic response shows a step drop at concentrations between $10^{-3.6}$ M and 10^{-4} M. Within this concentration range the sensitivity is increased by a factor ~ 20 compared to a potentiometric measurement (400 mV instead of 20 mV). The dynamic response remained stable, even after a period of 3 months and 120 measurements, whereas the

potentiometric response exhibited a significant drift. This stability is caused by the two identical ISEs which exhibit the same potential drift. For that reason the net potential between the ISEs remains approximately zero. Consequently, the response is not influenced by mutual potential drifts of both ISMs as they cancel out.

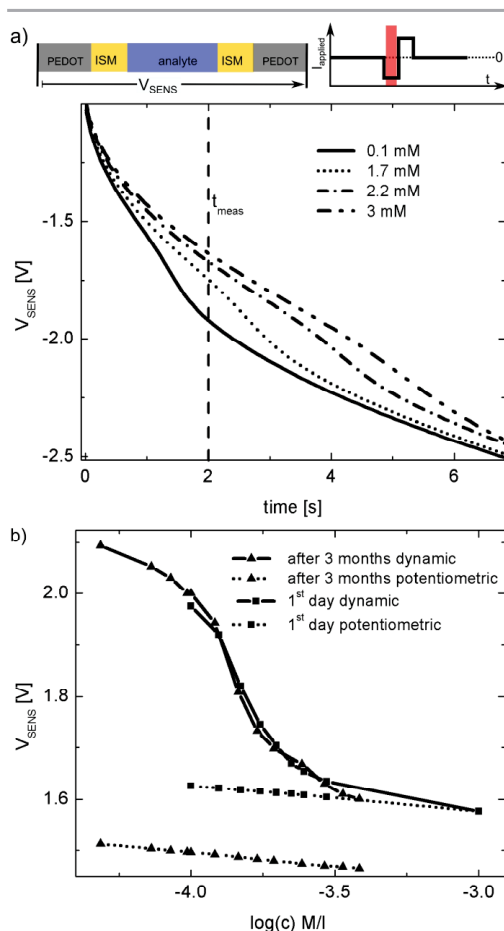


Figure 7: a) Response curve during a measurement pulse recorded in concentrations ranging from 0.1 mM to 10 M in a CaCl_2 background ($\sim 0.6 \mu\text{A}/\text{mm}^2$ (ISE_{in}) and $\sim 0.4 \mu\text{A}/\text{mm}^2$ (ISE_{out})). The time t_{meas} at which the potential for various sample K^+ concentrations was recorded, is marked by a dotted line. b) The potential measured at t_{meas} for various K^+ concentrations in a CaCl_2 background (solid) compared to the ISM potential measured using a conventional potentiometric measurement (dotted) at the first day (squares) and after three months (triangles). All measurements were carried out on the same device. In order to compare the potentials of the potentiometric measurements to the dynamic measurements, they were both shifted by the same constant value.

Conclusion & Outlook

In conclusion we have presented a unique ion sensing platform based on two solid contact ISEs (SC-ISEs) which were fabricated on a paper sheet, by simplest means, using drop casted PEDOT:PSS and Parafilm M[®] for sealing. This concept proved to be very promising. Using this simple setup a 20 fold sensitivity enhancement compared to a potentiometric measurement was

achieved without using a reference electrode. Due to the ISEs operated in series, potential drifts of the membranes cancel out and the response of this sensor turned out to be stable for at least 3 months and 120 measurements. The response is clearly well suited for cheap disposable threshold ion sensors under conditions with physiological backgrounds. The K^+ sensitive membrane served as a model and simply by exchanging the ionophore sensitivities toward other ions can be achieved. Thus, this concept can be extended to all sorts of analytical applications.

Acknowledgements

For financial support the Styrian Government (project BioOFET 2) is acknowledged.

Notes and references

^a NanoTecCenter Weiz Forschungsgesellschaft m.b.H., Franz-Pichler-Strasse 32, A-8160 Weiz, Austria.

^b Institute of Solid State Physics, Graz University of Technology, Petersgasse 16, A-8010 Graz, Austria

Electronic Supplementary Information (ESI) available See DOI: 10.1039/b000000x

¹ M. Tudorache and C. Bala, *Anal. Bioanal. Chem.* **388**, 565 (2007).

² C. Jimenez-Jorquera, J. Orozco, and A. Baldi, *Sensors* **10**, 61 (2010).

³ G. Hanrahan, D.G. Patil, and J. Wang, *J. Environ. Monit.* **6**, 657 (2004).

⁴ R. De Marco, G. Clarke, and B. Pejic, *Electroanalysis* **19**, 1987 (2007).

⁵ G. Crespo and E. Bakker, *RSC Adv.* **3**, 25461 (2013).

⁶ Y. Wang, H. Xu, J. Zhang, and G. Li, *Sensors* **8**, 2043 (2008).

⁷ J. Bobacka, A. Ivaska, and A. Lewenstam, *Chem. Rev.* **108**, 329 (2008).

⁸ E. Bakker, E. Pretsch, and P. Bühlmann, *Anal. Chem.* **72**, 1127 (2000).

⁹ A. Ceresa, A. Radu, S. Peper, E. Bakker, and E. Pretsch, *Anal. Chem.* **74**, 4027 (2002).

¹⁰ T. Sokalski, A. Ceresa, T. Zwickl, and E. Pretsch, *J. Am. Chem. Soc.* **119**, 11347 (1997).

¹¹ A. Malon, T. Vigassy, E. Bakker, and E. Pretsch, *J. Am. Chem. Soc.* **128**, 8154 (2006).

¹² G. Lisak, T. Sokalski, J. Bobacka, L. Harju, and A. Lewenstam, *Talanta* **83**, 436 (2010).

¹³ X.-G. Li, H. Feng, M.-R. Huang, G.-L. Gu, and M.G. Moloney, *Anal. Chem.* **84**, 134 (2012).

¹⁴ A. Radu, S. Peper, C. Gonczy, W. Runde, and D. Diamond, *Electroanalysis* **18**, 1379 (2006).

- ¹⁵ J. Kofler, K. Schmoltnner, A. Klug, and E.J.W. List-Kratochvil, *Appl. Phys. Lett.* **193305** (2014).
- ¹⁶ K. Schmoltnner, J. Kofler, A. Klug, and E.J.W. List-Kratochvil, *Adv. Mater.* **25**, 6895 (2013).
- ¹⁷ U. Mattinen, J. Bobacka, and A. Lewenstam, *Electroanalysis* **21**, 1955 (2009).
- ¹⁸ Y. Abbas, D. Balthazar de Graaf, W. Olthuis, and A. van den Berg, *Anal. Chim. Acta* **821**, 81 (2014).
- ¹⁹ W. Vonau, W. Oelßner, U. Guth, and J. Henze, *Sensors Actuators B Chem.* **144**, 368 (2010).
- ²⁰ S. Anastasova-Ivanova, U. Mattinen, A. Radu, J. Bobacka, A. Lewenstam, J. Migdalski, M. Danielewski, and D. Diamond, *Sensors Actuators B Chem.* **146**, 199 (2010).
- ²¹ T. Kakiuchi, T. Yoshimatsu, and N. Nishi, *Anal. Chem.* **79**, 7187 (2007).
- ²² T. Blaz, J. Migdalski, and A. Lewenstam, *Analyst* **130**, 637 (2005).
- ²³ A. Kisiel, H. Marcisz, A. Michalska, and K. Maksymiuk, *Analyst* **130**, 1655 (2005).
- ²⁴ H. Xu, Y. Pan, Y. Wang, G. Li, Y. Chen, and Y. Ye, *Meas. Sci. Technol.* **23**, 125101 (2012).
- ²⁵ S. Makarychev-Mikhailov, A. Shvarev, and E. Bakker, *J. Am. Chem. Soc.* **126**, 10548 (2004).
- ²⁶ M. Ghahraman Afshar, G.A. Crespo, and E. Bakker, *Anal. Chem.* **84**, 8813 (2012).
- ²⁷ S. Makarychev-Mikhailov, A. Shvarev, and E. Bakker, *Anal. Chem.* **78**, 2744 (2006).
- ²⁸ R. Ishimatsu, A. Izadyar, B. Kabagambe, Y. Kim, J. Kim, and S. Amemiya, *J. Am. Chem. Soc.* **133**, 16300 (2011).
- ²⁹ A. Shvarev and E. Bakker, *Anal. Chem.* **75**, 4541 (2003).
- ³⁰ A. Shvarev and E. Bakker, *Talanta* **63**, 195 (2004).
- ³¹ B. Grysakowski, A. Lewenstam, and M. Danielewski, *Diffus. Fundam.* **8**, 1 (2008).
- ³² T. Sokalski, P. Lingenfelter, and A. Lewenstam, *J. Phys. Chem. B* **107**, 2443 (2003).
- ³³ J.M. Zook, S. Bodor, R.E. Gyurcsányi, and E. Lindner, *J. Electroanal. Chem.* **638**, 254 (2010).
- ³⁴ J.M. Zook, R.P. Buck, R.E. Gyurcsányi, and E. Lindner, *Electroanalysis* **20**, 259 (2008).
- ³⁵ E. Bakker and a. J. Meir, *SIAM Rev.* **45**, 327 (2003).
- ³⁶ J.J. Jasielc, R. Filipek, K. Szyszkiewicz, J. Fausek, M. Danielewski, and a. Lewenstam, *Comput. Mater. Sci.* **63**, 75 (2012).
- ³⁷ H.-S. Park, S.-J. Ko, J.-S. Park, J.Y. Kim, and H.-K. Song, *Sci. Rep.* **3**, 2454 (2013).
- ³⁸ G. a. Crespo and E. Bakker, *RSC Adv.* **3**, 25461 (2013).

7.2 Hydrogen ion-selective electrolyte-gated field-effect transistor for pH-sensing

J. Kofler*, K. Schmoltner*, A. Klug, E. J. W. List-Kratochvil
Applied Physics Letter 104, 193305 (2014)

*both authors contributed equally.

Contribution: The author contributed equally with K. Schmoltner to experiments related to the ion-selective EGOFETs and sensor characterization. The author wrote the manuscript, finalized the manuscript together with the K. Schmoltner.



Hydrogen ion-selective electrolyte-gated organic field-effect transistor for pH sensing

Johannes Kofler, Kerstin Schmoltner, Andreas Klug, and Emil J. W. List-Kratochvil

Citation: *Applied Physics Letters* **104**, 193305 (2014); doi: 10.1063/1.4878539

View online: <http://dx.doi.org/10.1063/1.4878539>

View Table of Contents: <http://scitation.aip.org/content/aip/journal/apl/104/19?ver=pdfcov>

Published by the AIP Publishing

Articles you may be interested in

[Multianalyte biosensor based on pH-sensitive ZnO electrolyte–insulator–semiconductor structures](#)

J. Appl. Phys. **115**, 184701 (2014); 10.1063/1.4874182

[pH sensing properties of graphene solution-gated field-effect transistors](#)

J. Appl. Phys. **114**, 084505 (2013); 10.1063/1.4819219

[A pH sensor with a double-gate silicon nanowire field-effect transistor](#)

Appl. Phys. Lett. **102**, 083701 (2013); 10.1063/1.4793655

[Leaf-like carbon nanotube/nickel composite membrane extended-gate field-effect transistors as pH sensor](#)

Appl. Phys. Lett. **99**, 023108 (2011); 10.1063/1.3610554

[Electrolyte-gated organic field-effect transistors for sensing applications](#)

Appl. Phys. Lett. **98**, 153302 (2011); 10.1063/1.3581882

The announcement is set within an orange rectangular frame. On the left is a small portrait of André Anders. To the right, the 'AIP | Journal of Applied Physics' logo is displayed. Below the logo, the text reads: 'Journal of Applied Physics is pleased to announce **André Anders** as its new Editor-in-Chief'.

AIP | Journal of Applied Physics

Journal of Applied Physics is pleased to announce **André Anders** as its new Editor-in-Chief



Hydrogen ion-selective electrolyte-gated organic field-effect transistor for pH sensing

Johannes Kofler,^{1,a)} Kerstin Schmoltnner,^{1,a)} Andreas Klug,¹ and Emil J. W. List-Kratochvil^{1,2,b)}

¹NanoTecCenter Weiz Forschungsgesellschaft m.b.H., Franz-Pichler-Straße 32, A-8160 Weiz, Austria

²Institute of Solid State Physics, Graz University of Technology, Petersgasse 16, A-8010 Graz, Austria

(Received 1 April 2014; accepted 7 May 2014; published online 15 May 2014)

A H⁺ ion-selective electrolyte-gated organic field-effect transistor (IS-EGOFET) with a broad detection range between pH 3 and pH 12, is presented. This pH sensor relies on an integrated EGOFET used as a transducer in combination with an ionophore-doped polymeric ion-selective membrane serving as a sensing element. The broad detection range was possible through a dynamic measurement protocol comprising a readjustment of the gate voltage, which ensures a stable device operation at a constant working point. The effectiveness of this dynamic approach is confirmed by stability investigations. On the basis of this pH sensor concept, the importance of an appropriate gating electrolyte is highlighted, giving insights into the working mechanism of EGOFETs. © 2014 AIP Publishing LLC. [<http://dx.doi.org/10.1063/1.4878539>]

Glass electrodes, having a relatively high selectivity and a wide response range, are the most widely used devices for pH measurements in various samples. However, they also have a number of limitations, including high electrical resistance and brittleness. Particularly, for applications in bioanalysis such as *in-vivo* blood pH measurements, electrodes based on ionophore-doped liquid polymeric membranes are often preferred over traditional glass electrodes.¹ These ion-selective membranes (ISMs), containing neutral or charged ionophores, are available for the determination of a large number of organic and inorganic ions.² During the past decade, the chemical sensing abilities of ISMs have been significantly improved, resulting in a “new wave of ion-selective membranes.”³ If such powerful ion sensing elements are combined with suitable solid-state transducers, mass-producible, miniaturized ion-sensor systems with unforeseen analytical capabilities are within reach.³ Electrolyte-gated field-effect transistors (EGOFETs) proved to be ideal candidates as transducers for the detection of biomolecules such as DNA, dopamine, enzymes, and proteins in an electrolytic background with a constant ionic strength.^{4–7} Recently, we have shown that it is possible to use an EGOFET as a transducer in combination with a state of the art ISM as an active sensing element for selective and reversible Na⁺ ion detection.⁸ Moreover, EGOFETs are characterized by their small size, portability, low-energy consumption and low cost.^{9–11} An additional benefit of EGOFETs is that in contrast to the conventional ion-selective field-effect transistor (ISFET) architecture, the semiconductor is in direct contact with the electrolyte. Consequently, there is no need for elaborate and expensive encapsulation of the semiconductor. On the contrary, due to the formation of an electric double layer (EDL) at the semiconductor/electrolyte interface and a resulting high capacity (1–10 μF/cm²), a stable low-voltage operation

(<1 V) is possible.^{12–14} Therefore, they are ideal candidates, not only as transducers, but also as intrinsic signal amplifiers.¹⁵

Here, we demonstrate a selective and reversible EGOFET based pH sensor for a broad detection range between pH 3 and pH 12. First, the general requirements for gating electrolytes are investigated, giving insights into the working mechanism of EGOFETs. Subsequent stability investigations show the importance of operating the EGOFET at a constant low-voltage working point. This was ensured by the implementation of a dynamic measurement protocol which guarantees a constant effective gating potential independent of the sample composition.

The EGOFET based sensor was assembled as follows: The EGOFETs were fabricated on PET substrates (Melinex, DuPont Teijin Films) with gold source/drain electrodes (channel length ~6 μm, channel width ~3 mm) using regioregular poly(3-hexylthiophene) (P3HT) (Plexcore OS, Sigma-Aldrich) as organic semiconductor (for more details please refer to Ref. 8). The pH sensitive ionophore-doped polymeric ISMs were prepared as described by X. Liu *et al.*¹ but with a higher ionophore and salt content, reducing the influence of anion co-extraction at low pH values.¹⁶ The ISM membranes were prepared by drop-casting a high molecular weight polyvinyl chloride (31 wt.%, Selectophore grade), 2-nitrophenyl octyl ether (2-NPOE) (63 wt.%), sodium tetrakis[3,5-bis(trifluoromethyl)phenyl]borate (NaTTPB) (2 wt.%), and Hydrogen ionophore V (4 wt.%) in 4 ml tetrahydrofuran (THF) cocktail onto a glass slide. The drop-cast membrane was dried overnight at ambient conditions in a saturated THF environment and afterwards peeled off the glass slide for further implementation. The reservoir and the flow cell were fabricated via a soft molding process using polydimethylsiloxane (PDMS, Sylgard 184). Subsequently, the reservoir was placed on the EGOFET and filled with the inner filling solution. Finally, the ISM was sandwiched between the reservoir and the flow cell and sealed by applying a pressure with an appropriate fixture (see supplementary material (SM)). The 0.2M potassium phosphate buffer

^{a)}J. Kofler and K. Schmoltnner contributed equally to this work.

^{b)}Author to whom correspondence should be addressed. Electronic mail: emil.list-kratochvil@ntc-weiz.at

solutions (PBS) were adjusted to pH 7. To measure the response curve, the sample solution was buffered with 10 mM boric acid and 10 mM citric acid (unless noted otherwise) and drop-wise titrated with 0.5M NaOH while the pH was monitored with a calibrated glass electrode (Orion Thermo Sure Flow). All chemicals were obtained from Sigma Aldrich and were used as received. The electrical characterization of all devices was done in ambient conditions (at constant light conditions) using an Agilent B1500A Parameter Analyzer. All potentials were applied with respect to an Ag/AgCl reference electrode containing a 3M KCl inner filling solution.

The principle potentiometric sensing mechanism of this pH sensor is shown in Fig. 1: the EGOFET serves as a transducer and is in direct contact with an inner filling solution which is separated from the sample solution by the ISM. The sensing signal itself is given through the potential drop over the ISM, referred to as the membrane potential (E_{mem}). E_{mem} depends on the pH value of the sample relative to the pH value of the inner filling solution in a Nernstian fashion: $E_{mem} = E_0 + (RT/z_i F) \cdot \ln(pH_{sample}/pH_{inner\ filling})$, E_0 is a constant, R the gas constant, z_i the valency of the analyte ion, and F the Faraday's constant.¹⁷ During operation, a gate potential is applied to the sample solution with respect to the source contact through an Ag/AgCl reference electrode. The potential of the inner filling solution, which actually drives the EGOFET, is given through the sum of the membrane potential and the gate potential, and is further on referred to as effective gate potential. Generally, potentiometric measurements must have one polarizable, high impedance interface. In our case, the P3HT/inner filling solution interface should ideally be completely polarizable (no Faradaic current passes), whereas the Ag/AgCl gate electrode should be non-polarizable. Only if this is the case, it is ensured that the potential of the inner filling solution solely drops over the P3HT/electrolyte. Hence, the EGOFET serves as an impedance transformer, transforming the high impedance input-sensing signal of the effective gate potential into an amplified low impedance current signal (source-drain current). This is in contrast to the commonly used ion-selective electrodes (ISEs), where the polarizable and high impedance interface is provided by a potentiometer.

In order for this sensor concept to work, the inner filling solution of the sensor has to fulfill two conditions. First, it should allow for a good EGOFET performance in terms of transconductance and on/off ratio. This is the case if the inner

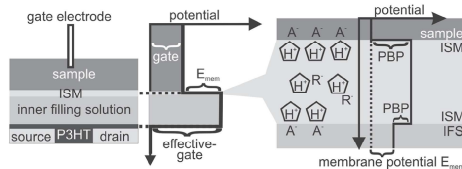


FIG. 1. Illustration of the sensing mechanism: a gate potential is applied to the sample solution relative to the source contact. The effective gate potential which drives the EGOFET is given through the sum of the gate and membrane potential (E_{mem}). E_{mem} stems from two Nernstian phase boundary potentials (PBP) at the ISM/inner filling solution (IFS) and at the sample/ISM interface, each depending on the respective pH value.

filling solution has a large electrochemical window which ensures a polarizable interface and, thus, a negligible leakage current (I_G) between the transistor and the gate. The second condition is related to the ISM: in order to guarantee a stable pH value and to avoid membrane potential drifts, pH buffers have to be used as an inner filling solution. Otherwise, processes such as co-extraction of counter-cations into the membrane and resulting diffusive transmembrane fluxes of H^+ lead to undesired pH value change of the inner filling solution.^{18–24} Furthermore, solvent polymeric membranes are permeable to CO_2 and other small neutral molecules which can also influence the pH value of the inner filling solution.^{25–27}

Here, a standard 0.2M phosphate buffer solution (PBS, pH 7), as commonly used in conventional ISE-setups, was employed as an inner filling solution. To verify whether the first condition is fulfilled, the EGOFET performance was studied without an ISM, i.e., the Ag/AgCl reference electrode was in direct contact with the inner filling solution (see the inset in Fig. 2). Figure 2 depicts the corresponding transfer (a) and output (b) characteristics, showing a good overall performance (on-current $\sim 1.7 \mu A$ and on/off ratio $\sim 2 \times 10^2$). These results are comparable with other values found in literature^{8,12,28} and prove the suitability of this buffer as a gating electrolyte. To demonstrate the effect of an inner filling solution which does not fulfill the aforementioned conditions (i.e., small electrochemical window), ascorbic acid ($10^{-2} M$) was added to the PBS. Fig. 2(c) shows the source-drain current (left) and gate current/leakage current (right) as a function of time: first, the EGOFET was gated with pure PBS (filled circles), subsequently with a phosphate buffer containing ascorbic acid and, finally, again with pure PBS. In case of ascorbic acid, the leakage current (open circles) increased by two orders of magnitude (from 10^{-10} to $10^{-8} A$) and the channel current decreased accordingly. Furthermore, the transfer characteristic was solely dominated

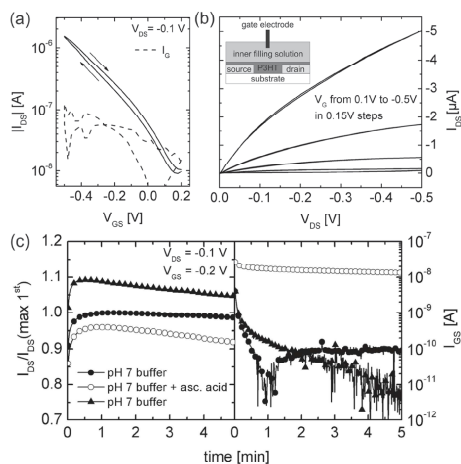


FIG. 2. Transfer (a) and output (b) characteristics of EGOFETs gated with a 0.2M phosphate buffer (PBS, pH 7); (c) source-drain current (left) and leakage current (right) as a function of time: first, the EGOFET was gated with PBS (filled circles), subsequently with PBS containing ascorbic acid (open circles), and finally, again with PBS (filled triangles).

by large leakage currents as shown in SM.²⁹ However, after replacing the ascorbic acid containing buffer with pure PBS again, the initial good transistor characteristics and low leakage currents were restored. Interestingly, the channel currents (at $V_{DS} = -100$ mV, $V_{GS} = -200$ mV) were slightly higher compared to the first measurement, indicating the absence of any degradation of the P3HT. Similar measurements were performed at higher gate potentials exhibiting the same trend (see SM).²⁹ The observed high steady-state gate currents can be ascribed to the ascorbic anion which is easily oxidized at the P3HT/electrolyte interface upon applying a negative potential to the gate electrode. Thus, the phosphate buffer containing ascorbic acid is a good example of a solution with a small electrochemical window. Another negative side effect at high gate currents can be a polarization of the membrane,^{30–33} which can lead to deviations from the linear Nernstian behavior and to a higher lowest-detection limit. These results highlight the importance of an appropriate inner filling solution and the separation of the EGOFET from the sample solution.

As discussed in our previous work,⁸ EGOFETs typically exhibit drifts. For that reason, stability investigations were carried out by measuring the drain and leakage currents at different gate voltages while keeping the source-drain potential constant. Fig. 3 shows the relative source-drain current changes for stepwise increased gate voltages. At gate voltages of -200 mV, -400 mV, and -600 mV negligible source-drain current drifts were observed within the measurement period of 8 min. High gate potentials of -800 mV lead to a significant channel current decrease of about 60% within 8 min indicating an irreversible degradation of the transistor. This is also confirmed by a significantly lower channel current of ~ 80 nA in comparison to the initial reference

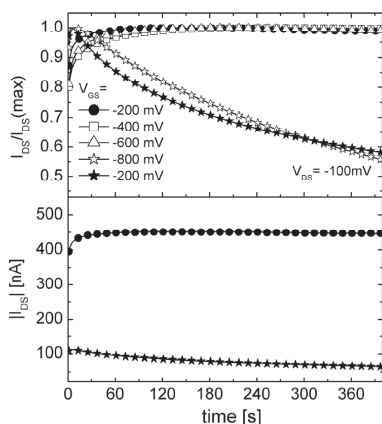


FIG. 3. (Top) Relative change of the source-drain current of an EGOFET gated with PBS as a function of time for different applied gate voltages: Open symbols represent measurements with stepwise increased gate voltages (-400 mV, -600 mV, -800 mV), closed symbols represent the subsequent reference measurements at -200 mV. The curves were normalized with respect to their maximum current. (Bottom) Absolute change of source-drain current at $V_{GS} = -200$ mV before and after applying elevated gate potentials for 8 min (>600 mV).

measurement at -200 mV (~ 450 nA). Moreover, the leakage current did not change, except during the first few seconds due to repolarization/charging and is typically ~ 1 nA.²⁹ The reason behind the observed channel current degradation is believed to be attributed to electrolysis and subsequent degradation of P3HT through oxygen oxidation^{34,35} and decrease of the charge carrier mobility due to ions/water molecules which diffuses into the organic semiconductor.³⁶

Regardless of the exact degradation mechanism, the results demonstrate that EGOFETs must be operated well below -600 mV in order to guarantee a stable operation. As the state of the art H^+ selective ISM membrane used in this work exhibits a broad detection range between pH 3 and pH 12 with a near Nernstian response of 52 mV/pH and a high selectivity,¹ the membrane potential can vary for more than 400 mV. Such a large membrane potential change would inevitably lead to instabilities/drifts of the EGOFET. Moreover, to maintain a stable working point, the effective gate potential has to be independent of the membrane potential and, thus, pH value of the sample. For that reason, a dynamic measurement protocol was used: the gate potential was adjusted dynamically by a feed-back loop keeping the source-drain current constant. The feedback loop was implemented using two Keithley 2400 SMUs which were controlled in real time via VBA-Excel. One SMU (source-drain SMU) measured the current at a constant source-drain voltage. The second one was connected to the gate electrode (gate SMU). Both SMUs shared a common ground. The accordingly adjusted gate potential change corresponds directly to the membrane potential change which eases data analysis. Another advantage of this measurement protocol is that it is not necessary to record the whole transfer curve in order to correlate the source-drain current changes with membrane potential changes/concentration changes. In our case, two solutions with known pH values are sufficient to calibrate the sensor.

The pH calibration curves of a boric/citric acid solution with a molarity of 10 mM each are shown in Fig. 4(a). Additionally, a calibration of a 5 mM boric/citric acid solution with and without a 10 mM NaCl background was recorded. The pH value was adjusted by titrating with a NaOH solution. As a result, the Na^+ concentration is increased at high pH values depending on the initial molarity of the citric and boric acid. Despite of a high concentration of the interfering alkali metal ion Na^+ , the response curve

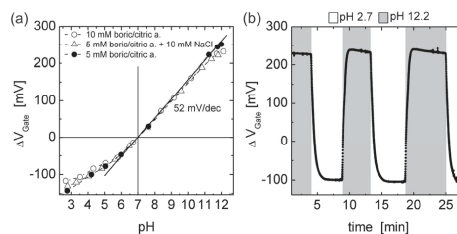


FIG. 4. (a) pH value calibration curves: gate voltage change as a function of the pH value; (b) response curve upon a pH-value change from pH 2.7 to pH 12.

reveals a near Nernstian slope between pH values 6 and 12, with a slope of 52 mV/dec. There is only a limited influence of interfering Na^+ ions at high pH values where the slope is slightly decreased. This is due to the high selectivity of the membrane over alkali metal ions.¹ At low pH values (<pH 6), anion interference leads to a deviation from the Nernstian slope (~25 mV/dec).¹ The anionic interference is increased with increasing anionic strength, i.e., with increasing NaCl or citric acid concentration. Fig. 4(b) shows the response curve of the sensor device exposed to a pH 12.2 buffer-solution and subsequently to a pH 2.7 buffer-solution. The response is reversible, and even long continuous measurements of 30 min did not show any significant drifts. The response time of this device is limited by the time necessary to flush the flow cell with the buffer solution.

In contrast to other sensor concepts based on EGOFETs,³⁷ the advantage of the presented IS-EGOFET is that the latter is not in direct contact with the sample solution, and the sensing signal solely relies on a highly selective ISM. Thus, it is ensured that the response is not influenced by any variations of the EGOFET-characteristics which depend on the composition of the gating solution due to a modification of the electrolyte/semiconductor interface.^{13,38}

In conclusion, a pH sensor based on a versatile ion-selective EGOFET concept comprising a highly selective state of the art H^+ membrane was demonstrated. Due to a dynamic measurement protocol pH detection within a broad detection range between pH 2.7 and pH 12 was possible. The EGOFET was operated at a constant and stable low-voltage working point independent of the sample composition. The pH sensor exhibited a linear near Nernstian response in the range between pH 6 and 12 and a sub Nernstian response between pH 2.7 and 6. Moreover, insights into the working mechanisms of EGOFETs were obtained by using an electrolyte with a small electrochemical window (adding ascorbic acid to PBS). The leakage current dramatically increased, while the transistor performance is not degraded permanently. This further highlights the advantage of the IS-EGOFET concept where the EGOFET is separated from various sample solutions by the ISM, paving the way for the application within relevant environments such as different body fluids.

For financial support, the Styrian Government (Project BioOFET 2, GZ:A3-11.B-36/2010-5) is acknowledged.

¹X.-J. Liu, B. Peng, F. Liu, and Y. Qin, *Sens. Actuators, B* **125**, 656 (2007).

²E. Bakker, P. Bühlmann, and E. Pretsch, *Chem. Rev.* **97**, 3083 (1997).

³J. Bobacka, A. Ivaska, and A. Lewenstam, *Chem. Rev.* **108**, 329 (2008).

⁴L. Kergoat, B. Piro, M. Berggren, M. C. Pham, A. Yassar, and G. Horowitz, *Org. Electron.* **13**, 1 (2012).

⁵S. Casalini, F. Leonardi, T. Cramer, and F. Biscarini, *Org. Electron.* **14**, 156 (2013).

⁶F. Buth, A. Donner, M. Sachsenhauser, M. Stutzmann, and J. A. Garrido, *Adv. Mater.* **24**, 4511 (2012).

⁷M. Magliulo, A. Mallardi, M. Y. Mulla, S. Cotrone, B. R. Pistillo, P. Favia, I. Vikholm-Lundin, G. Palazzo, and L. Torsi, *Adv. Mater.* **25**, 2090 (2013).

⁸K. Schmoltner, J. Kofler, A. Klug, and E. J. W. List-Kratochvil, *Adv. Mater.* **25**, 6895 (2013).

⁹P. Lin and F. Yan, *Adv. Mater.* **24**, 34 (2012).

¹⁰L. Kergoat, B. Piro, M. Berggren, G. Horowitz, and M.-C. Pham, *Anal. Bioanal. Chem.* **402**, 1813 (2012).

¹¹J. T. Mabeck and G. G. Malliaras, *Anal. Bioanal. Chem.* **384**, 343 (2006).

¹²L. Kergoat, L. Herlogsson, D. Braga, B. Piro, M.-C. Pham, X. Crispin, M. Berggren, and G. Horowitz, *Adv. Mater.* **22**, 2565 (2010).

¹³F. Buth, D. Kumar, M. Stutzmann, and J. A. Garrido, *Appl. Phys. Lett.* **98**, 153302 (2011).

¹⁴A. Laiho, L. Herlogsson, R. Forchheimer, X. Crispin, and M. Berggren, *Proc. Natl. Acad. Sci. U.S.A.* **108**, 15069 (2011).

¹⁵T. Cramer, A. Campana, F. Leonardi, S. Casalini, A. Kyndiah, M. Murgia, and F. Biscarini, *J. Mater. Chem. B* **1**, 3728 (2013).

¹⁶Z. Szigeti, T. Vigassy, E. Bakker, and E. Pretsch, *Electroanalysis* **18**, 1254 (2006).

¹⁷P. Bühlmann and L. D. Chen, in *Supramolecular Chemistry: From Molecular to Nanomaterials*, 1st ed., edited by J. W. Steed and P. A. Gale (Wiley, 2012), pp. 2539–2577.

¹⁸A. Ceresa, T. Sokalski, and E. Pretsch, *J. Electroanal. Chem.* **501**, 70 (2001).

¹⁹T. Zwickl and T. Sokalski, *Electroanalysis* **11**, 673 (1999).

²⁰E. Bakker, R. K. Meruva, E. Pretsch, and M. E. Meyerhoff, *Anal. Chem.* **66**, 3021 (1994).

²¹W. E. Morf, E. Lindner, and W. Simon, *Anal. Chem.* **47**, 1596 (1975).

²²T. Sokalski, A. Ceresa, M. Fibbioli, T. Zwickl, E. Bakker, and E. Pretsch, *Anal. Chem.* **71**, 1210 (1999).

²³T. Sokalski, T. Zwickl, E. Bakker, and P. Ernő, *Anal. Chem.* **71**, 1204 (1999).

²⁴W. E. Morf, M. Badertscher, T. Zwickl, N. F. De Rooij, and P. Ernő, *J. Phys. Chem. B* **103**, 11346 (1999).

²⁵E. Lindner and R. E. Gyurcsányi, *J. Solid State Electrochem.* **13**, 51 (2009).

²⁶E. Lindner and R. P. Buck, *Fresenius' J. Anal. Chem.* **364**, 22 (1999).

²⁷S. Y. Hyoung, S. C. Geun, and M. E. Meyerhoff, *Anal. Chim. Acta* **237**, 115 (1990).

²⁸K. Schmoltner, J. Kofler, A. Klug, and E. J. W. List-Kratochvil, *Proc. SPIE* **8831**, 88311N (2013).

²⁹See supplementary material at <http://dx.doi.org/10.1063/1.4878539> for influence of ascorbic acid in phosphate buffer solution on the transistor characteristics and gate current of EGOFETs after stressing with elevated gate potentials.

³⁰J. M. Zook, R. P. Buck, J. Langmaier, and E. Lindner, *J. Phys. Chem. B* **112**, 2008 (2008).

³¹M. G. Afshar, G. A. Crespo, and E. Bakker, *Anal. Chem.* **84**, 8813 (2012).

³²S. Makarychev-Mikhailov, A. Shvarev, and E. Bakker, *Anal. Chem.* **78**, 2744 (2006).

³³S. Makarychev-Mikhailov, A. Shvarev, and E. Bakker, *J. Am. Chem. Soc.* **126**, 10548 (2004).

³⁴H.-H. Liao, C.-M. Yang, C.-C. Liu, S.-F. Horng, and H.-F. Meng, *J. Appl. Phys.* **103**, 104506 (2008).

³⁵M. S. A. Abdou, F. P. Orfino, Y. Son, and S. Holdcroft, *J. Am. Chem. Soc.* **119**, 4518 (1997).

³⁶T. Cramer, T. Steinbrecher, T. Koslowski, D. Case, F. Biscarini, and F. Zerbetto, *Phys. Rev. B* **79**, 155316 (2009).

³⁷K. Melzer, A. M. M. Münzer, E. Jaworska, K. Maksymiuk, A. Michalska, and G. Scarpa, *Org. Electron.* **15**, 595 (2014).

³⁸A. M. Münzer, K. Melzer, M. Heimgreiter, and G. Scarpa, *Biochim. Biophys. Acta* **1830**, 4353 (2013).

7.3 Electrolyte-gated field-effect transistor for selective and reversible ion detection

K. Schmoltner*, J. Kofler*, A. Klug and E. J. W. List-Kratochvil,
Advanced Materials 25 (47), 6895–6899 (2013)

©WILEY-VCH Verlag GmbH & Co.

*both authors contributed equally.

Contribution: The author contributed equally with K. Schmoltner to experiments related to the ion-selective EGOFETs and sensor characterization. K. Schmoltner wrote the manuscript, finalized the manuscript together with the author.

Electrolyte-Gated Organic Field-Effect Transistor for Selective Reversible Ion Detection

Kerstin Schmoltner, Johannes Kofler, Andreas Klug, and Emil J. W. List-Kratochvil*

Organic field-effect transistors (OFETs) have already been proven to be suitable candidates as transducers for various sensor applications.^[1–4] Owing to their intrinsic amplification, OFET based sensors typically reveal a high sensitivity. In conjunction with the outstanding features of organic electronic devices such as economic production, integration on flexible substrates and biocompatibility, low-cost disposable sensor assemblies are not a future vision anymore. Especially, the emerging fields of medical diagnostics and environmental monitoring require sensor platforms for in-situ sensing of ions and biological substances in appropriate aqueous media. Within these fields, sensor arrays for multiple ion detection (e.g., Na⁺, K⁺, Ca²⁺, pH) for biomedical diagnostics, food-monitoring as well as for industrial process- and water-control are of particular interest.^[5] Regarding these sensing applications, electrolyte-gated organic field-effect transistors (EGOFETs) are the transducers of choice. In contrast to conventional ion-sensitive OFETs^[5–9] or FETs (ISFETs),^[10–12] where the analyte is in contact with a solid gate dielectric, EGOFETs benefit from a direct contact between the organic semiconductor and the analyte. The electric double layer of high capacitance (1–10 μF cm⁻²) formed at this interface enables low-voltage operation, which ensures a water-stable operation window, while the achieved source-drain currents (in the range of a few μA)^[13–15] are sufficiently high for further signal processing.^[6]

The high potential of electrolyte-gated OFETs was first indicated by Kergoat et al. who reported on the stable operation of water-gated OFETs.^[13] Recent advances in this field include the successful detection of biomolecules such as DNA, dopamine, enzymes and proteins.^[16–19] Additionally, the influence of pH and ionic strength of the electrolyte on the performance of EGOFETs were studied.^[3,14] However, to our knowledge no organic ion-selective EGOFET has been shown.

With this contribution we demonstrate a novel, modular and versatile EGOFET-sensor platform for reversible and selective ion detection. Based on an electrolyte-gated poly(3-hexylthiophene) thin film transistor and a state-of-the-art sodium ion

(Na⁺) selective membrane,^[20] a sensitive linear response in the range of 10⁻⁶ to 10⁻¹ M Na⁺ with a slope of ≈62 mV dec⁻¹ was achieved. Furthermore, this potentiometric sensor showed a reversible response and its selectivity was successfully tested against interfering potassium ions (K⁺). This new concept proves to be an important step towards a low-cost integrated ion-sensor array for selective multiple ion detection.

A schematic cross-section of the introduced ion-sensitive EGOFET is shown in Figure 1a, consisting of a bottom-contact poly(3-hexylthiophene) (P3HT) FET in direct contact with an optimized inner filling solution (water containing 10⁻² M NaCl), acting as an electrolyte gate and separated via a polyvinylchloride (PVC) based ion-selective membrane (ISM) from the analyte. The latter is in contact with an Ag/AgCl (3 M KCl) reference electrode. The mounted flow cell enables a continuous exposure of the sensor device to different salt concentrations. This architecture is modular and facilitates the realization of ion-selective EGOFETs for the detection of various ions “simply” by introducing appropriate ISMs. The latter are well-established components which are usually applied in ion-selective electrodes.^[21–23] Due to their vast dissemination they are available with a large variety of different ionophore-doped sensing membranes.^[24] Their working principle is not based on a selective transport through the membrane as, for example, in case of filtration, osmosis or gas separation. In contrast, it relies on the ion movement over a few nanometers within the charge separation layer at the sample/membrane interface, leading to an activity-dependent membrane potential. A detailed explanation of the function of such ISMs is, for example, given by Bühlmann et al.^[24] Important sensor parameters such as lowest detection limit and selectivity can be tuned by modifying the membrane.^[25]

In contrast to other OFET sensor concepts, this approach is potentiometric and no direct modification of the organic semiconductor takes place, which leads to a higher overall device stability. Moreover, since no binding happens at the interface (such as with enzymes etc.),^[18] reversible detection is possible by simply flushing the device using a mounted flow cell. Thus no complex recovery process is needed.

Figure 1 also shows the transfer (b) and output (c) characteristics of a typical Na⁺ sensitive EGOFET with deionized (DI) water as analyte and a 10⁻² M NaCl inner filling solution, exhibiting typical field-effect characteristics with a slight hysteresis. The transfer curve of this ion-sensitive EGOFET is shifted by ≈200 mV to the negative direction when the target ion in the analyte is increased to 10⁻² M Na⁺. This threshold voltage (V_{th}) shift originates from a non-zero membrane potential. In detail, this Nernstian membrane potential (see Figure 1a and Equation (1)) is determined by the ion activity difference between the analyte and the inner filling solution. As the ion activity of the inner

K. Schmoltner,^[†] J. Kofler,^[†] Dr. A. Klug,
Prof. Dr. E. J. W. List-Kratochvil
NanoTecCenter Weiz Forschungsgesellschaft mbH
Franz-Pichler Straße 32, A-8160 Weiz, Austria
E-mail: E.List@tugraz.at
Prof. Dr. E. J. W. List-Kratochvil
Institute of Solid State Physics
Graz University of Technology
Petersgasse 32, A-8010, Graz, Austria



^[†]K. Schmoltner and J. Kofler contributed equally to this work.

DOI: 10.1002/adma.201303281

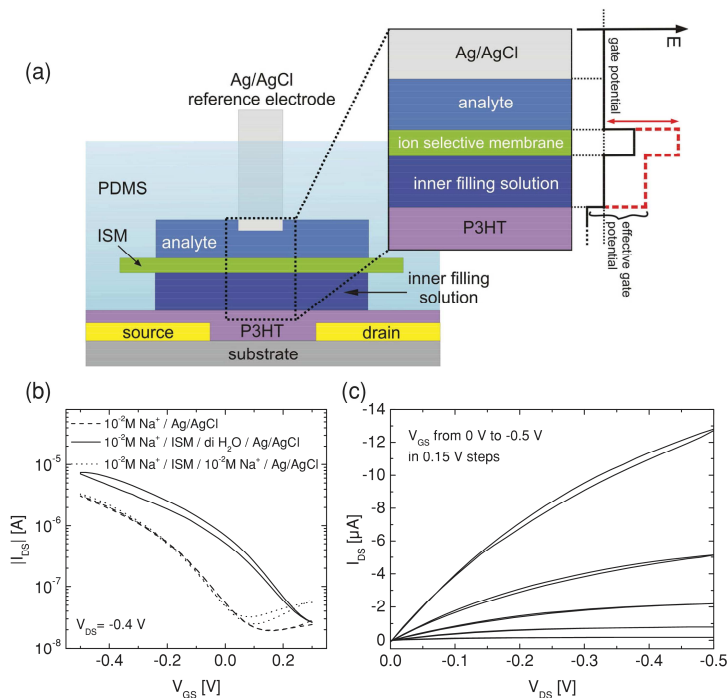


Figure 1. a) Cross section of an ion-sensitive EGFET: the bulk potentials in case of equal ion concentration in the analyte and the inner filling solution (black) as well as in case of lower concentration in the analyte (red dashed) are illustrated. b) Semilogarithmic transfer curve of a typical P3HT-based EGFET without (dashed line) and with implemented ISM using DI H₂O (solid line) and 10⁻² M Na⁺ solution (dotted line) as an analyte. c) Output characteristics of an ion-sensitive EGFET using DI H₂O as an analyte.

filling solution is kept constant and the potential of the analyte is predefined through the Ag/AgCl gate electrode, the potential of the inner filling solution is modulated solely by the ion activity in the analyte (see Figure 1a). In fact, it is the potential of the inner filling solution (gate potential + membrane potential), hereby referred to as effective gate potential, which controls the source-drain current. Therefore, if the concentration of the target ion in the analyte is equal to the concentration in the inner filling solution (10⁻² Na⁺), the membrane potential is zero and the effective gate voltage matches the applied gate voltage. Consequently no V_{th} shift is observed, and the characteristics are identical to an EGFET without a Na⁺ selective membrane where the Ag/AgCl gate electrode is directly immersed into the inner filling solution (see Figure 1b, dashed line). The reason for the insignificantly increased off-current of the transfer curve with an ISM (dotted line) is a slightly larger leakage current. The mobility with and without an ISM in the saturation region was estimated to be $\approx 2 \times 10^{-2} \text{ cm}^2 \text{ V}^{-1} \text{ s}^{-1}$ using a typical capacitance of $3 \text{ } \mu\text{F cm}^{-2}$ (for an Au/P3HT/water/Au system)^[13], which is in good agreement with other reported values.^[1,13] These results clearly demonstrate that the implementation of an ISM does not influence the overall performance (on/off ratio

$\approx 10^2$, maximum channel currents of $\approx 10 \text{ } \mu\text{A}$) of the underlying EGFET. However, when choosing the operational voltages, it is important to consider the effective applied gate potential which should be well below 0.7 V to ensure a stable device operation and to avoid degradation due to doping and hydrolyses.^[13,14]

In order to demonstrate the sensitivity of the ion-selective EGFET to Na⁺, the source-drain current was recorded at a constant gate and source-drain potential while the Na⁺ concentration in the water (analyte) was increased stepwise (see Figure 2a, $V_{DS} = -0.1 \text{ V}$, $V_{GS} = -0.2 \text{ V}$). The Na⁺ concentration was adjusted by adding a certain amount of different saline solutions (10⁻⁴ – 10⁻¹ M NaCl) to a larger reservoir (200 ml DI H₂O beaker) which was connected via PVC tubing to the flow cell and further to retracting micro syringes, producing a constant flow of 1 ml/min. As a sensitive response a source-drain current decrease of $\approx 250\text{--}500 \text{ nA dec}^{-1}$ (depending on the point of operation) was observed while varying the Na⁺ concentration between 10⁻⁶ M and 10⁻¹ M. The source-drain current decrease reflects the change in effective gate potential. The latter can be calculated by using the fitted transfer curve at $V_{SD} = -0.1 \text{ V}$ (see Supporting Information) of the EGFET without an ISM.

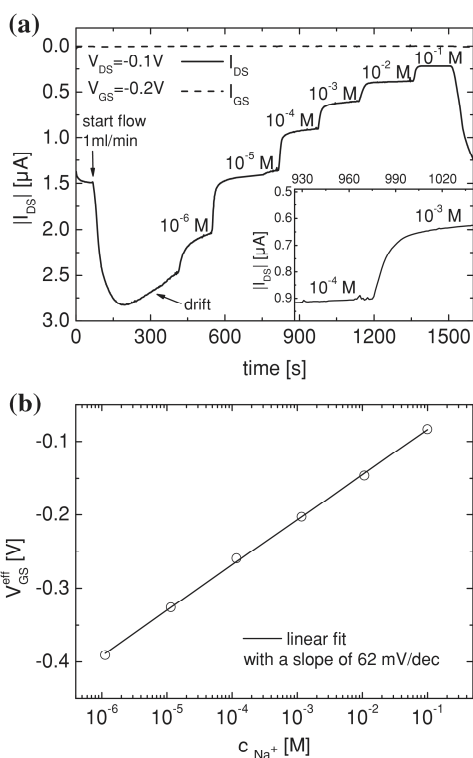


Figure 2. a) Source-drain current response to increasing Na^+ concentration of a typical ion-sensitive EGOFET with a PVC ion-selective membrane, exhibiting a response time of ≈ 30 s (see inset). b) Calculated effective gate potential versus Na^+ concentration (see Supporting Information).

Alternatively, the transfer curve of the EGOFET with an ISM can be used (as mentioned before), if the Na^+ concentration in the inner filling solution and the analytes are equal. Figure 2b shows the calculated effective gate voltage versus the Na^+ concentration following a linear relation with a slope of 62 mV dec^{-1} . Accordingly, the ion-selective PVC membranes were also tested in an ion-selective electrode configuration and the electrical characterization revealed a sensitive response of about 52 mV dec^{-1} (see Supporting Information). Both values are in good agreement with the theoretically predicted value of 59.2 mV dec^{-1} , calculated from the Nernst equation at 25°C , which describes the membrane potential across the membrane as follows^[23]

$$E = E^0 + \frac{RT}{z_1 F} \ln \left(\frac{a_{\text{analyte}}}{a_{\text{inner}}} \right) \quad (1)$$

where E^0 is a constant, R the gas constant, z_1 the valency of the analyte ion, F the Faraday's constant and a the corresponding activity of the target ion in the analyte and the inner filling

solution, respectively. Variations of about $\approx 7 \text{ mV dec}^{-1}$ are in the expected error range, considering the fitting model for the EGOFET transfer curve as well as degradation effects due to the long continuous measurements. Nevertheless, the obtained values for the effective applied gate potential represent good estimations.

The implementation of a flow cell was necessary to obtain a reversible sensor response and to lower the detection limit from 10^{-5} M Na^+ down to $\approx 10^{-6} \text{ M Na}^+$.^[26] This can be clearly seen by comparing the source-drain current before and after applying a flow of DI water through the cell (see Figure 2, first 300 s): if there is no flow, ions which diffuse out of the inner filling solution into the analyte lead to an artificially increased ion concentration in the vicinity of the ISM.^[27] This results in a decreased effective gate potential and further to a decreased source-drain current. If a flow is applied (after 300 s), this concentration is lowered, leading to a higher effective gate potential and consequently also to a higher source-drain current. These low Na^+ concentrations and the resulting high effective gate voltages (here $< -400 \text{ mV}$) lead to significant drifts (decreasing channel currents, see Figure 2a, 200–400 s). By increasing the concentration the effective applied gate voltage is decreased and the drift is reduced until it almost vanishes completely. Moreover, since no significant drift occurred when no voltages were applied, its origin is most probably ascribed to the electrolysis of water at the electrolyte/semiconductor interface leading to device degradation. This drift can in principle be avoided by keeping the effective gate potential constant at a stable operating point, regardless of the ion concentration in the analyte. However, this requires a readjusting of the gate potential by an appropriate feedback mechanism.^[28,29] The according adjustment of the gate potential corresponds directly to the membrane potential change and thus to the ion concentration in the analyte. An appropriate read-out circuit is currently under investigation.

Moreover, note that the herein reported lowest detection limit (10^{-6} M Na^+) is not a property of the ion-sensitive EGOFET itself, but is rather determined by the ISM and the inner filling solution. In detail, ion fluxes through the membrane typically limit the lowest detection limit. Suppression of these fluxes which leads to detection limits in the nano-molar range can be achieved e.g., by using thicker membranes or a lower Na^+ concentration in the inner filling solution.^[25,26,30]

Furthermore, the response time of ≈ 30 s is not a property of the ISM itself but rather related to how quickly the concentration within the flow cell reaches the concentration of the large reservoir (mixing time).^[24] Consequently, the response time can be lowered by increasing the flow rate and decreasing the dead volume.

The reversible and selective response of the ion-sensitive EGOFET is shown in Figure 3. It demonstrates a rather fast response when the concentration was varied between 10^{-4} M Na^+ (base line) and 10^{-3} M Na^+ . The selective response was tested with K^+ as interfering ion following 3 Na^+ concentration variation steps. The K^+ concentration was increased in a 10^{-4} M Na^+ background solution to 10^{-2} M K^+ (two orders of magnitude), showing a current variation of about 7%. In comparison, by increasing from 10^{-4} M Na^+ to 10^{-3} M Na^+ (one order of magnitude), a 5 times higher current change was

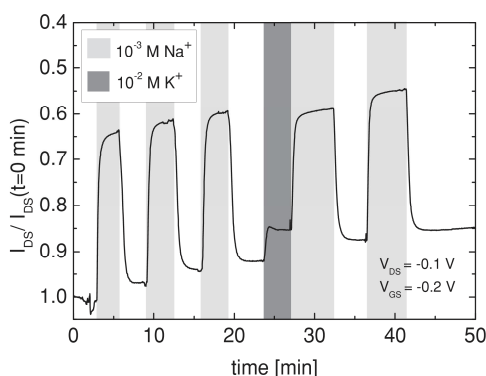


Figure 3. Response curve of a Na⁺ selective EGFOT. The source-drain current was measured while the Na⁺ concentrations were changed rapidly from 10⁻⁴ to 10⁻³ M and back. The selectivity was investigated by adding K⁺ to a 10⁻⁴ M Na⁺ background solution to obtain 10⁻² M K⁺.

detected, confirming the selectivity of the ion-sensitive EGFOT to Na⁺ ions. When the same PVC ISM was also characterized with respect to selectivity in an ion-selective electrode configuration between a range of 10⁻⁶ – 10⁻¹ M K⁺, the significant selective response to Na⁺ could be confirmed (see Supporting Information). The long-term current drift of ≈0.3% per minute at a reasonable gate voltage (see Figure 3), can be most likely ascribed to bias-stress effects. The long-term stability^[31] of the newly presented ion sensor is not a main topic in this letter but will be one of the challenges for the future when pursuing highly promising sensor concepts based on EGFOTs. However, considering the utilization of the presented ion sensor for rapid self-testing applications, the obtained small drifts during operation are in an acceptable range.

In conclusion, we have successfully demonstrated a novel sensor platform based on electrolyte-gated OFETs for selective and reversible ion detection. The novelty of this design compared to conventional ISFETs is the direct contact between the electrolyte and the semiconductor without the use of a solid dielectric, making low-voltage operation in aqueous media feasible. Furthermore, this architecture benefits from a modular approach, allowing for the detection of various ions simply by choosing an appropriate ion-selective membrane. The presented potentiometric sensor based on a Na⁺ sensitive PVC membrane showed a Nernstian behavior for a broad detection range between 10⁻⁶ M and 10⁻¹ M Na⁺. Moreover, a selective as well as reversible sensor response without a complex recovering process was achieved. These results constitute an important step towards a low-cost integrated sensor array for multiple ion detection facilitated by a facile integration of different state-of-the-art ISMs, being of high relevance for biomedical diagnostics, food-monitoring, industrial process- and water-control.

Experimental Section

The reservoir and the flow cell for the ion-sensitive EGFOTs were made of polydimethylsiloxane (PDMS, Sylgard 184) via a soft molding

process, including a curing step of ≈1 h at 100 °C. In order to seal off the flow cell and the reservoir of the inner filling solution, a pressure was applied by an appropriate fixture. The EGFOTs were fabricated on PET substrates (Melinex, DuPont Teijin Films) and the 50 nm gold source/drain (S/D) electrodes with 2 nm chromium adhesion layer were structured using conventional lift-off processing (channel length ≈7 μm, channel width ≈3 mm). Regioregular poly(3-hexylthiophene) (Plexcore OS purchased from Sigma-Aldrich) was deposited via spin-coating from a 4 g L⁻¹ toluene solution and dried at 60 °C in Argon (Ar) for ≈10 min and subsequently at 120 °C under high vacuum (p ≈ 4 × 10⁻⁵ mbar) for 1 h. All devices were assembled under inert atmosphere. In order to obtain a sensitive as well as selective response to sodium ions, a state-of-the-art ionophore-doped PVC based ISM as described by A. Cadogan^[20] was introduced. The ISM membranes were prepared by drop-casting a high molecular weight polyvinyl chloride (31 wt%, Selectophore grade), 2-nitrophenyl octyl ether (2-NPOE) (68 wt%), potassium tetrakis-((4-chlorophenyl)borate (KTPCIPB) (0.7 wt%) and sodium ionophore X (0.2 wt%) in 5 mL tetrahydrofuran (THF) cocktail onto a glass slide. The drop-cast membrane was allowed to dry overnight at ambient conditions and was peeled off the glass slide for further implementation. All of the chemicals mentioned above were obtained from Fluka Sigma-Aldrich and were used as received. Saline solutions were prepared in concentrations varying from 10⁻⁴ M to 10⁻¹ M NaCl (99.5%, p.a., ACS, ISO) and KCl (>99.0%) in deionized water, respectively. The electrical characterization of all devices was done in ambient air conditions (at same light conditions) using an Agilent B1500 Parameter Analyzer. Gradual channel approximation was used to calculate the field-effect mobility in the saturation regime.

Supporting Information

Supporting Information is available from the Wiley Online Library or from the author.

Acknowledgements

For financial support the Styrian Government (projects BioFOT 2 and MIEC-DEVS) is acknowledged.

Received: July 16, 2013
Revised: August 15, 2013
Published online: September 19, 2013

- [1] L. Kergoat, B. Piro, M. Berggren, G. Horowitz, M.-C. Pham, *Anal. Bioanal. Chem.* **2012**, *402*, 1813.
- [2] P. Lin, F. Yan, *Adv. Mater.* **2012**, *24*, 34.
- [3] J. T. Mabeck, G. G. Malliaras, *Anal. Bioanal. Chem.* **2006**, *384*, 343.
- [4] A. Klug, M. Denk, T. Bauer, M. Sandholzer, U. Scherf, C. Slugovc, E. J. W. List, *Org. Electron.* **2013**, *14*, 500.
- [5] A. Bratov, N. Abramova, A. Ipatov, *Anal. Chim. Acta* **2010**, *678*, 149.
- [6] C. Bartic, B. Palan, A. Campitelli, G. Borghs, *Sens. Actuators, B* **2002**, *83*, 115.
- [7] C. Gao, X. Zhu, J. Choi, C. H. Ahn, in *IEEE Transducers '03, The 12th International Conference on Solid State Sensors Actuators and Microsystems*, Boston **2003**, 1172.
- [8] C. Bartic, A. Campitelli, S. Borghs, *Appl. Phys. Lett.* **2003**, *82*, 475.
- [9] T. Ji, P. Rai, S. Jung, V. K. Varadan, *Appl. Phys. Lett.* **2008**, *92*, 233304.
- [10] P. Bergveld, *Sens. Actuators, B* **2003**, *88*, 1.
- [11] P. Bergveld, *IEEE Trans. Biomed. Eng.* **1970**, *BME* *17*, 70.
- [12] S. V. Dzyadevych, A. P. Soldatkin, A. V. El'skaya, C. Martelet, N. Jaffrezic-Renault, *Anal. Chim. Acta* **2006**, *568*, 248.

- [13] L. Kergoat, L. Herlogsson, D. Braga, B. Piro, M.-C. Pham, X. Crispin, M. Berggren, G. Horowitz, *Adv. Mater.* **2010**, *22*, 2565.
- [14] F. Buth, D. Kumar, M. Stutzmann, J. A. Garrido, *Appl. Phys. Lett.* **2011**, *98*, 153302.
- [15] A. Laiho, L. Herlogsson, R. Forchheimer, X. Crispin, M. Berggren, *Proc. Natl. Acad. Sci. U.S.A.* **2011**, *108*, 15069.
- [16] L. Kergoat, B. Piro, M. Berggren, M.-C. Pham, A. Yassar, G. Horowitz, *Org. Electron.* **2012**, *13*, 1.
- [17] S. Casalini, F. Leonardi, T. Cramer, F. Biscarini, *Org. Electron.* **2013**, *14*, 156.
- [18] F. Buth, A. Donner, M. Sachsenhauser, M. Stutzmann, J. A. Garrido, *Adv. Mater.* **2012**, *24*, 4511.
- [19] M. Magliulo, A. Mallardi, M. Y. Mulla, S. Cotroneo, B. R. Pistillo, P. Favia, I. Vikholm-Lundin, G. Palazzo, L. Torsi, *Adv. Mater.* **2013**, *25*, 2090.
- [20] A. Cadogan, Z. Gao, A. Lewenstam, A. Ivaska, D. Diamond, *Anal. Chem.* **1992**, *64*, 2496.
- [21] E. Bakker, E. Pretsch, *Anal. Chem.* **2002**, 420.
- [22] N. Abramova, A. Bratov, *Sensors* **2009**, *9*, 7097.
- [23] S. V. Lamaka, M. G. Taryba, M. L. Zheludkevich, M. G. S. Ferreira, *Electroanal.* **2009**, *21*, 2447.
- [24] P. Bühlmann, L. D. Chen, in *Supramolecular Chemistry: From Molecules to Nanomaterials* (Eds: P. A. Gale, J. W. Steed), John Wiley & Sons, Ltd., **2012**, pp. 2539–2577.
- [25] E. Bakker, E. Pretsch, *Trends in Anal. Chem.* **2001**, *20*, 11.
- [26] A. Ceresa, T. Sokalski, E. Pretsch, *J. Electroanal. Chem.* **2001**, *501*, 70.
- [27] S. Mathison, E. Bakker, *Anal. Chem.* **1998**, *70*, 303.
- [28] P. Bergveld, *Sens. Actuators* **1981**, *1*, 17.
- [29] P. Bergveld, *IEEE Trans. Biomed. Eng.* **1968**, *BME 15*, 102.
- [30] K. Schrolltner, F. Schlütter, M. Kivala, M. Baurngarten, S. Winkler, R. Trattning, N. Koch, A. Klug, E. J. W. List, K. Müllen, *Polym. Chem.* **2013**, *10.1039/c3py00089c*.
- [31] Z. Szigeti, T. Vigassy, E. Bakker, E. Pretsch, *Electroanal.* **2006**, *18*, 1254.

7.4 Ion-selective electrolyte-gated field-effect transistors: Prerequisites for proper functioning

J. Kofler, K. Schmoltner and E.J.W. List-Kratochvil,

Proceedings of SPIE 9185, Organic Semiconductors in Sensors and Bioelectronics VII, 91851U-1 (2014)

©Society of Photo Optical Instrumentation Engineers

Contribution: All experimental work. The author wrote the manuscript. The manuscript was finalized with K. Schmoltner.

Ion-selective electrolyte-gated field-effect transistors: Prerequisites for proper functioning

Johannes Kofler^a, Kerstin Schmoltn^a, Emil J. W. List-Kratochvil^{*a,b}

^a NanoTecCenter Weiz Forschungsgesellschaft m.b.H., Franz-Pichler-Straße 32, A-8160 Weiz, Austria

^b Institute of Solid State Physics, Graz University of Technology, Petersgasse 16, A-8010 Graz, Austria

ABSTRACT

Electrolyte-gated organic field-effect transistors (EGOFETs) used as transducers and amplifiers in potentiometric sensors have recently attracted a significant amount of scientific interest. For that reason, the fundamental prerequisites to achieve a proper potentiometric signal amplification and transduction are examined. First, polarizable as well as non-polarizable semiconductor- and gate-electrolyte- interface combinations are investigated by normal pulse voltammetry. The results of these measurements are correlated with the corresponding transistor characteristics, clarifying the functional principle of EGOFETs and the requirements for high signal amplification. In addition to a good electrical performance, the EGOFET-transducers should also be compatible with the targeted sensing application. Accordingly, the influence of different gate materials and electrolytes on the sensing abilities, are discussed. Even though all physical requirements are met, EGOFETs typically exhibit irreversible degradation, if the gate potential exceeds a certain level. For that reason, EGOFETs have to be operated using a constant source-drain operation mode which is presented by means of an H⁺ (pH) sensitive ion-sensor.

1. INTRODUCTION

Ion sensors are required in many fields ranging from food safety control, water quality monitoring to various applications in pharmaceutical and cosmetics industry. Especially within the emerging fields of medical diagnostics and environmental sensing, low-cost sensor platforms for in-situ sensing of ions and biological substances in appropriate aqueous media, are required. Within the field of environmental sensing, heavy metal contaminants such as lead and mercury, are one prevalent type of water pollutant. They are persistent in the environment, they are not decomposed naturally and tend to be accumulated in the food chain and ultimately in human beings. For that reason, heavy metal detection at part per billion (ppb) levels is essential. Well established methods to detect heavy metals in the low ppb range, such as inductively coupled plasma – mass spectrometry (ICP-MS) and anodic stripping voltammetry (ASV) require six-figure investments, regular maintenance and highly trained professionals. In order to meet established limits on a worldwide basis and to ensure a sustainable water safety, low cost, sensitive, selective, portable and easy to handle analytic sensing platforms are essential. In contrast to heavy metal detection, where smallest concentrations have to be detected, clinical diagnostic applications require high accuracy at a relatively high concentration in a highly interfering background. Consequently, a versatile ion sensing platform for clinical diagnostics and environmental analysis should span a wide concentration range while having a high selectivity and a high sensitivity.

* emil.list-kratochvil@ntc-weiz.at; phone +43 316 876 8003; <http://www.ntc-weiz.at/>

Ion selective membranes (ISMs) based on polymeric membranes containing neutral or charged carriers (ionophores) are available for the determination of a large number of inorganic and organic ions.¹ During the last decade, the chemical sensing abilities of ISMs have been improved to such an extent that it has resulted in a “new wave of ion-selective membranes”.² This was achieved due to considerable improvement of the lower detection limit, new membrane materials, new sensing concepts and deeper theoretical understanding of the potentiometric response of ISMs. A particularly important milestone was the demonstration of solid-contact ion selective electrodes (ISEs) for trace-level analysis.^{3–5} One of the major challenges is the downscaling of these ion sensors which would require suitable solid state transducers.^{4,5} Since electrolyte-gated field-effect transistors (EGOFETs) are characterized by small size, portability, low-energy consumption, and low costs^{6–8}, they are highly promising candidates. Furthermore, in comparison to ISEs which require high impedance, potentiometric measurements, all FET based transducers have the advantage of transforming the high impedance input signal into an amplified low impedance output signal right at the spot of the measurement. However, the additional specific advantage of EGOFETs over conventional ion-sensitive organic field-effect transistors (OFETs)^{9–11} or FETs (ISFETs)^{12–14}, is that the gate electrolyte is in direct contact with the semiconductor and not with a solid gate dielectric. Consequently, there is no need for elaborate and expensive encapsulation of the semiconductor. On the contrary: Due to the formation of an electric double layer (EDL) at the semiconductor/electrolyte interface and a thereof resulting high capacity (1–10 $\mu\text{F}/\text{cm}^2$)¹⁰, a stable low-voltage operation ($< 1 \text{ V}$) at high source-drain currents is possible. Most importantly, these source-drain currents (in the range of a few μA)^{15–17} are still sufficiently high for further signal processing.

The high potential of electrolyte-gated OFETs was first indicated by Kergoat et al. reporting on the stable operation of OFETs gated with water.¹⁵ Hence, EGOFETs were successfully used as transducers for the detection of biomolecules such as DNA, dopamine, enzymes and proteins in an electrolytic background with a constant ionic strength.^{18–21} Furthermore, we have shown that it is also possible to combine EGOFETs with state of the art ISM as an active sensing element for selective and reversible Na^+ and H^+ ion detection.^{22,23} The principle potentiometric sensing mechanism of this sensor concept is shown in Fig. 1. The EGOFET serves as a transducer and is in direct contact with an inner filling solution (gate electrolyte) which is separated from the sample solution by an ISM. The actual sensing signal is given through the potential drop over the ISM, referred to as the membrane potential (E_{mem}). E_{mem} depends on the ion activity within the sample relative to the ion activity of the inner filling solution in a Nernstian fashion: $E_{\text{mem}} = E_0 + (RT / z_i F) \cdot \ln(a_{\text{sample}} / a_{\text{inner filling}})$, E_0 is a constant, R the gas constant, z_i the valency of the analyte ion, F the Faraday’s constant.¹⁷ During operation, a gate potential is applied to the sample solution with respect to the source contact through an Ag/AgCl reference electrode. The potential of the inner filling solution, which actually drives the EGOFET, is given through the sum of the membrane potential and the gate potential, and is further on referred to as effective gate potential.

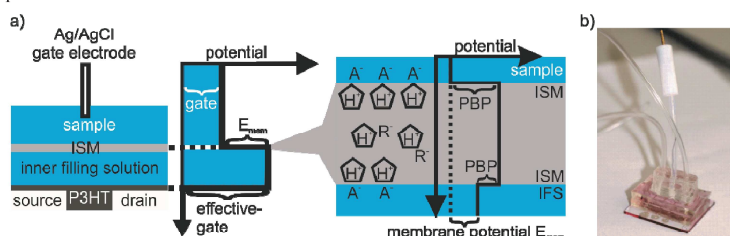


Figure 1: Illustration of the sensing mechanism of an ISM based ion selective EGOFET: a gate potential is applied to the sample solution relative to the source contact (a). The effective gate potential which drives the EGOFET is given through the sum of the gate and membrane potential (E_{mem}). E_{mem} stems from two Nernstian phase boundary potentials (PBP) at the ISM/inner filling solution (IFS) and at the sample/ISM interface, each depending on the respective pH value. Photograph of the sensing system with connected in and outlets (b).

EGOFETs used as transducers within such potentiometric sensing systems are of high interest to the scientific community. For that reason, the fundamental prerequisites to achieve a proper potentiometric signal transduction and amplification were investigated. The requirements imposed on the electrolytes and the gate electrodes are discussed in terms of electrical and sensing performance. First, polarizable and non-polarizable semiconductor- and gate-electrolyte- interface combinations are investigated by normal pulse voltammetry. The results of these measurements are correlated to the

corresponding transistor characteristics clarifying the distinct functional principle of EGOFETs and the basic conditions for high signal amplification. In addition to a good electrical performance, the EGOFET transducers should also be compatible with the targeted sensing application. Accordingly, the influence of different gate materials (PEDOT:PSS and Ag/AgCl) and electrolytes on the sensing abilities are discussed on the basis of potentiometric measurements. Even though all physical requirements are met, EGOFETs typically exhibit irreversible degradation, if the gate potential exceeds a certain level. For that reason, EGOFETs have to be operated using a constant source-drain operation mode which is presented by means of an H^+ (pH) sensitive ion-sensor.

2. EXPERIMENTAL

The EGOFETs and the electrodes for the normal pulse voltammetry measurements were fabricated on PET and glass substrates (Melinex, DuPont Teijin Films). The 50 nm gold source/drain (S/D) electrodes with 2 nm chromium adhesion layer were structured using conventional lift-off processing (channel length $\approx 7 \mu\text{m}$, channel width $\approx 3 \text{mm}$). The electrodes used for the normal pulse voltammetry had an area of 28mm^2 . Regioregular poly(3-hexylthiophene) (Plexcore OS purchased from Sigma-Aldrich) was deposited via spin-coating from a 4g L^{-1} toluene solution and dried at $60 \text{ }^\circ\text{C}$ in Argon (Ar) for $\approx 10 \text{min}$ and subsequently at $120 \text{ }^\circ\text{C}$ under high vacuum ($p \approx 4 \times 10^{-5} \text{mbar}$) for 1 h. All devices were assembled under inert atmosphere. The Na^+ selective ISM membranes were prepared by drop-casting a high molecular weight polyvinyl chloride (31 wt%, Selectophore grade), 2-nitrophenyl octyl ether (2-NPOE) (68 wt%), potassium tetrakis-((4-chlorophenyl)borate (KTpClPB) (0.7 wt%) and sodium ionophore X (0.2 wt%) in 5 mL tetrahydrofuran (THF) cocktail onto a glass slide. Whereas, the H^+ selective ISM membranes were prepared by drop-casting a high molecular weight polyvinyl chloride (31 wt%, Selectophore grade), 2-nitrophenyl octyl ether (2-NPOE) (63 wt%), sodium tetrakis[3,5-bis(trifluoromethyl)phenyl]borate (NaTFPB) (2 wt%) and Hydrogen ionophore V (4 wt%) in 4 mL tetrahydrofuran (THF) cocktail onto a glass slide. The K^+ selective ISM membranes were prepared by drop-casting a high molecular weight polyvinyl chloride (31 wt%, Selectophore grade), 2-nitrophenyl octyl ether (2-NPOE) (63 wt%), sodium tetrakis[3,5-bis(trifluoromethyl)phenyl]borate (NaTFPB) (0.5 wt%) and Potassium ionophore V (1 wt%) in 4 mL tetrahydrofuran (THF) cocktail onto a glass slide. The drop-cast membranes were allowed to dry overnight in a saturated THF environment conditions and were peeled off the glass slide for further implementation. All of the chemicals mentioned above were obtained from Fluka Sigma- Aldrich and were used as received. Saline solutions were prepared in concentrations varying from 10^{-4}M to 10^{-1}M NaCl (99.5%, p.a., ACS, ISO) and KCl (>99.0%) in deionized water, respectively. The 0.2 M potassium phosphate buffer solutions (PBS) were adjusted to pH 7. To continuously tune the pH value, the sample solution was buffered with 10 mM boric acid and 10 mM citric acid (unless noted otherwise) and drop-wise titrated with 0.5 M NaOH, while the pH was monitored with a calibrated glass electrode (Orion Thermo Sure Flow). The reservoir and the flow cell for the ion-sensitive EGOFETs were made of polydimethylsiloxane (PDMS, Sylgard 184) via a soft molding process, including a curing step of $\approx 1 \text{h}$ at $100 \text{ }^\circ\text{C}$. The flow cell was sealed by an appropriate fixture.

The electrical characterization of all devices was done in ambient air (at same light conditions) using an Agilent B1500 Parameter Analyzer. All potentials were applied with respect to an Ag/AgCl reference electrode containing a 3 M KCl inner filling solution. All normal pulse voltammetry measurements were carried out by a common three electrode setup: Pt counter electrode, Ag/AgCl reference electrode and a working electrode (electrode which is examined). The currents were measured after applying a potential pulse for 10 s on three different electrodes not revealing significant differences.

3. RESULTS AND DISCUSSION

3.1 Requirements of EGOFETs

In order to investigate the prerequisites to obtain an adequate electrical EGOFET performance, the semiconductor- (P3HT) and gate- electrolyte interfaces were examined separately. For that reason, Au electrodes and Au electrodes coated with P3HT (Au/P3HT electrodes) were fabricated and examined by normal pulse voltammetry measurements. Hence a potential was applied to the electrolyte relative to the respective electrode and the current was measured after a 10 s. This current is highly relevant to EGOFET devices, since it is directly related to the leakage current and to the potential drops at the semiconductor-/gate- electrolyte interfaces. Within this context, two representative interface types were examined, namely one polarizable (no faradaic current) and one non-polarizable interface (faradaic current passes) (see figure 2b). The measurement setup of the pulse voltammetry measurements is illustrated in figure 2a. The measured currents of Au/P3HT-PBS and Au-PBS interfaces are shown in figure 2c. The Au-PBS and the P3HT-PBS interfaces are polarizable within an electrochemical window of -500 mV to + 500 mV vs. an Ag/AgCl reference electrode. Thus, within this potential window, only negligible leakage current between the gate and the EGOFET device (source-/drain- pads, channel) will be flowing.

The currents flowing across Au|P3HT and Au electrodes in a PBS solution containing 0.01 M ascorbic acid are shown in figure 2d. The currents are magnitudes higher than their PBS counterparts. This can be ascribed to the ascorbic acid which easily oxidized or reduced and acts as a depolarizer. Consequently these interfaces are not polarizable and small potentials below +/- 500 mV already lead to currents in the range of a few μA . In both cases (PBS and PBS containing ascorbic acid), the currents flowing across the Au|P3HT electrodes at positive biases is magnitudes lower compared to Au electrodes. Since these currents are increasing significantly with time at potentials more positive than 500 mV (see figure 3a), the measured current depends on the history of the device, as indicated an arrow (see figure 2c).

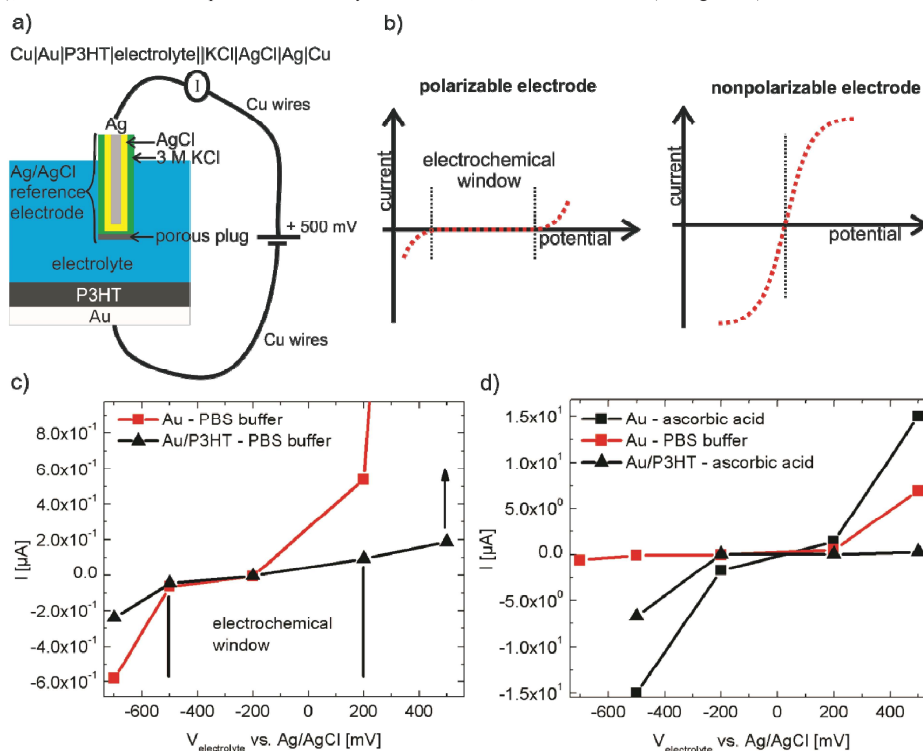


Figure 2: An illustration of the voltammetry measurement setup (a) and graphs of ideal polarizable and nonpolarized interfaces (b). The currents of the Au- and P3HT- PBS buffer and -ascorbic acid interfaces is shown in (c) and (d) respectively. The Au and P3HT- PBS buffer interface is polarizable within a ± 500 mV electrochemical window. Whereas the Au, P3HT-ascorbic acid solution interface is not polarizable and large currents > 1 mA are observed at voltages of -500 mV and $+500$ mV.

Figure 3a shows the current as a function of time at -500 mV, -700 mV and $+500$ mV, $+700$ mV with respect to an AgCl reference electrode of an Au/Au|P3HT electrodes. At a negatively biased gate electrolyte the current decreases with time, whereas at a positive bias the current increases. This could be ascribed to the p-type conduction of the P3HT. If the electrolyte is biased negatively, holes are injected from the underlying Au electrode to shield the external electric field induced by the potential difference between the gate and the gold electrode/P3HT. Consequently, the potential should ideally drop over the P3HT-electrolyte interface (see figure 3b). Whereas if the electrolyte is biased positively the potential drops over the whole P3HT coating as a result of the p-type conduction. The potential drop at the P3HT-electrolyte interface which drives the electrochemical reaction and thus the faradaic current is therefore reduced. However, the electric

field increases the migration of water/ions towards the gold pads. As the water/ion content is increased, the P3HT loses its blocking capabilities and the current starts to increase.

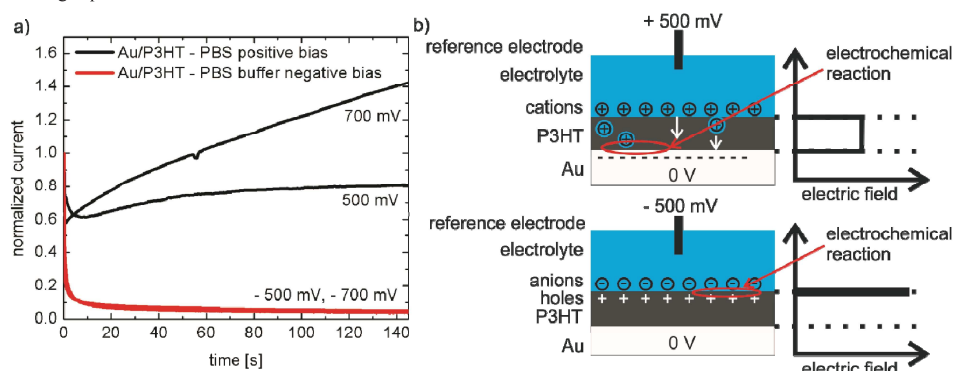


Figure 3: Normalized current as a function of time at positive and negative biased electrolyte solution (PBS) of an Au electrode coated with P3HT (a). The current was normalized by the initial current at time $t = 0$. At positive bias the current increases with time whereas at negative bias the current decreases. This could be attributed to an electric field which increases the ion/water migration towards the gold pad and as a result leads to decreasing blocking capabilities of the P3HT as illustrated in a simplified model (b).

The distinct EGOFETs functional principles corresponding to interface combinations examined by normal pulsed voltammetry, are shown in figure 4. Figure 4a shows a simplified circuit diagram of an EGOFET which neglects potential differences between source/drain/channel and describes the interfaces by capacitor in parallel to a resistor. The potential difference between the source/drain contacts and the gate electrolyte lead to an EDL formation with a high capacitance which controls the source-drain current. Ideally, the potential of the gate electrolyte should solely be given through the potential of the gate electrode; i.e. the effective gate potential should be independent of potential applied to the source/drain contacts. If this is not the case, the transistor does not show a proper transistor characteristic/amplification, since the whole applied gate potential would not drop at the P3HT-electrolyte interface. Thus, if the gate electrode-electrolyte interface and the P3HT-electrolyte interface is polarizable (R_{Gate} and R_{P3HT} large), the capacity of the gate electrode has to be significantly higher compared to the capacity of the source/drain contacts. That is why the EGOFET gated with a small area polarizable Au-gate electrode shows a poor performance compared to a porous large polarizable Pt-electrode (see figure 4b). These two cases mentioned above are certainly extreme cases. Practically, the transition between polarizing and non-polarizing interface is continuous and separating the capacitive contributions from the resistive contributions of the two interfaces is not possible. So far only polarizable gates-electrodes have been discussed. For that reason, the characteristics of a non-polarizable gate electrode (Ag/AgCl) using the same electrolyte (R_{Gate} small, R_{P3HT} large) are shown in figure 4c. In this case the capacity of the gate electrode does not matter and as the P3HT-electrolyte interface is polarizable, the characteristics are identical the ones obtained in figure 4b. Fig. 4d shows the transfer characteristics of an EGOFET gated with pure PBS, subsequently with a phosphate buffer containing ascorbic acid as a depolarizer and finally again with pure PBS. Due to the ascorbic acid the leakage current dominates the transistor characteristics. After replacing the ascorbic acid containing buffer with pure PBS again, the initial good transistor characteristics and low leakage currents are restored, not indicating any degradation of the P3HT. Thus, in this case the P3HT and gate-electrolyte interface are polarizable (R_{Gate} and R_{P3HT} are small).

To conclude there are two conditions to achieve a proper EGOFET performance in terms of amplifications: First, the P3HT-electrolyte interface has to be polarizable. Second, the gate electrode should either be non-polarizable or have a large capacitance.

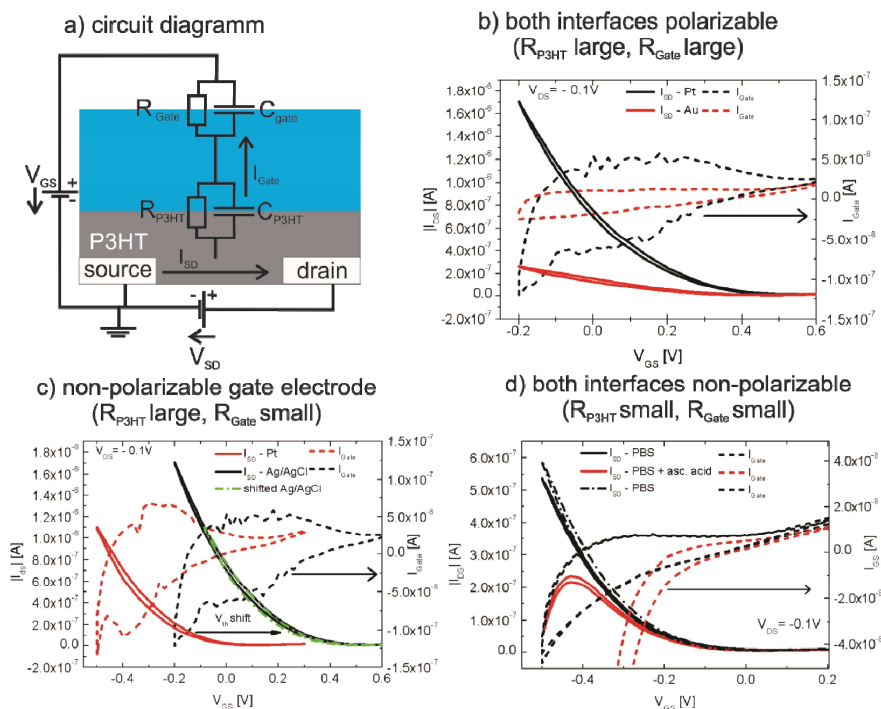


Figure 3: EGOFET operation modes: a) Simplified circuit diagram of the relevant interfaces of an EGOFET; b) transfer characteristics of an EGOFET gated with a small Au electrode (small C_{Gate}) is compared to an EGOFET gated with a Pt electrode (large C_{Gate}); c) transfer characteristics of an EGOFET gated with an Ag/AgCl electrode (non-polarizable) and a Pt electrode (polarizable). d) transfer-characteristics gated with an Ag/AgCl electrode and a PBS electrolyte containing ascorbic acid (non-polarizable) compared to a pure PBS electrolyte (polarizable).

3.2 Requirement of ion selective EGOFETS

In order to investigate the prerequisites to obtain a good performance with respect to the targeted sensing applications, the influence of electrolytes with varying ionic strength was examined first. Figure 5a shows the transfer characteristic of an EGOFET gated with a 10^{-2} M NaCl solution, subsequently with a 10^{-4} M NaCl solution and finally with a 10^{-4} M NaCl solution containing a 10^{-2} M $CaCl_2$ background. An Ag/AgCl reference electrode was used as a gate-electrode to ensure a constant gate potential which is independent of the electrolyte composition. The source drain currents are decreased with decreasing ionic strength. However, if the Cl⁻ concentration is kept constant using a $CaCl_2$ background, the transfer characteristics (including I_{Gate}) are almost unaltered. This can be attributed to a modification of the electrolyte/semiconductor interface depending on the concentration and type of the anion in the electrolyte.^{16,24}

Consequently, though it was already demonstrated that EGOFETS based on specifically designed semiconductors can be directly used as sensing elements for biomolecules such as DNA, dopamine, enzymes and proteins¹⁸⁻²¹ in a background of constant ionic strength, this approach does not seem to be suitable for the detection of metal ions such as Na⁺ or Pb²⁺ in analytes with varying ionic strength. First, only analytes with a large electrochemical window can be measured. This is not a drawback for biological analytes which have a known composition. Second, the EGOFET-characteristics non-selectively depend on the ionic strength/composition of the gating solution due to a modification of the electrolyte/semiconductor

interface. The advantage of the presented ion selective EGOFET is that, in contrast to other sensor concepts based on EGOFETs, the latter is not in direct contact with the sample solution. On the contrary, the EGOFET is in contact with an inner filling solution of constant composition and as a result, the sensing signal solely relies on a highly selective ISM (see figure 6a).

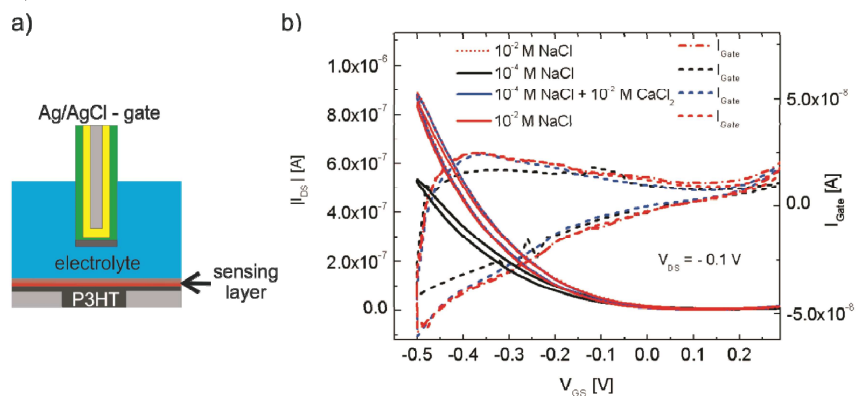


Figure 4: a) Illustration of an EGOFET using the semiconductor as a sensing layer; b) transfer characteristic of an EGOFET gated with a 10^{-2} M NaCl solution, with a 10^{-4} M NaCl solution and a 10^{-4} M NaCl solution containing a 10^{-2} M $CaCl_2$ background. An Ag/AgCl reference electrode was used as a gate-electrode to ensure a constant gating potential which is independent of the composition of the electrolyte.

Though various electrodes such as Pt or PEDOT:PSS can be used as a gate without changing the electrical performance of the EGOFETs, the electrochemical cell potential (gate electrode|analyte) typically changes with the sample composition. Figure 6b shows the electrode potential of a PEDOT:PSS electrode relative to a Ag/AgCl reference electrode. As the ionic strength is changed from 10^{-2} M KCl to 10^{-6} M KCl, the potential varies for ~ 80 mV. However, if the KCl concentration is decreased within a constant ionic NaCl background (10^{-2} M), keeping the ionic strength almost constant, the potential just varies for 20 mV. This potential drift would lead to a mixed signal between the sensing signal of the ISM and a non-selective signal from the gate electrode as shown in figure 6b. Consequently, Ag/AgCl reference electrodes which guarantee a constant potential independently from the sample composition have to be used, which is currently the major drawback of ion selective EGOFETs.

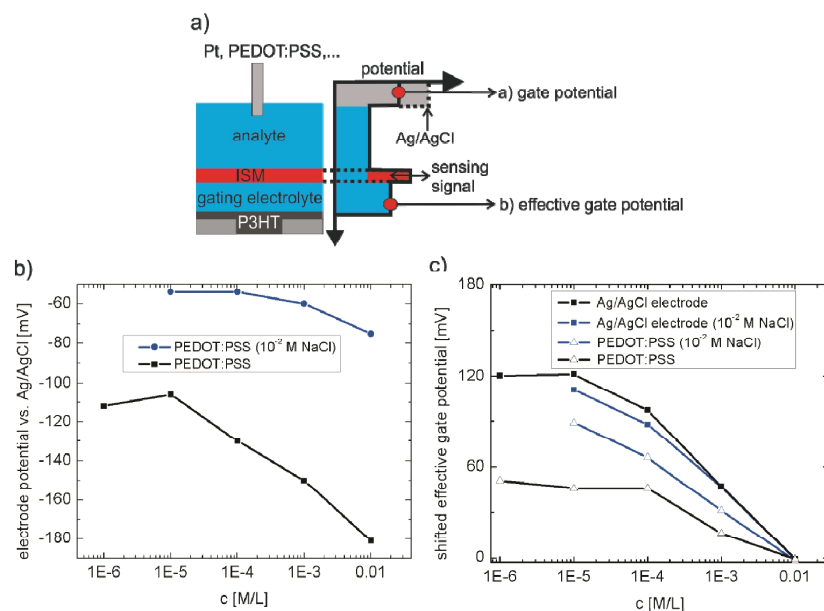


Figure 5: a) illustration of the functional principle of an ion selective EGOFET b) The electrode potential of PEDOT:PSS electrodes vs. the constant potential of a Ag/AgCl reference electrode as a function of K⁺ concentration. The potential was measured within a constant NaCl background (blue) and de-ionized water (black); c) Effective gate potentials of a K⁺ selective membrane measured with an Ag/AgCl reference electrode (squares) and with a PEDOT:PSS electrode (triangles) shifted to 0 mV at a concentration of 10⁻² M for better comparison. The potentials were measured with a constant NaCl background (blue) and de-ionized water (black).

The inner filling solution of the sensor has to fulfill two conditions. The first condition is related to the ISM; in order to guarantee a stable pH value and to avoid membrane potential drifts, pH buffers have to be used as an inner filling solution. Otherwise processes such as co-extraction of counter-cations into the membrane and resulting diffusive transmembrane fluxes of H⁺ lead to undesired pH value change of the inner filling solution.²⁵⁻³⁰ Furthermore, solvent polymeric membranes are permeable to CO₂ and other small neutral molecules which can also influence the pH value of the inner filling solution.^{4,31,32} Second, it should allow for a good EGOFET performance in terms of transconductance and on/off ratio (see previous section). This is the case if the inner filling solution has a large electrochemical window which ensures a polarizable interface and thus a negligible leakage current (I_G) between the transistor and the gate. Another negative side effect, is that high leakage currents densities can lead to a polarization of the membrane. Figure 7 shows the response curve of a Na⁺ selective ISM while applying a constant current. During EGOFET operation and a leakage current density of -10 nA/mm², cations are driven from the inner filling solution into the sample solution. Consequently, the Na⁺ concentration is increased, right in the vicinity of the ISM which leads to a higher lowest-detection limit. This also indicates that the area of the membrane has to have a certain size compared to the size of the transistor. Thus, typical leakage currents in the range of 1 nA require a minimum membrane size around 1 mm². The leakage current could also be used to pump ions from the sample into the inner filling solution (+10 nA/mm²), which could possibly lead to a lower detection limit. Unfortunately, as P3HT is a p-type conductor, this results in an EGOFET which is turned off.

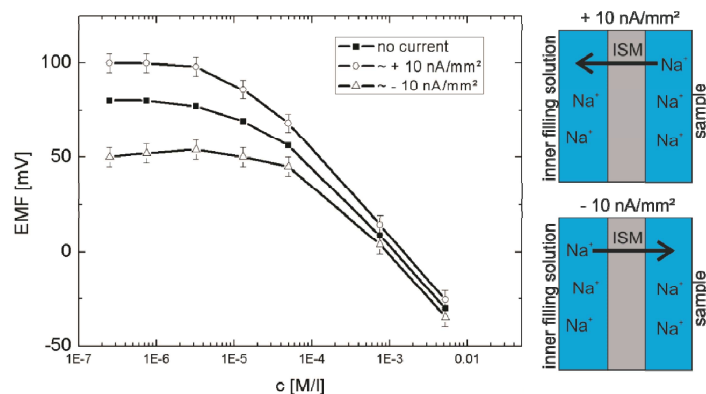


Figure 6: Membrane potential of a Na^+ selective membrane as a function of Na^+ concentration while applying a constant current (Na^+ ions flow from sample to inner filling solution) and negative currents (Na^+ ions flow from the inner filling solution to the sample). The potentials were not corrected for ohmic drops within the electrolyte. The error bars are due to noisy measurements. The current density ($\pm 10 \text{ nA/mm}^2$) is an estimation as the real surface area of the membrane which is slightly corrugated, is not exactly known.

3.3 Operation mode of ion selective EGOFETs

EGOFETs exhibit irreversible degradation if the gate potential exceeds -600 mV (using an Ag/AgCl gate-electrode) as shown by Kofler et al. ²³ Consequently, even if all requirements discussed in section 3.1 and 3.2 are fulfilled, EGOFETs must still be operated well below -600 mV in order to guarantee a stable operation. As typical membrane potentials can vary for more than $\pm 200 \text{ mV}$ (see figure 8), a working point at a gate potential of -400 mV can either lead to irreversible degradation (-600 mV) or negligible source-drain currents (-200 mV). For that reason, ion selective EGOFETs have to be operated at a constant working point and consequently also at a constant source-drain current. This implies that the effective gate potential has to be independent of the membrane potential and thus also ion activity within the sample. This can be achieved by adjusting the gate voltage through a feed-back loop which keeps a constant source-drain current level. The measurement signal is then given by the gate potential change required to keep the same source-drain current. Other than the operational stability, this operation mode has another benefit: The measured signal corresponds directly to the membrane potential change which eases data analysis (as shown in figure 8). As a result, it is not necessary to record the whole transfer curve in order to correlate the source-drain current changes with membrane potential changes/concentration changes. Two solutions with known pH values are sufficient to calibrate the sensor.

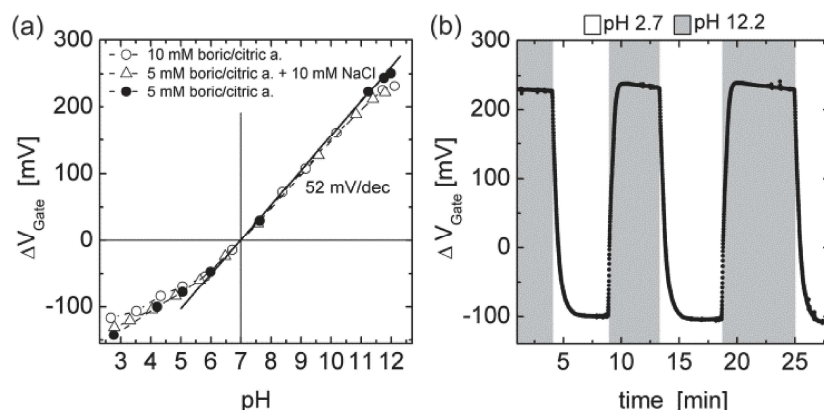


Figure 7: (a) pH value calibration curves of an H^+ selective EGOFET (PBS as an inner filling solution): gate voltage change as a function of the pH value; (b) response curve upon a pH-value change from pH 2.7 to pH 12. Figure taken from ref. 23.

4. SUMMARY AND CONCLUSION

The requirements imposed on ion selective EGOFETs were discussed. It is crucial that the whole gate potential actually drops at the semiconductor-electrolyte interface and that the leakage current flowing between the gate and the semiconductor is as small as possible. Consequently, the semiconductor – electrolyte interface should be polarizable. The electrolyte – gate interface, on the other hand must not be polarizable, as long as its capacity is larger than that of the EGOFET including the source/drain contacts. However, if analytes with varying ionic strength are investigated, a non-polarizable Ag/AgCl reference electrode (or other equivalent reference electrodes) is required to apply a concentration independent gate-potential. Furthermore, as the characteristics of the EGOFETs change non-selectively with the ionic strength of the gate electrolyte, the EGOFET should be in contact with a constant, well defined inner filling solution which is separated from the sample by an ISM. Accordingly, the sensing signal which solely relies on the highly selective ISM, is amplified and transduced into a low impedance output signal by the EGOFET. Even though all physical requirements are met, EGOFETs typically exhibit irreversible degradation, if the gate potential exceeds a certain level. For that reason, EGOFETs have to be operated using a constant source-drain operation mode which is presented by means of an H^+ (pH) sensitive ion-sensor.

ACKNOWLEDGEMENTS

For financial support, the Styrian Government (Project BioOFET 2, GZ: A3-11, B-36/2010-5) is acknowledged.

BIOOFET 2, GZ:A3-11.B-36/2010-5) IS ACKNOWLEDGED

REFERENCES

- [1] Bakker, E., Pretsch, E., Bühlmann, P., "Selectivity of potentiometric ion sensors.," *Anal. Chem.* **72**(6), 1127–1133 (2000).

- [2] Bobacka, J., Ivaska, A., Lewenstam, A., "Potentiometric Ion Sensors," *Chem. Rev.* **108**, 329–351 (2008).
- [3] Lisak, G., Sokalski, T., Bobacka, J., Harju, L., Lewenstam, A., "A study on lowering the detection limit with solid-state lead-selective electrodes," *Talanta* **83**(2), 436–440, Elsevier B.V. (2010).
- [4] Lindner, E., Gyurcsányi, R. E., "Quality control criteria for solid-contact, solvent polymeric membrane ion-selective electrodes," *J. Solid State Electrochem.* **13**(1), 51–68 (2009).
- [5] Bobacka, J., "Conducting Polymer-Based Solid-State Ion-Selective Electrodes," 7–18 (2006).
- [6] Lin, P., Yan, F., "Organic thin-film transistors for chemical and biological sensing," *Adv. Mater.* **24**(1), 34–51 (2012).
- [7] Kergoat, L., Piro, B., Berggren, M., Horowitz, G., Pham, M.-C., "Advances in organic transistor-based biosensors: from organic electrochemical transistors to electrolyte-gated organic field-effect transistors," *Anal. Bioanal. Chem.* **402**, 1813–1826 (2012).
- [8] Mabeck, J. T., Malliaras, G. G., "Chemical and biological sensors based on organic thin-film transistors," *Anal. Bioanal. Chem.* **384**(2), 343–353 (2006).
- [9] Bratov, A., Abramova, N., Ipatov, A., "Recent trends in potentiometric sensor arrays--a review," *Anal. Chim. Acta* **678**(2), 149–159, Elsevier B.V. (2010).
- [10] Bartic, C., Palan, B., Campitelli, A., Borghs, G., "Monitoring pH with organic-based field-effect transistors," *Sensors Actuators B* **83**, 115–122 (2002).
- [11] Ji, T., Rai, P., Jung, S., Varadan, V. K., "In vitro evaluation of flexible pH and potassium ion-sensitive organic field effect transistor sensors," *Appl. Phys. Lett.* **92**(23), 233304 (2008).
- [12] Bergveld, P., "The operation of an isfet as an electronic device," *Sensors And Actuators* **1**, 17–29 (1981).
- [13] Bergveld, P., "New Amplification Method for Depth Recording," *IEEE Trans. Biomed. Eng.* **BME-15**(2) (1968).
- [14] Dzyadevych, S. V., Soldatkin, A. P., El'skaya, A. V., Martelet, C., Jaffrezic-Renault, N., "Enzyme biosensors based on ion-selective field-effect transistors," *Anal. Chim. Acta* **568**(1-2), 248–258 (2006).
- [15] Kergoat, L., Herlogsson, L., Braga, D., Piro, B., Pham, M.-C., Crispin, X., Berggren, M., Horowitz, G., "A water-gate organic field-effect transistor," *Adv. Mater.* **22**, 2565–2569 (2010).
- [16] Buth, F., Kumar, D., Stutzmann, M., Garrido, J. a., "Electrolyte-gated organic field-effect transistors for sensing applications," *Appl. Phys. Lett.* **98**, 153302 (2011).
- [17] Laiho, A., Herlogsson, L., Forchheimer, R., Crispin, X., Berggren, M., "Controlling the dimensionality of charge transport in organic thin-film transistors," *Proc. Natl. Acad. Sci. U. S. A.* **108**(37), 15069–15073 (2011).
- [18] Kergoat, L., Piro, B., Berggren, M., Pham, M. C., Yassar, A., Horowitz, G., "DNA detection with a water-gated organic field-effect transistor," *Org. Electron.* **13**, 1–6, Elsevier B.V. (2012).
- [19] Casalini, S., Leonardi, F., Cramer, T., Biscarini, F., "Organic field-effect transistor for label-free dopamine sensing," *Org. Electron.* **14**(1), 156–163, Elsevier B.V. (2013).

- [20] Buth, F., Donner, A., Sachsenhauser, M., Stutzmann, M., Garrido, J. A., "Biofunctional electrolyte-gated organic field-effect transistors," *Adv. Mater.* **24**, 4511–4517 (2012).
- [21] Magliulo, M., Mallardi, A., Mulla, M. Y., Cotrone, S., Pistillo, B. R., Favia, P., Vikholm-Lundin, I., Palazzo, G., Torsi, L., "Electrolyte-gated organic field-effect transistor sensors based on supported biotinylated phospholipid bilayer," *Adv. Mater.* **25**, 2090–2094 (2013).
- [22] Schmoltnner, K., Kofler, J., Klug, A., List-Kratochvil, E. J. W., "Electrolyte-gated organic field-effect transistor for selective reversible ion detection," *Adv. Mater.* **25**, 6895–6899 (2013).
- [23] Kofler, J., Schmoltnner, K., Klug, A., List-Kratochvil, E. J. W., "Hydrogen ion-selective electrolyte-gated organic field-effect transistor for pH sensing Hydrogen ion-selective electrolyte-gated organic field-effect transistor for pH sensing," *Appl. Phys. Lett.*(104), 193305 (2014).
- [24] Melzer, K., Münzer, A. M. M., Jaworska, E., Maksymiuk, K., Michalska, A., Scarpa, G., "Polymeric ion-selective membrane functionalized gate-electrodes: Ion-selective response of electrolyte-gated poly (3-hexylthiophene) field-effect transistors," *Org. Electron.* **15**, 595–601, Elsevier B.V. (2014).
- [25] Ceresa, A., Sokalski, T., Pretsch, E., "Influence of key parameters on the lower detection limit and response function of solvent polymeric membrane ion-selective electrodes," *J. Electroanal. Chem.* **501**(1-2), 70–76 (2001).
- [26] Zwickl, T., Sokalski, T., "Steady-State Model Calculations Predicting the Influence of Key Parameters on the Lower Detection Limit and Ruggedness of Solvent Polymeric Membrane Ion-Selective Electrodes," *Electroanalysis* **11**, 673–680 (1999).
- [27] Morf, W. E., Lindner, E., Simon, W., "Theoretical Treatment of the Dynamic Response of Ion- Selective Membrane Electrodes," *Anal. Chem.* **47**(9), 1596–1601 (1975).
- [28] Sokalski, T., Ceresa, A., Fibbioli, M., Zwickl, T., Bakker, E., Pretsch, E., "Lowering the Detection Limit of Solvent Polymeric Ion-Selective Membrane Electrodes. 2. Influence of Composition of Sample and Internal Electrolyte Solution," *Anal. Chem.* **71**(6), 1210–1214 (1999).
- [29] Sokalski, T., Ceresa, A., Zwickl, T., Pretsch, E., "Large Improvement of the Lower Detection Limit of Ion-Selective Polymer Membrane Electrodes," *J. Am. Chem. Soc.* **119**(46), 11347–11348 (1997).
- [30] Morf, W. E., Badertscher, M., Zwickl, T., Rooij, N. F. De., Ernö, P., "Effects of Ion Transport on the Potential Response of Ionophore-Based Membrane Electrodes: A Theoretical Approach," *J. Phys. Chem. B* **103**, 11346–11356 (1999).
- [31] Lindner, E., Buck, R. P., "Calibration of a planar differential CO₂ probe," *Fresenius. J. Anal. Chem.* **364**, 22–27 (1999).
- [32] Hyoung, S. Y., Geun, S. C., Meyerhoff, M. E., "Differential ion-selective membrane electrode-based potentiometric gas-sensing cells with enhanced gas sensitivity," *Anal. Chim. Acta* **237**, 115–125 (1990).

7.5 Highly robust electron beam lithography lift-off process using chemically amplified positive tone resist and PEDOT:PSS as a protective coating

J. Kofler, K. Schmoltner, A. Klug, E. J. W. List-Kratochvil

Contribution: All experimental work. The author wrote the manuscript. The manuscript was finalized with K. Schmoltner.

Highly robust electron beam lithography lift-off process using chemically amplified positive tone resist and PEDOT:PSS as a protective coating

This content has been downloaded from IOPscience. Please scroll down to see the full text.

View [the table of contents for this issue](#), or go to the [journal homepage](#) for more

Download details:

This content was downloaded by: kofjo

IP Address: 129.27.171.12

This content was downloaded on 18/08/2014 at 08:37

Please note that [terms and conditions apply](#).

Highly robust electron beam lithography lift-off process using chemically amplified positive tone resist and PEDOT:PSS as a protective coating

Johannes Kofler¹, Kerstin Schmoltner¹, Andreas Klug¹ and Emil J W List-Kratochvil^{1,2}

¹ NanoTecCenter Weiz Forschungsgesellschaft m.b.H., Franz-Pichler-Straße 32, A-8160 Weiz, Austria

² Institute of Solid State Physics, Graz University of Technology, Petersgasse 16, A-8010 Graz, Austria

E-mail: emil.list-kratochvil@ntc-weiz.at

Received 3 April 2014, revised 20 June 2014

Accepted for publication 25 June 2014

Published 6 August 2014

Abstract

Highly sensitive chemically amplified resists are well suited for large-area, high-resolution rapid prototyping by electron beam lithography. The major drawback of these resists is their susceptibility to T-topping effects, sensitivity losses, and linewidth variations caused by delay times between individual process steps. Hence, they require a very tight process control, which hinders their potentially wide application in R&D. We demonstrate a highly robust electron beam lithography lift-off process using a chemically amplified positive tone 40XT photoresist in combination with an acidic conducting polymer (PEDOT:PSS) as a protective top-coating. Even extended delay times of 24 h did not lead to any sensitivity losses or linewidth variations. Moreover, an overall high performance with a resolution of 80 nm (after lift-off) and a high sensitivity ($<10 \mu\text{C}/\text{cm}^2$) comparable to other standard chemically amplified resists was achieved. The development characteristics of this resist-layer system revealed new insights into the immanent trade-off between resolution and process stability.

Keywords: chemically amplified resists, high-throughput electron beam lithography, electron beam lithography, PEDOT:PSS anti-charging layer, protective coating, lift-off

 Online supplementary data available from stacks.iop.org/JMM/24/095010/mmedia

(Some figures may appear in colour only in the online journal)

1. Introduction

Electron beam lithography (EBL), focused ion beam (FIB) lithography, and nanoimprint lithography (NIL) are the most established techniques for nanofabrication (structures sub $1 \mu\text{m}$). Among them, EBL is undoubtedly the most widely used tool for R&D [1–3]. In recent years, two main trends in EBL development are being pursued: first, the effort towards ultra-high resolution and pattern density (sub 30 nm) and second towards writing over large-areas with acceptable throughput and high resolution (sub 100 nm [4, 5]). In the case of a lift-off process, as discussed within this work, positive tone resists are

typically better suited than negative tone resists. First, positive tone resists typically have an intrinsic undercut due to backscattered electrons, and second, they usually require less exposure area for most applications (e.g. nanowires: only a single line has to be exposed). In the following work, we therefore focus on positive tone resists that are used for lift-off processes.

Ultra-high resolution (sub-30 nm) has already been demonstrated using common positive tone resists such as poly(methylmethacrylate) (PMMA) and ZEP-520A using nonstandard developers [6–9] as well as cold and sonication assisted development [10–13]. Although these resists have a high resolution, good repeatability, and stability, they are not

very sensitive. Typically they have sensitivities of $> 50 \mu\text{C}/\text{cm}^2$ (ZEP-520A [9, 10]) and $> 100 \mu\text{C}/\text{cm}^2$ (PMMA [14]), varying with the resist heights, the acceleration voltages, and the development procedures used. Due to their low sensitivity, the suitability of such resists is practically limited to small writing areas and low throughput applications. Although, the sensitivity can be increased using thin resist layers ($< 80 \text{ nm}$), low exposure voltages (5 keV [15]) and strong developers [2], these procedures lead to a low contrast and are not suited for lift-off processes. Another approach is to use high beam currents. However, this gives rise to undesired effects like reduced depth of focus, substrate heating and charging [4].

To overcome this drawback, highly sensitive chemically amplified resists (CA resists) can be used. Linewidths below 100 nm at sensitivities of $< 10 \mu\text{C}/\text{cm}^2$ were demonstrated with well-established chemically amplified positive tone resists such as UV88 [16, 17], AZPF514 [15], or IBM KRS-XE [18, 19]. Using state-of-the-art CA resists, even sub 30 nm resolutions were demonstrated [20–24]. In addition to their high sensitivity and etch resistance, CA resists have the benefit of mix & match applications, which combine EBL with photolithography: micron patterns such as the periphery and contact pads are exposed by photolithography, whereas high-resolution, submicron patterns are exposed by EBL, further increasing the throughput [17]. The drawback of such chemically amplified resists is that delay times at the order of minutes in between spin-coating, exposure, and post exposure bake lead to linewidth variations, to sensitivity losses, and, in the worst case, to T-topping effects [17, 25, 26]. These process instabilities are ascribed to basic air contaminants [27, 28] in combination with evaporation of the photoacid from the topmost resist layers [29], which induce an almost developer insoluble surface inhibition layer (SIL). This SIL is removed very slowly compared to the underlying exposed resist, retarding the actual development/ changing the effective development time. In order to obtain reproducible results, a very tight process control is required, which is most likely the reason why CA resists are not yet well established in R&D. Especially in case of high throughput mix & match processes, delay times between individual exposures are inevitable, requiring a resist system with an extraordinary stability. Another issue concerning CA resists is that due to their high sensitivity, shot noise effects get more prominent. This results in an exposure-related, increased line edge roughness (LER [30–33]) which ultimately limits the critical dimension (CD). In addition to shot noise, the LER is also greatly affected by resist properties such as resist graininess, acid generation efficiency, the acid diffusion, and concentration [33]. Within this context, chemically amplified molecular electron beam resists, which rely on small molecules, are of particular interest. They show promising results in terms of LER, resolution, and sensitivity [34–37]. However, these resists are currently not commercially available.

In this work, the commercially available 40XT positive tone CA photoresist is investigated as an EBL-resist for the first time. Since 40XT is also susceptible to severe SILs, resulting in process instabilities, highly conductive, acidic poly(3,4-ethylenedioxythiophene) poly(styrene-sulfonate) (PEDOT:PSS) was used as a protective coating. In order to determine the

optimal development parameters with respect to sensitivity and critical dimensions (CD), contrast curve and linewidth measurements were carried out. The stability of this new resist-protective-layer system was demonstrated by delay time investigations in air and vacuum. Even extended delay times of 24 h between exposure and post exposure bake (PEB) did not lead to sensitivity losses or linewidth variations. The working mechanism of this PEDOT:PSS protective coating is further discussed on the basis of dissolution rate studies. Additionally, due to the high conductivity of PEDOT:PSS, charging substrates can be structured without using a metal layer [38, 39].

2. Experimental

All SiO_2 substrates were cleaned as follows: rinsing with acetone, rinsing with isopropanol, blow-drying with dry N_2 , ultrasonic bath cleaning in isopropanol for 1 min., rinsing with de-ionized water (DI water), blow drying with N_2 . Subsequently a dehydration bake at 200°C for $> 10 \text{ min}$ was applied. The substrates were cooled to RT with dry N_2 before spin-coating the resist (no adhesion promoter such as HMDS was used). Baking and spin-coating steps were all carried out in a laminar flow box in a clean room facility. The photoresist 40XT from AZ Electronic Materials was diluted with AZ[®]EBR solvent (160 mg/mL). The diluted resist was spin coated on the substrates with 6000 rpm for 40 s and the soft bake (SB) was carried out at 110°C for 60 s leading to a resist height of 130 nm. The substrate was cooled down with dry N_2 for 60 s. Then the PEDOT:PSS (Clevios[™] PH 1000 diluted with 5% vol. isopropanol) was drop cast on top of the resist and left to settle for 40 s before spinning at 6000 rpm for 40 s. The samples coated with PEDOT:PSS were baked a second time at 110°C for 3 min on a hot plate if not specified otherwise. The thickness of the obtained PEDOT:PSS layer was $\sim 50 \text{ nm}$ (difference between initial resist height and resist height after applying the coating). Electron beam lithography was carried out with a Raith e-line system. All exposures were done at 20 kV acceleration voltage at a working distance of 7 mm and an aperture of $7.5 \mu\text{m}$. The post exposure bake (PEB) was carried out at 105°C for 60 s on a hot plate. After exposure the samples were developed by static immersion in the appropriate developer AZ[®] 726mif pure or diluted with de-ionized water (DI water). The standard delay times were as follows: $< 10 \text{ min}$ between SB and transfer to e-line; 1 h before exposure within the e-line in vacuum; the exposures were carried out within 15 min; 10 min after exposure within the e-line; $< 10 \text{ min}$ between transfer from the e-line and the PEB. After development, the samples were rinsed with DI water for 20 s and blow dried with dry N_2 . The metal layers (3 nm Cr adhesion layer and 30 nm Au) were deposited by thermal evaporation at a base pressure $< 10^{-6} \text{ mbar}$. Lift-off was carried out in an ultrasonic bath in NMP (N-Methyl-2-pyrrolidone) at 65°C .

All resist height measurements were done with a Veeco AFM in tapping mode. The contrast curves were obtained by measuring the remaining resist heights after development in the middle of $5 \mu\text{m}$ large rectangles exposed at varying dose. The rectangles were spaced $5 \mu\text{m}$ apart in order to avoid

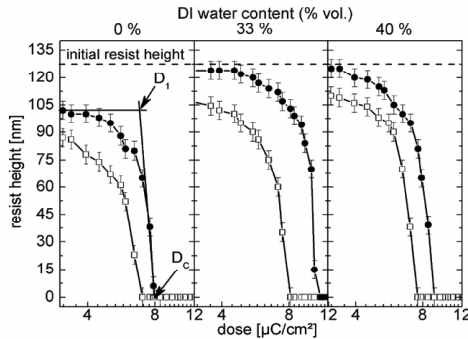


Figure 1. Remaining resist height after development on samples coated with PEDOT:PSS as a function of dose. The samples were developed in developers diluted with 0% vol., 33% vol. and 40% vol. DI water. The development times were 5 s (circles) and 10 s (open squares); 20 s (circles) and 60 s (open squares); and 120 s (open squares) respectively. The incipient dose D_1 and the sensitivity D_C used to calculate the contrast are indicated by arrows. The data points have been connected with lines as a guide to the eye. The error bars indicate the variance of the resist height.

influences of the proximity effect between adjacent structures. The contrast γ is given by the linear portion of the falling edge of the remaining resist height versus the logarithm of the dose $\gamma = \log(D_C/D_1)^{-1}$ [1] with D_C the clearing dose/sensitivity, and D_1 the incipient dose, as indicated in figure 1. The corresponding dissolution rates r at a given dose were calculated from the contrast curves and were defined as $r(\text{dose}) = (h_{\text{initial}} - h_{\text{rem}}(\text{dose}))/t_{\text{dev}}$ imposing a linear development. t_{dev} is the development time, h_{initial} corresponds to the initial resist height before development, and h_{rem} to the remaining resist height at a certain dose, after development. This linear approximation is valid, if the calculated dissolution rates are independent of the development time. This condition was fulfilled for the development times and developer dilutions studied within this work: the calculated dissolution rates measured at three different development times are equal within error bars (see supporting information). Very short development times, which are sensitive to retardations at the resist surface, might lead to different results. Furthermore, this approximation is also not valid if a SIL is present. The dissolution rates are subsequently used to calculate the dissolution selectivities. Similar as in [40], the dissolution selectivities (s_{diss}) at exposure dose values smaller than D_C are given by the dissolution rate at the corresponding dose divided through the dissolution rate of the unexposed resist ($s_{\text{diss}}(\text{dose}) = r(\text{dose})/r(\text{dose} = 0)$).

The dissolution rate of the unexposed resist (dark erosion rate) was obtained by a linear interpolation of the resist height plotted as a function of the development time (see supporting information). The corresponding resist heights were measured at different development times on separate substrates.

All linewidth and LER measurements were carried out after lift-off, and structures showing the characteristic ‘‘mouse bites’’ indicating an improper undercut were not considered. Thus,

the smallest linewidth specified in this work, referred to as the critical dimension (CD), corresponds to the resolution of the whole process including the lift-off. The linewidth measurements were done by averaging 20 line-scans with a step size of 2 nm (along the line) spaced 500 nm apart over a total distance of 2 μm . The LER were measured as described in [41]. All line scans and LER measurements were carried out using the same scan settings (aperture, working distance, etc.). In order to estimate the uncertainty, linewidth and LER measurements were carried out on two separate lines (exposed at the same dose at different positions on the substrate) on two separate substrates. The width variations between the lines were within ± 5 nm.

3. Results and discussion

3.1. Contrast curve and linewidth study

Since the presented 40XT-resist system was investigated for the first time, development process optimization was carried out first. In order to find the optimal development parameters contrast curves, dissolution selectivity curves and linewidth measurements for different developer dilutions and development times were conducted. Table 1 lists the resultant contrast values (γ) the CD and the normalized resist heights after development.

Figure 1 shows the corresponding contrast curves. Increasing development times (open symbols) generally led to a higher sensitivity (lower D_C) at the cost of a lower resist height in unexposed areas as well as a lower contrast. This well-known trade-off between sensitivity and contrast/resist height is improved using diluted developers: a sample that is developed for 120 s in a diluted developer (40% vol.) has a significantly higher remaining resist height and contrast (117 ± 5 nm and $\gamma = 10$) compared to samples developed for 10 s in a pure developer (95 ± 5 nm and $\gamma = 7$) at the cost of only a slightly lower sensitivity ($7 \mu\text{C}/\text{cm}^2$ instead of $7.5 \mu\text{C}/\text{cm}^2$).

Figure 2 shows the dissolution selectivity curves calculated from the contrast curves as described in the experimental section. The dissolution selectivity of diluted developers is higher at all exposure dose values smaller than the corresponding D_C . Accordingly, if an appropriate development time is chosen, diluted developers, will result in a higher final resist height and contrast at the same sensitivity. Since an ideal e-beam resist should have both, a high contrast and a high sensitivity [1], diluted developers and/or short development times are preferable. However, the lower limit of the development time is given by the time to clear the trench bottoms and to obtain an undercut for lift-off. Furthermore, development times below 10 s are difficult to handle practically. For that reason, in spite of having a high sensitivity, contrast, and small CD, a development time of 5 s with a pure developer was not considered because it leads to higher linewidth variations and a poor reproducibility.

Figure 3 compares the influence of the normalized exposure dose on the linewidth of samples developed for 10 s in a pure developer and for 60 s in a diluted developer (40% vol.). The samples developed in the pure developer exhibited a poor CD (110 nm) and their linewidths varied strongly upon exposure dose variations. Whereas the diluted developer yielded a

Table 1. Contrast, CD, sensitivity, and final resist height for different development parameters

Developer dilution [% vol. DI water]	Development time [s]	Contrast (γ)	Sensitivity (D_C) [$\mu\text{C}/\text{cm}^2$]	Critical dimension (CD) [nm]	Normalized resist height ^a
0%	5	8 ± 2	8	95 ± 10	83%
0%	10	7 ± 0.5	7	110 ± 5	73%
33%	20	14 ± 2	10.5	no undercut	95%
33%	40	10 ± 0.5	9	85 ± 5	89%
33%	60	9 ± 0.5	8	85 ± 5	86%
40%	60	11 ± 0.3	9	80 ± 5	95%
40%	120	10 ± 0.3	7.5	80 ± 5	90%

^a Remaining resist height after development normalized by the initial resist height (130nm) before development.

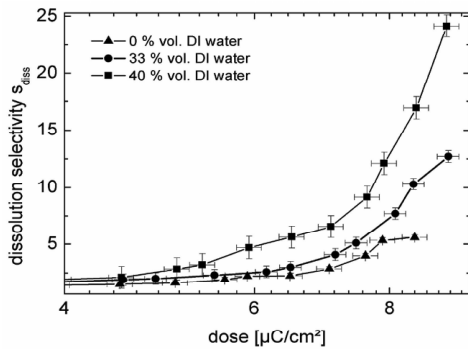


Figure 2. Dissolution selectivity curves of developers diluted with 0% vol. (triangles), 33% vol. (circles) and 40% vol. (squares) DI water. The data points have been connected with lines as a guide to the eye. The error bars on the x axis indicate dose uncertainties due to beam current variations, and on the y axis they indicate dissolution selectivity uncertainties originating from resist height variations.

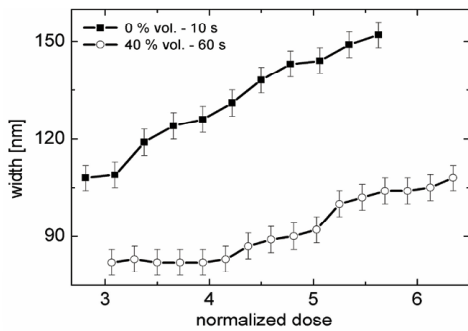


Figure 3. Linewidths after lift-off for varying exposure dose values normalized by the corresponding sensitivity values (D_C) taken from table 1. Development in a pure developer for 10 s (closed squares) and in a developer diluted with 40% vol. DI water for 60 s (open circles). The data points have been connected with lines as a guide to the eye. The error bars indicate the variance of the linewidths.

CD of 80 ± 5 nm, small linewidth variation upon increasing the dose and at the same time a very high sensitivity ($9 \mu\text{C}/\text{cm}^2$). Using these optimal development parameters, an array of 90 ± 5 nm wide lines, spaced 70 ± 5 nm apart, could be

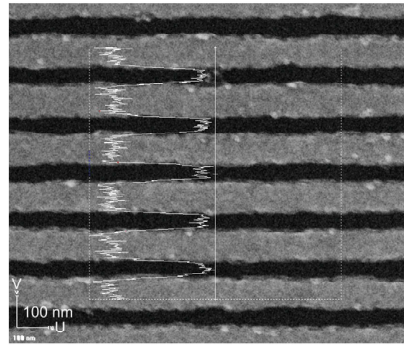


Figure 4. Line and space pattern: 90 nm wide gold lines on a SiO_2 substrate spaced 70 nm apart (80 nm half-pitch), structured with the presented lift-off process. The sample was developed for 60 s in a developer diluted with 40% vol. DI water.

achieved (see figure 4). The LER 3σ is 12 ± 0.6 nm on isolated lines and around 17 ± 1 nm in an array as shown in figure 4. These LER values are similar to the results obtained using NEB22 [31] and also seem to be similar to the results obtained for UVIII [42]. Though optimizing the PEB time and temperature could reduce the LER [41], 40XT cannot compete against state-of-the-art CA resists with LERs below 4 nm, as for example shown in [20, 34, 37]. However, this work does not aim to achieve the ultimate resolution and LER. The goal is to present a robust and cheap lift-off process with high throughput and acceptable resolution (sub 100 nm) with an easily commercially available resist.

3.2. PEDOT:PSS as a protection layer – delay time investigations

In order to study the performance of the PEDOT:PSS protective coating, delay time investigations were carried out using the development parameters obtained before (developer diluted with 40% vol. DI water and 60 s development time). Figure 5 compares the contrast curves of samples stored 24 h in either air or vacuum after exposure to samples that were not subjected to such extended delay times. In the case of PEDOT:PSS coated samples (open symbols), no changes of the contrast curves were observed. Whereas in the case of samples that were not coated with PEDOT:PSS (closed symbols),

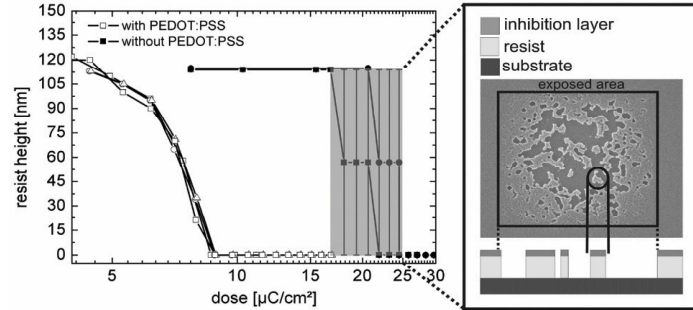


Figure 5. Contrast curves of samples coated with PEDOT:PSS (open symbols) and without PEDOT:PSS (closed symbols) developed in a developer diluted with 40% vol. DI water. The samples were subjected to different delay times after exposure: no extended delay (squares), stored 24 h in air (circles) or vacuum (triangles). In the case of samples without PEDOT:PSS, a severe SIL led to an inhomogeneous development at dose values close to D_C . This is also shown by the SEM image of a $5\ \mu\text{m}$ large, exposed rectangle (marked with a black square). Patches of the resist are completely developed, whereas others are not. Thus the resist height cannot be measured within this dose range, as indicated by large error bars and the grey area that marks the general ambiguity. The data points have been connected with lines as a guide to the eye.

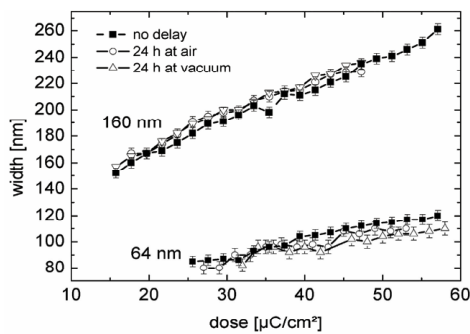


Figure 6. Widths of 160 nm / 64 nm wide and $5\ \mu\text{m}$ long rectangles (design) after lift-off of samples not subjected to an extended delay (closed squares), subjected to a 24 h delay in vacuum (open triangles) and 24 h in air (open circles) after exposure. The samples were coated with PEDOT:PSS and developed in a diluted developer with 40% vol. DI water for 60 s. The error bars indicate the standard variance of the widths. The data points have been connected with lines as a guide to the eye.

no visible dissolution at all was observable at the standard development time of 60 s, even if there was no extended delay. However, longer development times of 140 s led to an inhomogeneous development at dose values close to D_C , with patches of resist being completely developed and others that are not developed at all, as shown in figure 5 (right). The sensitivity of these samples shifted to higher values if they were stored in air for 24 h and samples that were stored in vacuum for 24 h were not developed at all. The extraordinary film life-time of the PEDOT:PSS coating is further demonstrated in figure 6. The widths of 64 nm and 160 nm wide rectangles did not show any significant linewidth variations, even if the samples were stored 24 h in vacuum. If the protection layer was omitted, no widths could be measured at all.

These results can be ascribed to the formation of an SIL in the absence of a PEDOT:PSS protective coating. The SIL results from a combination of three effects: basic air contaminants [27, 28]; evaporation of the photo acid from the resist surface [29, 43]; and evaporation of the residual solvent, which reduces the diffusion length of the photo acid and consequently the sensitivity of the resist [44]. An extended storage in vacuum, as is required for EBL exposure, augments the last two effects. Moreover, the contribution of the time to remove this SIL to the development time is increased with increasing developer selectivity. Accordingly, development processes that apply highly selective developers are very sensitive to SILs. As a diluted developer with a high selectivity was used, the short delay time in vacuum required to expose the sample was already sufficient to lead to a severe SIL. This can be avoided if a pure developer is used. In this case, the SIL is completely dissolved and no inhomogeneous development is observable. However, the magnitude of the SIL and therefore also the effective development time still varies, leading to severe sensitivity losses and linewidth variations (see supporting information (stacks.iop.org/JMM/24/095010/mmedia)).

To summarize, diluted and thus selective developers, which lead to desired properties such as high contrast, sensitivity, and resolution, inevitably result in process instabilities originating from an SIL. Fortunately, the PEDOT:PSS coating prevents the formation of such an SIL. Thus, the PEDOT:PSS coating not only leads to an extraordinary film life-time and a robust process, but also allows us to use a diluted developer leading to a high sensitivity and contrast, as well as resolution.

3.3. Working mechanism of the PEDOT:PSS layer

In order to further investigate the working mechanism of the PEDOT:PSS coating, the dissolution rate of an unexposed resist (dark erosion rate) was investigated. Figure 7 shows the dark erosion rate of samples coated with PEDOT:PSS compared to uncoated samples as a function of the soft bake (SB) time using

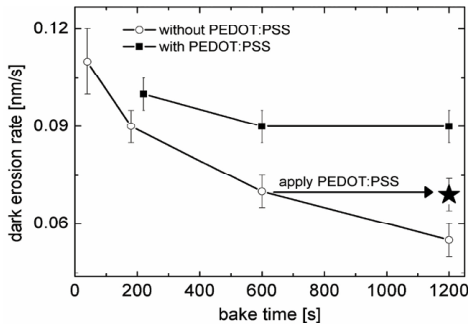


Figure 7. Dark erosion rate as a function of SB time at 110 °C in case of samples coated with PEDOT:PSS (closed symbols) and without PEDOT:PSS (open symbols) developed in a selective and diluted developer (40 vol.% DI water). The samples marked with a star were baked for 10 min before applying the protective PEDOT:PSS coating and baked again for 10 min after applying the coating. The error bars indicate the variance of the dark erosion rates (measured on three different samples). The data points have been connected with lines as a guide to the eye.

a selective and thus diluted developer (40 vol.% DI water). Samples coated with PEDOT:PSS baked for 3 min exhibit a slightly higher dark erosion rate compared to samples without PEDOT:PSS. It was reported that, in case of certain chemically amplified resists, acids diffuse into the resist, “artificially exposing” it, leading to an increased dark erosion rate [43, 45]. However, at long SB times of 10 min the dark erosion rate of samples coated with PEDOT:PSS remained almost constant. These results cannot be explained by an “artificially” exposed surface layer, which should lead to an increasingly dark erosion with increasing SB/diffusion time. It is most likely due to a solvent impermeable PEDOT:PSS coating as also observed by K. Petrillo *et al* [43] using polyaniline as a top-coat material. In the case of uncoated samples, the solvent content is slowly reduced with SB time leading to a decreasingly dark erosion rate (open symbols in figure 7). However, in the case of the PEDOT:PSS coated sample, this evaporation is impeded and the dark erosion rate remains almost constant, regardless of the SB time. This was further verified by baking a sample for 10 min, applying the PEDOT:PSS coating, and baking it a second time for 10 min. The result is marked by a star in figure 7. As the solvent evaporation was stopped after the first bake through the PEDOT:PSS coating, a subsequent bake did no longer had any influence on dark erosion rates. This is why the dark erosion rate of this sample is equivalent to the one without PEDOT:PSS, which was only baked one time for 10 min. This is also the reason why contrast curves and linewidths of PEDOT:PSS coated samples baked for 10 min at 110 °C instead of 3 min are almost unaltered (within error bars, see supporting info).

4. Conclusion and outlook

The chemically amplified 40XT positive tone photoresist was investigated as an EBL resist for the first time. Similar

to comparable chemically amplified resists, 40XT was also susceptible to severe surface inhibition layers depending on delay times, on the order of minutes, between individual process steps. It turned out that, especially diluted developers, which would lead to desired properties such as high contrast, sensitivity, and resolution, inevitably result in process instabilities. This can be ascribed to their high selectivity and their accompanied sensitivity towards any nonlinearities at the resist surface. Therefore, there is a practical trade-off between resolution/contrast and process stability. To overcome this, an acidic and conductive PEDOT:PSS protective top-coating was introduced. As a result, a highly robust and sensitive ($< 10 \mu\text{C}/\text{cm}^2$) lift-off process with a resolution of 85 nm (isolated line) and 90 nm/70 nm (line/space) was obtained. There were no significant linewidth or sensitivity variations observed, even if the samples were stored for 24 h in vacuum or air. This process is a good alternative to conventional EBL processes using standard chemically amplified resists such as UVIII and AZPF514, which all require a tight process control. This extraordinary stability will also render hybrid or mix & match lithography, where photolithography and EBL are combined, leading to inevitable delay times, practically feasible. As a consequence, it will be possible to structure micron patterns such as the periphery and contact pads by photolithography and submicron high-resolution patterns by EBL, further increasing the throughput. Such a versatile mix and match/hybrid lithography process is currently under investigation.

Acknowledgements

The authors wish to thank MicroChemicals for supplying the chemicals. For financial support, the Styrian Government (project MIEC-DEVs A3-11.M-32/2011-6) is acknowledged.

References

- [1] Grigorescu A E and Hagen C W 2009 *Nanotechnology* **20** 292001
- [2] Shokouhi B, Zhang J and Cui B 2011 *Micro Nano Lett.* **6** 992
- [3] Kolb F, Schmoltner K, Huth M, Hohenau A, Krenn J, Klug A, List E J W and Plank H 2013 *Nanotechnology* **24** 305501
- [4] Zhang J, Fouad M, Yavuz M and Cui B 2011 *Microelectron. Eng.* **88** 2196-9
- [5] Salerno M and Cingolani R 2007 *J. Micromech. and Microeng.* **17** 2414-9
- [6] Chen W and Haroon A 1993 *J. Vac. Sci. Technol. B* **11** 2519-23
- [7] Dial O, Cheng C C and Scherer A 1998 *J. Vac. Sci. Technol. B* **16** 3887-90
- [8] Thoms S, Macintyre D S and McCarthy M 1998 *Microelectron. Eng.* **41/42** 207-10
- [9] Mohammad M A, Koshelev K, Fito T, Zheng D A Z, Stepanova M and Dew S 2012 *Jpn. J. Appl. Phys.* **51** 06FC05
- [10] Tobing L Y M, Tjahjana L and Zhang D H 2012 *J. Vac. Sci. Technol. B* **30** 051601-01
- [11] Hu W, Sarveswaran K, Lieberman M and Bernstein G H 2004 *J. Vac. Sci. Technol. B* **22** 1711
- [12] Ocola L E and Stein A 2006 *J. Vac. Sci. Technol. B* **24** 3061

- [13] Cord B, Lutkenhaus J and Berggren K K 2007 *J. Vac. Sci. Technol. B* **25** 2013
- [14] Koshelev K, Ali Mohammad M, Fito T, Westra K L, Dew S K and Stepanova M 2011 *J. Vac. Sci. Technol. B* **29** 06F306-01
- [15] Tanenbaum D M, Lo C W, Isaacson M and Craighead H G 1996 *J. Vac. Sci. Technol. B* **14** 3829-33
- [16] Yasin S, Mumtaz A, Hasko D G and Ahmed H 2000 *Microelectron. Eng.* **53** 471-4
- [17] Yasin S, Khalid M N, Zhang Y and Hasko D G 2005 *Microelectron. Eng.* **78-79** 47-50
- [18] Medeiros R 2002 *J. Photopolym. Sci. Technol.* **15** 411-6
- [19] Merhari L, Gonsalves K., Hu Y, He W, Huang W-S, Angelopoulos M, Bruenger W., Dzionk C and Torkler M 2002 *Microelectron. Eng.* **63** 391-403
- [20] Cardineau B, Earley W, Fujisawa T, Maruyama K, Shimizu M, Sharma S, Petrillo K and Brainard R 2012 *J. Photopolym. Sci. Technol.* **25** 633-40
- [21] Thackeray J W, Aqad E, Kang S J and Spear-Alfonso K 2009 *J. Photopolym. Sci. Technol.* **22** 65-71
- [22] Thackeray J W et al 2007 *J. Photopolym. Sci. Technol.* **20** 411-8
- [23] Shimizu D, Maruyama K, Saitou A, Kai T, Shimokawa T, Fujiwara K, Kikuchi Y and Nishiyama I 2007 *J. Photopolym. Sci. Technol.* **20** 423-8
- [24] Inukai K, Maruyama K, Kawakami T, Ramkrishnan A, Hishiro Y and Kimura T 2013 *J. Photopolym. Sci. Technol.* **26** 691-5
- [25] Cui Z, Prewett P, Facility C M and Didecot C 1999 *Microelectron. Eng.* **46** 255-8
- [26] Krasnoperova A A, Turner S W, Ocola L and Cerrina F 1993 *J. Vac. Sci. Technol. B* **11** 2829
- [27] Nalamasu O, Reichmanis E, Hanson J E, Kanga R S, Heimbrook L A, Emerson A B and Baiocchi F A 1992 *Polym. Eng. Sci.* **32** 1565-70
- [28] MacDonald S A, Hinsberg W D, Wendt H R, Clecak N J, Willson C G and Snyder C D 1993 *Chem. Mater.* **5** 348-56
- [29] Fedynshyn T H, Thackeray J W, Georger J H and Denison M D 1994 *J. Vac. Sci. Technol. B* **12** 3888
- [30] Miller M a., Poppe W J, Neureuther A R, Liddle A and Harteneck B 2006 *J. Vac. Sci. Technol. B* **24** 3025
- [31] Lu B, Taylor J W, Cerrina F, Soo C P and Bourdillon A J 1999 *J. Vac. Sci. Technol. B* **17** 3345
- [32] Rio D, Constancias C, Saied M, Icard B and Pain L 2009 *J. Vac. Sci. Technol. B* **27** 2512
- [33] Kruit P and Steenbrink S 2005 *J. Vac. Sci. Technol. B* **23** 3033
- [34] Yang D X, Frommhold A, Xue X, Palmer R E and Robinson P G 2014 *J. Mater. Chem. C* **2** 1505
- [35] Gibbons F, Zaid H M, Manickam M, Preece J a, Palmer R E and Robinson A P G 2007 *Small* **3** 2076-80
- [36] Oizumi H, Tanaka Y, Kumise T, Shiono D, Hiramaya T, Hada H, Onodera J, Yamaguchi A and Nishiyama I 2007 *J. Photopolym. Sci. Technol.* **20** 403-10
- [37] Shiono D, Hada H, Sato K, Fukushima Y, Watanabe T and Kinoshita H 2009 *J. Photopolym. Sci. Technol.* **22** 737-41
- [38] Mohamed K, Alkaisi M M and Blaikie R J 2009 *Microelectron. Eng.* **86** 535-8
- [39] Angelopoulos M, Patel N, Jane M S, Nancy C, Rishton L and Rishton S A 1993 *J. Vac. Sci. Technol. B* **11** 2794
- [40] Thackeray J W, Denison M, Fedynshyn T H, Georger J, Mori J M and Orsula G W 1993 *J. Vac. Sci. Technol. B* **11** 2855
- [41] Yoshizawa M and Moriya S 2002 *J. Vac. Sci. Technol. B* **20** 1342
- [42] Yasin S, Hasko D G and Ahmed H 1999 *J. Vac. Sci. Technol. B* **17** 3390
- [43] Petrillo K, Bucchignano J and Angelopoulos M 1998 *J. Vac. Sci. Technol. B* **16** 3709
- [44] Asakawa K, Ushirogouchi T and Nakase M 1995 *J. Vac. Sci. Technol. B* **13** 833
- [45] Lee J K et al 2009 *J. Mater. Chem.* **19** 2986

